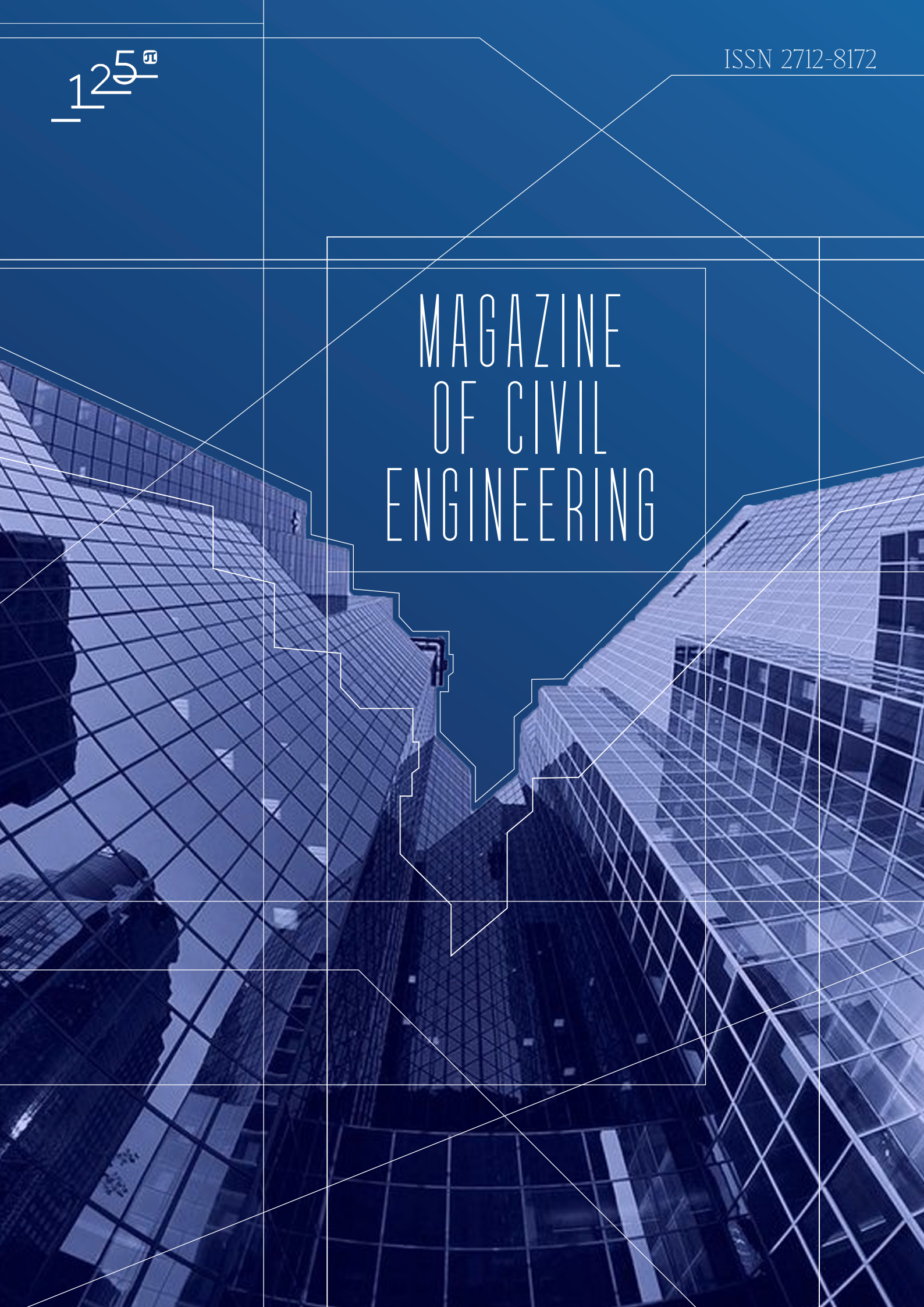


125<sup>th</sup>

ISSN 2712-8172

MAGAZINE  
OF CIVIL  
ENGINEERING



**Magazine of Civil Engineering**

ISSN 2712-8172

Online peer-reviewed open-access scientific journal in the field of Civil and Construction Engineering

**Founder and Publisher:** Peter the Great St. Petersburg Polytechnic University

This journal is registered by the Federal Service for Supervision of Communications, Information Technology, and Mass Media (ROSKOMNADZOR) in 2020. Certificate EI No. FS77-77906 issued February 19, 2020.

**Periodicity:** 8 issues per year

Publication in the journal is open and free for all authors and readers.

**Indexing:** Scopus, Web of Science (ESCI, RSCI), DOAJ, Compendex, Google Academia, Index Copernicus, ProQuest, Ulrich's Serials Analysis System, CNKI

**Corresponding address:** 29 Polytechnicheskaya st., Saint Petersburg, 195251, Russia

**Chief science editor:**

D.Sc., Galina L. Kozinetc

**Deputy chief science editors:**

D.Sc., Sergey V. Korniyenko

**Executive editor:** Ekaterina A. Linnik

**Translator, editor:** Irina Ye. Lebedeva

**Proofreader:** Philipp Chrysanthos S. Bastian

**DT publishing specialist:**

Anastasiya A. Kononova

**Contacts:**

E-mail: [mce@spbstu.ru](mailto:mce@spbstu.ru)

Web: <http://www.engstroy.spbstu.ru>

---

Date of issue: 30.09.2024

© Peter the Great St. Petersburg Polytechnic University. All rights reserved.

© Coverpicture – Polina A. Ivanova

**Editorial board:**

T. Awwad, PhD, professor, Damascus University, Syrian Arab Republic

A.I. Belostotsky, D.Sc., professor, StaDyO Research & Engineering Centre, Russia

A.I. Borovkov, PhD, professor, Peter the Great St. Petersburg Polytechnic University, Russia

M. Veljkovic, PhD, professor, Delft University of Technology, The Netherlands

R.D. Garg, PhD, professor, Indian Institute of Technology Roorkee (IIT Roorkee), India

M. Garifullin, PhD, postdoctoral researcher, Tampere University, Finland

T. Gries, Dr.-Ing., professor, RWTH Aachen University, Germany

T.A. Datsyuk, D.Sc., professor, Saint-Petersburg State University of Architecture and Civil Engineering, Russia

V.V. Elistratov, D.Sc., professor, Peter the Great St. Petersburg Polytechnic University, Russia

O.N. Zaitsev, D.Sc., professor, Southwest State University, Russia

T. Kärki, Dr.-Ing., professor, Lappeenranta University of Technology, Russia

G.L. Kozinetc, D.Sc., professor, Peter the Great St. Petersburg Polytechnic University, Russia

D.V. Kozlov, D.Sc., professor, National Research Moscow State Civil Engineering University, Russia

S.V. Korniyenko, D.Sc., professor, Volgograd State Technical University, Russia

Yu.G. Lazarev, D.Sc., professor, Peter the Great St. Petersburg Polytechnic University, Russia

M.M. Muhammadiev, D.Sc., professor, Tashkent State Technical University, Republic of Uzbekistan

H. Pasternak, Dr.-Ing.habil., professor, Brandenburgische Technische Universität, Germany

F. Rögner, Dr.-Ing., professor, Technology Arts Science TH Köln, Germany

V.V. Sergeev, D.Sc., professor, Peter the Great St. Petersburg Polytechnic University, Russia

T.Z. Sultanov, D.Sc., professor, Tashkent Institute of Irrigation and Agricultural Mechanization Engineers, Republic of Uzbekistan

A.M. Sychova, D.Sc., professor, Military Space Academy named after A.F. Mozhaysky, Russia

M.G. Tyagunov, D.Sc., professor, National Research University "Moscow Power Engineering Institute", Russia

M.P. Fedorov, D.Sc., professor, Peter the Great St. Petersburg Polytechnic University, Russia

D. Heck, Dr.-Ing., professor, Graz University of Technology, Austria

P. Cao, D.Sc., professor, Jilin University, China

A.G. Shashkin, D.Sc., PI Georekonstruktsiya, LLC, Russia

B.M. Yazyev, D.Sc., professor, Don State Technical University, Russia

**Contents**

Kirsanov, M.N., Luong, C.L. Simplified method for estimating the first natural frequency of a symmetric arch truss	13001
Suprun, V.A., Kovalenko, I.A, Ustinova, V.V. The GPR survey method in combination with destructive testing methods for the hydraulic structures technical condition studying	13002
Salih, A.G., Rashid, A.S., Salih, N.B. Effects of chicken bone powder mixed with limestone and cement on the clayey soil geotechnical characteristics	13003
Mirsaidov, M.M., Vatin, N.I., Mamasoliev, K. Bending of multilayer beam slabs lying on an elastic half-space	13004
Nesvetaev, G.V., Koryanova, Yu.I., Yazyev, B.M. Autogenous shrinkage and early cracking of massive foundation slabs	13005
Kozinetc, G.L., Kozinetc, P.V., Badenko, V.L. Response spectra at elevations of station dam equipment installation	13006
Glazunova, I.V., Sokolova, S.A., Shiryayeva, M.A. Filtration calculation to reduce the construction impact on hydrogeological conditions in the city	13007
Chepurnenko, A.S., Yazyev, B.M., Turina, V.S., Akopyan, V.F. Artificial intelligence models for determining the strength of centrally compressed pipe-concrete columns with square cross-section	13008
Shakir, R.R., Al-Haleem, Z. Abd. Evaluation of prior probability distribution of undrained cohesion for soil in Nasiriyah	13009
Sainov, M.P., Talalaev, N.S. Cut-off wall in foundation of reservoir dam and tailing dam: comparative evaluation	13010



Research article

UDC 624.04:531.391.3

DOI: 10.34910/MCE.130.1



## Simplified method for estimating the first natural frequency of a symmetric arch truss

M.N. Kirsanov  , C.L. Luong 

National Research University "Moscow Power Engineering Institute", Moscow, Russian Federation

✉ [c216@ya.ru](mailto:c216@ya.ru)

**Keywords:** Dunkerley method, Maple, analytical solution, lowest frequency, regular trusses, spectra of natural frequencies

**Abstract.** A planar model of a symmetric statically determinate arch truss is considered. The mass of the truss is evenly distributed over its nodes. The Maxwell–Mohr formula, assuming that the truss rods have the same cross-section, allows one to determine the stiffness matrix of a given structure. The Dunkerley method and a variant of the Rayleigh method are proposed to be used to estimate the first natural frequency of the truss. The mass of the structure is conditionally concentrated in its nodes. Only small vertical oscillations are considered. The generalization of a number of solutions for trusses with different number of panels to the general case is carried out by induction. A simplified method for calculating the first frequency based on the Rayleigh method is proposed. To simplify the sums of partial frequencies and squared frequencies included in the Rayleigh solution, the area of the curve limiting the frequency values is replaced by its approximate value, which is calculated by the triangle area formula. The solution includes the value of the maximum deflection of the truss from the action of a distributed load. The results obtained by different analytical methods are compared with the results obtained by the numerical method. All transformations were carried out analytically using the Maple computer mathematical system. The results showed that with an increase in the number of panels, the accuracy of the Dunkerley analytical estimate increases, and the proposed method changes insignificantly. Spectral constants and frequency safety regions were found in the spectra of a family of trusses of different orders.

**Citation:** Kirsanov, M.N., Luong, C.L. Simplified method for estimating the first natural frequency of a symmetric arch truss. Magazine of Civil Engineering. 2024. 17(6). Article no. 13001. DOI: 10.34910/MCE.130.1

### 1. Introduction

The characteristic properties of truss racks are low material consumption, ease of installation, ease of maintenance and convenient transportation. Therefore, this type of structure is widely applied in construction, mechanical engineering, aviation technology, shipbuilding, etc. One of the main tasks, when considering a structure in dynamics, is the calculation of the natural frequency of oscillation. The first, the lowest frequency is of particular importance to practice. To calculate the natural frequency of the truss oscillation in the general case, numerical methods are used based on the finite element method [1–3]. Usually only the upper or lower estimates of the first frequency are of interest, the Dunkerley (for the lower limit) or Rayleigh (for the upper limit) methods are used [4, 5]. A two-sided analytical estimate of the fundamental natural frequency of the spatial contour coverage was obtained in [6]. The formulas obtained based on the Dunkerley method are relatively simple, but in some cases, the accuracy of this method is not satisfactory. Usually the accuracy of the Dunkerley method ranges from 10 % to 45 %. General problems with conventional statically determinate trusses have been presented in [7, 8]. The formula for the lower estimate of natural oscillations of a planar regular externally statically indeterminate beam truss with a rectilinear upper chord was obtained in [9]. The existence of conventional statically determinate truss

systems was first announced in [10, 11]. Algorithms for calculating normal truss deflection based on inductive method using the ability of Maple notation have been used in [12, 13]. The lower limit of the first frequency by the Dunkerley method for a regular planar beam truss was obtained in [14]. In [15], a formula was derived for the dependence of the first frequency of natural vibrations of two span trusses on the number of panels. The dependence of the truss spatial deflection on the number of slabs in the Maple system is found in [16, 17]. Analytical calculations of elements of building structures using the method of superposition of analysis and expansions into series in the Maple computer mathematics system were used in [18, 19]. The spectrum of natural frequencies of the spatial model of a hexagonal rod prism and an analytical estimate of the first frequency were obtained in [20]. The Galerkin method for the analysis of non-linear parametric oscillations of plates was used in [21]. Vibrations and stability of a reinforced rectangular plate were studied in [22].

The Rayleigh method usually gives results with high accuracy. However, this method introduces overly complex formulas and in many cases may not provide a solution. In this paper, a variant of the Dunkerley method with relatively simple coefficients with good accuracy is proposed. The essence of this method is that if the potential energy is calculated from the sum of the potential energies of all the masses, then the sum of the kinetic energies of the masses is replaced by an approximate expression calculated from the maximum kinetic energy of one of the nodes. Refined versions of the Dunkerley method are considered in [23, 24].

## 2. Methods

### 2.1. The Truss Scheme

The truss under consideration is a symmetrical planar truss consisting of interconnected trusses with different number of slabs and different slopes (Fig. 1). The truss has a movable articulated support and a fixed articulation post. All truss posts have the same height  $h$ . The slope of the side (lower) parts of the truss with  $m$  panels is determined by the ratio  $b/a$ , the slope of the middle parts ( $n$  panels in each part) is  $c/a$ . Truss length  $L = a(m+n)$ . In a truss of  $\eta = 8(m+n) + 4$  rods, of which  $4(m+n)$  are in the upper and lower chords,  $4(m+n+1)$  rods form a lattice, and three rods are support rods. Using two balanced equations for each node, a closed system of equations for the forces in the rods and the reactions of the supports can be obtained. It is necessary to solve the problem of oscillation frequency in an analytical form.

It is assumed that the mass of the truss is concentrated in its nodes, oscillations occur along the vertical axis  $y$ .

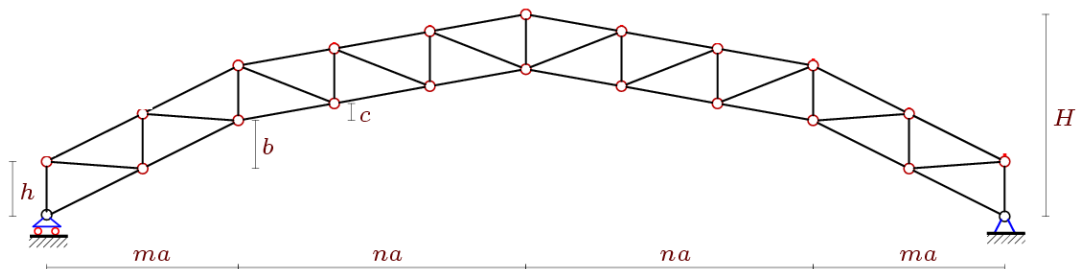


Figure 1. Truss,  $n = 3$ ,  $m = 2$ .

The coordinates of the nodes and the connection order of the bars in the structure are entered into the program like problems in discrete mathematics, the edges and vertices of the graph are specified. Fig. 2 shows the numbering order of the bars and the nodes, nodes and special feature bars are marked with formulas. The program to input coordinates into the Maple system has the following form:

```
> for i to 2*n+2*m+1 do
> x[i]:=a*(i-1);
> x[i+2*n+2*m+1]:=x[i];
> end:
> for i to m+1 do
> y[i]:=b*(i-1);
```

```

> y[i+m+2*n]:=m*b-b*i+b:
> end:
> for i to n do y[i+m+1]:=m*b+c*i; end:
> for i to n-1 do y[i+m+1+n]:=m*b+n*c-c*i; end:
> x[m3-2]:=0: y[m3-2]:=-4:
> x[m3-1]:=x[2*n+2*m+1]: y[m3-1]:=-4:
> x[m3]:= x[2*n+2*m+1]+3: y[m3]:=0:
> for i to 2*n+2*m+1 do
> y[i+2*n+2*m+1]:=y[i]+h:
> end:
    
```

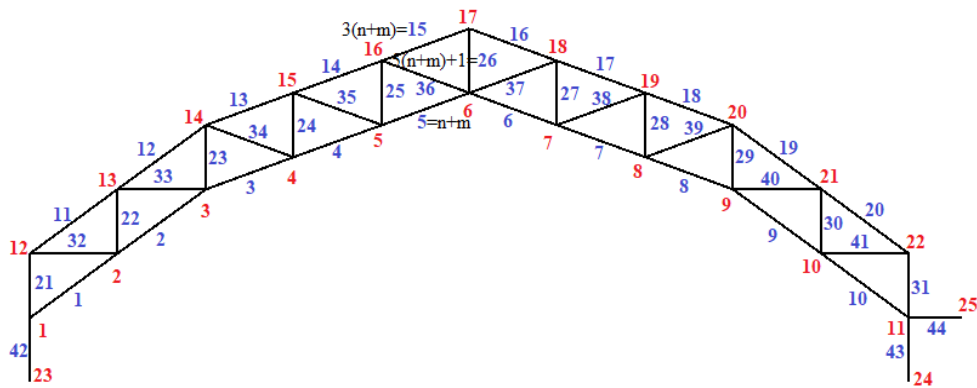


Figure 2. Numbering of bars and nodes,  $m = 3, n = 2$ . Supports are modeled by bars.

### 2.2. Dunkerley Method

The lowest estimate of the frequency of the first oscillations is obtained by the Dunkerley formula:

$$\omega_D^{-2} = \sum_{i=1}^K \omega_i^{-2}, \tag{1}$$

where  $\omega_p$  are partial frequencies calculated for each mass separately,  $K = 4n + 4m + 2$  is the number of degrees of freedom of the cargo system in the truss nodes.

To calculate the partial frequencies, we compose the mass  $\mu$  motion equation:

$$\mu \ddot{y}_p + D_p y_p = 0, \quad p = 1, 2, \dots, K. \tag{2}$$

The stiffness coefficient  $D_p$ , inverse to the compliance coefficient, is calculated using the Maxwell–Mohr formula:

$$\delta_p = 1/D_p = \sum_{\alpha=1}^{\eta-3} \left( S_{\alpha}^{(p)} \right)^2 l_{\alpha} / (EF). \tag{3}$$

From the Dunkerley formula for  $y_p = A_p \sin(\omega t + \varphi)$ ,  $\omega_p = \sqrt{D_p / \mu}$  follows. Hence, we have the expression for the Dunkerley frequency:

$$\omega_D^{-2} = \mu \sum_{p=1}^K \delta_p = \mu \Delta_n. \tag{4}$$

To obtain the dependence of the solution on the number of panels  $n$  in the crossbar and the number of panels  $m$  in the supporting parts, double induction is required. To do this, first, for  $m = 1$ , according to the solutions for a sequence of trusses with  $n = 1, 2, 3, \dots$ , a general formula is obtained, then the same

procedure is repeated for  $m = 2, 3, 4, \dots$ . A number of solutions obtained for various  $m$  are generalized to an arbitrary case. For  $m = 1$ , we have the following solution for the amount corresponding to vertical oscillations:

$$\begin{aligned} n = 1: \Delta_{(1,1)} &= (344a^3 + 842h^3 + 984d^3 + 163g^3) / (36EFh^2), \\ n = 2: \Delta_{(1,2)} &= (116a^3 + 346h^3 + 340d^3 + 153g^3) / (8EFh^2), \\ n = 3: \Delta_{(1,3)} &= (392a^3 + 1470h^3 + 1160d^3 + 1027g^3) / (20EFh^2), \\ n = 4: \Delta_{(1,4)} &= (446a^3 + 2093h^3 + 1326d^3 + 1995g^3) / (18EFh^2), \\ n = 5: \Delta_{(1,5)} &= (840a^3 + 4862h^3 + 2504d^3 + 5861g^3) / (28EFh^2), \\ &\dots \end{aligned}$$

Using the Maple system operators, the common terms of the resulting sequence of coefficients are calculated for the degrees of truss sizes:  $a^3$ ,  $h^3$ ,  $d^3$ ,  $g^3$ , where  $b = h$ ,  $c = h/2$ ,  $d = \sqrt{a^2 + h^2}$ ,  $g = \sqrt{4a^2 + h^2}$ . It follows from the formula that the dependence of the deflection on the number of panels and the dimensions of the structure has the form:

$$\Delta_n = (C_1 a^3 + C_2 h^3 + C_3 d^3 + C_4 g^3) / (h^2 EF). \quad (5)$$

The coefficients have the following formula:

$$\begin{aligned} C_{1,1} &= (8n^2 + 10n + 3) / 3, \\ C_{1,2} &= (4n^4 + 32n^3 + 50n^2 + 82n + 45) / 12, \\ C_{1,3} &= (8n^2 + 10n + 3) / 3, \\ C_{1,4} &= (16n^5 + 80n^4 + 200n^3 + 160n^2 + 39n) / 180. \end{aligned}$$

Similarly, when  $m = 2$ , the coefficients have the following formula:

$$\begin{aligned} C_{2,1} &= (16n^2 + 40n + 30) / 3, \\ C_{2,2} &= (2n^4 + 24n^3 + 81n^2 + 176n + 138) / 6, \\ C_{2,3} &= 16n^2 + 40n + 26, \\ C_{2,4} &= (16n^5 + 160n^4 + 600n^3 + 10400n^2 + 549n) / 180. \end{aligned}$$

Carry out the same process, when  $m = 3, 4, \dots$ , until  $m = 12$ , the general formula for the coefficients according to (5) is found and has the following form:

$$\begin{aligned}
C_1 &= \left( 4m^3 + 10m^2n + (8n^2 - 1)m \right) / 3, \\
C_2 &= \left( 6m^4 + 8(3n+2)m^3 + (32n^2 + 32n + 3)m^2 + \right. \\
&\quad \left. + 2(8n^3 + 8n^2 + 3n + 10)m + 4n^4 + 16n^3 + 2n^2 + 20n \right) / 12, \\
C_3 &= m \left( 32m^4 + 100m^3n + 20(4n^2 + 1)m^2 + 50mn + 40n^2 - 7 \right) / 45, \\
C_4 &= \left( 30m^4n + 120m^3n^2 + 20(8n^2 + 1)nm^2 + 40(2n^2 + 1)mn^2 + 16n^5 + 40n^3 - 11n \right) / 180.
\end{aligned}$$

The final expression for the dependence of the lowest limit of the first frequency on the geometrical parameters of the structure, including the number of plates in the crossbar and the load-bearing side truss, has the following form:

$$\omega_D = h \sqrt{\frac{EF}{\mu \left( C_1 a^3 + C_2 h^3 + C_3 d^3 + C_4 g^3 \right)}}. \quad (6)$$

The result can be checked by doing it in reverse order, that is first carry out induction on  $m$ , then on  $n$ .

### 2.3. A Simplified Version of the Calculation of the First Frequency

When using the Rayleigh method to find the upper estimate of the fundamental frequency, the biggest difficulty in deducing the dependence of the oscillator frequency on the number of plates is the denominator. The essence of the Rayleigh method is based on the law of conservation of energy. During each period of the harmonic oscillation, there is a conversion of potential energy to kinetic energy and vice versa. The transformation can be expressed as the following equation:

$$\omega_R^2 = \frac{\sum_{i=1}^K \tilde{u}_i}{\sum_{i=1}^K \mu \tilde{u}_i^2}, \quad (7)$$

where  $\tilde{u}_i = u_i / P = \sum_{\alpha=1}^{\eta-3} \tilde{S}_{\alpha}^{(P)} \tilde{S}_{\alpha}^{(i)} l_{\alpha} / (EF)$  – displacement amplitude of mass  $\mu$  at a node  $i$  under

the effect of load distributed on the nodes of the truss, is called the value of vertical nodal force  $P$ .

Notations are used:  $S_{\alpha}^{(P)}$  is the force in the rod  $\alpha = 1, \dots, \eta - 3$  from the action of the load  $P$ , uniformly

distributed over the nodes:  $\tilde{S}_{\alpha}^{(P)} = S_{\alpha}^{(P)} / P$ . Three support rods in this arrangement are assumed to be

rigid. The proposed method for the simplified calculation of the Rayleigh frequency consists in replacing the sums in (7) by half the value of the product of the truss-averaged value of the partial frequency and the number of degrees of freedom. This is illustrated in Figs. 3 and 4. The figure for a specific truss shows the distribution of partial frequencies over the nodes of the truss. In Fig. 4, on the horizontal axis, not the number

of marked nodes but the number of the list of  $u^*$  values ranked in ascending order. The sum  $\sum_{i=1}^N \tilde{u}_i$  can

be interpreted as the area bounded by the distribution curve. This area can be calculated more simply by sorting the frequencies in ascending order and calculating the area using the triangle area formula

$\sum_{i=1}^N \tilde{u}_i = Ku_*^* / 2$  (Fig. 4). Here  $u_*^*$  is the maximum deflection of the truss from the action of a single force

distributed over all nodes. From (7) a formula is obtained for an approximate expression of the frequency based on the simplified Rayleigh method:



$$\omega_*^2 = \frac{\sum_{i=1}^K \tilde{u}_i}{\sum_{i=1}^K \mu \tilde{u}_i^2} = 2 / (\mu K u_*). \tag{8}$$

The value of the maximum deflection is obtained by the formula  $u_* = \sum_{\alpha=1}^{\eta-3} \tilde{S}_\alpha^{(P)} \tilde{S}_\alpha^{(*)} l_\alpha / (EF)$ , where  $\tilde{S}_\alpha^{(*)}$  is the force in the rod with number  $\alpha$  from the action of a unit vertical force on the node, the deflection of which is tentatively estimated as maximum. This value for an arbitrary number of panels has the form:

$$u_* = (C_1 a^3 + C_2 h^3 + C_3 d^3 + C_4 g^3) / (h^2 EF). \tag{9}$$

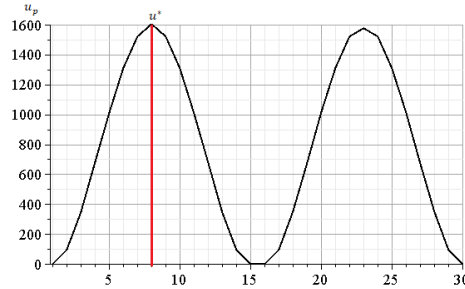


**Figure 3. The dependence of the coefficient  $u_p$  on the number of the truss node for  $m = 4, n = 3$ .**

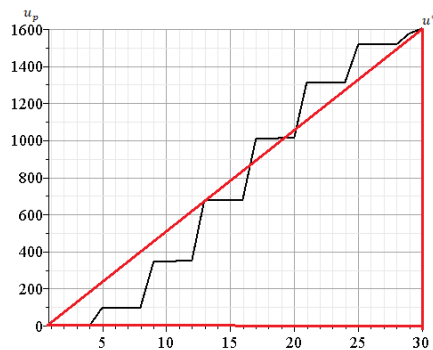


**Figure 4. Coefficients  $u_p$  in ascending order for  $m = 4, n = 3$ .**

Calculations testing the value of  $u_p$  for different values of  $m$  and  $n$  show that the maximum value of  $u_*$  falls on a node of order  $m + n + 1$ .

For  $m = 1$ , the calculations give the following sequence:

$$\begin{aligned}
 n=1: u_* &= \left(240a^3 + 2044h^3 + 19380d^3 + 633g^3\right) / \left(2EFh^2\right), \\
 n=2: u_* &= \left(560a^3 + 5096h^3 + 44120d^3 + 3139g^3\right) / \left(4EFh^2\right), \\
 n=3: u_* &= \left(320a^3 + 3128h^3 + 24740d^3 + 2867g^3\right) / \left(2EFh^2\right), \\
 n=4: u_* &= \left(180a^3 + 1895h^3 + 13710d^3 + 2294g^3\right) / \left(EFh^2\right), \\
 n=5: u_* &= \left(200a^3 + 2270h^3 + 15050d^3 + 3400g^3\right) / \left(EFh^2\right), \\
 &\dots
 \end{aligned}$$

Formulas for  $u_*$  are obtained similarly for  $m = 2, 3, \dots$ . The generalization of the series of these formulas to an arbitrary number of panels  $m$  gives the following final formulas:

$$\begin{aligned}
 C_1 &= m^2 + 2mn, \\
 C_2 &= \left(3m^3 + 2n^3 + 2(4n^2 + 1)m^2 + 4n^2 + 2(3n^2 + 1)m + 2n\right) / 4, \\
 C_3 &= m(5m^3 + 8m^2n + m + 4n) / 6, \\
 C_4 &= \left(12m^3n + 30m^2n^2 + 2n(10n^2 - 1)m + 4n^4 + 7n^2\right) / 48.
 \end{aligned} \tag{10}$$

The sequence of coefficients with this approach were relatively complex, for problems like this, there are many advantages to using the *rsolve* and *rgf\_findrecur* operators or the Maple operator to generalize to sequences.

Thus, the approximate value of the first frequency (8) is:

$$\omega_* = h \sqrt{\frac{EF}{\mu(2n + 2m + 1)(C_1a^3 + C_2h^3 + C_3d^3 + C_4g^3)}} \tag{11}$$

with coefficients (10).

This solution is obtained under the assumption that the three rods modeling the left movable and right fixed supports are rigid. This is why the summation in the Maxwell–Mohr formulas is carried out up to  $\eta - 3$ . However, this solution can be refined by conditionally accepting that all support rods have a length  $h$  and a modulus of elasticity  $E$ . Only the coefficient  $C_2$  in (10) will have a small difference:

$$C_2 = \left(3m^3 + 2n^3 + 2(4n^2 + 1)m^2 + 4n^2 + 2(3n^2 + 5)m + 10n + 4\right) / 4.$$

Considering that the new value of the coefficient  $C_2$  is greater than the initial one, and this coefficient is in the denominator of formula (11), the solution for the natural frequency, taking into account the elasticity of the supports, will be slightly smaller. This change has almost no effect on the magnitude of the natural frequency.

When  $m = n$ , the proposed simplified solution (11) has the form:

$$\begin{aligned}
 \omega_* &= \\
 &= 4h \sqrt{\frac{3EF}{\mu n \left( (67g^3 + 104d^3)n^3 + 228h^3n^2 + (72h^3 + 144a^3 + 40d^3 + 5g^3)n + 48h^3 \right)}}. \tag{12}
 \end{aligned}$$

### 3. Results and Discussion

#### 3.1. Numerical Example

To illustrate the dependence of the natural oscillator frequency on the number of panels found by the Dunkerley method, the new method has been proposed, and to evaluate the accuracy of the analytical solution, the first frequency from the frequency of the device natural motion of the structure will be found. Using the special operator Eigenvalues from the LinearAlgebra package, the Maple system finds eigenvalues and matrix vectors. The truss under consideration corresponds to the dimensions  $a = 5$  m,  $h = 4$  m. The cross-sectional area of the grids and supports is assumed to be the same:  $F = 4$  cm<sup>2</sup>. Elastic modulus of steel  $E = 2 \cdot 10^5$  MPa, mass at nodes  $\mu = 150$  kg. Fig. 5 shows the dependence on the number of panels of the frequency  $\omega_D$  according to the standard Dunkerley formula (6), the frequency  $\omega_*$  according to the simplified formula (11), and the numerically found value of the first frequency  $\omega_1$  of the spectrum of a system with  $K$  degrees of freedom.

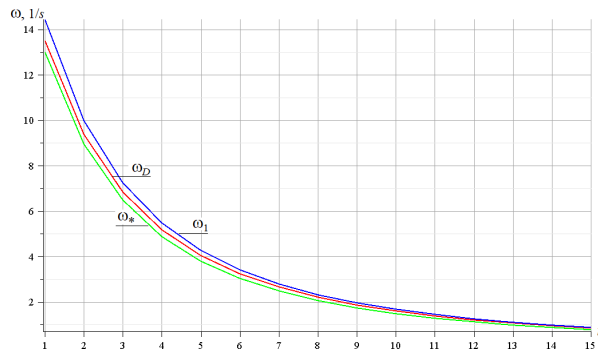


**Figure 5. Comparison of analytical solutions with numerical,  $m = 3$ . The first oscillation frequency of the truss  $\omega_1$  and its lower estimate  $\omega_D$  according to Dunkerley,  $\omega_*$  is the lower estimate according to the simplified formula.**

The Dunkerley method, its simplified version, and the numerical method for values do not differ too much. At the same time, over the entire range of values of the number of panels, as expected, the Dunkerley estimates are less than the first frequency of the spectrum obtained numerically, taking into account all degrees of freedom. From Fig. 5 it can be concluded that the more cells in the crossbar, the smaller the error obtained. The lower the truss height, the smaller the error.

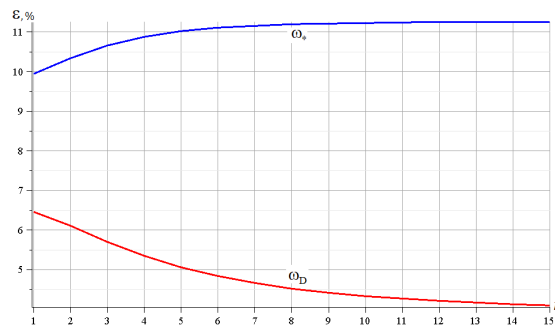


**Figure 6. Comparative error of methods,  $m = 3$ .**

Fig. 6 shows how the error of approximate solutions' changes as the number of tables changes. Values of relative error are introduced:  $\varepsilon = \left( \omega_1 - \omega_D \right) / \omega_1$ . With increasing truss order, the error of the Dunkerley method decreases and reaches a value of about 1 % with  $k > 12$ . In contrast, with the proposed method, with  $k < 8$ , the accuracy is gradually reduced, when  $k > 8$ , this error does not change at 12 %. In summary, for the selected design features, this value should not exceed 12 % for the proposed method and 6.5 % at most for the Dunkerley method.

#### 3.2. The Level Lines of the Value of the First Frequency

The level lines of the value of the first frequency in the  $m$ - $n$  axes, with increasing frequency, thicken (Fig. 7). The figure is constructed for the  $a = 5$  m,  $h = 10$  m and previous values of the mass, modulus of elasticity and stiffness of the rods. As the height of the truss decreases, the curves in this figure straighten.

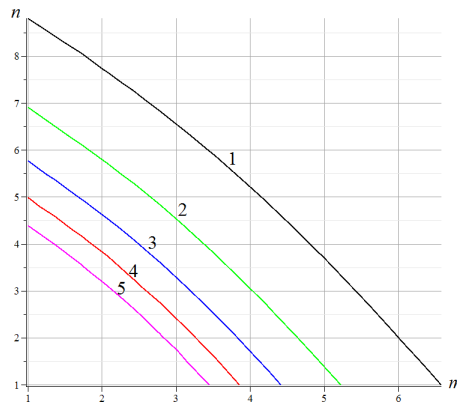


**Figure 7. First frequency level lines.**

**1:  $\omega = 4s^{-1}$ ; 2:  $\omega = 6s^{-1}$ ; 3:  $\omega = 8s^{-1}$ ; 4:  $\omega = 10s^{-1}$ ; 5:  $\omega = 12s^{-1}$ .**

The curves thicken with increasing frequency of natural oscillations. Outwardly, this resembles the Doppler effect for a moving source of oscillations, although, of course, it has a completely different nature.

### 3.3. Natural Frequency Spectra of Regular Trusses

Usually, high vibration frequencies are not used in engineering calculations, except in resonance case studies. The natural frequency of vibration caused by the operation of different equipment may coincide with the natural frequency of the structure's vibration. The natural frequency spectrum is used, for example, to monitor the dynamics of railway bridges [25, 26]. The frequency spectrum is also required for multi-scale modeling and design of sandwich metastructures with a lattice core to suppress broadband low-frequency vibrations [27].

The analytical method cannot account for these oscillation frequencies, but the well-tuned mathematical engine in numerical mode gives an interesting picture of the spectral set of conventional systems. In Fig. 8, twelve curves connect the points corresponding to the oscillation frequency of the truss of order  $n = 1, 2, \dots, 12$ . Each curve corresponds to a given truss, and the coordinates of the points on it are the frequencies. The horizontal axis shows the number of natural frequencies in the ordered spectrum.

Some features of the frequency distribution are noted here. All spectra are characterized by significant frequency jumps, and all higher frequencies of the spectrum are multiples. For the accepted truss sizes  $a = 5$  m,  $h = 4$  m,  $F = 4$  cm<sup>2</sup>, there appear to be frequencies of  $\omega_1 = 250s^{-1}$ ,  $\omega_2 = 520s^{-1}$ ,  $\omega_3 = 600s^{-1}$  (spectral constant) constant for rigs of different orders. The presence of this regularity allows one to predict several truss frequencies with large regularity as calculated by a truss with a small number of plates, which greatly simplifies the solution. The first frequency has a fairly accurate analytical estimate, which is found by the Dunkerley formula. A similar spectrum with multiple higher frequencies was obtained for a planar regular truss that allows kinematic changes for a certain number of panels [28].

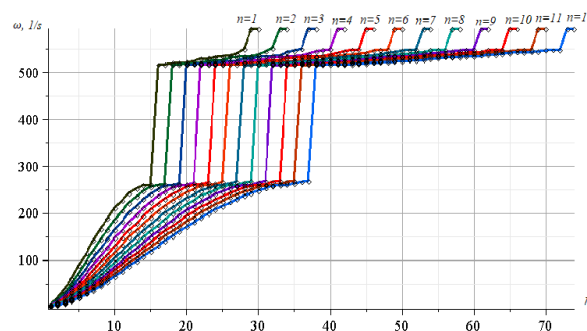


**Figure 8. Spectra of regular trusses,  $m = 6$ .**

It should also be noted the area of frequency safety, enclosed between frequencies  $\omega_1 = 250s^{-1}$  and  $\omega_2 = 520s^{-1}$  in the spectral picture. This means that placing on the truss some source of external excitation with a natural frequency from this gap guarantees the safety of the system from the occurrence of resonance. It is also characteristic that this area does not depend on the order of the truss (in this case, the number of panels  $n$ ).

#### 4. Conclusion

A new scheme for a statically determinate symmetric truss is proposed. The design under consideration could be used in the design of a bridge or other transport structure. The Dunkerley method and the proposed method allow one to obtain an analytical solution to estimate the first natural frequency of oscillation of a conventional truss. One of the objectives of the study was to obtain an analytical solution in the form of a relatively compact formula for the frequency of natural oscillations. Therefore, fairly strong assumptions were introduced into the model of the object: the oscillations of the nodes were assumed to be vertical, and neither physical nor geometric nonlinearities were taken into account. In favor of the latter, it should be noted that the oscillations were assumed to be small, where various nonlinearities are irrelevant.

Any other conventional mechanical system with a large number of degrees of freedom can also use this proposed method. The following main conclusions can be drawn from the analyzed results:

1. The coefficients obtained from the proposed method are much simpler than those obtained from the Dunkerley method, and the accuracy of these two methods is almost the same.
2. With an increase in the number of panels in the truss structure and a sufficiently large number of crossbars, the accuracy of the proposed method remains unchanged, while the accuracy of the Dunkerley method increases.
3. In the frequency spectrum of a family of regular trusses, spectral constants and a frequency safety region are found.

#### References

1. Macareno, L.M., Agirrebeitia, J., Angulo, C., Avilés, R. FEM subsystem replacement techniques for strength problems in variable geometry trusses. *Finite Elements in Analysis and Design*. 2008. 44(6–7). Pp. 346–357. DOI: 10.1016/j.finel.2007.12.003
2. Vatin, N., Havula, J., Martikainen, L., Sinelnikov, A.S., Orlova, A.V., Salamakhin, S.V. Thin-walled cross-sections and their joints: Tests and FEM-modelling. *Advanced Materials Research*. 2014. 945–949. Pp. 1211–1215. DOI: 10.4028/www.scientific.net/AMR.945-949.1211
3. Ignatyev, A.V., Ignatyev, V.A. On the Efficiency of the Finite Element Method in the Form of the Classical Mixed Method. *Procedia Engineering*. 2016. 150. Pp. 1760–1765. DOI: 10.1016/J.PROENG.2016.07.167
4. Kirsanov, M.N., Luong, C. Frequency spectrum of natural oscillations of the spatial structure of the rod pyramid. *Construction of Unique Buildings and Structures*. 2023. 107(2). Article no. 10702. DOI: 10.4123/CUBS.107.2
5. Komerzan, E.V., Maslov, A.N. Estimation of the L-shaped spatial truss fundamental frequency oscillations. *Structural Mechanics and Structures*. 2023. 37(2). Pp. 35–45. DOI: 10.36622/VSTU.2023.37.2.004
6. Kirsanov, M.N., Luong, C. Natural frequency spectra of spatial structure. *Construction of Unique Buildings and Structures*. 2023. 106(1). Article no. 10604. DOI: 10.4123/CUBS.106.04
7. Kaveh, A., Rahami, H., Shojaei, I. *Swift Analysis of Civil Engineering Structures Using Graph Theory Methods*. Springer, Cham, 2020. 302 p. DOI: 10.1007/978-3-030-45549-1
8. Ignatiev, V.A., Ignatiev, A.V. Metod konechnykh elementov v forme klassicheskogo smeshannogo metoda stroitel'noi mekhaniki (teoriia, matematicheskie modeli i algoritmy) [Finite element method in the form of a classical mixed method of structural mechanics (theory, mathematical models and algorithms)]. Moscow: ASV Publ., 2022. 306 p. DOI: 10.12731/978-5-4323-0431-5
9. Shchigol, E.D. The formula for the lower estimate of the natural oscillations of a flat regular girder truss with a rectilinear upper belt. *Structural Mechanics and Structures*. 2023. 37(2). Pp. 46–53. DOI: 10.36622/VSTU.2023.37.2.005
10. Hutchinson, R.G., Fleck, N.A. The structural performance of the periodic truss. *Journal of the Mechanics and Physics of Solids*. 2006. 54(4). Pp. 756–782. DOI: 10.1016/j.jmps.2005.10.008
11. Hutchinson, R.G., Fleck, N.A. Microarchitected cellular solids – the hunt for statically determinate periodic trusses. *Zeitschrift für Angewandte Mathematik und Mechanik*. 2005. 85(9). Pp. 607–617. DOI: 10.1002/zamm.200410208
12. Ivanitskii, A.D. Formulas for calculating deformations of a planar frame. *Structural Mechanics and Structures*. 2022. 34(3). Pp. 90–98. DOI: 10.36622/VSTU.2022.34.3.007
13. Komerzan, E.V., Lushnov, N.A., Osipova, T.S. Analytical calculation of the deflection of a planar truss with an arbitrary number of panels. *Structural Mechanics and Structures*. 2022. 33(2). Pp. 17–25. DOI: 10.36622/VSTU.2022.33.2.002
14. Komerzan, E.V., Maslov, A.N. Analytical evaluation of a regular truss natural oscillations fundamental frequency. *Structural Mechanics and Structures*. 2023. 37(2). Pp. 17–26. DOI: 10.36622/VSTU.2023.37.2.002

15. Petrenko, V.F. The natural frequency of a two-span truss. AlfaBuild. 2021. 20. Article no. 2001. DOI: 10.34910/ALF.20.1
16. Astakhov, S.V., Kirsanov, M.N., Vorobyev, O.V. Formulas for Calculating Deformations of Power Line Supports. IOP Conference Series: Earth and Environmental Science. 2022. 988(4). Article no. 052058. DOI: 10.1088/1755-1315/988/5/052008
17. Komerzan, E., Sviridenko, O. Static deformations of the truss of a composite spatial frame. Analytical solutions. Structural mechanics and structures. 2022. 35(4). Pp. 40–48. DOI: 10.36622/VSTU.2022.35.4.005
18. Matrosov, A.V. Computational Peculiarities of the Method of Initial Functions. Computational Science and Its Applications – ICCSA 2019. Springer, Cham, 2019. 11619. Pp. 37–51. DOI: 10.1007/978-3-030-24289-3\_4
19. Goloskokov, D.P. Analyzing simply supported plates using Maple system. 2014 International Conference on Computer Technologies in Physical and Engineering Applications (ICCTPEA). IEEE, 2014. Pp. 55–56. DOI: 10.1109/ICCTPEA.2014.6893273
20. Kirsanov, M. Model of a hexagonal prismatic truss. Oscillation frequency spectrum. Construction of Unique Buildings and Structures. 2023. 106(1). Article no. 10601. DOI: 10.4123/CUBS.106.1
21. Khodzhaev, D.A., Abdikarimov, R.A., Amabili, M., Normuminov, B.A. Parametric oscillations of a viscous-elastic orthotropic shell of variable thickness. Magazine of Civil Engineering. 2023. 120(4). Article no. 12010. DOI: 10.34910/MCE.120.10
22. Eshmatov, B.Kh., Abdikarimov, R.A., Amabili, M., Vatin, N. Nonlinear vibrations and dynamic stability of viscoelastic anisotropic fiber reinforced plates. Magazine of Civil Engineering. 2023. 118(2). Article no. 11811. DOI: 10.34910/MCE.118.11
23. Low, K.H. Modified Dunkerley formula for eigenfrequencies of beams carrying concentrated masses. International Journal of Mechanical Sciences. 2000. 42(7). Pp. 1287–1305. DOI: 10.1016/S0020-7403(99)00049-1
24. Rutenberg, A. A lower bound for Dunkerley's formula in continuous elastic systems. Journal of Sound and Vibration. 1976. 45(2). Pp. 249–252. DOI: 10.1016/0022-460X(76)90599-X
25. Vanova, P., Sun, Z., Odinson, O.-E., Jiang, Z. Dynamic response analysis of a model truss bridge considering damage scenarios. Engineering Failure Analysis. 2023. 151. Article no. 107389. DOI: 10.1016/j.engfailanal.2023.107389
26. Torres, B., Poveda, P., Ivorra, S., Estevan, L. Long-term static and dynamic monitoring to failure scenarios assessment in steel truss railway bridges: A case study. Engineering Failure Analysis. 2023. 152. Article no. 107435. DOI: 10.1016/j.engfailanal.2023.107435
27. Guo, J., Li, Y., Xiao, Y., Fan, Y., Yu, D., Wen, J. Multiscale modeling and design of lattice truss core sandwich metastructures for broadband low-frequency vibration reduction. Composite Structures. 2022. 289. Article no. 115463. DOI: 10.1016/j.compstruct.2022.115463
28. Kirsanov, M.N., Luong, C. Deformations and natural frequency spectrum of a planar truss with an arbitrary number of panels. AlfaBuild. 2022. 25. Article no. 2507. DOI: 10.57728/ALF.25.7

**Information about the authors:**

**Mikhail Kirsanov**

ORCID: <https://orcid.org/0000-0002-8588-3871>

E-mail: [c216@ya.ru](mailto:c216@ya.ru)

**Cong Luan Luong**

ORCID: <https://orcid.org/0000-0002-6848-0974>

E-mail: [luongcongluan96@gmail.com](mailto:luongcongluan96@gmail.com)

*Received 20.08.2024. Approved after reviewing 02.09.2024. Accepted 02.09.2024.*



Research article

UDC 626/627

DOI: 10.34910/MCE.130.2



## The GPR survey method in combination with destructive testing methods for the hydraulic structures technical condition studying

V.A. Suprun, I.A Kovalenko , V.V. Ustinova 

Federal Scientific Centre of Agroecology, Complex Melioration and Protective Afforestation of the Russian Academy of Sciences, Volgograd, Russian Federation

✉ [ustinova-v@vfanc.ru](mailto:ustinova-v@vfanc.ru)

**Keywords:** hydraulic structures, irrigation system, universal testing machine, GPR

**Abstract.** The study examined the technical condition of hydraulic structures (HS) to plan their reconstruction, restoration and development of protective measures. The Sarpinskaya Watering and Irrigation System (SWIS) in the Republic of Kalmykia was the object of study. Promising research and monitoring methods were used: testing of concrete core samples using universal testing machine MIM.4-1000 and ground penetrating radar probing (by the GPR OKO-3) with ground penetrating radar survey of HS. Based on the results obtained, it can be concluded that concrete and reinforced concrete structures on the territory of the SWIS (namely, pumping station No. 1) have low strength, which is explained by their long service life and the lack of major repairs. The studied core samples collapsed under a minimum load of 116...118 kN. This indicates severe wear of the concrete coating of HS, aggravated by the close occurrence of groundwater. Further destruction of the concrete coating is inevitable, and therefore urgent repair and reinforcement of the structures are required. The data obtained will be used as a basis for conducting an examination necessary for operational monitoring of the SWIS and decision-making, when developing protective measures to strengthen the structures.

**Funding:** The research was carried out within the framework of the state assignment "Reclamation complexes: assessment, condition control and process management using digital technologies" (FNFE-2022-0004).

**Citation:** Suprun, V.A., Kovalenko, I.A, Ustinova, V.V. The GPR survey method in combination with destructive testing methods for the hydraulic structures technical condition studying. Magazine of Civil Engineering. 2024. 17(6). Article no. 13002. DOI: 10.34910/MCE.130.2

### 1. Introduction

Irrigation canals and hydraulic structures (HS) play a key role in agriculture, providing a constant water supply for irrigation of fields. During the operation of HS, various types of damages occur. The study of the technical condition of HS is important for planning their reconstruction, restoration and development of further protective measures. Under conditions of intensive operation and exposure to natural factors, the following main types of damage occur on HS [1]: corrosion of water-saturated concrete in the zone of variable water level due to alternate freezing and thawing; mechanical damage to concrete masonry (chipping of corners of elements, crushing of concrete in separate zones, etc.); cracks caused by shrinkage or reaction of cement alkalis with aggregates containing active silica, and others.

Such scientists as V.S. Altunin, G.T. Balakay, A.V. Kolganov, B.S. Maslov, V.V. Noskewich, G.M. Nigmatov, I.V. Olgarenko, V.N. Shchedrin and others studied the technical condition of reclamation systems

[2–9]. The main direction in the works of these authors was the assessment of the condition of HS under construction and those already built where the main goal was to expand knowledge for further verification of design solutions and the formation of a regulatory and methodological framework.

M.L. Vladov, D.V. Dmitrievtsev, A.D. Zhigalin, O.Kh. Zhukov, S.V. Izumov, K.T. Iskakov, V.V. Kapustin, A.N. Ryzhakov, D.A. Solodovnikov, M.P. Shirobokov and others were engaged in research using ground penetrating radar (GPR) surveys [10–17]. The authors study and consider the issues of complex application of geophysical methods at the stages of design, construction and reconstruction of hydro-reclamation systems, with a description and operation of GPR and the use of the radar sounding method.

The work of D.A. Solodovnikov, N.M. Khavanskaya, N.V. Vishnyakov, A.A. Ivantsova, based on the use of geophysical monitoring, showed that the results of the using GPR monitoring contain more objective information about the depth of the groundwater table. Combining GPR profiling with a hypsometric profile of the terrain allows one to build a model of groundwater dynamics [14].

Such scientists as V.V. Borodychev, E.B. Dedova, A.V. Kolganov, T.N. Mandzhieva, V.A. Suprun, R.M. Shabanov and others conducted their research on the territory of the Sarpinskaya Watering and Irrigation System (SWIS) [18–24]. The research involves environmental monitoring of water bodies in the Republic of Kalmykia, including the SWIS, using methods of studying the biogeocenosis of inland water bodies.

The SWIS was chosen as the object of the present study. It is one of the largest objects of the reclamation complex of the Republic of Kalmykia. The climate of the republic can be characterized as sharply continental, semiarid and arid with cold winters (minimum temperature  $-37\text{ }^{\circ}\text{C}$ ) and hot summers (maximum temperature  $+44\text{ }^{\circ}\text{C}$ ). The SWIS was put into operation in 1968 and was used mainly for irrigation of rice fields. The water source of the system is the Volga River, on the bank of which, near Raygorod (the Volgograd Region), there is a water intake of a machine water lift that supplies irrigation water to the system. Water losses amount to 59 % of the annual volume of water intake (data obtained from the administration of the Oktyabrsky District of the Republic of Kalmykia). Most of the losses are associated with the physical wear of the system, equal to 92 % (data obtained from the administration of the Oktyabrsky District of the Republic of Kalmykia). During the entire period of operation of the system, only routine repairs of pumping stations (NS-2, NS-8, NS-9, etc.) were carried out, as well as repairs of earth dams and emergency repairs of failed system elements.

The republic is one of the most water-deficient regions of Russia. It is not provided with sufficient surface water resources, and the mineralization of the groundwater used for the needs of the population is constantly increasing. In some places, the mineralization index of natural groundwater is close to brines.

Thus, the purpose of this work is to determine the technical condition of the elements of irrigation systems to improve the reliability and environmental safety of their structural elements using non-destructive and destructive testing methods. The objectives of the study are:

- identifying patterns of changes in the physical and mechanical properties of materials of structures and structures during operation and obtaining data on the state of reinforcement and concrete in the studied samples from HS;
- obtaining up-to-date information on the condition, possible deformations and impacts of a natural and anthropogenic nature on structures using GPR;
- assessing the current technical condition of the elements of the SWIS.

To solve the problems associated with the wear and tear of HS and their timely repair, a more accurate assessment and forecast of the service life of HS is required. In accordance with the state assignment, field studies of the technical condition of HS at the SWIS were carried out in 2023. The results of these studies will help to identify defects and problem areas. It is necessary to develop a set of measures to improve the reliability and safety of HS, including more economically viable ways of current repair of structures.

## **2. Methods and Materials**

### **2.1. SWIS**

The SWIS is located in the north-east of the Republic of Kalmykia, in the Oktyabrsky and Maloderbetovskiy Districts. The following types of soil are typical for this area: saline light chestnut and brown semi-desert soils combined with salt marshes [2]. The total amount of precipitation is about 300 mm per year [1]. The average daily temperature varies in summer within the range of  $+23.5\text{ }^{\circ}\text{C}$ ... $+25.5\text{ }^{\circ}\text{C}$ , in particularly hot years it reaches an absolute maximum of  $+40\text{ }^{\circ}\text{C}$ ... $+44\text{ }^{\circ}\text{C}$ . In winter, the average



temperatures are negative  $-12\text{ }^{\circ}\text{C} \dots -7\text{ }^{\circ}\text{C}$ , the minimum temperature in January is  $-37\text{ }^{\circ}\text{C} \dots -35\text{ }^{\circ}\text{C}$ . Sometimes the temperature drops to  $-40\text{ }^{\circ}\text{C}$  and below [3].

## 2.2. Technical Studies of HS

In 2023, georadolocation survey was carried out at certain SWIS sites in the Oktyabrsky District of the Republic of Kalmykia using the GPR OKO-3. Concrete samples were taken from some sections of the concrete lining of the drainage channel for further study in the laboratory (Fig. 1).



**Figure 1. Places of concrete cores sampling.**

To obtain complete and accurate information about the HS condition, a destructive testing method, “Core sampling and testing” was used, which was carried out on selected sections of HS with the use of a diamond drilling rig (Fig. 2).



**Figure 2. Process of cutting the cores using a diamond drilling rig.**

The cores were taken from the area of pumping station No. 1 of the SWIS. The sampling site was chosen taking into account the minimum possible damage to HS, at a distance of 600 mm from the joints and edges of the coating, in the area free from reinforcement. The number and location of drilling spots are determined by local conditions.

After cutting, the concrete core samples were sent to the laboratory to determine their strength by measuring the minimum force required for destruction. The number of samples in the series was 6 pieces (Fig. 3).



**Figure 3. Concrete samples from the SWIS.**

Compression tests of samples were carried out in the laboratory of the Federal Scientific Centre of Agroecology, Complex Melioration and Protective Afforestation of the Russian Academy of Sciences on universal testing machine MIM.4-1000 (Fig. 4). The laboratory analysis consisted of a static load with its constant growth rate, and the subsequent calculation of stresses taking into account the elastic work of the material.



**Figure 4. Testing of a core sample using a universal testing machine MIM.4-1000.**

The cut-out part of the structure used for the testing was formed and hardened during HS construction under the same conditions and under the same load as the rest of the structure, which means that the results of testes represent the state of HS nearby.

However, after the core was extracted, such a structural characteristic as load-bearing capacity of the structure under study may change. Therefore, it is recommended to extract a concrete sample only with the marks made in advance by the developer, so that the loss of a part of the structure would not affect its strength characteristics in any way. The place, from which the core was removed, was filled with concrete and the surface was leveled.

The GPR survey was performed at the place where the core samples were taken (Fig. 1). The GPR survey of HS was carried out using the GPR OKO-3, manufactured by JSC Geotech (Russia), equipped with a 2-frequency antenna unit 150+400 MHz (Fig. 5).



**Figure 5. The GPR survey.**

Both antennas of the device are shielded, which prevents electromagnetic radiation from entering the upper half-space of the device, and suppresses reflection from objects of the upper half-space [25]. The 150 MHz antenna probes the soil to a depth of up to 12 m with a resolution (minimum size of detectable objects) of 0.35 m. The 400 MHz antenna provides probing to a depth of 5 m but with a more accurate resolution of 0.15 m. In this work, due to the small capacities of the probed soils, the main instrument was the 400 MHz antenna, the 150 MHz antenna served as a control.

The GPR method is based on the reflection of electromagnetic waves from surfaces, on which electrical properties change. It makes it possible to solve a wide range of applied tasks, in particular: the study of geological sections with determination of capacities layers and types of rocks; determination of the position of the groundwater level; identification of defects in building structures; identification of foreign bodies in the ground, and others [12].

The electromagnetic pulse emitted by the GPR is reflected from any objects or inhomogeneities in it that have electrical permeability or conductivity different from the medium. Such inhomogeneities may include voids, interfaces between layers of different rocks, areas with different humidity, etc. The receiving antenna converts the reflected signal into digital and stores it for further processing. When a GPR scans the surface of the area under study, a radar image or profile appears on the screen, which can be used to determine the location, depth and extent of objects.

### 3. Results and Discussion

The results of the conducted research show that concrete samples taken from the concrete lining of the drainage channel have low strength, which is natural, given the service life of structures and the lack of major repairs of concrete and reinforced concrete structures. The table shows the data obtained in the laboratory of the Federal Scientific Centre of Agroecology, Complex Melioration and Protective Afforestation of the Russian Academy of Sciences using a universal testing machine (Table 1).

**Table 1. Research results obtained using the MIM.4-1000 testing machine.**

No	Concrete core sample	Sample diameter, mm	Sample length, mm	Mechanical stress $R(cp)$ , MPa	Ultimate compressive strength, kN	Year of HS commissioning
1	1	63.40	110	47.1	150	1968
2	2	63.20	111	34.3	148	1968
3	3	63.10	109	41.2	118	1968
4	4	63.40	110	34.3	116	1968
5	5	63.35	110	38.2	118	1968
6	6	63.37	111	29.1	116	1968

From Table 1, it can be seen that samples No. 3, 4, 5, 6 were destroyed at a minimum load of 116...118 kN. These data indicate a strong wear of the concrete coating of HS, which is complicated by the close occurrence of groundwater, which will cause further damage to the coating.

The graph in Fig. 6 shows fluctuations and a subsequent sharp increase in the load during compression of the core sample on a universal testing machine. This graph is typical for all selected cores, since destruction occurs throughout the area under study.

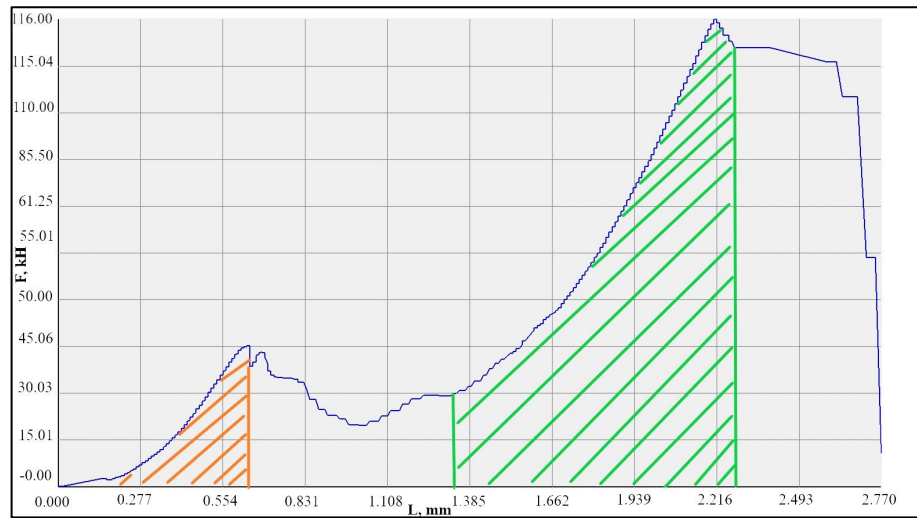


**Figure 6. Deformation diagram of the core sample, kN.**

When loading the test sample, in the area highlighted in orange in Fig. 6, there is an increase in the deformation curve from 0 to 42 kN. A repeated jump can be observed in the area highlighted in green. In this part, the graph has a stronger amplitude from 30 to 116 kN.

The graph shows that the deformation runs along the layering with an exorbitant characteristic. It follows from this that the site is subject to destruction.

Conducting research using the GPR OKO-3 allowed us to obtain the following results.

1. Graphs of time sections recorded by the variable density method, on which the horizontal axis indicates the distance in meters, and the vertical axis indicates the time of arrival of reflected signals in nanoseconds. In subsequent work in the GeoScan32 program, when processing signals, interference is weakened or removed from the record as much as possible, and useful ones are highlighted [15].
2. The electrical properties of metals are fundamentally different from the properties of any soils, therefore, their detection in the soil by the GPR method does not cause significant difficulties, provided that metal objects are found within the probing depth of the device and linear dimensions exceed the resolution of the device. Concrete structures in the soil also cause changes in the propagation of electromagnetic fields (Fig. 7, 8).

The geimage (Fig. 7) shows the revealed inhomogeneities of the body: surface local fractures and voids in the reinforced concrete structure of the structure, when scanning with the antenna side of the AB 150/400 MHz, having a width in plan of 0.5...1.5 m and directed across the body of the dam. In this image, we can observe fluctuations through the entire body of the concrete channel bed and up to 12.5 m, which can be formed by voids in the body of the dam [25].

Fig. 8 shows the result of a detailed study of the zone, which was carried out by scanning using the AB 150/400 MHz antenna unit. Some of these zones are visually distinguishable in the lower part of the slope in the form of leaks and filtration passing through the body of the structure. This filtration can be traced from a depth of 0.06–0.40 m to the groundwater level.

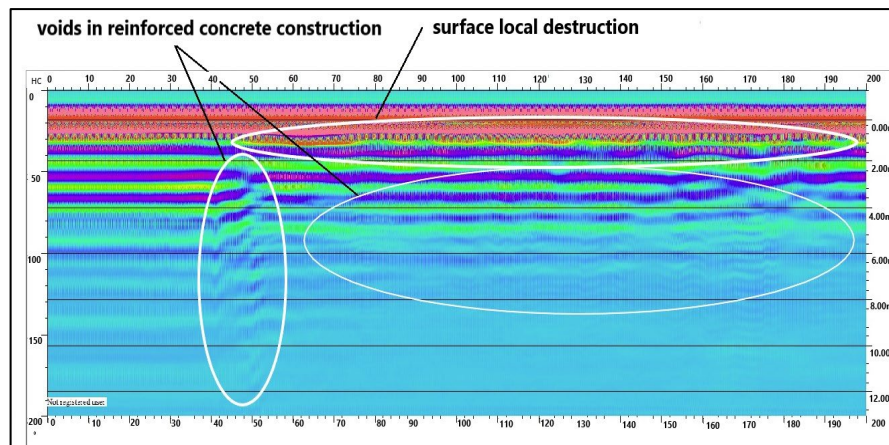


Figure 7. Image from the GPR OKO-3.

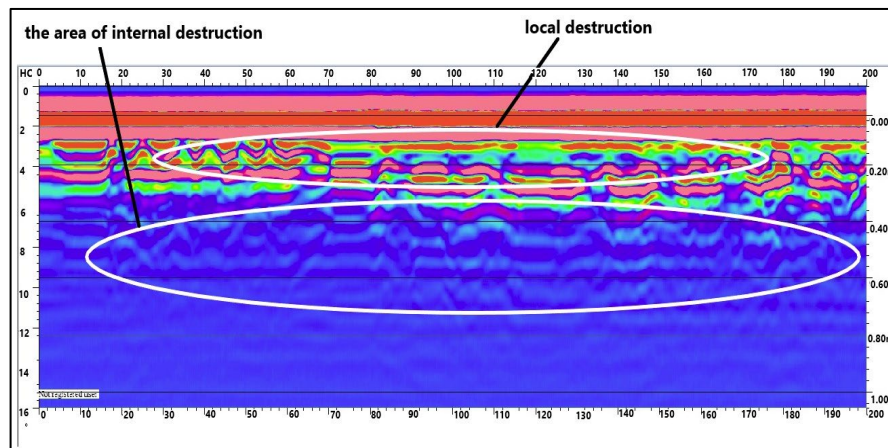


Figure 8. Image from the GPR OKO-3.

#### 4. Conclusions

Based on the results obtained, it can be concluded that:

1. Concrete and reinforced concrete structures on the territory of the SWIS, namely pumping station No. 1, have low strength, which is due to the long service life of the structures and the lack of major repairs. Tests of concrete core samples showed that the samples collapsed at a minimum load of 116...118 kN. This indicates severe wear of the concrete coating of HS, which is aggravated by the close occurrence of groundwater. Further destruction to the concrete coating is inevitable, which requires urgent repair and reinforcement of the structures.
2. The study of the concrete coating using the GPR method on the territory of the SWIS using the GPR OKO-3 with a 2-frequency antenna unit of 150+400 MHz during the diagnosis of the technical condition allowed us to identify the following. Pronounced voids of soil decompression under the concrete base of the body of the dam. Water filtration points through the body of the dam. All of them are characterized by an increase in soil moisture from 3 to 40 %, interpreted through a change in its dielectric constant, which leads to the expansion of the concrete base of a part of HS. Due to the rise of groundwater to the base of the body of the dam, the strength of individual elements of HS is subjected to greater wear, which will lead to the rapid destruction of the concrete coating.
3. The use of non-destructive testing methods, using modern equipment, allows us to carry out a survey of HS with high accuracy and to identify problem areas in time to further ensuring the safety of HS and the rational use of water resources for the development of the agricultural potential of the region.

#### References

1. Borul'ko, V.G., Ertai, A.B. Glavnoe o chrezvychainykh situatsiiakh na gidrotekhnicheskikh sooruzheniakh v tselom i v chastnosti gidromeliorativnogo kompleksa [The main thing about emergency situations at hydraulic structures in general and in particular at the hydromelioration complex]. *Gidromelioratsiia zemel' i vodnoe khoziaistvo* [Land reclamation and water management]. Moscow: RGAU-MSKHA, 2022. Pp. 285–291.
2. Altunin, V.S. *Meliorativnye kanaly v zemlianykh ruslakh* [Reclamation channels in earthen channels]. Moscow: Kolos, 1979. 255 p.
3. Balakay, G.T., Kupriyanova, S.V. Technical condition of Russia's reclamation systems and proposals for their restoration. *Ways of Increasing the Efficiency of Irrigated Agriculture*. 2020. 1(77). Pp. 5–9.
4. Kolganov, A.V., Baev, O.A., Baklanova, D.V. Results of field studies of the main canal in the republic of Kalmykia. *Environmental Engineering*. 2022. 3. Pp. 108–114. DOI: 10.26897/1997-6011-2022-3-108-114
5. Maslov, B.S., Tarasov, A.K. About the first perfect irrigation system in the steppe zone of Russia. *Melioration and Water Management*. 2013. 6. Pp. 11–14.
6. Noskewich, V.V., Gorshkov, V.Yu., Baydikov, S.V., Ugryumov, I.A. Investigation of soil dam state by set of geophysical methods. *Power Technology and Engineering*. 2019. 5. Pp. 30–37.
7. Nigmatov, G.M., Maklakov, A.S., Rotaru, A.N., Gaifullin, Z.G. Assessment of the technical condition of dams using dynamic and geophysical testing methods. *Civil Security Technology*. 2021. 18(1(67)). Pp. 46–53. DOI: 10.54234/CST.19968493.2021.18.1.67.9.46
8. Tkachyev, A.A., Olgarenko, I.V. Urgent problems of water distribution management in main canals of irrigation systems. *Scientific Journal of Russian Scientific Research Institute of Land Improvement Problems*. 2021. 11(2). Pp. 1–23. DOI: 10.31774/2222-1816-2021-11-2-1-23
9. Shchedrin, V.N., Manzhina, S.A. Osnovnye printsipy i podkhody k vosstanovleniiu meliorativnogo kompleksa Rossii [Basic principles and approaches to the restoration of the melioration complex of Russia]. *Materialy mezhdunarodnoi nauchno-*

- prakticheskoi konferentsii "Rol' melioratsii v obespechenii proizvodstvennoi bezopasnosti" [Proceedings of the international scientific and practical conference "The role of land reclamation in ensuring food security"]. Moscow: Kostiakovskie chteniia, 2022. Pp. 138–145.
10. Zhigalin, A.D., Vladov, M.L., Kapustin, V.V. Geofizicheskie tekhnologii dlia resheniia ekologicheskikh, arkhologicheskikh i inzhenernykh zadach [Geophysical technologies for solving environmental, archaeological and engineering problems]. Materialy obshcherossiiskoi nauchno-prakticheskoi konferentsii "Inzhenerno-ekologicheskii izyskaniia – normativno-pravovaia baza, sovremennye metody i oborudovanie" [Proceedings of the All-Russian scientific and practical conference "Engineering and environmental surveys – regulatory framework, modern methods and equipment"]. Moscow: Geomarketing, 2019. Pp. 83–91.
  11. Zhukov, O.Kh., Dmitriev, D.V. Primenenie georadara dlia izucheniia sostoiianiia zemlianogo polotna zheleznykh dorog [Application of ground penetrating radar to study the condition of railway roadbeds]. Railway Track and Facilities. 2011. 12. Pp. 27–29.
  12. Ryzhakov, A.N., Kuzmitchev, A.A., Martynov, D.V., Kolganov, A.V. The use of geoinformation technologies for involvement of agricultural lands located in the zone of reclamation systems influence into irrigation. Land Reclamation and Hydraulic Engineering. 2022. 12(4). Pp. 186–203. DOI: 10.31774/2712-9357-2022-12-4-186-203
  13. Shirobokov, M.P., Ivanov, A.A., Pudova, N.G. Primenenie kompleksa geofizicheskikh metodov dlia obsledovaniia sostoiianiia gidrotekhnicheskikh sooruzhenii na primere gruntovoi plotiny v sostave MGES (Kareliia) [Application of a set of geophysical methods for surveying the condition of hydraulic structures using the example of an earth dam as part of a small hydroelectric power station (Karelia)]. Sbornik trudov konferentsii "Goevraziia-2021. Geologorazvedka v sovremennykh realiiakh" [Proceedings of the conference "GeoEurasia-2021. Geological exploration in modern realities"]. Tver: PoliPRESS, 2021. Pp. 35–36.
  14. Solodovnikov, D.A., Khavanskaya, N.M., Vishnyakov, N.V., Ivantsova, E.A. Methodical basis of geophysical monitoring of ground water river floodland. South of Russia: Ecology, Development. 2017. 12(3). Pp. 106–114. DOI: 10.18470/1992-1098-2017-3-106-114
  15. Isakov, K.T., Mukanova, Zh.A., Baranchuk, K.I., Oralbekova, Zh.O., Omarkhanova, D.Zh. Characteristics and the interface of the signal database according to GPR data. Bulletin of L.N. Gumilyov Eurasian National University. Technical Sciences and Technology Series. 2019. 4(129). Pp. 91–100. DOI: 10.32523/2616-7263-2019-129-4-91-100
  16. Izumov, S.V. Vozmozhnost' ispol'zovaniia georadarov dlia inzhenerno-geologicheskikh izyskaniia pri proektirovanii i rekonstruktsii avtomobil'nykh dorog [Possibility of using ground penetrating radars for engineering and geological surveys during the design and reconstruction of highways]. Sbornik trudov konferentsii "Strategiia razvitiia geologicheskogo issledovaniia nedr: nastoiashchee i budushchee (k 100-letiiu MGRI-RGGRU)" [Proceedings of the conference "Strategy for the development of geological exploration of the subsurface: present and future (on the 100th anniversary of MGRI-RGGRU)"]. Moscow: Fil'trotkani, 2018. Pp. 119–120.
  17. Shevchenko, V.A., Izumov, S.V., Mironov, S.I., Pol'torykhin, K.S. Application of techniques of geophysics in land reclamation. Melioration and Water Management. 2017. 6. Pp. 44–46.
  18. Borodychev, V.V., Dedova, E.B., Sazanov, M.A. Water of the Republic of Kalmykia and measures to improve water complex. Doklady Rossiiskoi Akademii sel'skokhoziaistvennykh nauk [Reports of the Russian Academy of Agricultural Sciences]. 2015. 4. Pp. 41–45.
  19. Dedova, E.B., Dedov, A.A., Ivanova, V.I., Mandzhieva, T.N. Problemy vodopol'zovaniia i funktsionirovaniia vodokhoziaistvennogo kompleksa Respubliki Kalmykiia [Problems of water use and functioning of the water management complex of the Republic of Kalmykia]. Osnovnye rezul'taty nauchnykh issledovaniia instituta za 2018 god [The main results of the institute's scientific research in 2018]. Moscow: All-Russian Research Institute for Hydraulic Engineering and Land Reclamation, 2019. Pp. 64–73.
  20. Suprun, V.A. Ochistka i povtornoe ispol'zovanie drenaznykh vod risovykh orositel'nykh sistem: dissertatsiia kandidata tekhnicheskikh nauk [Treatment and reuse of drainage water from rice irrigation systems. Cand. tech. sci. diss]. Moscow, 2022. 156 p.
  21. Tokseit, D., Isakov, K., Boranbaev, S. Technique for processing signals from a source emitted by a georadar. University Proceedings. 2022. 1(86). Pp. 323–332. DOI: 10.52209/1609-1825\_2022\_1\_323
  22. Baklanova, D.V., Kolganov, A.V., Baev, O.A. Computational study of water loss from unlined canals taking into account the geological and soil features of the North of Kalmykia. Land Reclamation and Hydraulic Engineering. 2023. 13 (2). Pp. 281–298. DOI: 10.31774/2712-9357-2023-13-2-281-298
  23. Shirokova, V.A., Dedova, A.A., Shabanov, R.A., Dedova, E.B. Agroekologicheskii monitoring sostoiianiia Sarpinskoi obvodnitel'no-orositel'noi sistemy [Agroecological monitoring of the state of the Sarpinskaya irrigation system]. Materialy mezhdunarodnoi nauchno-prakticheskoi konferentsii "Tsifrovizatsiia zemlepol'zovaniia i kadastrov: tendentsii i perspektivy" [Proceedings of the international scientific and practical conference "Digitalization of land use and cadastres: trends and prospects"]. Moscow: State University of Land Use Planning, 2020. Pp. 496–500.
  24. Shiriaeva, M.A., Suprun, V.A. Issledovanie ionnogo sostava vody s Sarpinskoi orositel'no-obvodnitel'noi sistemy dlia tekhnologii povtornogo ispol'zovaniia drenazno-sbrosnogo stoka s primeneniem prirodnykh mineral'nykh sorbentov [Study of the ionic composition of water from the Sarpinskaya Irrigation and Watering System for the technology of reuse of drainage and discharge runoff using natural mineral sorbents]. Materialy mezhdunarodnoi nauchno-prakticheskoi konferentsii "Kompleksnyi podkhod k nauchno-tekhnicheskoi obespecheniiu sel'skogo khoziaistva" [Proceedings of the international scientific and practical conference "An integrated approach to scientific and technical support for agriculture"]. Ryazan: Ryazan State Agrotechnological University, 2020. Pp. 87–92.
  25. Sakhterov, V.I., Averin, A.A., Popov, A.V., Prokopovich, I.V. The investigation of pulsed GPR antennas. Vserossiiskaia otkrytaia nauchnaia konferentsiia "Sovremennye problemy distantsionnogo zondirovaniia, radiolokatsii, rasprostraneniia i difraktsii voln" [All-Russian Open Scientific Conference "Modern Problems of Remote Sensing, Radar, Wave Propagation and Diffraction"]. Murom: Murom Institute of the Vladimir State University, 2022. Pp. 485–488. DOI: 10.24412/2304-0297-2022-1-485-488

### **Information about the authors:**

**Veronika Suprun, PhD in Technical Sciences**

E-mail: [suprun-v@vfanc.ru](mailto:suprun-v@vfanc.ru)

**Ivan Kovalenko,**

ORCID: <https://orcid.org/0009-0001-3147-6613>

E-mail: [kovalenko-i@vfanc.ru](mailto:kovalenko-i@vfanc.ru)

**Viktoriya Ustinova,**

ORCID: <https://orcid.org/0000-0001-6490-7072>

E-mail: [ustinova-v@vfanc.ru](mailto:ustinova-v@vfanc.ru)

*Received: 29.11.2023. Approved after reviewing: 23.09.2024. Accepted: 24.09.2024.*



Research article

UDC 624

DOI: 10.34910/MCE.130.3



## Effects of chicken bone powder mixed with limestone and cement on the clayey soil geotechnical characteristics

A.G. Salih<sup>1</sup> ✉, A.S. Rashid<sup>1</sup>, N.B. Salih<sup>2</sup>

<sup>1</sup> School of Civil Engineering, University Teknologi Malaysia, Johor Bahru, Johor, Malaysia

<sup>2</sup> Department of Water Resources Engineering, College of Engineering, University of Sulaimani, Sulaimaniyah, Northern Iraq

✉ [asmaagheyathsalih@gmail.com](mailto:asmaagheyathsalih@gmail.com)

**Keywords:** clayey soil, soil stabilization, waste chicken bone powder, strength improvement, unconfined compressive strength

**Abstract.** Soil stabilization is aiming to enhance the geotechnical properties of soils. Traditionally, it has relied on conventional materials, such as cement and lime. However, the growing awareness of environmental sustainability has prompted researchers to explore alternatives, including waste. The employment of waste helps reduce waste deposited in landfills and decrease greenhouse gas emissions. The literature revealed that adding wastes to clay significantly improves clay's mechanical characteristics. This study has identified alternative methods of trash disposal that would be economically and environmentally beneficial. The effect of chicken bone powder with limestone and cement on clay has been investigated. Liquid limit and plasticity index have decreased, and unconfined compressive strength of samples treated with 10%CBP+5%LS and 10%CBP+5%C up to 28 days have been increased by 2.69-fold and 4.82-fold, respectively. A reduction in the soil's cohesion from 37.079 to 35.115 kPa and an increment in the internal frictional angle from 0.66° to 2.10° has been discovered for the mix of 10%CBP+5%LS. Compression and swell index reductions were observed with the addition of 10%CBP+5%LS and 10%CBP+5%C. From scanning electron microscopy, the binder materials caused the samples to indicate a dense and compact matrix and reduced the porosity.

**Citation:** Salih, A.G., Rashid, A.S., Salih, N.B. Effects of chicken bone powder mixed with limestone and cement on the clayey soil geotechnical characteristics. Magazine of Civil Engineering. 2024. 17(6). Article no. 13003. DOI: 10.34910/MCE.130.3

### 1. Introduction

Soil quality is an essential consideration in infrastructure development [1]. The geotechnical challenges associated with varying site conditions can be mitigated through adjustments in foundation design and soil stabilization techniques [2, 3]. By adapting these methods to the specific needs of a project, engineers can ensure the long-term stability and safety of buildings, roads, and foundations, contributing to sustainable infrastructure development [4, 5]. Soil stabilization techniques might be the most cost-effective way to solve the issue depending on the required particulars. Soil stabilization is the process of modifying soils physically and chemically to improve their mechanical characteristics [6]. The primary objectives of soil stabilization include increasing load-bearing capacity, reducing soil settlement, enhancing soil durability, and mitigating environmental impacts.

To enhance the shear strength of soils, numerous stabilizing methods and additives have been used for a period of time. The two main techniques used nowadays to increase shear strength are either stabilization techniques can be mechanical or chemical. Compaction or the addition of fibrous and other non-biodegradable reinforcement to the soil are two examples of mechanical stabilization. Further, chemical stabilization involves the addition of chemicals or other materials to enhance the ongoing soil.



Portland cement (C), lime (L), fly ash, bitumen, calcium chloride, cement kiln dust, steel slag, limestone (LS), enzymes, and many other natural materials are a few of the chemicals or materials used today [7–15].

The majority of frequently used soil-stabilizing substances, such as C, L, and coal fly ash, all contain variable amounts of calcium. One of the most common, widely applicable, and simple methods for improving the geotechnical characteristics of clayey soils is by using L and C stabilization [16, 17]. Calcium, the essential component required for stabilizing soil and enhancing its strength, can be provided by both L and C. The availability of calcium varies depending on the type and purity of L employed as a stabilizing agent. The chemical reaction between L and soil consists mostly of two phases. When adding L, the first phase, sometimes referred to as an immediate or short-term treatment or stabilization, starts to take place within a few hours or days. At this step, three primary chemical processes occur – cationic exchange, flocculation-agglomeration, and carbonation. It may take months or years to finish the second phase, which makes up the majority of the pozzolanic reaction. It is regarded as a long-term treatment [4, 16, 18]. While L has some benefits in lowering the plasticity index (PI) of very plastic soils [19], C has the feature of enhancing soil strength in addition to decreasing the PI. The reaction between the silica from the soil and the  $\text{Ca}(\text{OH})_2$  from the L might result in the formation of C-S-H in L-soil systems [15]. A pozzolanic reaction is the name for this process. Additionally, calcium and alumina may combine to form the cementitious compound C-A-H [20, 21]. In this context, when C hydrates, it composes C-S-H and produces  $\text{Ca}(\text{OH})_2$ , whereas the pozzolanic reaction produced known as C-S-H has been proven to be crucial for maintaining and enhancing soil's engineering qualities [19, 21, 22]. Generally, the C stabilization method demands the addition of 5 to 14 % C by the volume of the compacted mixture being stabilized [23, 24]. Bhuvaneshwari et al. [25] and Anggraini et al. [26] reported that 5 % L additive is a sufficient amount for the stabilization of dispersive soils.

Basically, conventional stabilizers like C and L have been widely used but raise concerns related to carbon emissions and resource consumption. As a result, there is a growing interest in utilizing waste materials as alternatives for soil stabilization, aligning with the principles of sustainability and circular economy.

Many studies revealed that the characteristics of soil strength, compaction, and settlement are considerably enhanced by the addition of various waste materials to parent clay. Essentially, the resulting mechanical properties depend mainly on the type of the added mineral and treatment duration [27, 28]. When bones are burned (calcinated), white, powdery ash is remaining. Calcium phosphate is the main component. Tricalcium phosphate, or  $\text{Ca}_3(\text{OH})(\text{PO}_4)_3$ , represents the hydroxyapatite form of bone ash [29, 30]. Ayininuola and Akinniyi [29] stated that bone ash is chemically inert, free of organic matter, and has very high heat transfer resistance; it also has good non-wetting features. Ayininuola and Shogunro [31] carried out laboratory investigations to study the influence of bone ash on soil shear strength and revealed that bone ash had a significant role in increasing its shear strength. The shear strength of the soil was increased by between 22.4 and 105.2 % above the strengths of the corresponding control tests when bone ash was added to soil samples. On the other hand, all samples reached their highest shear strengths at 7 % stabilization with bone ash [31, 32]. However, there is still cause for concern regarding the embodied energy used to produce bone ash. This is because, notwithstanding the benefit of minimizing the environmental pollution caused by these wastes, calcining bone ash at a temperature of between 650 and 900 °C after open-air burning has a high cost [33, 34].

To address problems related to soil instability, researchers are now creating and investigating effective uses for agricultural and environmental waste products. This study has identified alternative methods of trash disposal that would be economically beneficial and environmentally friendly. Thus, the study aims to investigate the possibility of utilizing waste chicken bone powder (CBP) – which is yet material containing calcium – as a soil stabilizer. Therefore, to improve clayey soils, the utilization of waste CBP as well as LS and C as partially eco-friendly alternatives was investigated in the current study. For samples of clayey soil, the additives were put in a variety of percentages. Then, to investigate the potential of such additives in reducing the LS and C content as well as improving the engineering properties of the clayey soil, a comparative analysis was made between the CBP-LS-treated soil mix and the CBP-C-treated soil mix.

## 2. Materials and Test Methods

### 2.1. Materials

#### 2.1.1. Soil

The clayey soil in southern parts of Sulaimaniyah City was investigated for this research. As a result of weathered portions of the parent rock and foraminifera in the soil, the deposit in this location is primarily

made up of soft dark grey, silty clay, and clayey silt. Soil samples were taken from a depth near the surface, put in plastic bags, and transferred to the laboratory. Classification tests were carried out based on the ASTM standards [35–38] to determine the priority geotechnical properties of the collected soil. The natural water content in the soil sample used in this investigation ranged from 23 to 34 %. As illustrated in Fig. 1(a), the preliminary observation of the soil revealed that it is fine-grained soil. By performing the basic tests required for soil classification, the characteristics of the soil were determined. The soil sample contains 51.17 % clay, 45.44 % silt, and 3.39 % sand, according to the results of the sieve analysis and the grain distribution curve shown in Fig. 2. Moreover, the basic properties of the soil sample are 2.67 specific gravity, 48 % liquid limit (LL), 23 % plastic limit (PL), and 25 % PI. Table 1 lists the geotechnical characteristics of the soil. The natural soil sample was classified as low plasticity clay (CL) by the Unified Soil Classification System (USCS) [39]. The compaction test was conducted to obtain the optimum moisture content (OMC) and maximum dry density (MDD) of the natural soil sample as presented in Table 1. These results were used for the preparation of remolded soil samples for the study tests. Fig. 3 present the scanning electron microscope (SEM) micrograph and its elemental spectrum of the studied soil.

### 2.1.2. Chicken bone powder

Chicken bones were collected from the waste of food. The bones were carefully washed with water multiple times, released from the meat, and then rinsed once more repeatedly to get eliminate any surface impurities. Firstly, the bones were air-dried and then put in the oven at 50–60 °C to ensure they were fully dry. Then a grinder was used to crush the dried bones into a homogeneous mixture as presented in Fig. 1(c). Accordingly, the study employed an average particle size of less than 425 µm, which was obtained using a sieve size of 425 µm (sieve No. 40).

### 2.1.3. Crushed limestone

The sample of crushed LS used in this study was obtained from the Tlazait crusher in Iraq, which is located 30 kilometers to the southeast of Sulaimaniyah city. The crushed LS was chosen as a waste material. The waste LS used was easily crushed, whitish, and had a sub-rounded particle shape. To employ the crushed rock for laboratory use, it was passed through sieve No. 40 (425 µm) as indicated in Fig. 1(b). The sample of crushed LS had a specific gravity of 2.81 according to the ASTM standard [38].

### 2.1.4. Cement

For the present study, the required amount of Bazyan Portland cement was obtained locally and used as a soil stabilizer additive. Both C and LS have a pozzolanic reaction that requires a period of time. They will create bonds among soil particles that tie them together and hence result in a strong soil structure.



Figure 1. The materials used (a) clayey soil, (b) limestone, and (c) waste chicken bone.

**Table 1. Geotechnical properties of clayey soil.**

Physical properties	Clay	Standard
Liquid limit, %	48	
Plastic limit, %	23	ASTM D 4318
Plasticity index, %	25	
Sand content, %	3.39	
Silt content, %	45.44	ASTM D 422
Clay content, %	51.17	
Passing sieve no. 200, %	96.61	
Soil classification	Lean Clay	ASTM D 2487
Optimum moisture content, %	20	ASTMD 698
Max dry density, g/cm <sup>3</sup>	1.694	
Specific gravity, $G_s$	2.67	ASTM D 854

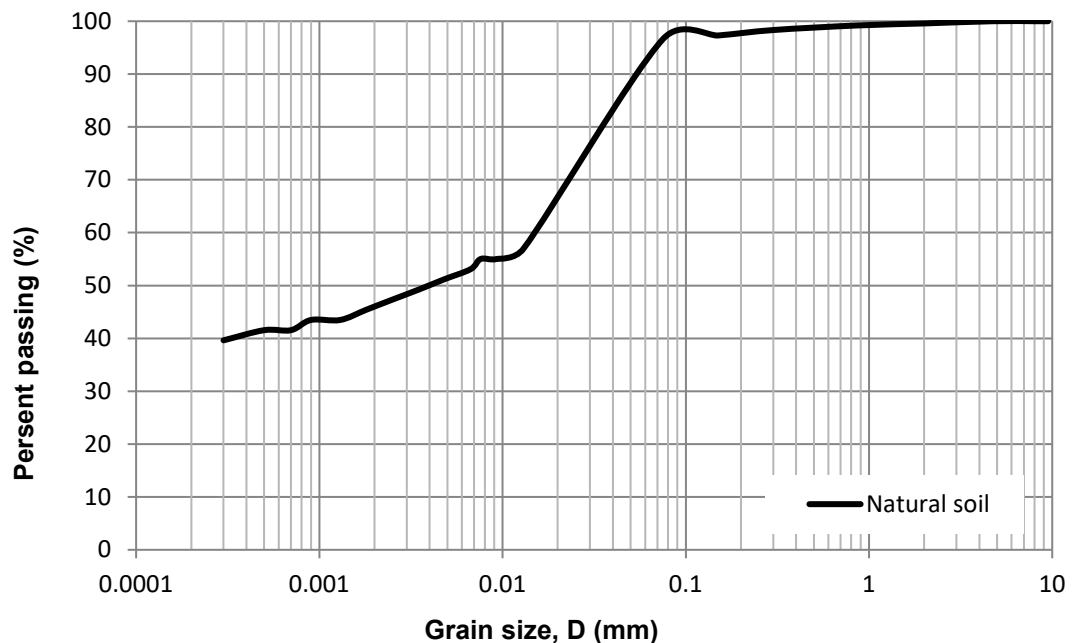
**Figure 2. Grain size distribution curve for the natural clayey soil.**

Table 2 lists the materials' chemical compositions by the weight percentage of the total chemical composition as determined by X-ray fluorescence (XRF) testing. Table 2 shows that the clay soil sample has a high content of silica ( $\text{SiO}_2 = 49.4\%$ ) and a lower content of alumina ( $\text{Al}_2\text{O}_3 = 9.25\%$ ).

On the other hand, the oxide composition of the LS showed that it consisted of majorly of calcium oxide (87.12%) with traces of magnesium oxide (0.96%), silicon oxide (0.6%), and potassium oxide (0.1%). Furthermore, C was mostly consists of calcium oxide (65.03%) and silicon oxide (18.4%), whereas CBP mostly consists of calcium oxide (53.25%), phosphorus pentoxide (37.46%), and silicon oxide (1.5%). Ojuri et al. [4] reported that cow bone powder does not contain enough calcium oxide to be considered a cementitious material.

However, Adeyemi et al. [40] have noted that when employed that cow bone powder as a partial substitute for L in the presence of water at room temperature, it produces insoluble compounds with cementitious capabilities.

**Table 2. The chemical composition obtained from (X-ray fluorescence analysis) of the natural soil and the additives for soil stabilization under study.**

Chemical compound	Minerals	Clay soil, %	Chicken bone powder, %	Limestone, %	Cement, %
Silicon dioxide	SiO <sub>2</sub>	49.4	1.5	0.6	18.4
Sulfur trioxide	SO <sub>3</sub>	0.44	1.74	0.58	
Iron (III) oxide	Fe <sub>2</sub> O <sub>3</sub>	6.37	0.26	0.15	2.537
Aluminum oxide	Al <sub>2</sub> O <sub>3</sub>	9.25	0.7	0.49	3.439
Calcium oxide	CaO	16.45	53.25	87.12	65.03
Magnesium oxide	MgO	9.003	1.77	0.96	2.748
Potassium oxide	K <sub>2</sub> O	4.28	0.48	0.1	
Chlorine	Cl	0.7		0.0013	0.013
Sodium oxide	Na <sub>2</sub> O	–	0.016	0.0031	
Phosphorus pentoxide	P <sub>2</sub> O <sub>5</sub>	0.07	37.46	0.02	
Tricalcium aluminate	C <sub>3</sub> A	–	–	–	4.83

The SEM micrograph of untreated clay is displayed in Fig. 3. The image illustrates the detection of hexagonal particles and the flaky texture of the clay, which almost disappeared after the addition of additives as presented in Fig. 10.

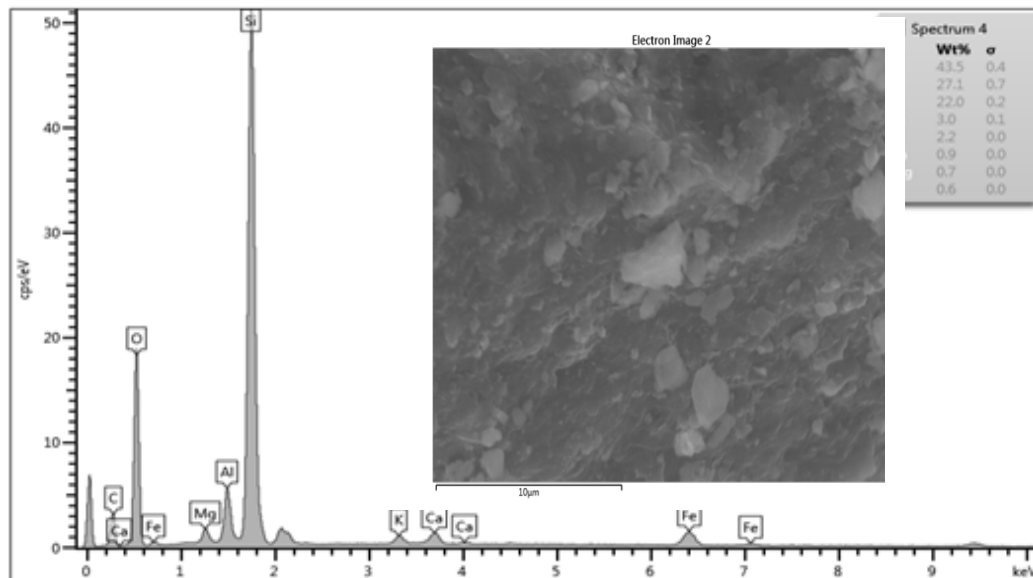


**Figure 3. SEM image of clay soil.**

## 2.2. Sample Preparation and Methods

The soil sample was put in the oven at 110 °C, then left to be dried for 24 hours. The soil sample was well mixed after being pulverized with a plastic mallet and then passed through a No. 4 sieve on a flat surface to achieve a uniform distribution. In order to investigate the geotechnical characteristics of the treated clayey soil, and look into the impact of the CBP with a separate mix of LS, or C, some of the geotechnical experiments, such as the Atterberg limit, unconfined compressive strength (UCS), direct shear, and 1-D consolidation tests were conducted. All samples were remolded using the moist tamping method with a dry density of 1.694 g/cm<sup>3</sup> (95 % of MDD), and 20 % water content (OMC). The compaction characteristics of soil samples were evaluated using the Standard Proctor test and as presented previously in Table 1. Manual mixing was used in every part, and each step was monitored carefully to ensure a uniform mixture. The samples, which had been carefully compacted in particular molds prepared for each experiment, were taken out of the molds, placed in plastic bags, and kept in safe containers at about 25 °C in the laboratory for various treatment periods.

SEM and X-ray diffraction (XRD) analysis were carried out to obtain a better understanding of the microscale's interaction mechanism of the CBP and the soil particles, in addition to the LS and C mixture. The central zone of the samples was used to collect the specimens.

According to ASTM D2166/D2166M-16 [41], the UCS tests were carried out on cylindrical samples with dimensions 38 mm in diameter and 76 mm in height for both the untreated and treated remolded soil samples. The samples were remolded and then sealed in plastic bags and cured at constant humidity and room temperature of 25 °C to allow for chemical reaction. The soil was mixed with the specified distilled water to produce the necessary water contents.

Firstly, the soil was treated with CBP of 2.5, 5, 7.5, and 10 % of the total dry weight of the soil at curing time periods of 7 days in order to evaluate the effect of time on the strength of the treated materials for UCS tests. To compare the UCS behavior of the tested samples, the stress-strain curves were plotted.

Secondly, other samples were prepared for each additive with the optimum value of the CBP, obtained from the results of UCS tests as mentioned in the previous step. Both crushed LS and C were added individually to the optimum value of CBP with the clay soil mix by utilizing the replacement method with percentages of 5 % in order to increase the soil's bearing capacity and stiffness. This dosage was selected for subsequent experiments and tests.

In a similar manner, separated mixtures of soil, 10%CBP+5%LS, 10%CBP+5%C, and 20 % of water content were prepared in order to be used for the direct shear tests. The prepared mixtures were then placed into the direct shear test squared mold of 60 × 60 × 20 mm in accordance with ASTM D3080 standard [42]. The direct shear test samples were made, sealed with a plastic bag, and allowed to cure for 28 days. To determine the shear strength parameters, shear stress-normal stress curves were developed (internal friction angle and cohesion).

The intention of the 1-D consolidation test is to determine the compressibility characteristics of the soil samples on the remolded samples of treated and untreated soil. The ASTM D2435 standard [43] provides the basis for the test. The consolidation tests were carried out over a single curing time period of 28 days. Brass oedometer rings of 50 mm in diameter and 19 mm in height were used for all consolidation tests. The additional load that was imposed was twice as much as the previous one. Thus, with a loading interval of 24 hours, the samples were loaded gradually as 2, 4, 8, and 16 kg. At 2 kg of normal stress, the unloading was accomplished. In order to plot the compression curves (void ratio versus applied vertical stress), the deformations of the samples during the test were recorded.

However, these materials and additives percentages were used and compared in order to address the strength development of materials to evaluate the best combinations of soils and stabilizing agents.

### 3. Results and Discussion

#### 3.1. The Effect of the Additives on the Consistency Limits

The results obtained from this study showed that the LL and PI decreased with the addition of binders. For the sample treated with 10%CBP+5%LS, there was a reduction in the PI values from 25 to 20.59 % due to the LL value decrease from 48.1 to 43.09 %, and the PL value decreased from 23 to 22.5 %. In addition, in the treated sample with 10%CBP+5%C, the PI value decreased from 25 to 11.07 % due to the LL value decrease from 48.1 to 39.1 %, and the PL value increased from 23 to 28.03 %.

The remarked behavior may be due to the partial replacement of the plastic soil particles with CBP and other binders that are non-plastic material with a reduction in clay content. Basically, the amount of clay in the soil controls its plasticity, which decreases as the percentage of clay fractions decreases [1, 29, 44, 45]. Further, chemical reactions between the soil and the binders may be responsible for this reduction. The significant reduction in LL for the sample treated with 10%CBP+5%C may be caused by the rapid hydration of the C that leads to a decrease in the amount of water available in the mixture to be absorbed by the other contents.

Abdalqadir et al. [46] reported in their study on clayey soil stabilization with LS that the reduction in the double-layer thickness of clay particles was the matter of this reduction in consistency limits, which was caused by the cation exchange reaction, which increases the attraction force and causes the particles to flocculate.

#### 3.2. The Effect of the Additives on the Unconfined Compressive Strength

Unconfined compressive strength values are considered the primary criterion for evaluating the enhanced strength of the treated soil [47, 48]. Fig. 4 displays the relation stress versus axial strain for treatment duration of 7 days for samples containing soil with CBP of 2.5, 5, 7.5, and 10 % mix. These curves illustrate the effect of CBP on the UCS of clay soil samples. The UCS of the untreated sample was 66.6 kPa. However, there are considerable increases in the UCS values of all CBP-clay samples. It can be seen that the UCS increased and reached its maximum resistance with the addition of CBP of up to 10 % as the UCS was 120.133 kPa, and the UCS of the clayey soil was increased by 80.29 %.

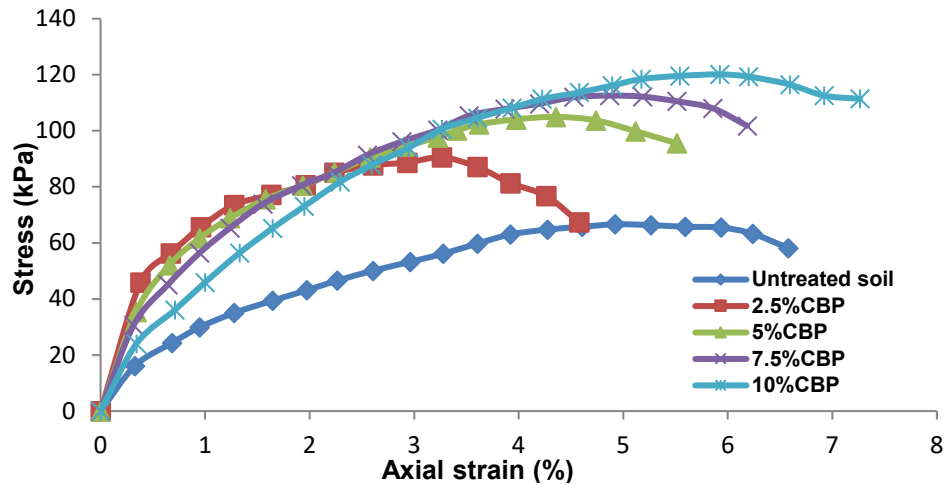


**Figure 4. UCS results for different CBP % contents.**

Furthermore, the achieved results showed that by increasing the CBP dosage, the strength increased and the failure strain increased accordingly, besides, the treated sample stiffness was decreased. The failure strain of the treated soil increased from 3.26 to 4.35, 4.86, and 5.92 % for the 2.5, 5, 7.5, and 10 % of CBP mix, respectively, showing an increase in flexibility. Overall, the treated soil samples exhibited more stiffness than the untreated soil samples. Therefore, the addition of LS or C was suggested for the soil stiffness and brittleness enhancement.

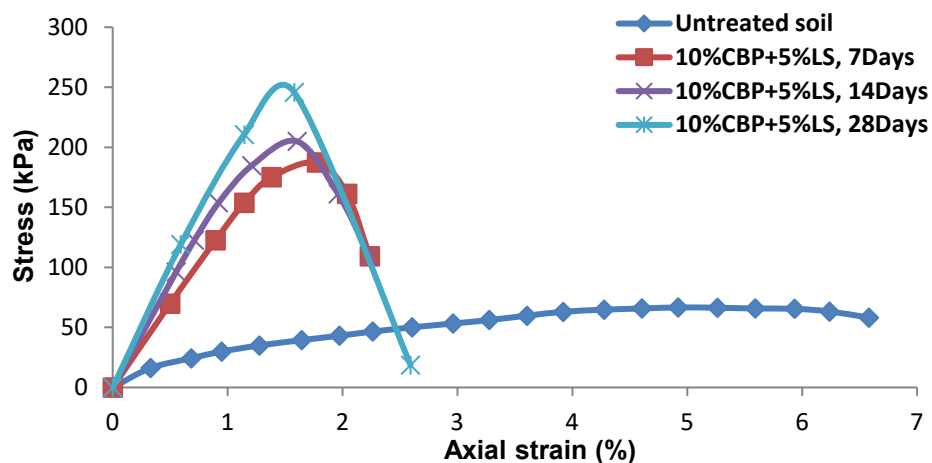


**Figure 5. UCS results of 10%CBP+5%LS contents with different curing ages.**

Fig. 5 illustrates the UCS results for samples treated with 10%CBP+5%LS contents. By comparing the result of UCS as presented in Figs. 4 and 5 for curing ages of 7, 14, and 28 days; all samples provided more strength and less ductility at failure strain compared to the untreated soil sample and the samples treated with CBP only. The failure strain decreased from 4.92 % for untreated soil to less than 2 % for treated soil showing decreased flexibility, thus, the brittleness of the treated samples with 10%CBP+5%LS further increased and subsequently resulted in non-plastic deformation.

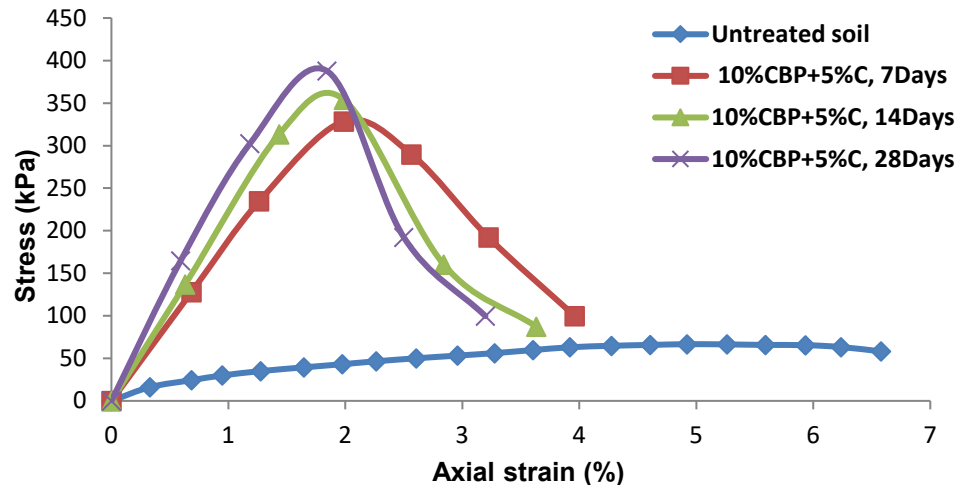


**Figure 6. UCS results of 10%CBP+5%C contents with different curing ages.**

The pozzolanic reaction property of the LS and C increases the strength of the treated soil, but as the plasticity of the soil is decreased by the addition of additives, the soil sample becomes more brittle.

Similarly, after the treatment duration of 7, 14, and 28 days, samples treated with 10%CBP+5%C represented more UCS strength but less ductility at failure strain compared to the untreated samples and samples treated with only CBP as presented in Fig. 6. The failure strain decreased from 4.92 % for untreated soil to less than 2 % for treated soil showing less flexibility and more brittleness. This behavior may come as a result of the influence of cementation reactions on the reduction of soil plasticity.

Due to the time effect, which created the environment for long-term pozzolanic reactions, the specimens' ductility decreased, therefore, extending the curing time improved the development of mechanical strength, which was caused by the completion of chemical reactions.

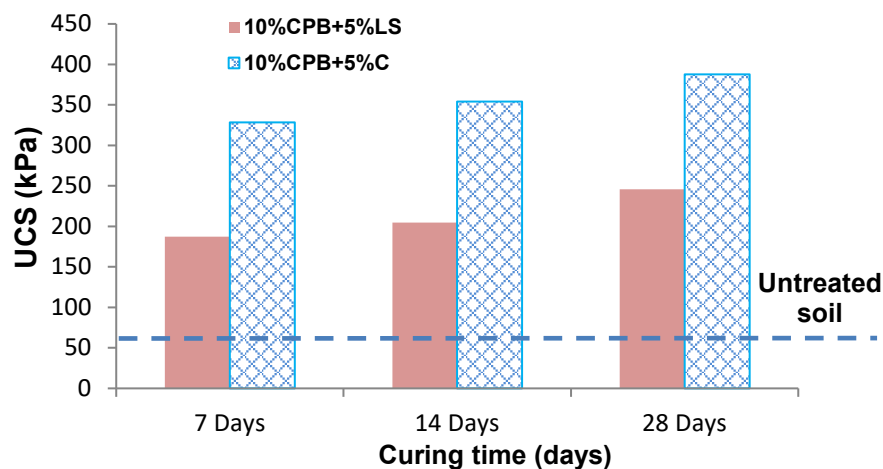


**Figure 7. Effect of additives on the UCS of clayey soil.**

Overall, for the resulting material, the UCS values of C-treated soil were higher than the LS-treated soil at all curing days as illustrated in Fig. 7. For samples treated with 10%CBP+5%LS and 10%CBP+5%C up to 28 days; the strength was increased by more than 2.69-fold and 4.82-fold, respectively, compared to the UCS of the untreated sample. Thus, using C is ideal when strength improvement is required. Two elements may be involved in Portland cement's ability to acquire increased strength. Firstly, the  $\text{Ca}(\text{OH})_2$  crystals produced as a by-product of the hydration of calcium silicates are significantly more reactive as they are pure and fine. This gives the required calcium for the ion exchange process. Secondly, with the hydration of C, a stiff network was created similar to that in mortar or concrete which mainly depends on the amount of the added C. This variation in the utilized material may be of significant employ when various properties are required from the same soil.

A study conducted by Ojuri et al. [4] concluded that the cow bone powder and L efficiently reacted to form cementitious materials that improved the soil's strength properties. The results obtained from the present study agree with the findings of Ojuri et al. [4], and Adeyemi et al. [40].

### 3.3. The Effect of the Addition on Shear Strength Parameters

Fig. 8 shows the effect of different additives on clay soil results from the direct shear test. Cohesion and angle of internal friction are each determined by the y-intercept and line gradient, respectively. With the addition of CBP and LS or C, the strength of soil samples increased. This strength increase was due to water content reduction in the treated samples. While the pH-raising additives create an ideal environment for the stabilizing process, so the soil density tends to increase upon stabilization. Based on Table 3, the samples treated with the CBP-C content reached the highest shear strength with the cohesion of 48.143 kPa in comparison with the strength of samples treated with CBP-LS or untreated clayey soil strength. As well known, soil plasticity is a factor that controls the corresponding cohesion of the samples. It was presented earlier that the addition of 10%CBP+5%LS and 10%CBP+5%C reduced the PI of the mixture by 17.64 and 55.72 %, respectively. Therefore, with the addition of CBP-C content, there is a noticeable increase in cohesion, and further, the angles of internal friction increased up to 1.54°.

In contrast, the addition of 10%CBP+5%LS reduced the cohesion to 35.115 kPa, while the internal friction increased to 2.1°. Results indicated that the LS content had a greater influence on the friction angle than the cohesion and that relatively controlled by the surface friction of the particles, which has a great impact on the structure and stability of the sample. It is evident that because of the relatively significant amount of coarser particles in samples that had appeared, the larger particles in the samples were broken and filled with pores during the shearing test process, which makes the adhesion between particles lesser, and further decreases the soil's cohesion. Thus, the friction force on the particle surface is increased and soil cohesiveness is decreased as a result of the particles' evident edge angle.

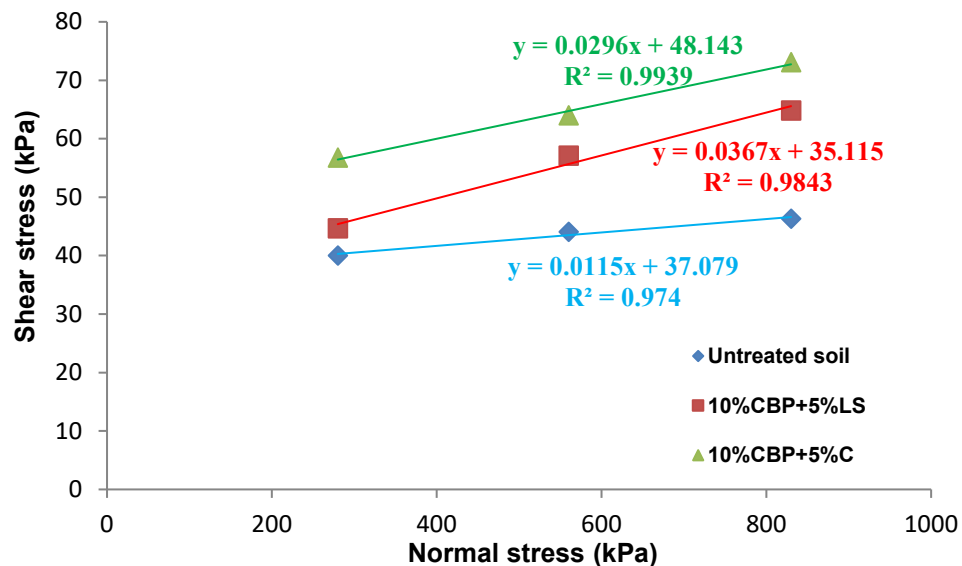


Figure 8. Strength envelope lines of untreated and treated soil.

Table 3. Cohesion and angle of internal friction for samples with different material additives.

Sample description	Untreated sample	Soil+10%CBP+5%LS	Soil+10%CBP+5%C
Cohesion (kPa)	37.079	35.115	48.143
Angle of shear resistance (°)	0.66	2.10	1.54

These results showed a good agreement with results obtained by Ojuri et al. [4]; the 10%L addition improved the internal friction while reducing the soil cohesiveness. Moreover, 6% L + 7 % cow bone powder + 1 % plastic waste stabilized low plasticity soil showed a similar pattern thus, with the addition of additive materials, the soil cohesiveness decreased, while the angle of internal friction increased [4].

### 3.4. The Effect of the Addition on Compressibility Characteristics

As seen in Fig. 9, the coefficients of consolidation ( $C_c$ ) and the expansion index ( $C_r$ ) decreased with the addition of the stabilizing binder 10%CBP+5%LS and 10%CBP+5%C. With the addition of 10%CBP+5%LS, the values of  $C_c$  and  $C_r$  decreased by 71.07 and 1.84 %, respectively. Likewise, the value of  $C_c$  and  $C_r$  decreased by 74.21 and 54.6 %, respectively for samples treated using 10%CBP+5%C. The reduction in  $C_c$  and  $C_r$  comes as a result of the influence of the stabilizing additives on reducing the void ratio among the clay soil particles in the treated samples, as well as the stiffness increase contributed to this reduction. From all curves, it can be observed that clayey soil with CBP achieved the lowest  $C_c$  and  $C_r$ .



with the addition of C compared to LS. Therefore, the addition of 10%CBP+5%LS and 10%CBP+5%C to the clayey soil will reduce its settlement potential. These results agree with the findings of Ojuri et al. [4].

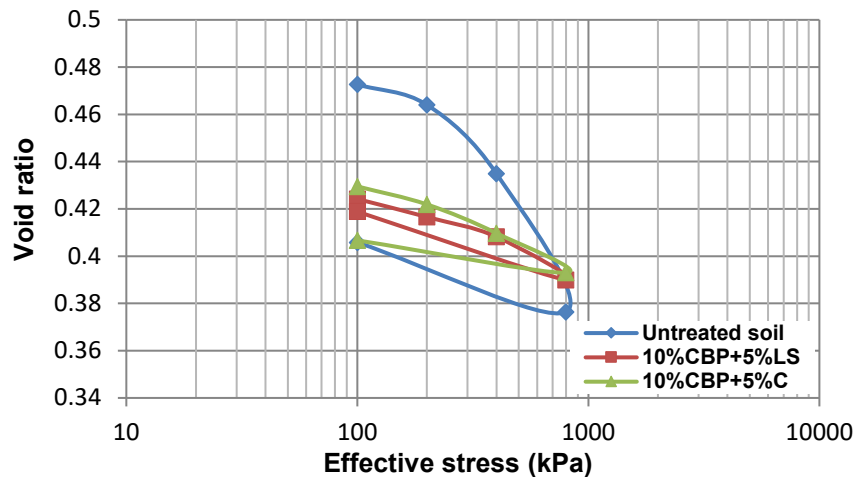


**Figure 9: Void ratio versus effective stress curves from the consolidation test on untreated and treated soil with 10%CBP+5%LS and 10%CBP+5%C.**

### 3.5. Microstructural Mechanisms of the Additives Mix on the Microstructure

As seen in Fig. 10(a), untreated clayey soil has large voids between the soil particles to appear as dark patches. The microstructural analysis utilizing SEM indicated denser materials for the treated samples which resulted in decreasing the voids between the soil particles as shown in Fig. 10(b), (c), and (d). The particles of these denser materials have closer contact and stronger bonding due to the addition of 10 % of CBP as the soil stabilizer as clarified in Fig. 10(b). Thus, increasing the soil density will enhance the compressive strength of the treated clayey soil as presented in images (c) and (d) for samples treated with 10%CBP+5%LS and 10%CBP+5%C, respectively.

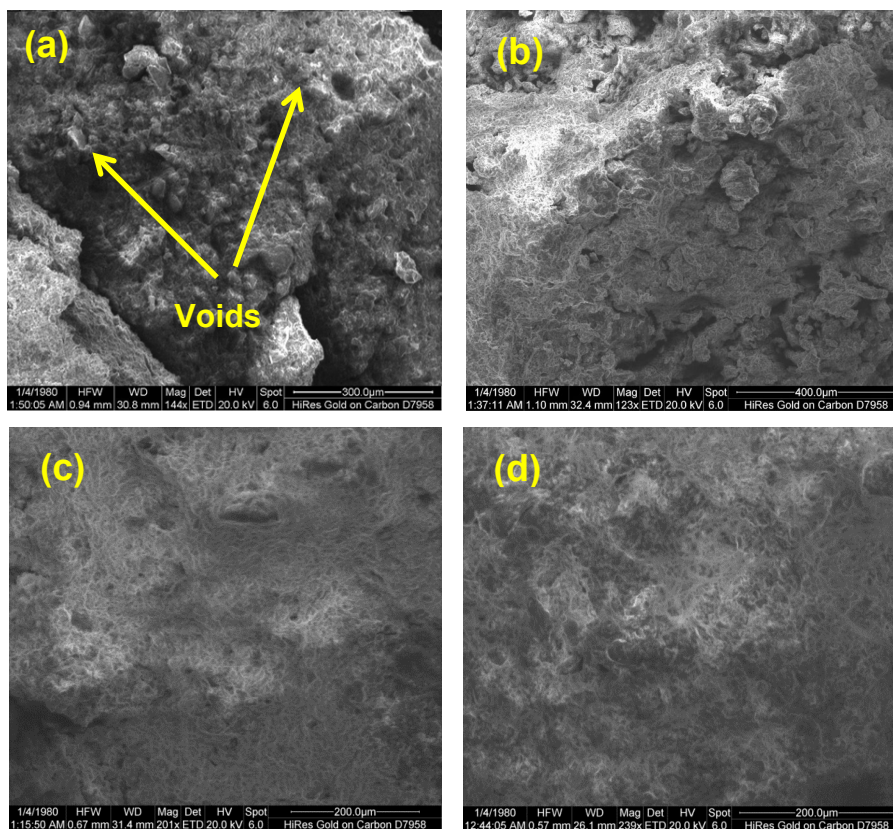


**Figure 10. SEM images of (a) untreated soil, (b) sample treated with 10%CBP after 7 days, (c) sample treated with 10%CBP+5%LS after 28 days, and (d) sample treated with 10%CBP+5%C after 28 days.**

The effect of LS and C relies mainly on their chemical reaction with soil components when there is water present, as well as the quantity of stabilizer agent, which is used. In this regard, the SEM analysis was employed to observe the structural changes and to better understand the interactions between the soil and additives.

It is noteworthy that the primary aspect affecting the void ratio of the texture is the shape of the particles. Among the analysis of particle matter, it is found that the arrangement of texture particles in the treated sample in image (d) is relatively dense, and multiple paths for cemented bonds (C-SH gel) are formed between particles in different forms of contact. In the texture particle system, numerous of these cemented bonds crisscross one another to create a network that is adequate to resist both the weight of the particle system and external loads. The production of C-S-H has a significant effect on the mechanical properties of the sample which is reflected in the strength development of the soil sample. Fewer voids remain as a result of the particle's range in angularity, which lowers the void ratio.

In general, as calcium-based stabilizers, L, and C are usually utilized to strengthen the soil during the hydration and pozzolanic processes [49].

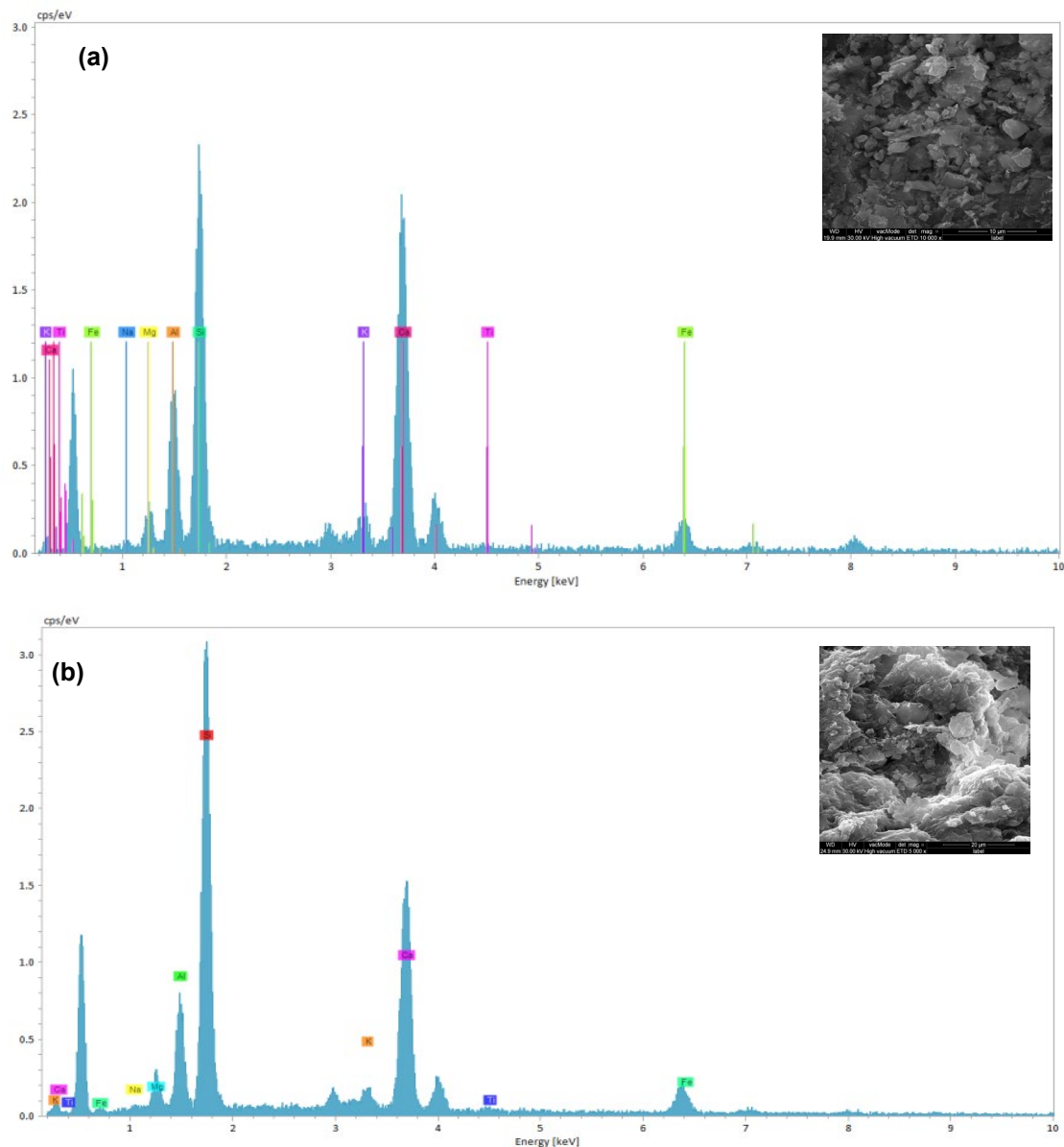


**Figure 11. SEM micrograph and its elemental spectrum of a selected particle obtained by EDS analysis of sample: (a) 10%CBP+5%LS and (b) 10%CBP+5%C.**

According to Fig. 11, this study found that the development of new hardened cementitious compounds has a principal effect that enhanced the UCS and shear strength characteristics of CBP-LS-treated soil and CBP-C-treated soil. The outcomes of the microstructural test revealed that the growth and deposition of cementing compounds caused morphological changes at the edges of soil particles. The soil texture changes when the soil particles get closer to one another. The clayey soil is mainly composed of

silica ( $\text{SiO}_2$ ) and alumina ( $\text{Al}_2\text{O}_3$ ), while LS and C are mostly composed of calcium ions. The most important chemical composition values belong to calcium in LS and C; silicon and aluminum in the soil are presented in Table 2. The addition of LS or C ( $\text{Ca}^{+2}$ ) strengthens the bond between the soil particles. The soil mineralogy, LS content, and short-term reactions are the factors affecting LS-treated soil. On the other hand, C reactions are time-dependent and take a long time to complete since these reactions depend on temperature, the amount of calcium present, the pH level, and the proportion of silica in the soil minerals [50]. Substantially, SEM images revealed that the pozzolanic reaction coated the soil particles and created a closed matrix, which made the voids less evident and reduced the consolidation coefficient as well as the expansion index.

#### 4. Conclusions

This research investigated the effect of CBP with the addition of LS and C individually to a clay matrix. The conclusions obtained throughout the investigations for this research can be listed as follows:

1. The study yielded in LL and PI values to be decreased with the addition of additives.
2. The results from UCS (which were considered the primary indicator to evaluate the effectiveness of CBP as a stabilizer) revealed that the 10%CBP mix produced the best improvement for the soil strength.
3. According to results obtained from UCS for samples treated with 10%CBP+5%LS and 10%CBP+5%C up to 28 days; the strength was increased by more than 2.69-fold and 4.82-fold respectively compared to the UCS of the untreated sample.
4. Generally, the rate of UCS development of the clayey soil samples stabilized with CBP and C or LS is enhanced as the curing duration is increased.
5. The direct shear components were notably achieved. The soil cohesion was reduced from 37.079 to 35.115 kPa, but the angle internal frictional was increased from  $0.66^\circ$  to  $2.10^\circ$  for the mix 10%CBP+5% of LS. While, for the mix 10%CBP + 5 % of C, the soil cohesiveness and the internal frictional angle were increased from 37.079 to 48.143 kPa, and from  $0.66^\circ$  to  $1.54^\circ$  respectively.
6. Reduction in both the compression index  $C_c$  and swell index  $C_s$  were observed with the addition of 10%CBP+5%LS and 10% CBP+5%C content.
7. Portland cement modification with CBP exhibited higher UCS and shear strength values than limestone modification for all samples when mixed with clayey soil and CBP for all curing ages.
8. According to the SEM analysis, the addition of the binder materials caused the stabilized samples to indicate a dense and compact matrix as well as reduced the soil porosity which resulted in increasing the mechanical strength.

#### References

1. Salih, A.G. Review on granitic residual soils' geotechnical properties. *Electronic Journal of Geotechnical Engineering*. 2012. 176. Pp. 2645–2658.
2. Karkush, M.O., Yassin, S. Improvement of Geotechnical Properties of Cohesive Soil Using Crushed Concrete. *Civil Engineering Journal*. 2019. 5(10). 2110–2119. DOI: 10.28991/cej-2019-03091397
3. Karkush, M.O., Yassin, S.A. Using Sustainable Material in Improvement the Geotechnical Properties of Soft Clayey Soil. *Journal of Engineering Science and Technology*. 2020. 15(4). Pp. 2208–2222.
4. Ojuri, O.O., Osagie, P., Oluayemi-Ayibowu, B.D., Fadugba, O.G., Tanimola, M.O., Chauhan, V.B., Jayejeje, O.O. Eco-friendly stabilization of highway lateritic soil with cow bone powder admixed lime and plastic granules reinforcement. *Cleaner Waste Systems*. 2022. 2. Article no. 100012. DOI: 10.1016/j.clwas.2022.100012
5. Salih, A.G., Rashid, A.S.A., Salih, N.B. Finite Element Analysis of the Load-Settlement Behavior of Large-Scale Shallow Foundations on Fine-Grained Soil Utilizing Plaxis 3D. *Current Trends in Geotechnical Engineering and Construction*. ICGECI 2022. Springer. Singapore, 2023. DOI: 10.1007/978-981-19-7358-1\_22
6. Rashid, A.S.A., Latifi, N., Meehan, C.L. Sustainable Improvement of Tropical Residual Soil Using an Environmentally Friendly Additive. *Geotechnical and Geological Engineering*. 2017. 35. Pp. 2613–2623. DOI: 10.1007/s10706-017-0265-1
7. Fattah, M.Y., Nareeman, B.J., Salman, F.A. A Treatment of Expansive Soil Using Different Additives. *Acta Montanistica Slovaca*. 2010. 15(4). 290–297.
8. Baloochi, H., Aponte, D., Barra, M. Soil Stabilization Using Waste Paper Fly Ash: Precautions for Its Correct Use. *Applied Sciences*. 2020. 10(23). Article no. 8750. DOI: 10.3390/app10238750
9. Abdalqadir, Z.K., Salih, N.B. An Experimental Study on Stabilization of Expansive Soil Using Steel Slag and Crushed Limestone. *Sulaimani Journal for Engineering Sciences*. 2020. 7(1). Pp. 37–48. DOI: 10.17656/sjes.10120
10. Salih, N.B., Abdalla, T.A. Characterization of the Geotechnical Properties of CL Soil Improved by Limestone. *Arabian Journal of Geosciences*. 2022. 15. Article no. 604. DOI: 10.1007/s12517-022-09871-0
11. Salih, N.B., Abdalla, T.A. Stabilization of Low Plasticity Clay Soil Utilizing Crushed Limestone. *Jordan Journal of Civil Engineering*. 2022. 16(2). Pp. 219–228.

12. Karkush, M.O., Ali, H.A., Ahmed, B.A. Improvement of Unconfined Compressive Strength of Soft Clay by Grouting Gel and Silica Fume. Springer Series in Geomechanics and Geoengineering. 1. Proceedings of China-Europe Conference on Geotechnical Engineering. Springer. Cham, 2018. Pp. 546–550. DOI: 10.1007/978-3-319-97112-4\_122
13. Karkush, M.O., Almurshedi, A.D., Karim, H.H. Investigation of the Impacts of Nanomaterials on the Micromechanical Properties of Gypseous Soils. *Arabian Journal for Science and Engineering*. 2023. 48. Pp. 665–675. DOI: 10.1007/s13369-022-07058-z
14. Karkush, M.O., Al-Murshedi, A.D., Karim, H.H. Investigation of the Impacts of Nano-clay on the Collapse Potential and Geotechnical Properties of Gypseous Soils. *Jordan Journal of Civil Engineering*. 2020. 14(4). Pp. 537–547.
15. Salih, A.G., Rashid, A.S.A., Salih, N.B. Evaluation the Effects of Waste Glass Powder Mixed with Hydrated Lime on the Unconfined Compressive Strength of Clayey Soil. *E3S Web Conferences*. 2023. 427. Article no. 01022. DOI: 10.1051/e3sconf/202342701022
16. Tan, E.H., Zahran, E.M., Tan, S.J. A review of chemical stabilisation in road construction. *IOP Conference Series Materials Science and Engineering*. 2020. 943. 2<sup>nd</sup> International Conference on Materials Technology and Energy. Article no. 012005. DOI: 10.1088/1757-899X/943/1/012005
17. Zhang, R., Long, M., Zheng, J. Comparison of Environmental Impacts of Two Alternative Stabilization Techniques on Expansive Soil Slopes. *Advances in Civil Engineering*. 2019. 1. Article no. 9454929. DOI: 10.1155/2019/9454929
18. Deboch, F.M. Recent Literatures Review on Stabilization of Lateritic Soil. *International Journal of Scientific Research Engineering & Technology*. 2018. 7(11). Pp. 765–774.
19. Firoozi, A.A., Guney Olgun, C., Firoozi, A.A., Baghini, M.S.H. Fundamentals of soil stabilization. *International Journal of Geo-Engineering*. 2017. 8. Article no. 26. DOI: 10.1186/s40703-017-0064-9
20. Little, D.N. *Handbook for Stabilization of Pavement Subgrades and Base Courses with Lime*. Kendal/Hunt Publishing Company, 1995. 219 p.
21. Bhattacharja, S.A., Bhatta, J.I., Todres, H.A. Stabilization of Clay Soils by Portland Cement or Lime— A Critical Review of Literature. *PCA R&D Serial*. 2003. 60(1). Pp. 124–133.
22. Pan, Y., Rossabi, J., Pan, C.H., Xie, X. Stabilization/solidification characteristics of organic clay contaminated by lead when using cement. *Journal of Hazardous Materials*. 2019. 362. Pp. 132–139. DOI: 10.1016/j.jhazmat.2018.09.010
23. Adetayo, O.A., Amu, O.O., Ilori, A.O. Cement Stabilized Structural Foundation Lateritic Soil with Bone Ash Powder as Additive. *AZOJETE*. 2019. 15(2). Pp. 479–487.
24. Al-Gharbawi, A.S.A., Najemalden, A.M., Fattah, M.Y. Expansive Soil Stabilization with Lime, Cement, and Silica Fume. *Applied Sciences*. 2023. 13(1). Article no. 436. DOI: 10.3390/app13010436
25. Bhuvaneshwari, S., Soundra, B., Robinson, R.G., Gandhi, S.R. Stabilization and microstructural modification of dispersive clayey soils. *Proceedings of the First Sri Lankan Geotechnical Society (SLGS) International Conference on Soil and Rock Engineering*. Colombo, 2007. Pp. 1–7.
26. Anggraini, V., Huat, B.B.K., Asadi, A., Nahazanan, H. Effect of coir fiber and lime on geotechnical properties of marine clay soil. *7th International Congress on Environmental Geotechnics*. Melbourne, 2014. Pp. 1430–1437.
27. Khitab, A., Riaz, M.S., Jalil, A., Khan, R.B.N., Anwar, W., Khan, R.A., Arshad, M.T., Kirgiz, M.S., Tariq, Z., Tayyab, S. Manufacturing of Clayey Bricks by Synergistic Use of Waste Brick and Ceramic Powders as Partial Replacement of Clay. *Sustainability*. 2021. 13(18). Article no. 10214. DOI: 10.3390/su131810214
28. Bih, N.L., Mahamat, A.A., Chinweze, C., Ayeni, O., Bidossèssi, H.J., Onwualu, P.A., Boakye, E.E. The Effect of Bone Ash on the Physicochemical and Mechanical Properties of Clay Ceramic Bricks. *Buildings*. 2022. 12(3). Article no. 336. DOI: 10.3390/buildings12030336
29. Ayininuola, G.M., Akinniyi, B.D. Bone Ash Influence on Soil Consolidation. *Malaysian Journal of Civil Engineering*. 2016; 28(3). Pp. 407-422. DOI: 10.11113/mjce.v28.15984
30. Ifka, T.M., Palou, M.T., Bazelova, Z. Influence of CaO and P<sub>2</sub>O<sub>5</sub> of bone ash upon the reactivity and the burnability of cement raw mixtures. 2012. *Ceramics – Silikáty*. 56(1). Pp. 76–84.
31. Ayininuola, G.M., Sogunro, A.O. Bone Ash Impact on Soil Shear Strength. *International Journal of Environmental, Earth Science and Engineering*. 2013. 7(11). Pp. 793–797.
32. Iorliam, A.Y., Obam, S.O., Owinizi, S.A. Improvement of black cotton soil with cattle bone powder. *American Journal of Scientific and Industrial Research*. 2012. 3(3). Pp. 175–180. DOI: 10.5251/ajsir.2012.3.3.175.180
33. Emeka, E. Stabilization of laterites with industrial wastes: a recent and comprehensive review. *International Journal of Advancements in Research & Technology*. 2015. 4(11). Pp. 69–87.
34. Obianyo, I.I., Mahamat, A.A., Nneka, E., Stanislas, T.T., Geng, Y., Chibuzor, K., Odusanya, S., Onwualu, A.P., Soboyejo, A.B. Performance of lateritic soil stabilized with combination of bone and palm bunch ash for sustainable building applications. *Cogent Engineering*. 2021. 1(8). Pp. 1921673. DOI: 10.1080/23311916.2021.1921673
35. American Society for Testing and Materials (ASTM). *Standard Test Methods for Liquid Limit, Plastic Limit, and Plasticity Index of Soils*. ASTM International. West Conshohocken, 2005.
36. American Society for Testing and Materials (ASTM). *Standard Test Method for Particle Size Analysis of Soils*. ASTM International. West Conshohocken, 2007.
37. American Society for Testing and Materials (ASTM). *Standard Test Methods for Laboratory Compaction Characteristics of Soil Using Standard Effort*. ASTM International. West Conshohocken, 2014.
38. American Society for Testing and Materials (ASTM). *Standard Test Method for Specific Gravity of Soil Solids by Water Pycnometer*. ASTM International. West Conshohocken, 2014.
39. American Society for Testing and Materials (ASTM). *Standard Practice for Classification of Soils for Engineering Purposes (Unified Soil Classification System)*. ASTM International. West Conshohocken, 2011.
40. Adeyemi A, Williams K, Rotimi S, Dolapo Y, Chewe K. Utilization of pulverised cow bone (PCB) for stabilizing lateritic soil. *African Journal of Science, Technology, Innovation and Development*. 2017. 9(4). Pp. 411–416. DOI: 10.1080/20421338.2017.1340395
41. ASTM, D2166-13/D2166M-16. *Standard Test Method for Unconfined Compressive Strength of Cohesive Soil*. ASTM International. West Conshohocken, 2016.
42. ASTM D3080. *Standard Test Method for Direct Shear Test of Soils under Consolidated Drained Conditions*. ASTM International. West Conshohocken, 2011.

43. ASTM D2435. Standard test methods for one-dimensional consolidation properties of soils using incremental loading. ASTM D2435. ASTM International. West Conshohocken, 2011.
44. Arora, K.R. Soil Mechanics and Foundation Engineering. Standard. Publishers Distributors. Delhi, 2008. 118 p.
45. Salih, A.G., Ismael, A.M. Influence of clay contents on drained shear strength parameters of residual soil for slope stability evaluation. International Journal of GEOMATE. 2019. 17(59). Pp. 166–172. DOI: 10.21660/2019.59.38987
46. Abdalqadir, Z.K., Salih, N.B., Salih, S.J.H. Using Steel Slag for Stabilizing Clayey Soil in Sulaimani City-Iraq. Journal of Engineering. 2020; 7 (26), 145–157. DOI: 10.31026/j.eng.2020.07.10
47. Spagnoli, G., Seidl, W., Romero, E., Arroyo, M., Gómez, R., López, J. Unconfined compressive strength of sand-fines mixtures treated with chemical grouts. Geotechnical Aspects of Underground Construction in Soft Ground. 1<sup>st</sup> ed. CRC Press, 2021. Pp. 829–835. DOI: 10.1201/9780429321559-109
48. Federal Highway Administration. Chemical Grouts for Soils. Report no. FHWA-RD-77-51, Washington, 1977.
49. Tamassoki, S., Daud, N.N.N., Jakarni, F.M., Kusun, F.M., Rashid, A.S.A., Roshan, M.J. Compressive and Shear Strengths of Coir Fibre Reinforced Activated Carbon Stabilised Lateritic Soil. Sustainability. 2022. 14(15). Article no. 9100. DOI: 10.3390/su14159100
50. Jawad, I.T., Taha, M.R., Majeed, H.Z., Khan, T.A. Soil stabilization using lime: Advantages, disadvantages and proposing a potential alternative. Research Journal of Applied Sciences, Engineering and Technology. 2014. 8(4), Pp. 510–520.

**Information about the authors:**

**Asmaa Salih,**

E-mail: [asmaagheyathsalih@gmail.com](mailto:asmaagheyathsalih@gmail.com)

**Ahmad Safuan A. Rashid,**

E-mail: [ahmadsafuan@utm.my](mailto:ahmadsafuan@utm.my)

**Nihad Bahaaldeen Salih,**

E-mail: [nihad.salih@univsul.edu.iq](mailto:nihad.salih@univsul.edu.iq)

*Received 15.02.2023. Approved after reviewing 08.02.2024. Accepted 10.09.2024.*



Research article

UDC 69

DOI: 10.34910/MCE.130.4



## Bending of multilayer beam slabs lying on an elastic half-space

M.M. Mirsaidov <sup>1</sup> , N.I. Vatin <sup>2</sup>  , K. Mamasoliev <sup>3</sup> 

<sup>1</sup> Tashkent Institute of Irrigation and Agricultural Mechanization Engineers, Tashkent, Uzbekistan

<sup>2</sup> Peter the Great St. Petersburg Polytechnic University, St. Petersburg, Russian Federation

<sup>3</sup> Samarkand State Institute of Architecture and Civil Engineering, Samarkand, Uzbekistan

 [vatin@mail.ru](mailto:vatin@mail.ru)

**Keywords:** multilayer beam slab, interaction, half-space, shear stress, filler, rigidity, discreteness, contact conditions, regularity

**Abstract.** Mathematical models and analytical methods for solving contact problems of multilayer beam slabs lying on an elastic base are developed, considering the reactive normal and shear pressures of the base. In this case, an elastic filler is inserted between each pair of beam slabs. The rigidity of the filler placed between the slabs can differ in each layer. Each slab beam is subject to external loads and pressure of the filler. The stiffness coefficients of beam slabs are discrete and variable. The lower beam slab, which has a two-way connection with the elastic base, is under the influence (except for external loads) of reactive normal and shear pressure of the base. The mathematical model of the problem includes closed systems of integro-differential equations with corresponding boundary conditions. To solve the problem, an analytical method based on the approximation of Chebyshev orthogonal polynomials was used. The solution to the problem is reduced to the study of infinite systems of algebraic equations. The regularity of the resulting infinite system of equations is proven. To solve it, the reduction method was used. A test example is considered and a numerical solution to algebraic equations is obtained. The internal force factors arising in the beam slab are also investigated. Based on the analysis of numerical results, some new results were identified, i.e., a significant influence of the filler and the reactive pressure of the base on the internal force factors of the beam slab, etc.

**Funding:** This research was funded by the Ministry of Science and Higher Education of the Russian Federation within the framework of the state assignment No. 075-03-2022-010 dated 14 January 2022 and No. 075-01568-23-04 dated 28 March 2023 (Additional agreement 075-03-2022-010/10 dated 09 November 2022, Additional agreement 075-03-2023-004/4 dated 22 May 2023), FSEG-2022-0010.

**Citation:** Mirsaidov, M.M., Vatin, N.I., Mamasoliev, K. Bending of multilayer beam slabs lying on an elastic half-space. Magazine of Civil Engineering. 2024. 17(6). Article no. 13004. DOI: 10.34910/MCE.130.4

### 1. Introduction

Numerous scientific studies are devoted to the influence of contacting structural elements. Various physical models describe these relationships. Recently, the number of scientific articles in this sphere has increased dramatically; various aspects of modeling and analysis of contacting elements by mechanical parameters are presented in these articles.

Plate Behavior under Various Conditions were studied in [1–3]. The article [1] presents an effective theoretical solution for studying the time-dependent characteristics of elastic plates on layered soil. The study compares numerical results with the finite element method (FEM). It investigates the influence of load

shape, plate rigidity, material anisotropy, and soft soil layers on the plate-soil system's dynamic behavior. The findings emphasize the significant impact of shallow weak layers and the increasing flexibility of the plate with decreasing burial depth.

Research in [2] proposes a strain recovery method based on surface strain measurements for analyzing large deflections in thin-plate structures. The authors develop an algorithm for strain field reconstruction and create an experimental platform to control strain under different loading conditions. Comparisons between theoretical and experimental data yield valuable insights into surface strain behavior under various loads.

A comparative study in [3] explores the nonlinear vibrations of plates fabricated from polymeric materials. The research derives governing equations for plates made of polymers and polymer composites, considering first-order shear deformations. Verification results are presented to validate the approach's accuracy.

Plate Design and Optimization were studied in [4, 5]. In [4], it introduces a novel Moving Morphable Component (MMC)-based approach for the topological design of rigid plate structures. This approach utilizes stiffeners as optimization building blocks. The research demonstrates the efficiency and effectiveness of the proposed method through numerical examples. Notably, a three-dimensional model for rigid bodies is presented, contrasting with traditional approaches. The study in [5] combines experimental and numerical analysis to assess the ultimate strength and fracture behavior of reinforced plates under combined biaxial compression and lateral loads. The results reveal that lateral pressure significantly enhances the ultimate bearing capacity.

Foundation Modeling and Analysis were done in [6–8]. In [6] and [7], the problem of determining the internal stresses of multilayer slabs was considered. In these studies, the slabs of buildings and structures foundations are considered beam slabs, and the effect of the beam on the internal tension forces in beam slabs is evaluated.

Building upon uniaxial load testing of orthotropic plates, [8] proposes an interaction function based on axial loads and shear forces. The research establishes interaction formulas for bending and failure under combined loading scenarios. The proposed formulas demonstrate excellent agreement with test results for bending interaction curves and fracture envelopes.

Dynamic Modeling and Optimization were proposed in [9, 10]. The research [9] presents a dynamic modeling approach for multi-plate structures connected by nonlinear hinges. The method utilizes Chebyshev polynomials to create dynamic models for each plate. The Rayleigh–Ritz method is then employed to derive the characteristic equation for determining the eigenfrequencies of multi-plate structures. In [10], the research focuses on optimizing the placement of longitudinal stiffeners in steel plates under pure bending. The obtained results are validated against established findings to ensure accuracy.

Simplified Models and Contact Mechanics were studied in [11, 12]. The study [11] explores one-dimensional linearly elastic models for composite layered beams. The results are compared with a two-dimensional finite element model under plane stress conditions. The findings demonstrate good agreement between the simplified multilayer sandwich model and experimental data. A mathematical model was constructed in [12] for the contact interaction between two plates with distinct elastic moduli. This model accounts for physical and structural nonlinearities. The method of variational iteration is employed to solve the governing partial differential equations, leading to a set of ordinary differential equations.

References [13, 14] provide comprehensive reviews on the development of mathematical models, methods for elastic analysis of non-homogeneous rigid bodies, and models for elastic and viscoelastic foundations in oscillating systems.

A broader range of studies, encompassing references [15–31], delve into the behavior of non-homogeneous elastic and viscoelastic systems, particularly their interaction with soil under various loading conditions. These studies offer valuable analyses of internal force factors and stress states within various systems under environmental interaction.

Along with these studies, a sufficient number of scientific works have been conducted to date, devoted to various structures interacting with media under dynamic impacts.

In [32], radial vibrations of cylindrical panels of finite length were considered using the concept of wave propagation in periodic structures. Several new results were obtained and it was shown that with the correct choice of a periodic element, it is possible to determine the boundary frequencies and corresponding modes in all propagation bands.

In [33], an assessment of large displacements of prismatic beams of variable cross-sections subjected to concentrated impacts was done. The resulting large amplitudes at the first frequency were estimated by the FEM and approximately by using polynomial functions.

The study in [34] describes the free waves propagation in a two-dimensional periodic plate using the FEM. In this case, infinite plates are considered a combination of periodic plates on an orthogonal array of simple, evenly-spaced linear supports. The eigenfrequency of the infinite plate was obtained for different wave propagation constants in two directions of the plate.

In [35], based on the theory of thin and thick plates, the vibration and energy flow of a fixed reinforced plate are studied using the finite integral transform method. It is found that including the rotational inertia of the beam and plate in the model affects only the component of the energy flow controlled by the moment coupling but not the component controlled by the shear force coupling.

In reference [36], the propagation of one-dimensional axial waves in an infinitely long periodically supported cylindrically curved panel exposed to a supersonic air flow was investigated. A line of instability was identified. The limiting frequency values and flutter pressure parameters are compared with the critical flutter state of a single curved panel by two methods – the exact method and the FEM.

Currently, many different methods have been developed for assessing the strength parameters of structures in contact interaction with elastic half-spaces under static and dynamic loads.

Despite this, today many questions related to the assessment of internal force factors arising in a structure working together with the soil base under the impact of static loads remain open.

Therefore, this study is devoted to an urgent problem of the development of mathematical models and analytical methods for assessing the internal force factors of multilayer beams lying on an elastic base.

## 2. Methods

### 2.1. The Beamslab Configuration

A  $n$ -layered beam slab interacting with a linearly deformable half-space is considered. Unlike [28], a more general model is presented here, which assumes the normal and shear pressure of the base on the strip slab. It is assumed that between each pair of beam slabs, there is an elastic filler. At that, normal external loads  $q_i$  and pressure of the filler  $q_{z,i+1}$ ,  $q_{z,1}$  act on each  $i$ -th beam slab. The first (lower) beam slab fits snugly to the base, i.e., a tear-free contact hold. It is assumed that vertical  $q_i$  and horizontal  $T_1$  external loads and reactive normal  $p$  and tangential  $\tau$  pressures of the base act on the lower beam slab. Each beam slab has different mechanical characteristics of the material, i.e., the stiffness coefficients of the beam slabs  $D_i$  are discretely variable. It is also assumed that the length of each beam slab is the same, i.e.,  $2l$ , the height is different, i.e.,  $h_i$ , and the width equals one (Fig. 1).

Then, the problem of bending of  $n$ -layered beam slabs interacting with an elastic base is considered, an  $n$ -layered structure works with the base, considering the normal and shear pressure of the base on the strip slab under the impacts of static loads. It is required to develop a mathematical model and analytical methods for assessing the internal force factors, considering the pressure of the base and filler arising on strip slabs under various static loads.

### 2.2. Mathematical Model of the Problem

In the mathematical model, the origin of the system of rectangular Cartesian coordinates  $xOy$  is located at the center of symmetry of the lower beam slab (Fig. 1). If the deflection of the  $i$ -th beam slab is denoted by  $y_i$ , then the following functional dependencies  $y_i = y_i(x)$ ;  $q_i = q_i(x)$ ;  $p = p(x)$ ;  $\tau = \tau(x)$ ;  $i = 1, 2, \dots, n$  hold on the segment  $[-l; l]$ .

The pressure of the filler is assumed to be proportional to the differences in deflections connecting the beams of the slab  $q_{z,i} = k_i(y_{i+1} - y_i)$ .





The set of equations (1), (2), (3), (4), and (5) are the resolving equations of the problem, and they form a system of closed equations. The closedness of the system of resolving equations confirms the correctness of the problem under consideration.

### 3. Results and Discussion

#### 3.1. Solution Method

The dimensionless coordinates equal to the ratio of absolute coordinates to the half-length of the beam slab were used and expressed in similar equations in matrix form for convenience.

A series in orthogonal  $T_n(x)$  Chebyshev polynomials of the first kind approximates the normal and shear stresses of the elastic half-space:

$$(p, \tau) = (1-x^2)^{-\frac{1}{2}} \sum_{n=0}^{\infty} (A_n, B_n) T_n(x). \quad (6)$$

Here,  $A_n, B_n$  are the unknown constants to be determined.

The substitute (6) into the equilibrium equation (4), and considering the orthogonality of the polynomials, gives the relations:

$$A_0 = R / (\pi l); \quad A_1 = 2M / (\pi l^2); \quad B_0 = T / (\pi l). \quad (7)$$

Here, the Chebyshev norm was used defined by the following formulas:

$$\|T_n(x)\| = \pi, \text{ for } n = 0; \quad \|T_n(x)\| = \frac{\pi}{2}, \text{ for } n \neq 0. \quad (8)$$

Formulas (3), which determine the vertical and horizontal displacements of the surface points of the elastic base, considering (6), are written as:

$$(V, U) = \pi \alpha_1 \left[ (-A_0, -B_0) \ln 2 + \sum_{n=1}^{\infty} (A_n, B_n) T_n(x) / n \right] + 2 \alpha_1 \left[ (B_0, -A_0) \arcsin x - \sum_{n=1}^{\infty} (B_n, -A_n) U_n(x) / n \right]. \quad (9)$$

Here,  $U_n(x)$  are the Chebyshev polynomials of the second kind.

For simplicity, a two-layer beam slab interacting with an elastic base is considered. The system of differential equations (1) takes the following form:

$$\frac{D_2}{l^4} y_2^{IV} = q_2 - k_1(y_2 - y_1); \quad \frac{D_1}{l^4} y_1^{IV} = q_1 + k_1(y_2 - y_1) - p - \frac{h_1}{2l} \tau'. \quad (10)$$

The general solution of the system of differential equations (10), considering (6), is represented in the following form:

$$(y_1, y_2) = \frac{l^4}{D_1 + D_2} \left\{ (1, 1) F_{1,q}(x) + (-D_2, D_1) \frac{1}{l^4} F_{2,q}(x) - (1, 1) \sum_{n=0}^{\infty} [A_n f_{p,n}(x) + B_n f_{\tau,n}(x)] + \right. \\ \left. + (-D_2, D_1) \frac{1}{l^4} \sum_{n=0}^{\infty} [A_n \phi_{p,n}(x) + B_n \phi_{\tau,n}(x)] \right\}. \quad (11)$$

Here:

$$F_{1,q}(x) = \sum_{i=1}^4 C_i \frac{x^{4-i}}{(4-i)!} + f_q(x); \quad F_{2,q}(x) = \sum_{i=1}^4 C_{i+4} u_i(\alpha x) + \phi_q(x);$$

are the integration constants;  $u_i(x)$  are the known functions [6]:

$$f_q^{IV}(x) = q_1(x) + q_2(x); \varphi_q(x) = \frac{l^4}{4\alpha^3} \int_0^x u_4 [\alpha(x-5)] \left[ \frac{q_2(5)}{D_2} - \frac{q_1(3)}{D_1} \right] ds; \quad (12)$$

$$f_{p,n}^{IV}(x) = (1-x^2)^{-1/2} T_n(x); \quad f_{\tau,n}'''(x) = \frac{h_1}{2l} f_{p,n}^{IV}(x); \quad (13)$$

$$\left( \varphi_{p,n}(x), \varphi_{\tau,n}(x) \right) = \frac{l^4}{4\alpha^3} \frac{1}{D_1} \int_0^x u_4 [\alpha(x-s)] \left( f_{p,n}^{IV}(s), f_{\tau,n}^{IV}(s) \right) ds. \quad (14)$$

Expression (2), which determines the horizontal displacements of the points of the slab foot, considering (6) and (11), takes the following form:

$$u_\tau = \frac{(1-\nu_1^2)e^2}{h_1 E_1} \left[ B_{1,n}x + B_{2,i} + \sum_{n=0}^{\infty} B_n f_{\tau,n}'(x) \right] - \frac{h_1}{2l} y_1'. \quad (15)$$

The contact conditions (5) are used to determine the unknown coefficients  $A_n, B_n$ . In this case, expressions (9), (11), and (15) are put into equations (5), respectively, and both equations are multiplied by the expression  $(1-x^2)^{-1/2} T_k(x)$ . After that, integrate the equations on the variable  $x$  in  $[-1; 1]$ . In the integration, the orthogonality of polynomials is used, and it is possible to get the following results:

$$\begin{aligned} a_{1,k} + \sum_{n=0}^{\infty} (a_{1,n,k} A_n + b_{1,n,k} B_n) &= \pi^2 \alpha_1 \frac{A_k}{2k}; \\ a_{2,k} + \sum_{n=0}^{\infty} (a_{2,n,k} A_n + b_{2,n,k} B_n) &= \pi^2 \alpha_1 \frac{B_k}{2k}; \\ k &= 2, 3, 4, \dots \end{aligned} \quad (16)$$

The following notation is used:

$$a_{1,k} = \frac{l^4}{D_1 + D_2} \int_{-1}^1 \left\{ F_{1,q}'(x) + f_q(x) - \frac{D_2}{e^4} F_{2,q}'(x) \right\} (1-x^2)^{-1/2} T_k(x) dx; \quad (17)$$

$$a_{2,k} = \int_{-1}^1 \left\{ \frac{(1-\nu_1^2)l^2}{h_1 E_1} (B_{2,\tau}x + B_{2,\tau}) + \frac{l^4}{2h_1(D_1 + D_2)} F_{1,q}'(x) - \frac{D_2}{e^4} F_{2,q}'(x) \right\} (1-x^2)^{-1/2} T_k(x) dx; \quad (18)$$

$$a_{1,n,k} = -\frac{e^4}{D_1 + D_2} \int_{-1}^1 \left[ f_{p,n}(x) + \frac{D_2}{e^4} \varphi_{p,n}(x) \right] (1-x^2)^{-1/2} T_k(x) dx; \quad (19)$$

$$a_{2,n,k} = -\frac{e^4}{2h_1(D_1 + D_2)} \int_{-1}^1 \left[ f_{p,n}'(x) + \frac{D_2}{e^4} \varphi_{p,n}'(x) \right] (1-x^2)^{-1/2} T_k(x) dx; \quad (20)$$

$$b_{1,n,k} = -\frac{e^4}{D_1 + D_2} \int_{-1}^1 \left[ f_{\tau,n}(x) + \frac{D_2}{e^4} \varphi_{\tau,n}(x) \right] (1-x^2)^{-1/2} T_k(x) dx; \quad (21)$$

$$b_{2,n,k} = \int_{-1}^1 \left\{ \frac{(1-\nu_1^2)e^2}{h_1 E_1} f_{\tau,n}'(x) + \frac{e^4}{2h_1(D_1 + D_2)} \left[ f_{\tau,n}'(x) - \frac{D_2}{e^4} \varphi_{\tau,n}'(x) \right] \right\} (1-x^2)^{-1/2} T_k(x) dx. \quad (22)$$

The integration by parts can eliminate the singularity in integrals (17), (18), (19), (20), (21), and (22) and bring the integrals to a convenient form for calculation and evaluation.

System (16) is an infinite system of algebraic equations with respect to unknown coefficients  $A_n, B_n$ . For solving system (16) the reduction method is proposed.

The patterns of pressure distribution along the base are determined by substituting the obtained values of coefficients  $A_n, B_n$  into (6). Expression (6) is put into formulas (9) and (11) to find displacements of beam slabs and base points. Based on these formulas, the internal stress factors in beam slabs are determined according to certain rules of the elasticity theory. Thus, the solution to the problem is reduced to the study of a system of infinite algebraic equations of the form (21). The existence of a bounded solution to the system (21) is equivalent to the existence of solutions for the problem under consideration.

### 3.2. The Existence of a Bounded Solution of the System of Equations

Since a regular system has a unique bounded solution, the regularity of the system (16) is studied. The convergence of the following sequences consisting of free coefficients  $a_{1,k}, a_{2,k}$  of the system (16) is studied. That is, the meeting of the following conditions is analyzed to study the regularity:

$$|a_{1,k}| < \infty, |a_{2,k}| < \infty, k = 2, 3, 4, \dots \quad (23)$$

Integrating integrals (17) and (18) by parts, applying the Cauchy–Bunyakhovsky inequalities, and considering the continuity of the integrands gives the following estimates:

$$(a_{1,k}, a_{2,k}) < (a_1, a_2) \frac{1}{2k} \|P_{k-1}^{(1/2, 1/2)}(x)\|^{1/2}. \quad (24)$$

Here,  $\|P_{k-1}^{(1/2, 1/2)}(x)\|^{1/2}$  is the norm of Jacobi polynomials. The following designations are introduced:

$$a_1 = \left\{ \int_{-1}^1 \left| \frac{e^4}{D_1 + D_2} \left[ F'_{1,q}(x) - \frac{D_2}{e^4} F'_{2,q}(x) \right] (1-x^2)^{1/2} \right|^2 dx \right\}^{1/2}, \quad (25)$$

$$a_2 = \left\{ \int_{-1}^1 \left| \frac{(1-\nu_1^2)l}{h_1 E_1} (B_{2,\tau} + B_{1,\tau}x) - \frac{h_1 l^3}{2(D_1 + D_2)} \left[ F''_{1,q}(x) - \frac{D_2}{l^4} F''_{2,q}(x) \right] (1-x^2)^{1/2} \right|^2 dx \right\}. \quad (26)$$

Considering the given estimate (24), it is certain that inequality (23) holds.

Now, the following numerical series, consisting of the coefficients of unknowns  $A_n, B_n$  of the system (16), are considered:

$$\sum_{n=0}^{\infty} (|a_{1,n,k}| + |a_{2,n,k}| + |b_{1,n,k}| + |b_{2,n,k}|). \quad (27)$$

If series (27) is a convergent series, then the sum of the series depends on the parameter  $k$ . Therefore, denoting the sum of series (27) by  $S_k$  gives the following sequence:

$$\{S_k\}, k = 2, 3, 4, \dots \quad (28)$$

The next step is studying the convergence of sequence (28). For each summand of the common term of series (27), determined by formulas (19), (20), (21), and (22) separately, the following estimates could be obtained:

$$|a_{1,n,k}| \leq \frac{e^4}{D_1 + D_2} (P_{n-3} + \frac{D_2}{e^4} u P_{n-2}) P_{k-1}; \quad |a_{2,n,k}| \leq \frac{e^4}{D_1 + D_2} \frac{h_1}{2l} (P_{n-2} + \frac{D_2}{e^4} u P_{n-2}) P_{k-1} \quad (29)$$

$$|b_{1,n,k}| \leq \frac{e^4}{D_1 + D_2} (P_{n-2} + \frac{D_2}{e^4} u P_{n-2}) P_{k-1}; \quad |b_{2,n,k}| \leq \frac{(1-\nu_1^2)e}{h_1 E_1} P_{n-1} + \frac{h_1 e^3}{2(D_1 + D_2)} (P_{n-1} + \frac{D_2}{e} u P_{n-1}) P_{k-1}. \quad (30)$$

In obtaining these estimates, integration by parts in integrals (19), (20), (21), and (22) is applied. Then, the Cauchy–Bunyakhovsky inequality and the following notation is used:

$$u = \max |u_1(x), u_2(x), u_3(x), u_4(x)|, \quad -1 \leq x \leq 1 \quad (31)$$

$$|b_{1,n,k}| \leq \frac{e^4}{D_1 + D_2} (P_{n-2} + \frac{D_2}{e^4} u P_{n-2}) P_{k-1}; P_{n-2} = \frac{1}{4n(n-1)} \|P_{n-1}^{(3/2,3/2)}(x)\|^{1/2}; P_{n-3} = \frac{1}{8n(n-1)(n-2)} \|P_{n-3}^{(7/2,7/2)}(x)\|^{1/2}. \quad (32)$$

Substituting (29) and (30) into (27), and considering (28) gives the following:

$$S_k \leq P_k \left\{ \frac{l^4}{D_1 + D_2} \sum_{n=3}^{\infty} P_{n-3} + \frac{D_2}{D_1 + D_2} u \left( 3 + \frac{h_1}{2l} \right) \sum_{n=2}^{\infty} P_{n-2} + \left[ \frac{(1-\nu_1^2)l}{h_1 E_1} + \frac{h_1 l^3}{2(D_1 + D_2)} \left( 1 + \frac{D_2}{l^4} u \right) \right] \sum_{n=1}^{\infty} P_{n-1} \right\}. \quad (33)$$

Considering (31) and (32) in inequality (33) verifies that each series on the right-hand side of inequality (33) are convergent. Therefore, the following limit holds:

$$\lim_{k \rightarrow \infty} S_k = 0. \quad (34)$$

Since estimates (23) and (34) are true, then the infinite system of algebraic equations (16) is regular. Thus, the reduction method (23)–(34) can be applied to solve the system (16). As a result, the infinite system of algebraic equations (16) can be solved using the reduction method.

### 3.3. Test Case

The test case is the problem of bending a two-layer beam slab interacting with an elastic base when loaded with a uniformly distributed external load of the following form:

$$q_1(x) = q_1 = const, \quad q_2(x) = q_2 = const.$$

Due to the symmetry of external loads, (6) and (7) will take the following form:

$$(\rho, \tau) = (1-x^2)^{-1/2} \sum_{n=0}^{\infty} (A_{2n} T_{2n}(x), B_{2n+1} T_{2n+1}(x)), \quad A_0 = 2(q_1 + q_2) / \pi. \quad (35)$$

Expressions (9) are written in the following form:

$$(V, U) = \pi \alpha_1 \left[ (-A_0, 0) \ln 2 + \sum_{n=1}^{\infty} \left( A_{2n} \frac{T_{2n}(x)}{2n}, B_{2n-1} \frac{T_{2n-1}(x)}{2n-1} \right) \right] + 2\alpha_1 \left[ (0, -A_0) \arcsin x - \sum_{n=1}^{\infty} \left( B_{2n-1} \frac{U_{2n-1}(x)}{2n-1}, A_{2n} \frac{U_{2n}(x)}{2n} \right) \right]. \quad (36)$$

Beam slab deflections that satisfy the boundary conditions of the problem are written as:

$$(\bar{y}_1, \bar{y}_2) = \frac{l^4}{D_1 + D_2} \left\{ (1, 1)(q_1 + q_2) \left( \frac{x^4}{24} - \frac{x^2}{2} \right) - \sum_{n=1}^{\infty} A_{2n} \left[ \left( \frac{D_2}{D_1}, 1 \right) F_{1,2n}(x) + (1, -1) f_{2n}(x) \right] - \frac{h_1}{2l} \sum_{n=1}^{\infty} B_{2n-1} \left[ \left( \frac{D_2}{D_1}, 1 \right) F_{2,2n}(x) + (1, -1) f'_{2n-1}(x) \right] \right\}. \quad (37)$$

Here,  $\bar{y}_1, \bar{y}_2$  are the relative deflections equal to  $\bar{y}_1(x) = y_1(x) - y_1(0); \quad \bar{y}_2 = y_2(x) - y_2(0);$

$$(F_{1,2n}(x), F_{2,2n-1}(x)) = (\varphi_{5,2n}; \omega_{5,2n-1}) u_1(\alpha x) + (\varphi_{7,2n}; \omega_{7,2n-1}) u_3(\alpha x) + \frac{D_1}{l^4} (\varphi_{2n-1}(x); \omega_{2n-1}(x)); \quad (38)$$

$$(\varphi_{5,2n}, \varphi_{7,2n}) = \int_0^1 \{ (u_4(\alpha); u_2(\alpha)) u_2[\alpha(1-s)] + (2u_1(\alpha) - 2u_3(\alpha)) u_1[\alpha(1-s)] \} (1-s^2)^{-1/2} T_{2n}(s) ds; \quad (39)$$

$$\begin{aligned}
 (\omega_{5,2n-1}, \omega_{7,2n-1}) = & -\frac{h_1}{2lD_1} \int_0^1 \{ (u_4(\alpha); u_2(\alpha)) u_2[\alpha(1-s)] + \\
 & + (2u_1(\alpha) - 2u_3(\alpha)) u_1[\alpha(1-s)] \} [(1-s^2)^{-1/2} T_{2n}(s)]' ds.
 \end{aligned} \tag{40}$$

The horizontal displacement of the foot point of the beam slab, which satisfies the boundary conditions, is represented in the following form:

$$u_\tau = -h_1^2 l^2 / (12D_1) T_x - y' h_1 / (2l). \tag{41}$$

Next, the system (16) is solved in correspondence to this example (41).

Here, the solution is restricted to eight equations relative to eight unknowns  $A_0, A_2, A_4, A_6, A_8, B_1, B_3, B_5, B_7$ .

The calculations are performed for the following values of the parameters of the slab and base [6]:

$$l = 500 \text{ cm}, h_1 = h_2 = 45 \text{ cm}, q_1 = q_2 = q, \nu_1 = \nu_2 = 0.167$$

$$E_1 = E_2 = 1.25 \cdot 10^5 \text{ kg/cm}^2, \nu_0 = 0.3, E_0 = 5 \cdot 10^2 \text{ kg/cm}^2$$

The modulus of elasticity and Poisson's coefficients obtained for slabs and elastic base correspond to concrete slabs and clay-sand soils, respectively.

Calculations will be performed separately according to the following numerical values of the stiffness coefficients of the filler  $k$  [kPa]: 24.52; 49.03; 73.55; 122.5; 171.6.

These values correspond to elastic materials with very low, low, and moderate porosity in the order in which the filler layer stiffness coefficients are written [31].

Table 1 gives the calculation results. The analysis of the results obtained shows that an increase in the values of the stiffness coefficients of the filler  $k$  does not lead to a significant change in the numerical values of the algebraic equations. A change in the numerical values of the stiffness coefficients of the filler  $k$  does not lead to a significant change in the pressures in the base. Retaining three terms in the series in the expansion of the pressure in the base in terms of orthogonal Chebyshev polynomials is ensured by sufficient accuracy in determining the internal force factors in the beam slab.

**Table 1. Numerical values of coefficients  $A_{2n}, B_{2n-1}$  for different values of stiffness coefficients of the filler  $k$ .**

$k$ [kPa]	24.52	49.03	73.55	122.5	171.6
$A_0 / q$	1.273239	1.273239	1.273239	1.273239	1.273239
$A_2 / q$	-0.308264	-0.306441	-0.304161	-0.302753	-0.301269
$A_4 / q$	-0.041247	-0.040962	-0.037824	-0.033472	-0.031643
$A_6 / q$	0.002193	0.002081	0.001973	0.001746	0.001385
$A_8 / q$	0.0003427	0.0003165	0.0002761	0.0002472	0.0002169
$B_1 / q$	0.817618	0.806977	0.793185	0.784676	0.778634
$B_3 / q$	-0.427618	-0.421738	-0.415627	-0.410698	-0.407164
$B_5 / q$	-0.044363	-0.041764	-0.037954	-0.031761	-0.030118
$B_7 / q$	0.001394	0.001169	0.000875	0.000554	0.000347

The solutions to the system of algebraic equations presented in Table 1 differ from the quantities in the table presented in [6] by the characteristics of the equations and the numerical amount of the unknowns in it. From Table 1, it is possible to determine the numerical value of the unknowns of the system of algebraic

equations in order to perform the project calculations with the required accuracy. In particular, for calculations with an accuracy of 0.01, it is enough that the number of unknowns in the system of algebraic equations is six.

Table 2 shows the highest values of bending moments  $M_{1,\tau}$  and  $M_{2,\tau}$  of the beam slabs (for  $x = 0$ ). It shows the values of bending moments  $M_1$  and  $M_2$ , obtained without considering the shear stresses given in [6].

**Table 2. The highest values of bending moments in beam slabs.**

$k$ [kPa]	24.52	49.03	73.55	122.5	171.6
$M_{1,\tau} / (ql^2)$	0.025764	0.0241627	0.023866	0.023219	0.022761
$M_1 / (ql^2)$	0.103563	0.103012	0.099073	0.098169	0.091864
$M_{2,\tau} / (ql^2)$	0.016191	0.016843	0.017384	0.018175	0.019568
$M_2 / (ql^2)$	0.069591	0.071368	0.072437	0.074981	0.077576

The analysis of the results obtained allows to draw the following conclusions: with a decrease in the stiffness coefficients of the filler  $k$ , the bending moments in the first beam slab increase, and in the second beam slab, they decrease; with an increase in the stiffness of the filler  $k$ , the bending moments of the beam slab significantly approach each other; at the accepted values of the stiffness coefficients of the filler  $k$ , an account for the shear stresses in the base leads to a significant (up to 24%) decrease in the bending moments of the first and second beam slabs (Table 2).

#### 4. Conclusions

1. A mathematical model was developed for the problem of bending of multilayer beam slabs interacting with an elastic half-space, taking into account shear stresses in the base.
2. An analytical method was proposed for solving the problem of bending of multilayer beam slabs interacting with an elastic half-space based on the approximation of Chebyshev polynomials.
3. The regularity of the infinite system of algebraic equations obtained by solving the problem was proved.
4. The required number of summands of the terms of the series was established with expanding the solution of the unknown pressure of the base into a series of Chebyshev polynomials.
5. The pattern of changes in the stiffness of the filler and their influence on the force factors in multilayer beam slabs was established.
6. A decrease in the force factors of multilayer beam slabs was established, considering shear stresses in the multi-layer plates.

#### References

1. Jia, M., Yang, Y., Ai, Z. Time history response of an elastic thin plate on a transversely isotropic multilayered medium due to vertical loadings. *Computers and Geotechnics*. 2021. 134. Article no. 104058. DOI: 10.1016/j.compgeo.2021.104058
2. Wang, W., Lu, Y., Zhao, D., Zhang, J., Bai, X. Research on large deflection deformation reconstruction of elastic thin plate based on strain monitoring. *Measurement*. 2020. 149. Article no. 107000. DOI: 10.1016/j.measurement.2019.107000
3. Mao, J.J., Lai, S.K., Zhang, W., Liu, Y.Z. Comparisons of nonlinear vibrations among pure polymer plate and graphene platelet reinforced composite plates under combined transverse and parametric excitations. *Composite Structures*. 2021. 265. Article no. 113767. DOI: 10.1016/j.compstruct.2021.113767
4. Li, L., Liu, C., Zhang, W., Du, Z., Guo, X. Combined model-based topology optimization of stiffened plate structures via MMC approach. *International Journal of Mechanical Sciences*. 2021. 208. Article no. 106682. DOI: 10.1016/j.ijmecsci.2021.106682
5. Ma, H., Xiong, Q., Wang, D. Experimental and numerical study on the ultimate strength of stiffened plates subjected to combined biaxial compression and lateral loads. *Ocean Engineering*. 2021. 228. Article no. 108928. DOI: 10.1016/j.oceaneng.2021.108928
6. Mirsaidov, M., Mamasoliev, Q. Contact problems of multilayer slabs interaction on an elastic foundation. *IOP Conference Series: Earth and Environmental Science*. 2020. 614. Article no. 012089. DOI: 10.1088/1755-1315/614/1/012089
7. Mirsaidov, M., Mamasoliev, K., Ismayilov, K. Bending of Multilayer Slabs Lying on Elastic Half-Space, Considering Shear Stresses. *Lecture Notes in Civil Engineering*. 182. *Proceedings of MPCPE 2021*. Springer. Cham, 2022. Pp. 93–107. DOI: 10.1007/978-3-030-85236-8\_8

8. Wang, B., Chen, X., Sun, X., Chen, P., Wang, Z., Chai, Y. Interaction formulae for buckling and failure of orthotropic plates under combined axial compression/tension and shear. *Chinese Journal of Aeronautics*. 2022. 35(3). Pp. 272–280. DOI: 10.1016/j.cja.2021.01.021
9. Cao, Y., Cao, D., He, G., Ge, X., Hao, Y. Modelling and vibration analysis for the multi-plate structure connected by nonlinear hinges. *Journal of Sound and Vibration*. 2021. 492. Article no. 115809. DOI: 10.1016/j.jsv.2020.115809
10. Vu, Q., Papazafeiropoulos, G., Graciano, C., Kim, S. Optimum linear buckling analysis of longitudinally multi-stiffened steel plates subjected to combined bending and shear. *Thin-Walled Structures*. 2019. 136. Pp. 235–245. DOI: 10.1016/j.tws.2018.12.008
11. Szeptyński, P. Comparison and experimental verification of simplified one-dimensional linear elastic models of multilayer sandwich beams. *Composite Structures*. 2020. 241. Article no. 112088. DOI: 10.1016/j.compstruct.2020.112088
12. Awrejcewicz, J., Krysko, V.A., Zhigalov, M.V. Contact interaction of two rectangular plates made from different materials with an account of physical nonlinearity. *Nonlinear Dynamics*. 2018. 91. Pp.1191–1211. DOI: 10.1007/s11071-017-3939-6
13. Tokovyy, Y., Chyzh, A., Ma, C. An analytical solution to the axisymmetric thermoelasticity problem for a cylinder with arbitrarily varying thermomechanical properties. *Acta Mechanica*. 2019. 230. Pp.1469–1485. DOI: 10.1007/s00707-017-2012-3
14. Tokovyy, Y., Ma, C. Elastic Analysis of Inhomogeneous Solids: History and Development in Brief. *Journal of Mechanics*. 2019. 35(5). Pp. 613–626. DOI: 10.1017/jmech.2018.57
15. Sultanov, K.S., Vatin, N.I. Wave Theory of Seismic Resistance of Underground Pipelines. *Applied Sciences*. 2021. 11(4). Article no. 1797. DOI: 10.3390/app11041797
16. Mirsaidov, M.M., Dusmatov, O.M., Khodjabekov, M.U. Stability of nonlinear vibrations of plate protected from vibrations. *Journal of Physics: Conference Series*. 1921. First International Conference on Advances in Smart Sensor, Signal Processing and Communication Technology (ICASSCT 2021). IOP Publishing. Goa, 2021. Pp.19–20. DOI: 10.1088/1742-6596/1921/1/012097
17. Mirsaidov, M., Dusmatov, O., Khodjabekov, M. Mode Shapes of Transverse Vibrations of Rod Protected from Vibrations in Kinematic Excitations. *Lecture Notes in Civil Engineering*. 170. Proceedings of FORM 2021. Springer. Cham, 2022. Pp 217–227. DOI: 10.1007/978-3-030-79983-0\_20
18. Ikonin, S.V., Sukhoterina, A.V. The effect of design on interaction of foundation slabs with the base. *Magazine of Civil Engineering*. 2019. 89(5). Pp. 141–155. DOI: 10.18720/MCE.89.12
19. Schreiber, Ph., Mittelstedt, Ch. Buckling of shear-deformable unsymmetrically laminated plates. *International Journal of Mechanical Sciences*. 2022. 218. Article no. 1069995. DOI: 10.1016/j.ijmecsci.2021.106995
20. Zhao, X., Chang, P. Free and forced vibration of double beam with arbitrary end conditions connected with a viscoelastic layer and discrete points. *International Journal of Mechanical Sciences*. 2021. 209. Article no. 106707. DOI: 10.1016/j.ijmecsci.2021.106707
21. Zhang, L., Pellegrino, A., Townsend, D., Petrinic, N. Temperature Dependent Dynamic Strain Localization and Failure of Ductile Polymeric Rods under Large Deformation. *International Journal of Mechanical Sciences*. 2021. 204. Article no. 106563. DOI: 10.1016/j.ijmecsci.2021.106563
22. Shao, D., Wang, Q., Tao, Y., Shao, W., Wu, W. A unified thermal vibration and transient analysis for quasi-3D shear deformation composite laminated beams with general boundary conditions. *International Journal of Mechanical Sciences*. 2021. 198. Article no. 106357. DOI: 10.1016/j.ijmecsci.2021.106357
23. Mirsaidov, M., Sultanov, T., Yarashov, J., Toshmatov, E. Assessment of dynamic behaviour of earth dams taking into account large strains. *E3S Web of Conferences*. 2019. 97. Article no. 05019. DOI: 10.1051/e3sconf/20199705019
24. Sultanov, T.Z., Khodzhaev, D.A., Mirsaidov, M.M. The assessment of dynamic behavior of heterogeneous systems taking into account non-linear viscoelastic properties of soil. *Magazine of Civil Engineering*. 2014. 45(1). Pp. 80–89, 117–118. DOI: 10.5862/MCE.45.9
25. Sultanov, K.S., Khusanov, B.E., Rikhsieva, B.B. Underground pipeline strength under non-one-dimensional motion. *IOP Conference Series: Materials Science and Engineering*. 2020. 883(1). Article no. 012023. DOI: 10.1088/1757-899X/883/1/012023
26. Sultanov, K.S., Khusanov, B.E., Rikhsieva, B.B. Longitudinal waves in a cylinder with active external friction in a limited area. *Journal of Physics: Conference Series*. 2020. 1546(1). Article no. 012140. DOI: 10.1088/1742-6596/1546/1/012140
27. Mirsaidov, M., Boytemirov, M., Yuldashev, F. Estimation of the Vibration Waves Level at Different Distances. *Lecture Notes in Civil Engineering*. 170. Proceedings of FORM 2021. Springer. Cham, 2022. Pp. 207–215. DOI: 10.1007/978-3-030-79983-0\_19
28. Mirsaidov, M.M., Mamasoliev, K. Contact interaction of multilayer slabs with an inhomogeneous base. *Magazine of Civil Engineering*. 2022. 115(7). Article no. 11504. DOI: 10.34910/MCE.115.4
29. Mirsaidov, M.M., Sultanov, T.Z., Rumi, D.F. An assessment of dynamic behavior of the system “structure – foundation” with account of wave removal of energy. *Magazine of Civil Engineering*. 2013. 39(4). Pp. 94–105, 126–127. DOI: 10.5862/MCE.39.10
30. Mirsaidov, M.M., Sultanov, T.Z., Sadullaev, A. Determination of the stress-strain state of earth dams with account of elastic-plastic and moist properties of soil and large strains. *Magazine of Civil Engineering*. 2013. 40(5). 59–68. DOI: 10.5862/MCE.40.7
31. Jurayev, D.J., Vatin, N., Sultanov, T.Z., Mirsaidov, M.M. Spatial stress-strain state of earth dams. *Magazine of Civil Engineering*. 2023. 118(2). Article no. 11810. DOI: 10.34910/MCE.118.10
32. Pany, C., Parthan, S., Mukherjee, S. Vibration analysis of multi-supported curved panel using the periodic structure approach. *International Journal of Mechanical Sciences*. 2002. 44(2). Pp. 269–285. DOI: 10.1016/S0020-7403(01)00099-6
33. Pany, C. Large amplitude free vibrations analysis of prismatic and non-prismatic tapered cantilever beams. *Pamukkale University Journal of Engineering Sciences*. 2023. 29(4). Pp.370–376. DOI: 10.5505/pajes.2022.02489
34. Pany, C. An Insight on the Estimation of Wave Propagation Constants in an Orthogonal Grid of a Simple Line-Supported Periodic Plate Using a Finite Element Mathematical Model. *Frontier in Mechanical Engineering. Solid and Structural Mechanics*. 2022. 8. Article no. 926559. DOI: 10.3389/fmech.2022.926559
35. Guo, H., Zhang, K. An analytical model for the analysis of vibration and energy flow in a clamped stiffened plate using integral transform technique. *Journal of Vibroengineering*. 2024. 26(4). Pp. 918–935. DOI: 10.21595/jve.2024.23604
36. Pany, C., Parthan, S. Flutter analysis of periodically supported curved panels. *Journal of Sound and Vibration*. 2003. 267(2). Pp. 267–278. DOI: 10.1016/S0022-460X(02)01493-1



**Information about the authors:**

**Mirziyod Mirsaidovich Mirsaidov**, Doctor of Technical Sciences

ORCID: <https://orcid.org/0000-0002-8907-7869>

E-mail: [mirsaidov1948@mail.ru](mailto:mirsaidov1948@mail.ru)

**Nikolai Ivanovich Vatin**, Doctor of Technical Sciences

ORCID: <https://orcid.org/0000-0002-1196-8004>

E-mail: [vatin@mail.ru](mailto:vatin@mail.ru)

**Kazokboy Mamasoliev**

ORCID: <https://orcid.org/0000-0003-3371-5742>

E-mail: [q-mamasoliev@mail.ru](mailto:q-mamasoliev@mail.ru)

Received 03.05.2024. Approved after reviewing 29.08.2024. Accepted 31.08.2024.



Research article

UDC 693.547

DOI: 10.34910/MCE.130.5



## Autogenous shrinkage and early cracking of massive foundation slabs

G.V. Nesvetaev , Yu.I. Koryanova , B.M. Yazyev 

Don State Technical University, Rostov-on-Don, Russian Federation

✉ [koryanova.yi@mail.ru](mailto:koryanova.yi@mail.ru)

**Keywords:** kinetics of heat dissipation, autogenous shrinkage, stress level, massive monolithic structure

**Abstract.** The risk of early cracking due to temperature gradients in the early period of concrete hardening of massive monolithic reinforced concrete structures determines the relevance of research into the possibilities of regulating temperature-shrinkage stresses. An important task is to improve the algorithm for calculating temperature-shrinkage stresses due to temperature gradients and autogenous shrinkage, taking into account the kinetics of heat dissipation of concrete, heat exchange conditions, and ambient temperature. Numerous factors influencing the formation of temperature-shrinkage stresses determine the relevance of the use of numerical methods for modeling temperature fields and stresses, which requires dependencies of changes in heat generation and temperature gradients over time, temperature deformations and autogenous shrinkage deformations, tensile strength of concrete, elastic modulus, creep coefficient. *Purpose of the study:* obtaining dependencies describing changes in the kinetics of heat dissipation and strength, taking into account the properties of cements and the presence of additives; methodology for taking into account autogenous shrinkage deformations when calculating stress values; modeling the stress-strain state of a massive monolithic structure in the early period of hardening and comparison of calculated and experimental values, taking into account the influence of autogenous shrinkage of concrete on the stress level. *Materials and methods:* modeling temperature fields and stresses from temperature differences and autogenous shrinkage depending on the class and kinetics of heat dissipation and hardening of concrete; experimental studies of temperature fields and stresses in the early period of hardening. *Results:* the equations describing the kinetics of heat dissipation, strength, and autogenous shrinkage of concrete up to 5 days old depending on concrete hardening rate are proposed. It is shown that failure to take autogenous shrinkage into account can lead to an overestimation of the tensile stress level, depending on the concrete class and the autogenous shrinkage value by up to 30 %. An algorithm is proposed for calculating the kinetics of the stress level in the early period of hardening of massive monolithic structures, taking into account the deformations of autogenous shrinkage, the class, and hardening rate of concrete. The expediency of limiting the temperature difference “center-top” depending on the required reliability in the range from 20...23 °C to 26...28 °C is substantiated.

**Citation:** Nesvetaev, G.V., Koryanova, Yu.I., Yazyev, B.M. Autogenous shrinkage and early cracking of massive foundation slabs. Magazine of Civil Engineering. 2024. 17(6). Article no. 13005. DOI: 10.34910/MCE.130.5

### 1. Introduction

The risk of early cracking due to temperature gradients in the early period of concrete hardening of massive monolithic reinforced concrete structures determines the relevance of regulating the temperature regime of concrete hardening. Particularly effective is the combination of prescription (limiting cement content, using low exothermic cements and hardening retardant additives) and technological factors, for example, regulating heat loss to level out temperature gradients [1–3].

An important task is to improve the algorithm for calculating temperature stresses due to temperature gradients in the early period of construction of a massive monolithic structure, taking into account the kinetics of heat dissipation of concrete, heat exchange conditions, and ambient temperature. According to [4], the level of tensile stresses  $u = \sigma_t / f_{ctm}$  ( $R_{bt}$  in the Russian Code of Regulations 63.13330.2018 “Concrete and reinforced concrete structures. General provisions”)  $> 1$  was noted after approximately 3.5 days of aging. In [5], the level of tensile stresses  $u = \sigma_t / f_{ctm}$  ( $\sigma_t / R_{bt}$  in the Russian Code of Regulations 63.13330.2018)  $> 1$  at a design concrete strength of 80 MPa was recorded after approximately 54 hours of hardening. In [6], when the maximum temperature in the center of the slab was reached after 72 hours, the value  $\sigma_t = 2.43$  MPa was recorded, which is higher than the axial tensile strength of class C20/25 (B25 in the Russian Code of Regulations 63.13330.2018) concrete at design age. The maximum temperatures in the center of the structures can exceed 70 °C, the time to reach the maximum temperature can be from 24 to 72 hours or more, and the “center-top” temperature difference, which determines the level of tensile stresses, according to the authors, can exceed 30 °C with standardized permissible values up to 20 °C.

The above predetermines the relevance of research in the field of regulating the temperature regime of hardening and preventing early cracking of massive monolithic reinforced concrete structures [7]. The numerous prescription and technological factors influencing the formation of temperature stresses in the early period of concrete hardening of monolithic structures determines the relevance of using modeling to study temperature fields and stresses using numerical methods [1, 3, 8]. Calculation of the stress level requires the dependencies of the change in the “center-top” temperature gradients and temperature deformations, the tensile strength of concrete, the elastic modulus, and the creep coefficient over time [1, 9]. Calculation of temperature gradients requires data on the kinetics of heat dissipation of hardening concrete. In addition, when calculating temperature stresses, with rare exceptions [1], the deformations of autogenous shrinkage of concrete are ignored, especially when the overlap time of layers is more than 4 hours, when using concrete mixtures from different suppliers (with different cements), the values of which depend on prescription factors and can make certain adjustments to the assessment of stresses. The value of autogenous shrinkage of concrete at any time depends on the class of concrete, the properties of cement [10–12]. Some factors can influence on the kinetics [13] and the value of autogenous shrinkage, for example the different additives and conditions, such as internal curing [14], calcium carbonate whiskers [15], nanofibrillated cellulose [16], temperature rising inhibitor [17], and others. And, with increasing class of concrete, it can exceed the shrinkage deformation during drying [18, 19], and depending on the class of concrete can be 0.5...0.83 of the total shrinkage (shrinkage during drying + autogenous shrinkage) [18], and according to [19] – 0.32...0.38. Since the use of high-strength concrete is finding increasing application in the construction of building foundations due to the increase in the number of storeys, assessing the contribution of autogenous shrinkage to the formation of the stress field in the early period of hardening of massive monolithic structures is an urgent task. In this regard, the purpose of this work is:

- obtaining dependencies describing changes in the kinetics of heat dissipation and strength, taking into account the properties of cements and the presence of additives;
- methodology for taking into account deformations of autogenous shrinkage, when calculating the magnitude of stresses;
- modeling the stress-strain state of a massive monolithic structure in the early period of hardening and comparing of calculated and experimental values.

## 2. Materials and Methods

The research included modeling and experimental determination of the parameters of temperature fields and concrete deformations of a massive monolithic structure. The modeling methodology is based on the principles presented below.

The determination of temperature field parameters was carried out according to the method [20] depending on the concrete class C20/25 – B40 (B40 in the Russian international standard GOST 25192-2012 “Concretes. Classification and general technical requirements”, between C30/37 and C35/45) with specific heat dissipation at the age of 28 days respectively from 130 to 190 mJ/m<sup>3</sup> (for example, in [21], the simulation was performed for concrete with a specific heat dissipation of 140 mJ/m<sup>3</sup>). In order to exclude factors that do not have a significant impact on the result of this study, the main objective of which is to assess the effect of autogenous shrinkage of concrete, taking into account the properties of cement, on the level of stress in the early period of hardening, the following assumptions were made:

- uninsulated upper surface, ambient temperature of 20 °C and initial concrete temperature of 20 °C;
- a statically determinate slab is erected on a concrete foundation.

Since the Russian Codes of Regulations (63.13330.2018, 70.13330.2012, 435.1325800.2018) do not contain quantitative criteria for crack resistance in the early period of hardening, the following condition is adopted as a criterion:

$$\sigma_{\tau} < R_{t,\tau}/1,5, \quad (1)$$

where  $\sigma_{\tau}$  is the value of tensile stress at time  $\tau$ ;  $R_{t,\tau}$  is the ultimate strength of concrete under axial tension at time  $\tau$ ; 1,5 is the safety factor for concrete under tension (in the Russian Code of Regulations 63.13330.2018).

The relative heat dissipation of hardening concrete due to the hydration of Portland cement under normal conditions is described by the equation [20]:

$$Q_{\tau} = Q_{28} \cdot \exp\left(k \cdot \left(1 - \left(\frac{28}{\tau}\right)^d\right)\right), \quad \tau > 1, \quad (2)$$

where  $\tau$  is the time (days);  $k$ ,  $d$  are the coefficients, the values of which proposed by the authors are presented in Table 1.

In this case, the relative heat dissipation is considered as an indicator of the degree of cement hydration:

$$\frac{\alpha_{\tau}}{\alpha_{28}} = f\left(\frac{Q_{\tau}}{Q_{28}}\right). \quad (3)$$

When hardening under normal conditions, the change in the relative compressive strength of concrete  $f_{c,\tau}/f_{c,28}$  ( $R/R_{28}$  in the Russian international standard GOST 25192-2012) over time is described by the equation 3.2 EN 1992-1-1:

$$\frac{f_{c,\tau}}{f_{c,28}} = \exp\left(s \cdot \left(1 - \sqrt{\frac{28}{\tau}}\right)\right), \quad \tau > 1. \quad (4)$$

As is known, the compressive strength of concrete depends on the porosity of concrete and the hardening temperature, in connection with which the concepts "reduced age" or "degree of maturity" are used [22, 23]:

$$f_c = f(P), \quad \text{or} \quad \frac{f_c}{f_{P=0}} = \exp(k \cdot P), \quad (5)$$

and the porosity of concrete depends on the degree of hydration of the cement:

$$P = f(\alpha) = k \left( \frac{1}{\rho_c} + \frac{W}{C} \right) - \left( \frac{(1+n)\alpha}{\rho_{cs}} + \frac{1-\alpha}{\rho_c} \right), \quad (6)$$

therefore, the tensile strength of concrete  $f_{cm}$  at time  $\tau$  depends on the relative heat dissipation at this moment and there is a relationship of the form [24]:

$$\frac{f_{cm,\tau}}{f_{cm,28}} = b \cdot \left( \frac{Q_{\tau}}{Q_{28}} \right)^x. \quad (7)$$

To take into account the influence of temperature conditions other than normal, the dependence of the ultimate strength of concrete from the "reduced age" ("degree of maturity") [20, 23], similar to (2), in which the value  $\tau_r$  is defined as:

$$\tau_r = \frac{\sum Q_i \tau_i}{T_a} - \tau_s, \quad (8)$$

where  $Q_i$  is the amount of heat dissipation per period  $\tau_i$ ;  $T_a$  is an average concrete temperature over a controlled hardening period;  $\tau_s$  is the duration of the induction period (a parameter adjusted to take into account different setting times due to different mix temperatures caused by the use of retarding/accelerating admixtures).

The value of autogenous shrinkage  $\varepsilon_{ca}(\infty)$  according to EN 1992-1-1 is determined by the formulas:

$$\varepsilon_{ca}(\infty) = 2.5(f_{ck} - 10)10^{-6}; \quad (9)$$

$$\varepsilon_{ca}(t) = \beta_{as}(t)\varepsilon_{ca}(\infty); \quad (10)$$

$$\beta_{as}(t) = 1 - \exp(-0.2t^{0.5}). \quad (11)$$

Using (3) and taking  $f_{ck} = f_{c,\tau}$ , and instead of 10 taking  $10f_{c,\tau}/f_{c,28}$ , after some transformations, we obtain a function connecting the kinetics of autogenous shrinkage and the kinetics of compressive strength of the form:

$$\frac{\varepsilon_{ca,\tau}}{\varepsilon_{ca,5}} = f\left(\frac{f_{c,\tau}}{f_{c,5}}\right) = f\left(\frac{R_\tau}{R_{28}}\right). \quad (12)$$

These dependencies make it possible to consider the kinetics of heat dissipation, strength, and autogenous shrinkage in relation to each other.

Experimental studies of temperature fields and deformations of concrete of a massive monolithic structure in the early period of hardening were carried out by the authors using temperature and deformation sensors [25]. The ultimate axial tensile strength of concrete  $f_{ctm}$  ( $R_{bt}$  in the Russian Code of Regulations 63.13330.2018), the modulus of elasticity of concrete  $E_0$ , the creep coefficient of concrete  $\varphi$  at any time were calculated as a function of the ultimate compressive strength  $f_{cm}$  ( $R_b$  in the Russian Code of Regulations 63.13330.2018), taking into account the degree of concrete maturity, according to (7) time [20, 24]:

$$f_{ctm} = 0.29 \cdot f_{cm}^{0.6}; \quad (13)$$

$$E_0 = 1000 \cdot \frac{0.05 \cdot f_{cm} + 57}{1 + \frac{29}{3.8 + f_{cm}}}; \quad (14)$$

$$\varphi(\tau) = \frac{8000}{(E_0(\tau))^{0.785}}. \quad (15)$$

Tensile stresses from temperature deformations  $\varepsilon_T$  at any time were calculated using the formula [9]:

$$\sigma_T = \frac{k_r \cdot E_0 \cdot \alpha \cdot \Delta T}{(1 + \varphi)} = \frac{k_r \cdot E_0 \cdot \varepsilon_T}{(1 + \varphi)} \quad (16)$$

and taking into account the deformations of autogenous shrinkage  $\varepsilon_{ca}$  according to the formula:

$$\sigma_T = \frac{k_r \cdot E_0 \cdot (\varepsilon_T + \varepsilon_{ca})}{(1 + \varphi)}. \quad (17)$$

### 3. Results and Discussion

The kinetics of heat dissipation, compressive strength of concrete and autogenous shrinkage are described by the equation:

$$Y_{\tau} = Y_{[\tau]} \cdot \exp \left( k \cdot \left( 1 - \left( \frac{[\tau]}{\tau} \right)^d \right) \right), \quad (18)$$

the coefficients  $k$ ,  $d$  of which for concrete based on cements with different hardening kinetics (with different hydration rates) are presented in Table 1.

**Table 1. Coefficient values in (18) for concretes with different hardening kinetics.**

Properties of concrete, $Y$	Coefficient	$f_{c,2}/f_{c,28}$ according to EN 206.1			
		Rapid > 0.5	Medium 0.3–0.5	Slow 0.15–0.3	Very slow < 0.15
Compressive strength, $R(f_{c,\tau})$	$k$ (s)	< 0.25	0.25–0.43	0.43–0.7	$\geq 0.7$
	$d$			0.5	
	$[\tau]$			28	
Heat dissipation, $Q_{\tau}$	$k$	$\geq 0.15$	0.16–0.2	0.21–0.24	> 0.24
	$d$	$\geq 0.45$	0.46–0.51	0.52–0.62	> 0.62
	$[\tau]$			28	
Autogenous shrinkage, $\varepsilon_{CA,\tau}$	$k$	$\geq 0.33$	0.3–0.4	> 0.4	–
	$d$	$\geq 0.65$	0.66–0.9	> 0.9	–
	$[\tau]$		5		–

Fig. 1 shows the calculated values according to (18) kinetics of heat dissipation under normal hardening conditions.

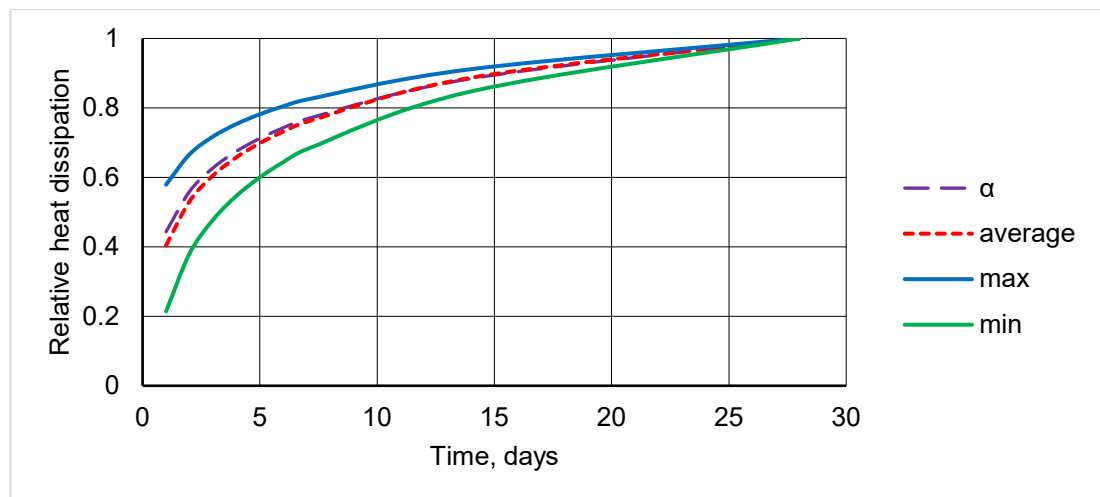


**Figure 1. Relationship between relative heat dissipation and age of concrete under normal conditions.  $\alpha$  – average statistical values for hydration kinetics for normally hardening concrete; max, min – according to (18) for quickly and slowly hardening concrete according to Table 1; average – average between max and min.**

As is known, the value of autogenous shrinkage depends on the properties of cement, the presence of additives and can differ significantly (Table 2, 3) from the values according to (9). Autogenous shrinkage develops most intensively under normal conditions during the first 5–7 days [10].

**Table 2. Values of autogenous shrinkage of concrete of various classes.**

Concrete class	Autogenous shrinkage, ( $10^6$ )	
	EN 1992-1-1	Data of the authors with different admixtures and additives
C20/25	25	17...72 (0.68...2.88)
C60/75	125	110...360 (0.88...2.88)

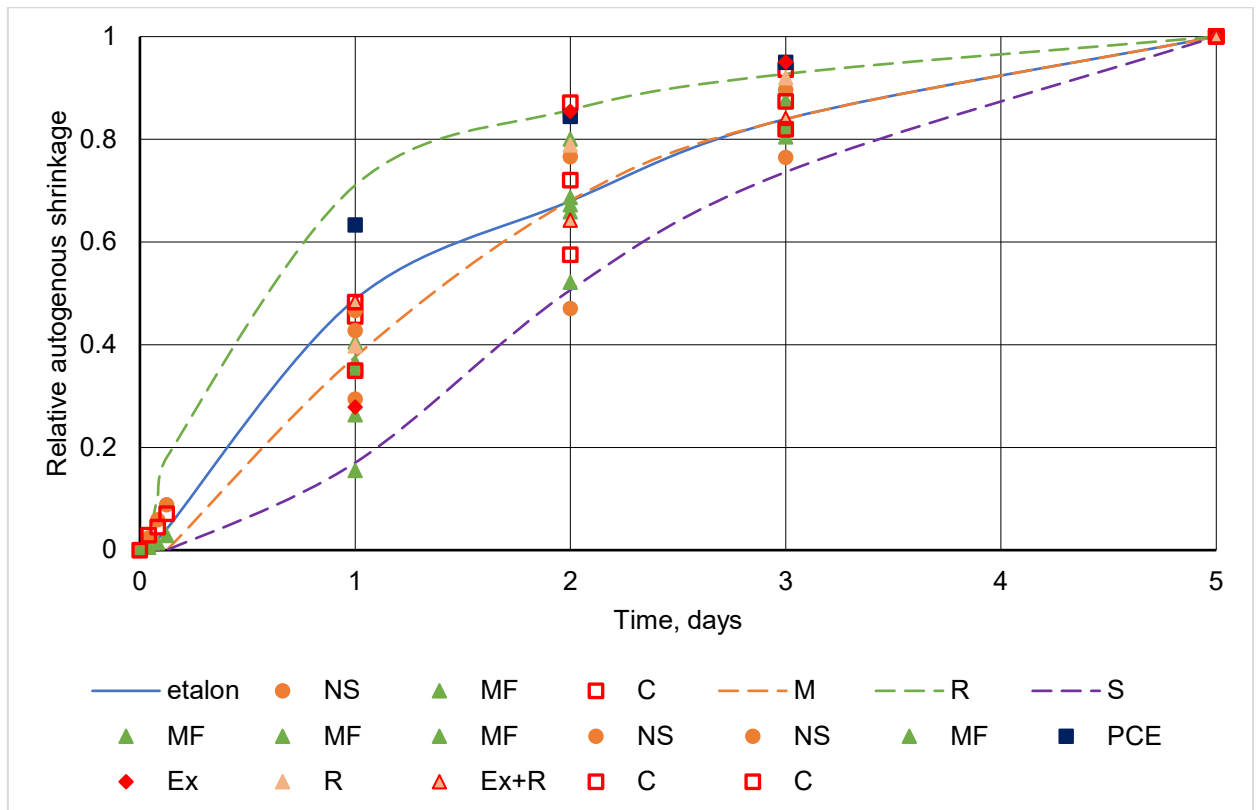
**Table 3. Autogenous shrinkage values.**

Data	Autogenous shrinkage, ( $10^6$ )			
	Cement paste		Concrete or mortar <sup>1</sup>	
	72 h	120 h	72 h	120 h
[11]	1200	1470	(120–240)*	(147–295)*
[26]	600	750	(60–120)*	(75–150)*
	300	390	(30–60)*	(39–78)*
[13]			2000 <sup>1</sup> (800–1000)*	
			1100 <sup>1</sup> (440–550)*	
			950 <sup>1</sup> (238–475)*	
			450 <sup>1</sup> (180–225)*	
[27]	250	275	(25–50)*	(27.5–55)*

\* according to our forecast

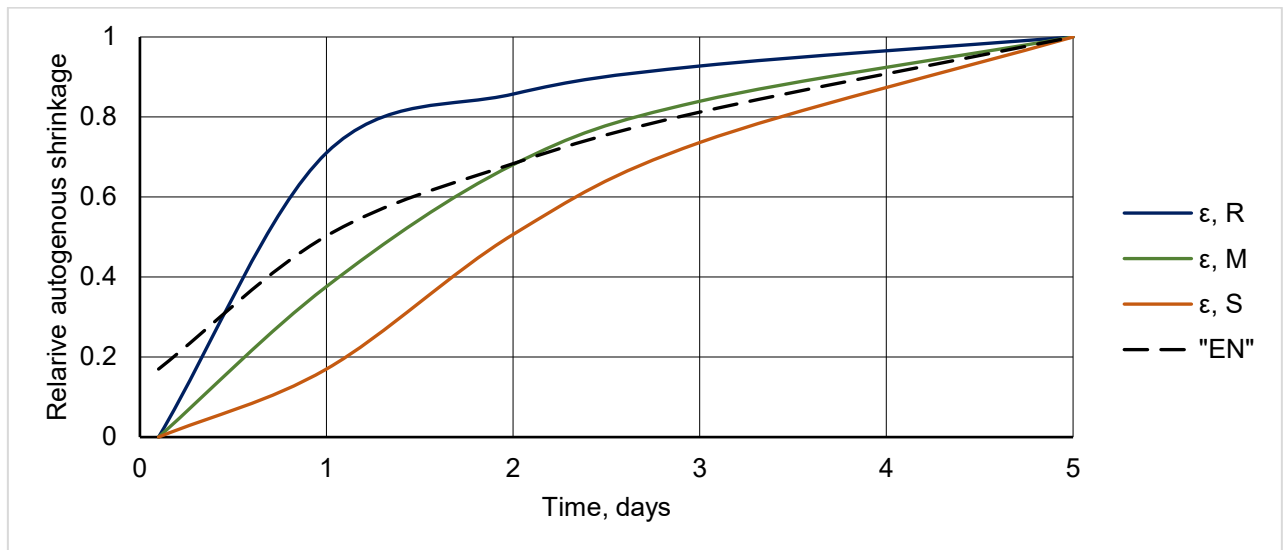
It is obvious that autogenous shrinkage deformations can vary over a very wide range. In this study, values at the age of 28 days were taken from  $20 \cdot 10^{-6}$  for C20/25 to  $80 \cdot 10^{-6}$  ( $\epsilon$ ) and  $160 \cdot 10^{-6}$  ( $2\epsilon$ ) for B40 (by the Russian Code of Regulations 63.13330.2018).

Fig. 2 shows the measured values of autogenous shrinkage of concrete according to Table 2 in the first 5 days of hardening. It is obvious that the kinetics of autogenous shrinkage, especially in the first two days of hardening, varies significantly depending on the individual characteristics of cements and additives.



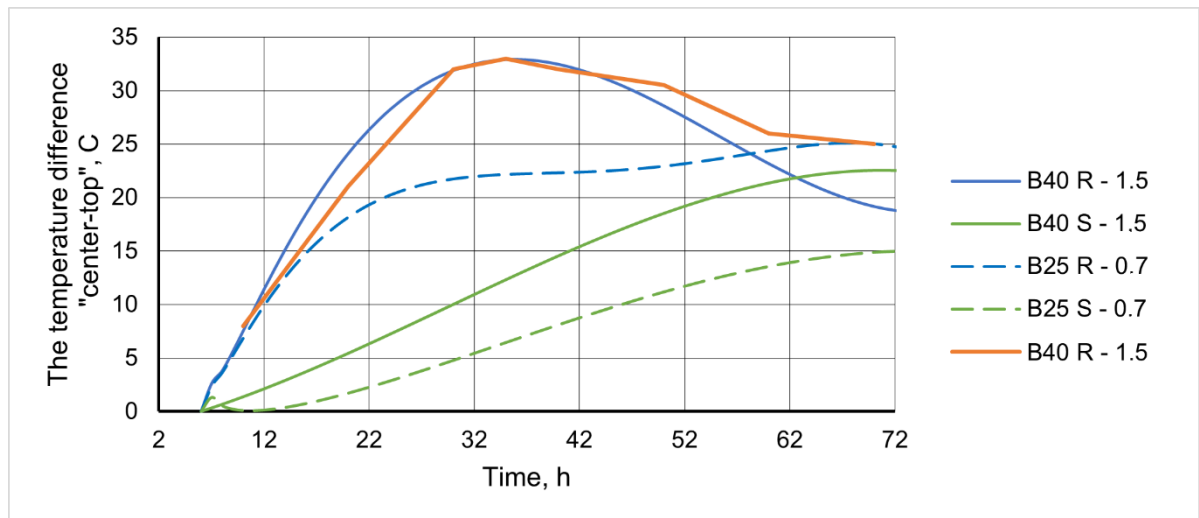
**Figure 2. Kinetics of autogenous shrinkage. Etalon – without admixture, 1–15 with different PCE, MF, NS superplasticizers; Ex; R; C – expansion additive, hardening accelerator, complex additive; R – rapid; M – medium; S – slow according to Table 1.**

Fig. 3 shows a comparison of the kinetics of the calculated values of autogenous shrinkage according to Table 1 with the values according to (9–11). A good compliance for type “M” concrete according to Table 1 with values according to EN 1992-1-1 for  $\tau > 2$  is obvious.



**Figure 3. Kinetics of autogenous shrinkage.  $\epsilon$ , R;  $\epsilon$ , M;  $\epsilon$ , S – according to (16); “EN” – according to EN 1992-1-1.**

Fig. 4 shows the calculated “center-top” temperature difference of foundation slabs 0.7 and 1.5 m thick made of fast-hardening concrete of classes C20/25 (B25) – B40 and the “center-top” temperature difference measured during the construction of a real foundation slab 1.5 m thick made of class B40 concrete. According to data, for example, [28], a temperature difference between “center-top” of up to 28.7 °C was noted, while deformations on the surface reached values of 126–137  $\mu\text{s}$ .



**Figure 4. Relationship between “center-top” temperature difference of foundation slabs 1.5 m and 0.7 m thick. B25...B40 – 1.5 (0.7) – design values for concrete of the corresponding classes; B40 R – 1.5  $\Theta$  – measured values; R, S – rapid and slow hardening concrete.**

### 3.1. Theoretical Prerequisites for Constructing a Calculation Methodology

Calculation of the kinetics of the stress level from temperature-shrinkage deformations in the early period of hardening of massive monolithic structures can be implemented using the following algorithm:

- depending on the class and hardening kinetics of cement (concrete) according to (18), the kinetics of heat dissipation is determined;
- according to the method, for example, [29], temperature fields are calculated with the determination of the temperature in the center and on the surface of the structure and the temperature difference “center-top” at any time of the analyzed period  $\tau$ ;
- average temperature for the analyzed hardening period  $T_a$  is determined;



- according to (8), the degree of concrete maturity is determined at any time during the analyzed period  $\tau$ ;
- reduced hardening time  $\tau_a$  is determined for the analyzed period;
- compressive strength of concrete is determined at any time of the analyzed period  $\tau$  according to (4) with  $\tau = \tau_r$ ;
- determined by (13–15) concrete tensile strength, elastic modulus, and creep coefficient at any time  $\tau$  are calculated;
- according to (18), the magnitude of autogenous shrinkage deformations at any time  $\tau$  is calculated;
- according to (16) or (17), the magnitude of stress and the level of stress at any time  $\tau$  are calculated.

Fig. 5 shows the calculated and measured values of the stress level in the first 5 days of hardening during the early period of hardening of a foundation slab 1.5 m thick. The value  $\tau_s = 0$  in (8) is accepted.

The ratio of the stress level without taking into account autogenous shrinkage to the stress level taking into account autogenous shrinkage according to EN 1992-1-1 is 1.36 for concrete of class B40 and 1.09 for concrete of class B25. If the autogenous shrinkage deformation exceeds 2.5 times relative to the data in EN 1992-1-1 (Table 2), for class B40 concrete, the ratio of stress levels is 2.15. Comparison of the influence of autogenous shrinkage increased relative to (9) for concrete classes C20/25 and B40 clearly shows the increase in influence with increasing autogenous shrinkage, which increases with increasing class of concrete.

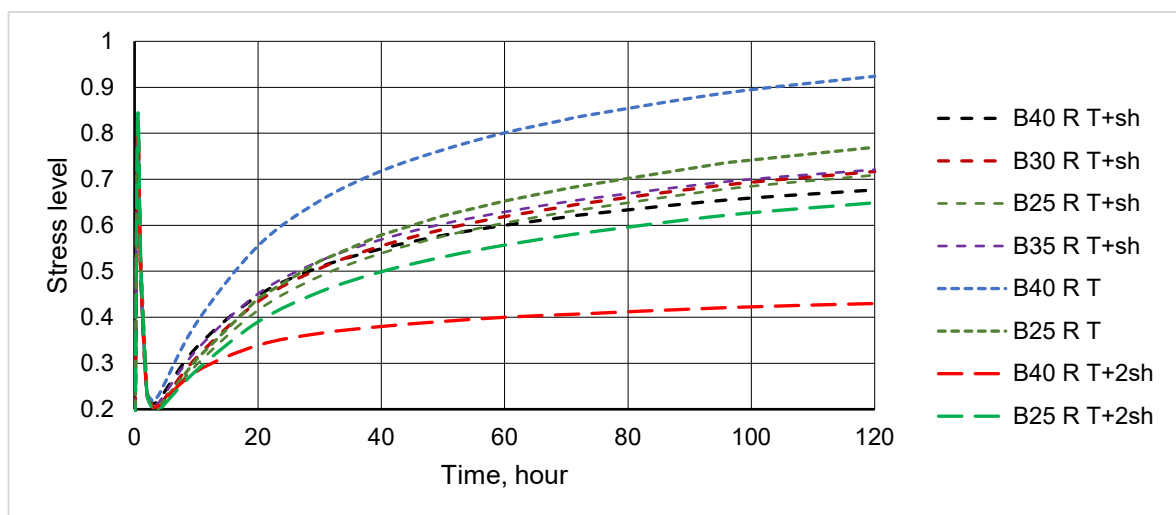


**Figure 5. Dependence of the calculated values of the stress level in the early period of hardening of a foundation slab 1.5 m thick. B25...40 R T+sh, T+2sh – calculated values taking into account the influence of autogenous shrinkage for concrete of the corresponding classes; B25...40 R T – without taking into account the influence of autogenous shrinkage.**

Fig. 6 shows the dependence of the stress level on the temperature difference “center-top” according to calculated and measured [25] results. The dependence of the stress level on the temperature difference “center-top” is described by the equation:

$$U(\sigma) = k\Delta T, \quad (19)$$

with  $k = 0.029$  for calculated values without taking into account autogenous shrinkage and  $k = 0.033$  for measured values.

It is in good agreement with the values measured in a real structure [20]. Taking the value  $[u] = 1/1.5 = 0.67$  for the calculated value of the permissible level of tensile stresses, we obtain for the permissible temperature difference “center-top” according to experimental data and the model the value  $\Delta T = 20\text{--}23$  °C, at  $[u] = 0.85$  we get  $\Delta T = 26\text{--}28$  °C. According to modeling data [30], at a temperature difference of 29 °C, the stress level was approximately 0.55, which is lower than the values according to

our data. This once again confirms the relevance of research in this area. In [28], very different results, when modeling using five different techniques, were also obtained.

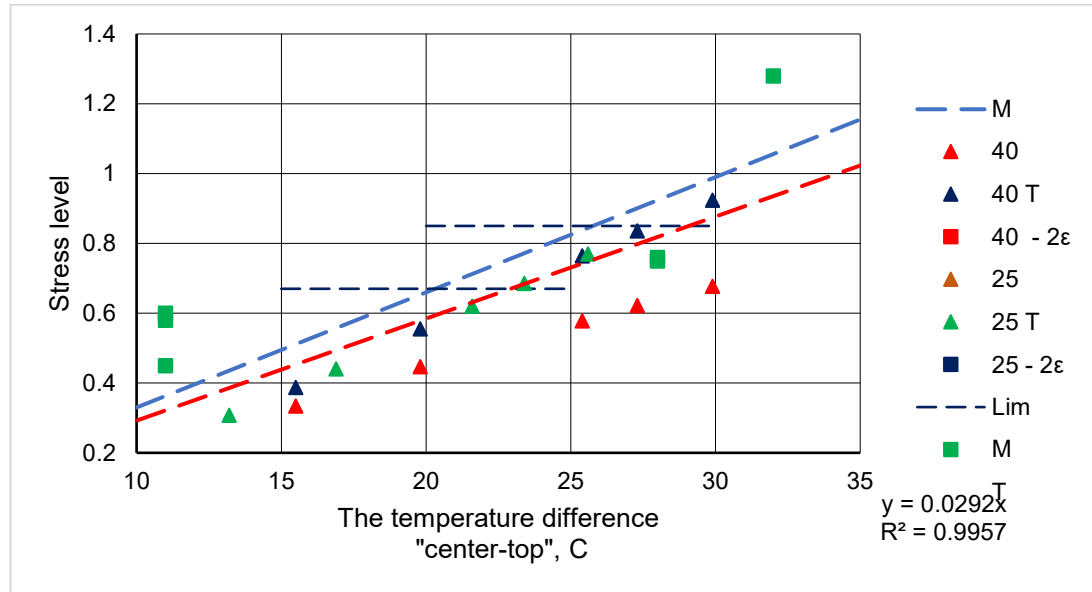


**Figure 6. Dependence of the stress level on the temperature difference “center-top”. 25...40 – calculated values for the corresponding class of quick-hardening concrete; T – excluding autogenous shrinkage; 2ε – with autogenous shrinkage doubled relative to (8); M – measured values; Lim – limit values.**

#### 4. Conclusions

1. The relationship between the kinetics of heat dissipation, strength, and autogenous shrinkage is shown and the corresponding calculation equations are presented. A classification of concretes based on the kinetics of the above properties is proposed.
2. The effect of some superplasticizing and mineral additives on the kinetics of autogenous shrinkage is shown.
3. An algorithm is proposed for calculating the stress level in the early (up to 5 days) period of hardening of massive monolithic slab foundations, taking into account autogenous shrinkage and the degree of maturity of concrete at any time. It is shown that failure to take autogenous shrinkage into account, when determining temperature-shrinkage deformations and stresses, can lead to an overestimation of the tensile stress level, depending on the concrete class and the value of autogenous shrinkage by up to 30 % or more.
4. An equation is obtained for the dependence of the tensile stress level on the “center-top” temperature difference for the structures under consideration. Comparison of the calculated values based on the simulation results and the values measured on the real structure showed a difference within 15 %.
5. A conclusion was made about the advisability of limiting the temperature difference “center-top” depending on the required reliability in the range from 20...23 °C to 26...28 °C.

#### References

1. Aniskin, N.A., Nguyen, T.-C. Influence factors on the temperature field in a mass concrete. E3S Web of Conferences. 2019. 97. Article no. 05021. DOI: 10.1051/e3sconf/20199705021
2. Sheng, X., Xiao, S., Zheng, W., Sun, H., Yang, Y., Ma, K. Experimental and finite element investigations on hydration heat and early cracks in massive concrete piers. Case Studies in Construction Materials. 2023. 18. Article no. e01926. DOI: 10.1016/j.cscm.2023.e01926
3. Schackow, A., Eftting, C., Gomes, I.R., Patrui, I.Z., Vicenzi, F., Kramel, C. Temperature variation in concrete samples due to cement hydration. Applied Thermal Engineering. 2016. 103. Pp. 1362–1369. DOI: 10.1016/j.applthermaleng.2016.05.048
4. Dobretsova I.V., Galaktionov D.E. Temperaturnyi rezhim i termonapriazhennoe sostoianie massivnykh zhelezobetonnnykh elementov konstruktiv AES pri ikh vozvedenii [Temperature conditions and thermal stress state of massive reinforced concrete elements of NPP structures during their construction]. Gidroenergetika. Novye razrabotki i tekhnologii [Hydropower. New developments and technologies]. St. Petersburg, 2013. Pp. 55–60.

5. Bjøntegaard, Ø. Basis for and practical approaches to stress calculations and crack risk estimation in hardening concrete structures – State of the art FA 3 Technical performance. SP 3.1 Crack free concrete structures. SINTEF Building and Infrastructure, 2011.
6. Struchkova, A.Y., Barabanshchikov, Yu.G., Semenov, K.S., Shaibakova, A.A. Heat dissipation of cement and calculation of crack resistance of concrete massifs. *Magazine of Civil Engineering*. 2018. 78(2). Pp. 128–135. DOI: 10.18720/MCE.78.10
7. Wu, S., Huang, D., Lin, F., Zhao, H., Wang, P.X. Estimation of cracking risk of concrete at early age based on thermal stress analysis. *Journal of Thermal Analysis and Calorimetry*. 2011. 105. Pp. 171–186. DOI: 10.1007/S10973-011-1512-Y
8. Semenov, K., Barabanshchikov, Yu. Thermal Cracking Resistance in Massive Concrete Structures in the Winter Building Period. *Applied Mechanics and Materials*. 2015. 725–726. Pp. 431–441. DOI: 10.4028/www.scientific.net/AMM.725-726.431
9. Mehta, P.K., Monteiro, P.J.M. *Concrete: Microstructure, properties and materials*. 3<sup>rd</sup> ed. McGraw-Hill. New York, 2006. 239 p. DOI: 10.1036/0071462899
10. Panchenko, A.I., Harchenko, I.Ya., Vasiliev, S.V. Durability of Concretes with Compensated Chemical Shrinkage. *Stroitel'nye Materialy (Construction Materials Russia)*. 2019. 8. 48–53. DOI: 10.31659/0585-430x-2019-773-8-48-53
11. Bentz, D.P., Haecker, C.-J., Hansen, K.K., Jensen, O.M., Oleson, J.F., Stang, H. Influence of Cement Particle-Size Distribution on Early Age Autogenous Strains and Stresses in Cement-Based Materials. *Journal of the American Ceramic Society*. 2001. 84(1). Pp. 129–135.
12. Smolana, A., Klemczak, B., Azenha, M., Schlicke, D. Experiences and analysis of the construction process of mass foundation slabs aimed at reducing the risk of early age cracks. *Journal of Building Engineering*. 2021. 44. Article no. 102947. DOI: 10.1016/j.jobbe.2021.102947
13. Kumarappa, D.B., Peethamparan, S., Ngami, M. Autogenous shrinkage of alkali activated slag mortars: Basic mechanisms and mitigation methods. *Cement and Concrete Research*. 2018. 109. Pp. 1–9. DOI: 10.1016/j.cemconres.2018.04.004
14. Tutkun, B., Barlay, E.S., Yalçınkaya, Ç., Yazıcı, H. Effect of internal curing on shrinkage and cracking potential under autogenous and drying conditions. *Construction and Building Materials*. 2023. 409. Article no. 134078. DOI: 10.1016/j.conbuildmat.2023.134078
15. Wen, S., Li, Y., Yao, G., Cao, M. Effect of calcium carbonate whiskers on the setting behavior, autogenous shrinkage, drying shrinkage, and micro-structure of cement paste. *Journal of Materials Science*. 2024. 59(16). Pp. 7028–7043. DOI: 10.1007/s10853-024-09573-w
16. De Souza, L.O., de Souza, L.M.S., de Andrade Silva, F., Mechtcherine, V. Effect of nanofibrillated cellulose on shrinkage of cement pastes. *Materials and Structures*. 2024. 57(4). Article no. 53. DOI: 10.21203/rs.3.rs-3296733/v1
17. Lingye, L., Wenwen, L., Zhang, C., Pengfei, Z., Tian, W. Influence of temperature rising inhibitor on temperature and stress field of mass concrete. *Case Studies in Construction Materials*. 2023. 18. Article no. e01888. DOI: 10.1016/j.cscm.2023.e01888
18. Tazawa, E., Miyazawa, S. Influence of autogenous shrinkage on cracking in high-strength concrete. 4th International Symposium on Utilization of High Strength/High Performance Concrete. 2. Paris, 1996. Pp. 321–330.
19. Persson, B. Conditions for Carbonation of Durable Silica Fume. 5<sup>th</sup> International Workshop on Material Properties and Design – Durable Concrete Structures. EDIFICATIO Verlag GmbH. Freiburg and Unterengstringen, 1998. Pp. 415–433.
20. Koryanova, Y.I., Nesvetaev, G.V., Chepurmenko, A.S., Sukhin, D.P. On the issue of modeling thermal stresses during concreting of massive reinforced concrete slabs. *Engineering Journal of Don*. 2022. 6.
21. Zeng, Y., Zeng, Y., Jiang, D., Liu, S., Tan, H., Zhou, J. Curing parameters' influences of early-age temperature field in concrete continuous rigid frame bridge. *Journal of Cleaner Production*. 2021. 313. Article no. 127571. DOI: 10.1016/j.jclepro.2021.127571
22. Fairbairn, E.M.R., Silvano, M.M., Toledo Filho, R.D., Alves, J.L.D., Ebecken, N.F.F. Optimization of mass concrete construction using genetic algorithms. *Computers & Structures*. 2004. 82(2–3). Pp. 281–299. DOI: 10.1016/j.compstruc.2003.08.008
23. Wade, S.A., Schindler, A.K., Barnes, R.W., Nixon, J.M. Evaluation of the Maturity Method to Estimate Concrete Strength. ALDOT Research Project 930-590. Highway Research Center and Department of Civil Engineering at Auburn University, 2006. 307 p.
24. Nesvetaev, G.V., Koryanova, Yu.I. Forecasting the Strength Gaining Kinetics of the Concrete Hardening in the Abnormal Conditions. *Modern Trends in Construction, Urban and Territory Planning*. 2023. 2(4). Pp. 59–68. DOI: 10.23947/2949-1835-2023-2-4-59-68
25. Nesvetaev, G.V., Koryanova, Yu.I., Sukhin, D.P. Experimental study of the stress-strain state of a massive reinforced concrete foundation slab in the early period of hardening. *The Eurasian Scientific Journal*. 2023. 15(3). Article no. 17SAVN323.
26. Koenders, E.A.B., van Breugel, K. Numerical modelling of autogenous shrinkage of hardening cement paste. *Cement and Concrete Research*. 1997. 27(10). Pp. 1489–1499. DOI: 10.1016/S0008-8846(97)00170-1
27. Abate, S.Y., Park, S., Kim, H.-K. Parametric modeling of autogenous shrinkage of sodium silicate-activated slag. *Construction and Building Materials*. 2020. 262. Article no. 120747. DOI: 10.1016/j.conbuildmat.2020.120747
28. Smolana, A., Klemczak, B., Azenha, M., Schlicke, D. Early age cracking risk in a massive concrete foundation slab: Comparison of analytical and numerical prediction models with on-site measurements. *Construction and Building Materials*. 2021. 301. Article no. 124135. DOI: 10.1016/j.conbuildmat.2021.124135
29. Semenov, K., Kukolev, M., Zaichenko, N., Popkov, S., Makeeva, A., Amelina, A., Amelin, P. Unsteady Temperature Fields in the Calculation of Crack Resistance of Massive Foundation Slab During the Building Period. *Proceedings of ECECE 2019*. Springer. Cham, 2020. Pp. 455–467.
30. Zhang, J., Zhang, H., Zhao, Y., Xu, W., Su, M., Ge, J., Qiang, S. Relationship between Ambient Temperature and Reasonable Heat Dissipation Coefficient of Mass Concrete Pouring Blocks. *Materials*. 2024. 17(10). Article no. 2187. DOI: 10.3390/ma17102187

**Information about the authors:**

**Grigory Nesvetaev**, Doctor of Technical Sciences

ORCID: <https://orcid.org/0000-0003-4153-1046>

E-mail: [nesgrin@yandex.ru](mailto:nesgrin@yandex.ru)

**Yulia Koryanova**, PhD in Technical Sciences

ORCID: <https://orcid.org/0000-0002-2341-9811>

E-mail: [koryanova.yi@mail.ru](mailto:koryanova.yi@mail.ru)

**Batyr Yazyev**, Doctor of Technical Sciences

ORCID: <https://orcid.org/0000-0002-5205-1446>

E-mail: [ps62@yandex.ru](mailto:ps62@yandex.ru)

Received: 07.06.2024. Approved after reviewing: 16.09.2024. Accepted: 17.09.2024.



Research article

UDC 626


DOI: 10.34910/MCE.130.6



## Response spectra at elevations of station dam equipment installation

G.L. Kozinetc , P.V. Kozinetc, V.L. Badenko 

Peter the Great St. Petersburg Polytechnic University, St. Petersburg, Russian Federation

 [kozinets\\_gl@spbstu.ru](mailto:kozinets_gl@spbstu.ru)

**Keywords:** concrete station dam, rock foundation, earthquake, natural frequency, waveform, finite element method, response spectrum, equipment

**Abstract.** The object of the study is a concrete station dam of a run-of-river hydroelectric power plant (HPP). A review of publications on the methods of calculating the dynamic responses of structures is presented. The calculation studies were carried out using the finite element method. The initial data for the calculation are the physical characteristics of the concrete material, steel and rock foundation, the geometric parameters of the dam obtained as a result of engineering surveys and strength calculations of the structure. To determine the natural frequencies and vibration modes of the station dam, eight dynamic calculations of the structure and foundation system were performed for eight design nodes at the equipment installation marks. An analysis is presented describing the dam vibrations and response spectra at the equipment installation marks of the station dam. The issues of strength and stability of the station dam are not included in this study, but were taken into account when determining the geometric dimensions of the structure. To calculate the response spectra at the structure marks, a finite element model of the “structure-foundation” station dam of the Nizhne-Bureyskaya HPP was built. The construction of the calculation model was based on the geometric and physical parameters of the station dam and foundation. The accelerogram is selected in accordance with the design period of the station dam of the Nizhne-Bureyskaya HPP, which is 0.23 sec. It corresponds to the first form of oscillations with a frequency of 4.43 Hz. Using the calculated accelerogram, eight dynamic calculations of the “structure-foundation” system were performed for eight calculated nodes at the elevations of the HPP equipment installation. The solution of the equations of motion with decomposition by the initial oscillation forms was performed for each of the eight calculated nodes. The calculated nodes were determined based on the condition of the location of the HPP equipment on them.

**Citation:** Kozinetc, G.L., Kozinetc, P.V., Badenko, V.L. Response spectra at elevations of station dam equipment installation. Magazine of Civil Engineering. 2024. 17(6). Article no. 13006. DOI: 10.34910/MCE.130.6

### 1. Introduction

The object of the research is a concrete station dam of a run-of-river hydroelectric power plant (HPP), which is part of the main structures of HPPs. A special feature of HPPs is the presence of numerous equipment located at various elevations. Thus, mechanical and crane equipment is located at the water intake marks of the HPP. The water intake valves are closed in case of repair of the hydraulic unit. Turbine and transformer equipment is located at the elevations of the turbine room of the HPP. At the outlet marks of the HPP, there is mechanical and crane equipment for the outlet pipes. The outlets are closed during repair of the turbine equipment.

The concrete station dam ensures the supply of water to hydraulic units through a water intake device. The station structure consists of a water intake part of the dam, a water supply path, which includes

a spiral chamber and suction pipes. On the upstream side of the HPP, there is a water intake part, on the downstream side, there are rear HPPs and a part of the dam that drains water from the hydraulic units. Lifting mechanisms are mounted on the bulls, designed to block the water intake openings. There is a lot of equipment located at the station dam elevations; therefore, it is mandatory to calculate the seismic load on this equipment.

When designing a station dam in zones of seismic activity, response spectra are calculated at various elevations of equipment installation. The action of seismic waves causes vibrations of the structure. The higher the mark, the stronger the amplitude of the oscillations.

A feature of calculating the response spectrum of a station dam is that the model considers several factors, such as the presence of a soil foundation in the model and the effect of water on the pressure face of the dam.

In the scientific literature, there are several studies of the seismic response of hydraulic structures to dynamic loads using numerical modeling methods.

The article [1] presents an analysis of response spectra, which estimates the peak response directly from the calculated earthquake spectrum. The study includes the effects of dam interactions with water and foundation, which are known to play an important role in the response of a dam to an earthquake. This paper provides a comprehensive assessment of the accuracy of the response spectrum studies by comparing them with the results obtained from monitoring the response spectrum of a dam. The modeling was carried out using the finite element method, including a dam-water-foundation model. A comparison of the results showed that the response spectrum procedure estimates stresses with a satisfactory degree of accuracy for the preliminary design stage of new dams and safety assessment of existing dams.

The article [2] is devoted to the analysis of the safety of concrete dams. Most existing station dams were designed without taking into account their dynamic behavior; therefore, monitoring their condition is of great importance to determine the appropriate safety level. This study provides a framework for dynamic monitoring of the structural health of concrete station dams under changing operating conditions.

The paper [3] presents an analysis of the dimensions of the foundation base in the dam-foundation-reservoir system. The study applied the finite element method to model mass, damping and wave propagation effects in foundations of dam-foundation-reservoir systems using ABAQUS software. The boundary condition is used to model the semi-infinite foundation and damping. Various mechanisms for modeling foundations, earthquake impacts, and boundary conditions in a given area are described. The implementation of the boundary condition in the program by the finite element method is verified by comparing it with the analytical results.

The article [4] presents a practical methodology with an example of determining the seismic resistance of concrete gravity dams using nonlinear seismic analysis from an accelerogram using simulation. Nonlinear seismic analysis is performed for ten tests at multiple ground motion levels until each test indicates an error. The ground motion variable includes ten sets of acceleration time histories obtained from actual earthquake records and mapped to a target response spectrum.

Many articles and books are devoted to the methods for numerically solving the problems of structure dynamics [5–9]. Among the scientists who studied seismic resistance and dynamic characteristics of structures, it is worth noting the works of Ya.M. Aizenberg, S.P. Timoshenko, L.A. Rozin [10].

The aim of the study is to determine the natural frequencies and analyze the vibration modes of the station dam, as well as to calculate the response spectra for further analysis of the seismic resistance of the equipment [11–13].

The study was carried out based on a model of the Nizhne-Bureyskaya HPP dam with a rock foundation (Fig. 1).

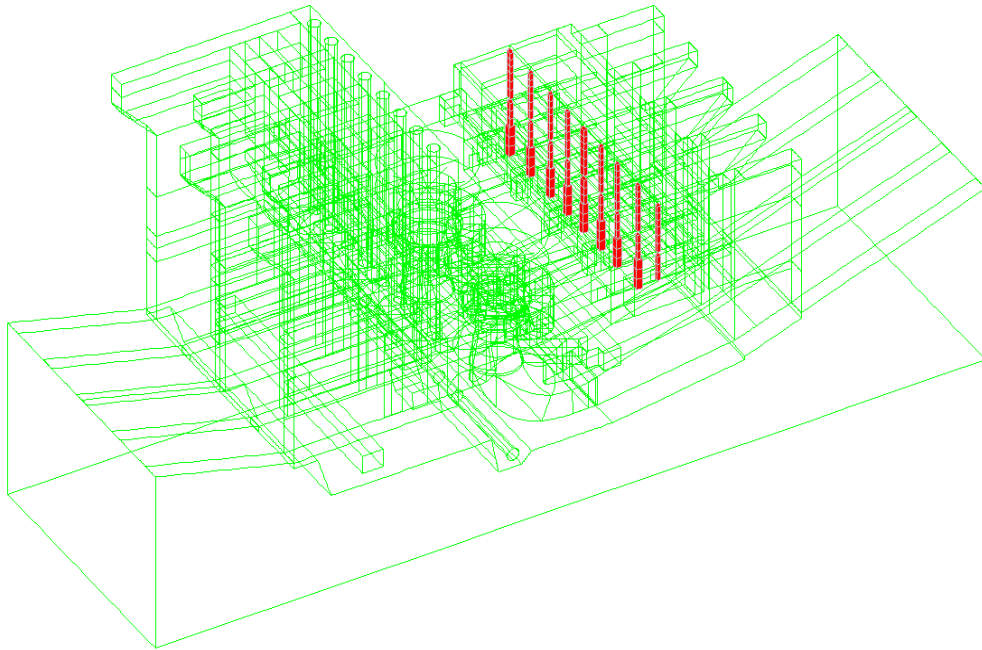


**Figure 1. Three-dimensional geometric model of a station dam with a base.**

## 2. *Materials and Methods*

The method describes the procedure for calculating seismic load response spectrum for equipment located at the station dam levels.

To calculate the response spectra at the elevations of the structure, a finite element “structure-foundation” model of the station dam of the Nizhne-Bureyskaya HPP was constructed. The “structure-foundation” model was divided into three-dimensional 4-node elements of the tetrahedron – TETRA, interconnected at the nodes. Coordinate system: OX axis – along the flow, OZ axis – across the flow, OY axis – vertically upward.

The calculation area was automatically divided into the following elements:

- The maximum size of a rock foundation element is 4 m.
- The maximum size of a concrete structure element is 1.5 m.
- In the areas where the rock foundation and concrete structure are connected, the grid has been increased to 1 m.
- Number of model nodes: 877615.

Description of boundary conditions:

- The nodes on the lower edge of the rock foundation are secured against movement and rotation along all axes.
- The nodes on the vertical faces of the rock foundation are secured against movement in the direction perpendicular to each face.
- The dimensions of the foundation soil are selected vertically to the depth of solid rocks without cracks. The depth of the soil layer is 30 m.
- The problem is solved in an elastic setting.

The issues of strength and stability of the station dam are not included in this study, but were taken into account when determining the geometric dimensions of the structure, which were used as input data for this work.

Computational studies were carried out within the framework of the spatial formulation of the problem by the finite element method [14–17] using the SolidWorks program. The method and its application in structural calculations are presented in [18–23]. The methodology for monitoring the condition of structures is presented in [24]. The calculation model was constructed on the basis of the geometric and physical parameters of the station dam and the foundation. The calculated model of the structure is presented in Fig. 2.

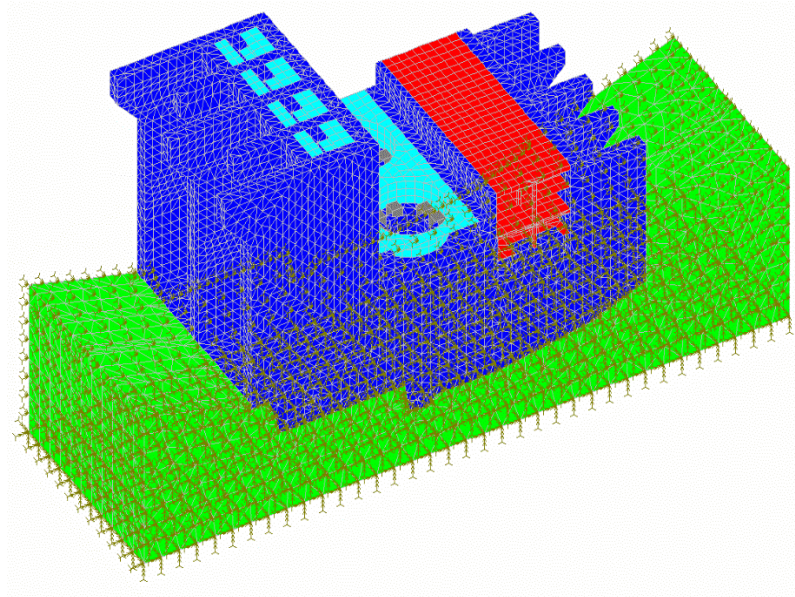


**Figure 2. Finite element calculation model of a station dam with boundary conditions.**

The initial data for the calculation are the physical characteristics of the material of concrete, steel and rock foundation, the geometric parameters of the station dam of the Nizhne-Bureyskaya HPP on the Bureya River, obtained as a result of engineering surveys and calculations of the strength of the structure. For dynamic calculations, an accelerogram of the dynamic seismic impact was used, obtained by the results of microseismic zoning at the station dam construction site.

The main objectives of the study are as follows:

1. Construction of a mathematical dynamic model “dam-foundation” of the station dam of the Nizhne-Bureyskaya HPP, including geometric construction, division into finite elements, setting the material properties and boundary conditions.
2. Determination of natural frequencies and vibration modes of the station dam. In this case, the calculation period corresponding to the first form of oscillation was determined. Based on the calculated period, a 3-component calculated accelerogram of the seismic impact was selected, in which the predominant period along the horizontal component G1 corresponded to the calculated period of the station dam.
3. Dynamic calculation based on the selected calculated 3-component accelerogram.
4. Calculation of response spectra at given nodes at the station dam marks and construction of graphs of response spectra at given nodes and tables of digitization of spectral curves.

### 3. Results and Discussion

#### **First stage of research**

Fig. 2 shows the finite element calculation model of the structure, together with the foundation. Boundary conditions are specified on the model.

#### **Physical characteristics of materials**

The station dam is made of hydraulic concrete class B20. Calculated resistance of concrete under compression  $R_b = 11700$  kPa and tension  $R_{bt} = 900$  kPa for the limit states of the first group.

Modulus of elasticity of concrete in compression and tension  $E_b = 3 \times 10^7$  kPa. The coefficient of transverse deformation of concrete (Poisson's ratio) for massive structures  $\nu = 0.15$ . Density of concrete  $\rho_b = 2.36$  t/m<sup>3</sup>.

The metal frame of the HPP building is welded from sheet steel 09G2S GOST 19281–2014 (similar to DIN 13Mn6, JIS SB49, GB 12Mn).

Density  $p = 7.85$  t/m<sup>3</sup>.

Modulus of elasticity  $E = 2.1 \times 10^8$  kPa.



Poisson's ratio  $\nu = 0.2$ .

Thermal expansion coefficient  $\alpha = 1.2 \times 10^{-5} \text{ } ^\circ\text{C}^{-1}$ .

The rock foundation is composed of granites. Physical and mechanical properties and thermophysical characteristics of granite rock foundation are:

Density  $\rho = 2.65 \text{ t/m}^3$ .

Elastic modulus  $E = 1.3 \times 10^7 \text{ kPa}$ .

Poisson's ratio  $\nu = 0.35$ .

Adhesion  $c = 400 \text{ kPa}$ . Angle of internal friction  $\phi = 39^\circ$ .

Thermal expansion coefficient  $\alpha = 1.4 \times 10^{-5} \text{ } ^\circ\text{C}^{-1}$ .

### Second stage of research

At the next stage, the calculation of the natural frequencies and vibration modes of the structure with the foundation was carried out.

In this calculation, the first 50 natural frequencies of the dam-foundation were obtained from 4.43 to 24.24 Hz (from 27.84 to 152.24 rad/sec). The first natural waveform with a frequency of 4.43 Hz is shown in Fig. 3.

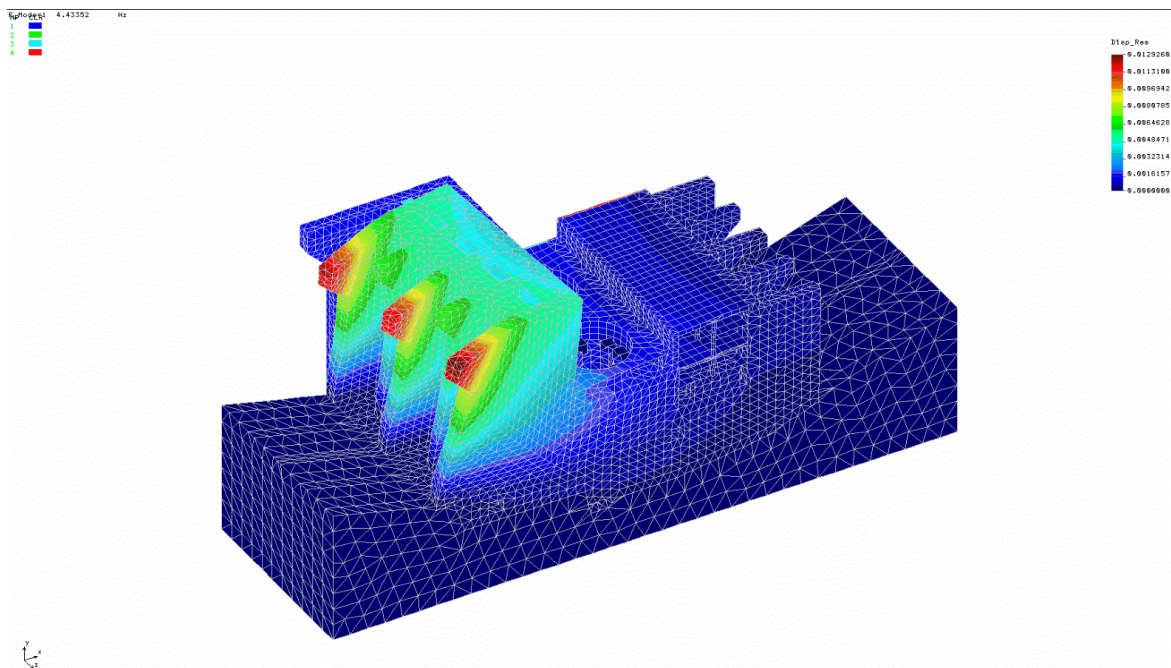


**Figure 3. The first natural mode of vibration with frequency  $f = 4.43 \text{ Hz}$ . General oscillations of the water intake part of the station dam with shift and rotation of the bulls across the flow.**

Calculation period  $T$  corresponding to the first mode of dam vibrations with frequency  $f = 4.43 \text{ Hz}$  amounts to  $T = 0.23 \text{ sec}$ .

$$T = \frac{1}{f} = \frac{1}{4.43} = 0.23 \text{ sec} . \quad (1)$$

The response spectra at the equipment installation marks were determined using a calculated three-component accelerogram for the MPE (maximum probable earthquake) level of 7 points at the station dam site of the Nizhne-Bureyskaya HPP (Fig. 4).

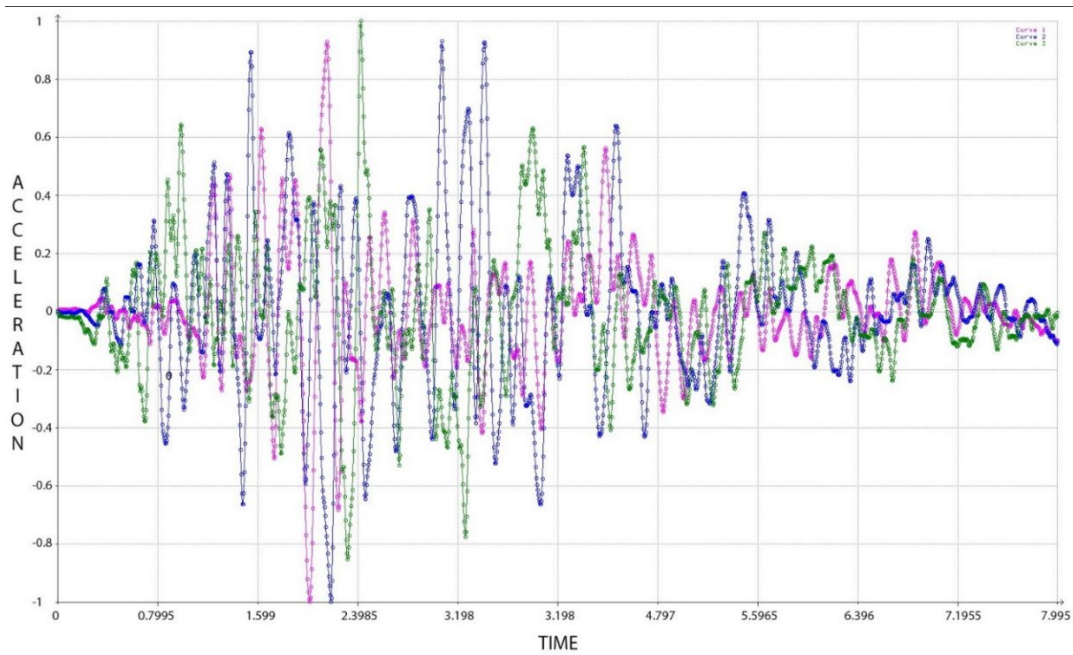


**Figure 4. Calculated three-component accelerogram [25]: red line – horizontal component G1, along the OX axis; blue line – horizontal component G2, along the OZ axis; green line – vertical component B1, along the OY axis.**

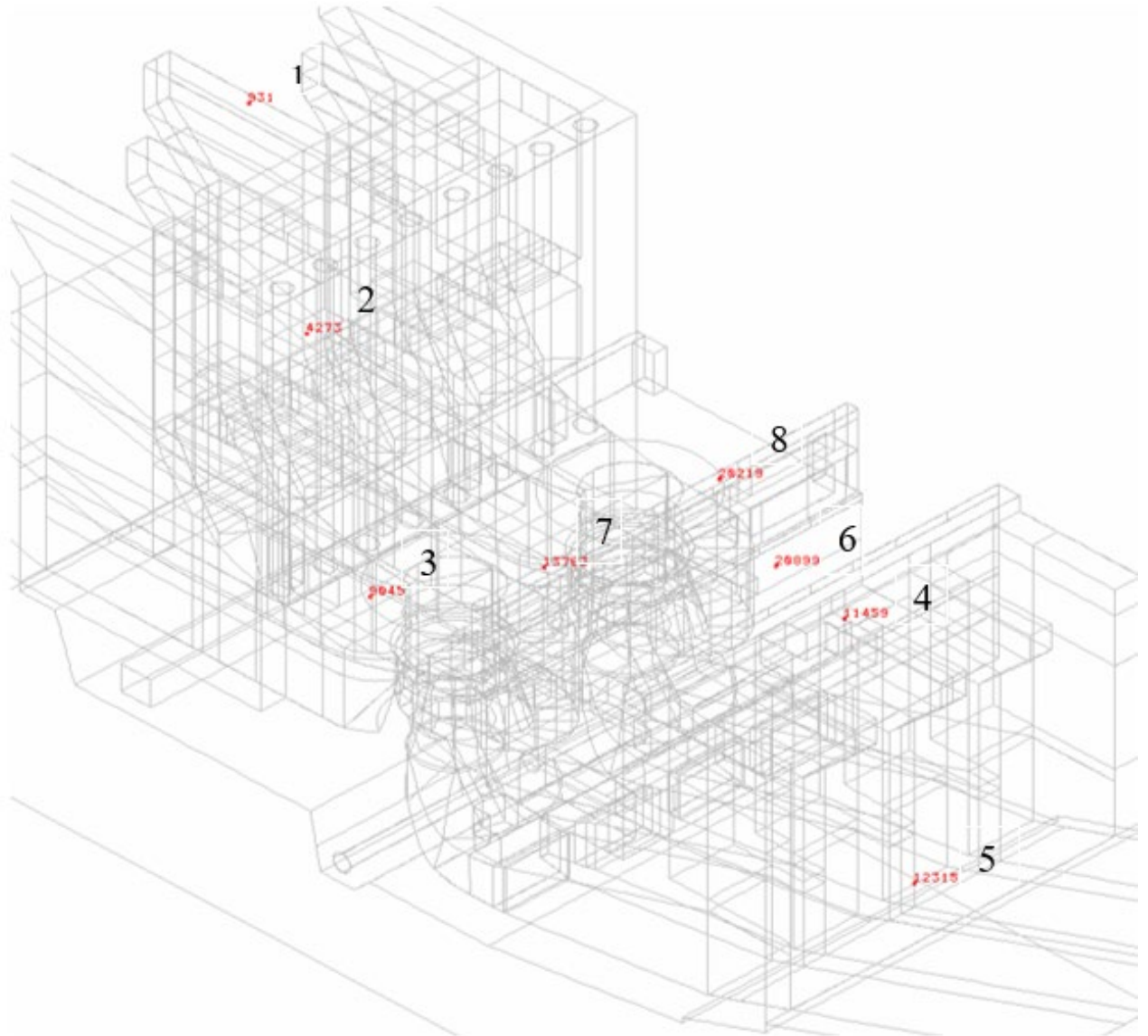
The choice of this accelerogram was made in accordance with the calculated period of the station dam of the Nizhne-Bureyskaya HPP, which is 0.23 sec, which corresponds to the first form of oscillation with a frequency of 4.43 Hz.

The predominant period for the horizontal component G1 is 0.24 sec, G2 is 0.16 sec, for the vertical component is 0.26 sec.

### ***Third stage of research***

Using the calculated accelerogram, eight dynamic calculations of the structure-foundation system were performed for eight calculation nodes at the installation marks of HPP equipment. The solution of the equations of motion with expansion in terms of the initial vibration modes was performed for each of the eight calculated nodes. The calculated nodes are determined from the conditions for the location of HPP equipment on them, Fig. 5.

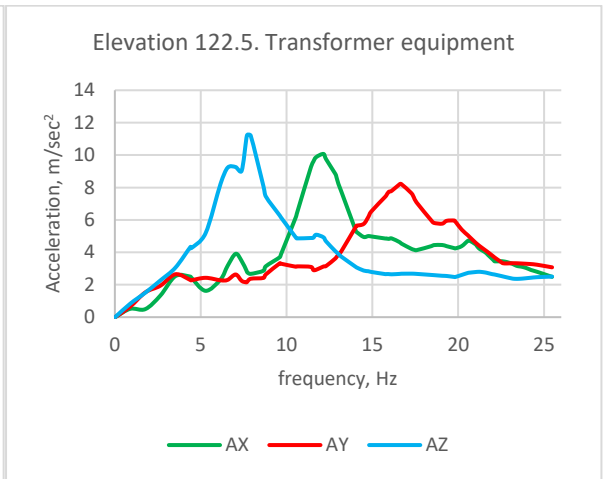
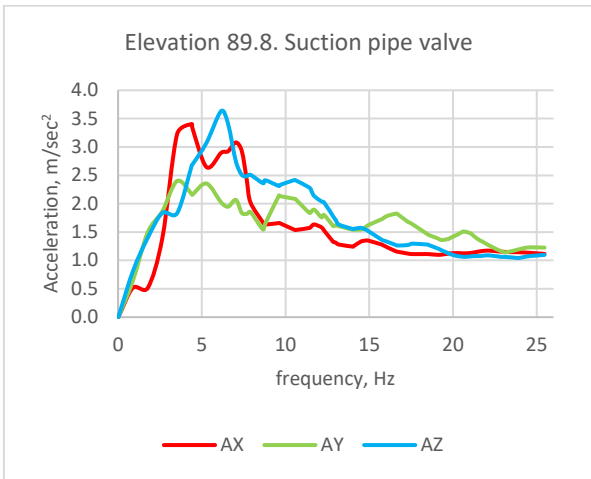
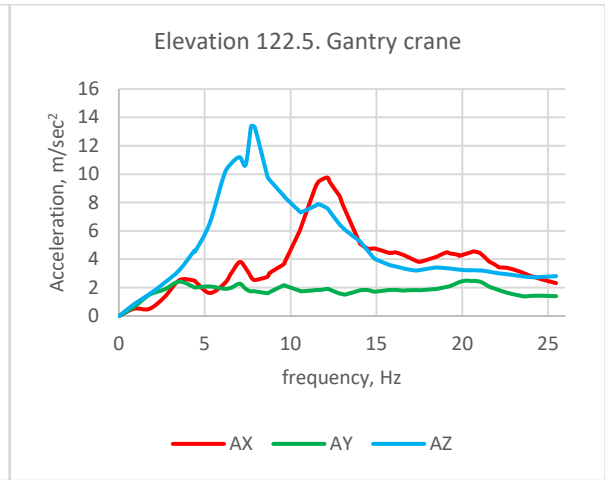
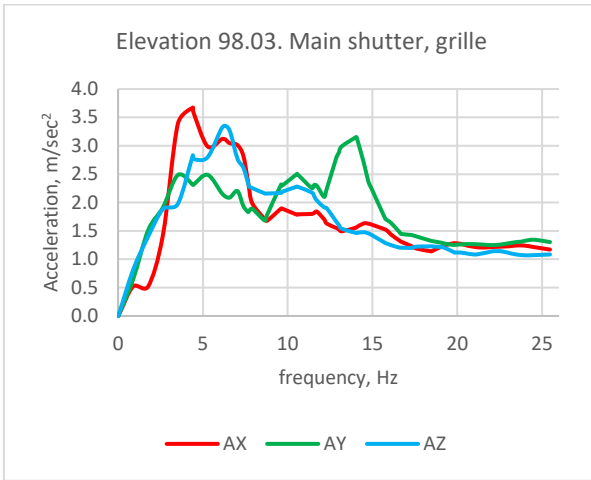
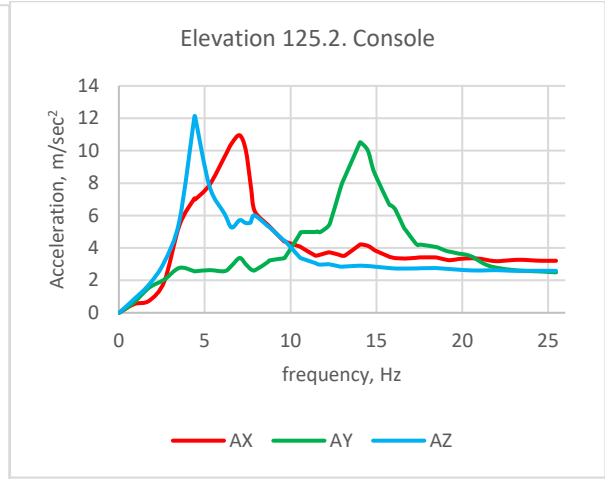
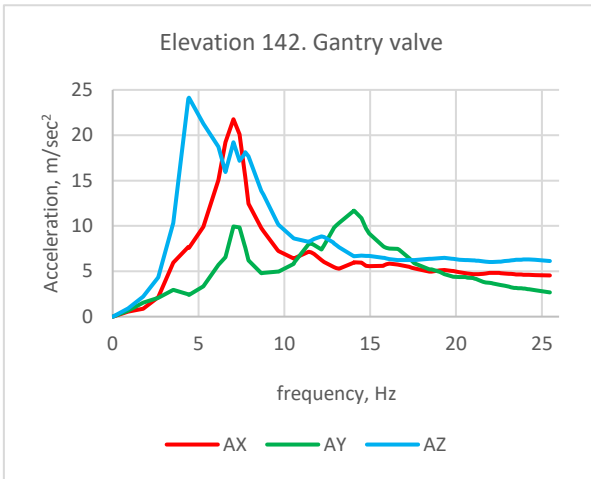
1. Gantry valve, water inlet, elevation 142, node 931;
2. Console, water inlet, elevation 125.2, node 4273;
3. Main shutter, grate, water inlet, elevation 98.03, node 9045;
4. Gantry crane, suction pipes, elevation 122.5, node 11459;
5. Main valve, suction pipes, elevation 89.8, node 12315;
6. Transformer equipment, transformer site, elevation 122.5, node 20899;
7. Stator support, power unit, elevation 111.535, node 13763;
8. Spacer jack support, aggregate block, elevation 114.8, node 20219.



**Figure 5. Equipment at station dam marks.**

***Fourth stage of research***

Floor-by-floor response spectra were calculated at the installation marks of the station dam equipment, and graphs of acceleration  $m/sec^2$  versus frequency Hz were obtained along all three axes (Fig. 6). Three-component spectral curves are presented. Table 1 shows the maximum acceleration values and the corresponding frequencies at the equipment installation marks for two horizontal AX and AZ and one vertical AY axes. The resulting spectra can be used to calculate equipment installed at the station dam elevations.



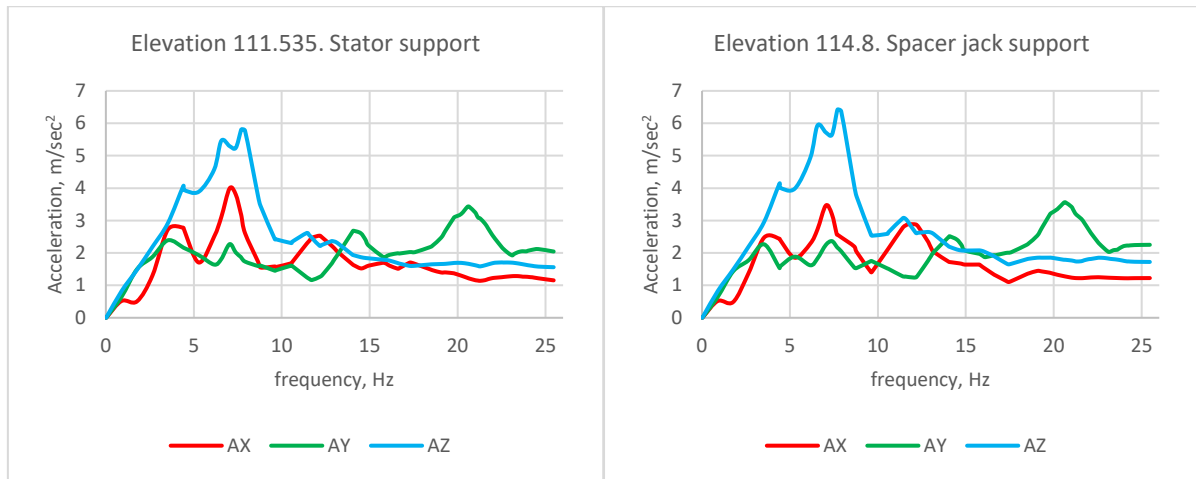


**Figure 6. Response spectra at station dam elevations. Dependence of acceleration  $m/sec^2$  on frequencies Hz: red line – horizontal accelerations AX (along the flow); green line – vertical accelerations AY; blue line – horizontal accelerations AZ (across the flow).**

**Table 1. Maximum acceleration values and corresponding frequencies at equipment installation marks.**

№	Equipment name	Mark on the structure	Acceleration $m/sec^2$ , Frequency Hz	Acceleration $m/sec^2$ , Frequency Hz	Acceleration $m/sec^2$ , Frequency Hz
			AX; FX	AZ; FY	AY; FZ
1	Gantry valve, water inlet	Elevation 142	7; 21.8	14; 11.7	4.4; 24
2	Console, water inlet	Elevation 125.2	7; 11	14.1; 10.5	4.4; 12.1
3	Main shutter, grille, water inlet	Elevation 98.03	4.4; 3.6	14; 3.2	6.2; 3.3
4	Gantry crane, suction pipes	Elevation 122.5	12.2; 9.8	3.5; 2.4	7.9; 13.3
5	Main valve, suction pipes	Elevation 89.8	4.4; 3.4	3.5; 2.4	4.4; 3.4
6	Transformer equipment, transformer site	Elevation 122.5	17.3; 7.7	12.3; 9.7	7.9; 11.2
7	Stator support, power unit	Elevation 111.535	7.4; 3.8	21.2; 3.1	7.7; 5.8
8	Spacer jack support, power unit	Elevation 114.8	7; 3.5	20.7; 3.6	7.7; 6.3

The parameters of the selected accelerogram are consistent with the research data of [12], in which, during an earthquake greater than 7 points, the prevailing period  $T$  multiplied by the peak acceleration  $A_{max}$  and the corresponding time  $t$  can be described by the parameter  $B$ , which is determined by the earthquake magnitude.

$$B = A_{max} g T \tau = 0.95 \times 9.81 \times 0.24 \times 2 = 4.47 \text{ m} = 447 \text{ cm} . \quad (2)$$

For our study, parameter  $B$  is equal to 447 cm, which corresponds to a magnitude of 6.5 points, which is the calculated magnitude for the design area of the Nizhne-Bureyskaya HPP with a MPE level of 7 points.

Thus, when comparing the results of the study with the data of [12], the reliability of the determination of the accelerogram parameters used to calculate the response spectra of the concrete dam of the HPP is confirmed.

#### 4. Conclusions

- Calculations of the response spectra at the installation elevations of mechanical equipment corresponding to the seismic impact of a MPE level of 7 points were performed. The calculations of

the response spectra were used in the designs of the mechanical equipment of the Nizhne-Bureyskaya HPP, performed at JSC Lengidrostal.

10. The response spectra of the floors represent the calculated seismic load for each unit of equipment installed at the elevations of the station dam. The response spectra at the elevations were the calculated seismic load for the equipment of JSC Power Machines. As a result of the study, the points of the design area's estimated magnitude were found to correspond to the research data of Academician A.I. Savich et al.
11. The scientific novelty lies in the presented and implemented method for calculating the response spectra determined at the equipment installation marks, considering the choice of parameters of the estimated accelerogram.

## References

1. Løkke, A., Chopra, A.K. Response Spectrum Analysis of Concrete Gravity Dams Including Dam-Water-Foundation Interaction. *Journal of Structural Engineering*. 2015. 141(8). Article no. 04014202. DOI: 10.1061/(ASCE)ST.1943-541X.0001172
2. Sevieri, G., De Falco, A. Dynamic structural health monitoring for concrete gravity dams based on the Bayesian inference. *Journal of Civil Structural Health Monitoring*. 2020. 10(2). Pp. 235–250. DOI: 10.1007/s13349-020-00380-w
3. Mohammadnezhad, H., Ghaemian, M., Noorzad, A. Seismic analysis of dam-foundation-reservoir system including the effects of foundation mass and radiation damping. *Earthquake Engineering and Engineering Vibration*. 2019. 18. Pp. 203–218. DOI: 10.1007/s11803-019-0499-4
4. Ghanaat, Y., Patev, R.C., Chudgar, A.K. Seismic fragility analysis of concrete gravity dams. *Proceedings of the 15<sup>th</sup> World Conference on Earthquake Engineering*, Lisbon, 24–28 September 2012.
5. Rybakov, V., Jos, V., Raimova, I., Kudryavtsev, K. Modal analysis of frameless arches made of thin-walled steel profiles. *IOP Conference Series: Materials Science and Engineering*. 2020. 883. Article no. 012197. DOI: 10.1088/1757-899X/883/1/012197
6. Zarubin, P.E., Baranovskij, M.Yu., Tarasov, V.A. Tekla Structures – is innovation of structures's calculation. *Construction of Unique Buildings and Structures*. 2013. 5(10). Pp. 1–8.
7. Kozinec, G.L. Generalization of the Methodology of Studying the Durability of Segmental Gates. *Power Technology and Engineering*. 2018. 52(4). Pp. 395–399. DOI: 10.1007/s10749-018-0964-7
8. Verret, D., LeBoeuf, D. Dynamic characteristics assessment of the Denis-Perron dam (SM-3) based on ambient noise measurements. *Earthquake Engineering & Structural Dynamics*. 2022. 51(3). Pp. 569–587. DOI: 10.1002/eqe.3580
9. Arbain, A., Ahmad Mazlan, A.Z., Zawawi, M.H., Mohd Radzi, M.R. Vibration Analysis of Kenyir Dam Power Station Structure Using a Real Scale 3D Model. *Civil and Environmental Engineering Reports*. 2019. 29(3). Pp. 48–59. DOI: 10.2478/ceer-2019-0023
10. Rozin, L.A., Chernysheva, N.V. Algorithm of combined method of 3D analysis for the boundary problems in infinite medium. *Materials Physics and Mechanics*. 2017. 31(1–2). Pp. 82–85.
11. Savich, A.I., Bronshtein, V.I., Groshev, M.E., Gaziev, E.G., Il'in, M.M., Rechitskii, V.I., Rechitskii, V.V. Sticheskoie i dinamicheskoe povedenie Saiano-SHushenskoj arochno-gravitatsionnoj plotiny [Static and dynamic behavior of the Sayano-Shushenskaya arch-gravity dam]. *Gidrotekhnicheskoe Stroitel'stvo*. 2013. 3. Pp. 2–13.
12. Savich, A.I., Burdina, N.A. On the Relationships between the Fundamental Parameters of Calculation Accelerograms. *Power Technology and Engineering*. 2016. 50. Pp. 38–47. DOI: 10.1007/s10749-016-0656-0
13. Rybakov, V., Lalin, V., Pecherskikh, M., Saburov, D. Accounting for rotational inertia in calculating structures for seismic impact. *AIP Conference Proceedings*. 2023. 2612(1). Article no. 040034. DOI: 10.1063/5.0113989
14. Pereira, S., Magalhães, F., Gomes, J.P., Cunha, Á., Lemos, J.V. Dynamic monitoring of a concrete arch dam during the first filling of the reservoir. *Engineering Structures*. 2018. 174. Pp. 548–560. DOI: 10.1016/j.engstruct.2018.07.076
15. Gordan, B., Raja, M.A., Armaghani, D.J., Adnan, A. Review on Dynamic Behaviour of Earth Dam and Embankment during an Earthquake. *Geotechnical and Geological Engineering*. 2022. 40. Pp. 3–33. DOI: 10.1007/s10706-021-01919-4
16. Chen, J., Jia, Q., Xu, Q., Fan, S., Liu, P. The PDEM-based time-varying dynamic reliability analysis method for a concrete dam subjected to earthquake. *Structures*. 2021. 33. Pp. 2964–2973. DOI: 10.1016/j.istruc.2021.06.036
17. Boulanger, R.W. Nonlinear Dynamic Analyses of Austrian Dam in the 1989 Loma Prieta Earthquake. *Journal of Geotechnical and Geoenvironmental Engineering*. 2019. 145(11). Article no. 05019011. DOI: 10.1061/(ASCE)GT.1943-5606.0002156
18. Wang, J.-T., Jin, A.-Y., Du, X.-L., Wu, M.-X. Scatter of dynamic response and damage of an arch dam subjected to artificial earthquake accelerograms. *Soil Dynamics and Earthquake Engineering*. 2016. 87. Pp. 93–100. DOI: 10.1016/j.soildyn.2016.05.003
19. Miquel, B., Bouaanani, N. Accounting for Earthquake-Induced Dam-Reservoir Interaction Using Modified Accelerograms. *Journal of Structural Engineering*. 2013. 139(9). Pp. 1608–1617. DOI: 10.1061/(ASCE)ST.1943-541X.0000726
20. Zacchei, E., Molina, J.L. Application of artificial accelerograms to estimating damage to dams using failure criteria. *Scientia Iranica*. 2020. 27(6). Pp. 2740–2751. DOI: 10.24200/sci.2018.50699.1824
21. Rebez, A., Sandron, D., Santulin, M., Peruzza, L., Tamaro, A., Eusebio, M., Mucciarelli, M., Slejko, D. Input accelerograms and expected accelerations for some dam sites in southern Italy. *Proceedings of the 33<sup>rd</sup> Conference of the National Solid Earth Geophysics Group (NGTGS)*, Bologna, 25–27 November 2014. 2. Caratterizzazione sismica del territorio. Centro Stampa della Regione Emilia-Romagna. Bologna, 2014. Pp. 48–57.
22. Alegre, A., Carvalho, E., Matsinhe, B., Mendes, P., Oliveira, S., Proença, J. Monitoring vibrations in large dams. *HYDRO2019. Concept to Closure: Practical Steps*. 2019.
23. Aliberti, D., Cascone, E., Biondi, G. Seismic Performance of the San Pietro Dam. *Procedia Engineering*. 2016. 158. Pp. 362–367. DOI: 10.1016/j.proeng.2016.08.456
24. Badenko, V., Volgin, D., Lytkin, S. Deformation monitoring using laser scanned point clouds and BIM. *MATEC Web of Conferences. International Scientific Conference on Energy, Environmental and Construction Engineering (EECE-2018)*. 2018. 245. Article no. 01002. DOI: 10.1051/mateconf/201824501002

25. Kozinetc, G.L., Kozinetc, P.V. The calculation of the dynamic characteristics of the spillway of the dam. Magazine of Civil Engineering. 2022. 113(5). Article no. 11312. DOI: 10.34910/MCE.113.12

**Information about the authors:**

**Galina Kozinetc**, Doctor of Technical Sciences

E-mail: [kozinets\\_gl@spbstu.ru](mailto:kozinets_gl@spbstu.ru)

**Pavel Kozinetc**

E-mail: [pavelkozinetc@yandex.ru](mailto:pavelkozinetc@yandex.ru)

**Vladimir Badenko**, Doctor of Technical Sciences

ORCID: <https://orcid.org/0000-0002-3054-1786>

E-mail: [vbadenko@gmail.com](mailto:vbadenko@gmail.com)

Received: 26.07.2024. Approved after reviewing: 19.09.2024. Accepted: 29.09.2024.



Research article

UDC 624.131

DOI: 10.34910/MCE.130.7



## Filtration calculation to reduce the construction impact on hydrogeological conditions in the city

I.V. Glazunova<sup>1</sup> , S.A. Sokolova<sup>1</sup> , M.A. Shiryayeva<sup>2</sup> 

<sup>1</sup> Moscow Timiryazev Agricultural Academy, Moscow, Russian Federation

<sup>2</sup> F.F. Erisman Federal Scientific Center of Hygiene of Rospotrebnadzor, Moscow, Russian Federation

✉ [ivglazunova@mail.ru](mailto:ivglazunova@mail.ru)

**Keywords:** civil engineering, filtering features, grounds, water table, drainage, construction, plot, dewatering

**Abstract.** The paper presents the results of the research conducted to justify construction works within the intensively developed and still developing city area. The study area was located structurally and tectonically within the lowered part of the grabens bounded by regional gaps. The second from the surface aquifer was confined. The aim of the research was to evaluate the effect of lowering of the water table during construction work and laying utility lines on the filtration properties of soils, as well as on existing buildings and highways. Analytical dependencies for the infinite linear perturbation source scheme in an infinite soil layer were proposed and improved. The conducted modeling showed that the estimated maximum depression at the design point under the multi-storey non-residential administrative building was 4.4 m, which was less than the maximum allowable deformations. It was revealed that the maximum water inflows were observed at lowering of water table over the entire limited area of 20–40 m length simultaneously; therefore, the obtained analytical solution should be increased by 22.4 %. It was found that the average discharges depend proportionally on the amount of subsidence in the water table lowering area, with the relationship between the average discharges being linear regardless of the design scheme. The building subsidence due to water table lowering was calculated and a model for geofiltration calculations was developed in Microsoft Excel. The model calculations showed that the maximum subsidence of the soil at the design point of the multi-storey non-residential administrative building did not exceed the maximum allowable deformation values.

**Citation:** Glazunova, I.V., Sokolova, S.A., Shiryayeva, M.A. Filtration calculation to reduce the construction impact on hydrogeological conditions in the city. Magazine of Civil Engineering. 2024. 17(6). Article no. 13007. DOI: 10.34910/MCE.130.7

### 1. Introduction

The studied area is structurally and tectonically located within the lowered part of the grabens bounded by regional gaps.

The constructed site is located within the valleys of small rivers flowing through the city. In particular, on the site along the construction of the city highway, there are also small basins of small rivers. It should be noted that within the floodplains of small rivers, with shallow bedding of the moraine roof and insignificant thickness of fluvio-glacial deposits, the area becomes waterlogged. Therefore, the problem of assessing and predicting changes in the filtration properties of soils in conditions of intensive urban development is relevant.



When considering the situation in the modern scientific community, it is revealed that the closest to this issue are the researches of Prof. V.V. Vedernikov in the field of water regime forecasting in the aeration zone. In our study, in contrast to the above study, differential nonlinear equations with specified parameters of the range of application area are used [1].

As an aside from the previously considered hydrogeological conditions of urban areas development (M.V. Bolgov et al.), large megapolis with dense building are characterized by more intensive development and frequent reconstruction of both roads and buildings, which must be taken into account when calculating filtration flows in construction [2].

Most works in the considered research area (S.F. Aver'anov, I.S. Pashkovskii, etc.) consider agricultural areas and the impact of irrigated and drained meliorations on filtration flows in soils without an emphasis on built-up areas [3, 4].

Various types of construction work, civil engineering and laying of utility lines substantially affect changes in hydrogeological conditions and, in particular, the water regime, which, in turn, has a significant impact on the subsidence and deformation of buildings [5–8]. This is especially relevant when laying utility lines in urbanized areas. One of the most important problems and practical tasks at construction sites and when laying utilities, when designing hydraulic structures, linear engineering systems, etc. is the prediction of the water regime in the aeration zone and the groundwater regime. Therefore, the assessment of the filtration calculation to reduce the factors of the impact of utility lines on hydrogeological conditions within the urban districts is relevant, especially in the constantly changing conditions of urban development and reconstruction of cities.

The aim of the research is to evaluate the filtration calculations of water lowering during construction works on utility lines in the watersheds of the small rivers within the built-up urban area to reduce the factors of the impact of utility lines on the hydrogeological conditions within urban districts.

Such tasks as modeling to reveal patterns of changes in the subsidence of buildings depending on the water table were considered.

## 2. *Material and Methods*

The research was conducted to justify construction works in the territory of megapolis on the example of some districts of Moscow.

This structural depression includes structural-erosive valleys of the Moscow River of different ages [9–13]. Geomorphologically, the area under consideration lies within the plain of fluvioglacial interflaves. This part of the upland is characterized by smooth relief forms with indistinct watersheds of small rivers, with absolute surface elevations of 150–190 m and relative elevations above the flat depressions of 5–10 m, which were previously waterlogged.

The hydrogeological conditions of the area under consideration within the upper part of the section are characterized by the presence of three aquifers: supra-moraine, Upper Jurassic and Upper Carboniferous (Fig. 1).

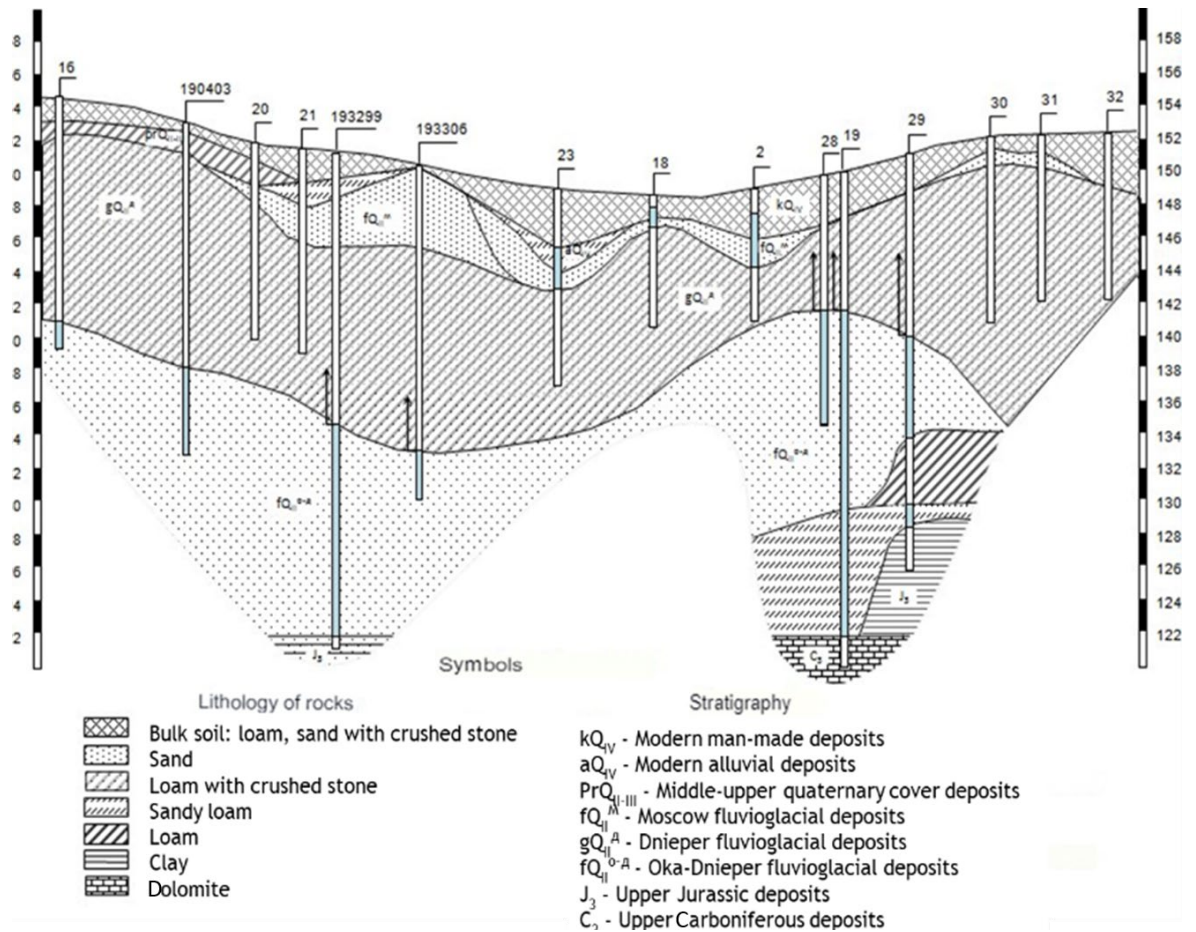


**Figure 1. Geological and hydrogeological cross-section (the figure was compiled by the authors based on the results of some studies, expertise and other data from various free resources).**

The upland aquifer is the first from the surface at a depth of 1–4 m, is partially distributed and is characterized by sandy deposits above the upper part of moraine and low filtration properties of moraine deposits. The thickness of the horizon is 0.3–5.0 m, water conductivity varies from 1 to 20 m<sup>2</sup>/day. The water-retaining foundation is loams 3–15 m thick.

The Upper Jurassic aquifer, widespread throughout the area under consideration, is the second from the surface and is a confined aquifer. The filtration structure of the groundwater in the aquifer is rather complex due to the irregularity of the infiltration supply and the heterogeneity of the underlying water-bearing Jurassic clays. The total thickness of the aquifer is 10–20 m, the filtration coefficient is 2 m/day, the water permeability is 20–40 m<sup>2</sup>/day. The water-bearing foundation is clayey deposits of the Upper Jurassic.

The analysis showed that the technical and moral deterioration of fixed assets at almost all operating construction sites, expiration of the standard service life of technical facilities and utility lines, reduction in the volume of reconstruction and repair work, force one to improve the existing ones and look for new ways to reduce the environmental hazard of techno-natural system functioning.

Analytical methods for solving differential equations of groundwater filtration are used to assess the impact of construction work on hydrogeological conditions. When predicting changes in groundwater levels, it is advisable to use the basic differential nonlinear steady-state filtration equation for planar-flat flow [14, 15]:

$$\frac{\partial}{\partial x} \left( T \frac{\partial H}{\partial x} \right) + \frac{\partial}{\partial y} \left( \frac{\partial H}{\partial y} \right) = 0, \tag{1}$$

where  $H$  is the hydraulic head, m;  $T$  is the reservoir conductivity, m<sup>2</sup>/day;  $x$  and  $y$  are the coordinates, m.

The general solution of equation (1) is represented as [16, 17]:

$$H(x, t) = H_e + \Delta H(x, t), \tag{2}$$

where  $H_e$  is the head of the original steady-state flow;  $\Delta H(x, t)$  is the change in the head caused by the disturbance boundary.

In order to solve equation (1), the condition of theoretically instantaneous filling of the channel and instantaneous onset of undercut filtration stage is assumed, i.e. the following initial and boundary conditions:

$$\Delta H(x, 0) = 0 \quad \text{and} \quad \Delta H(0, t) = \Delta H^0. \quad (3)$$

For an instantaneous level change at the boundary, the calculation formula (solution) has a general form [18, 19]:

$$\Delta H = \Delta H^0 \times F(x; t), \quad (4)$$

where  $\Delta H$  is the change in groundwater level at the distance  $x$  (m) from the boundary of the flow disturbance after the time period  $t$  (days);  $\Delta H^0$  is the value of the change in the horizon level at the line of the well contour, m;  $F(x, t)$  is a special function, depending on the nature of the flow disturbance and boundary conditions, whose values are given [20, 21].

For a semi-constrained flow with an imperfect boundary, the value of additional hydrodynamic resistance must be taken into account by lengthening the flow  $\Delta L_t$  by the time-dependent value  $t$  during unsteady flow. When solving the problem in this way, the equation has the following form [22, 23]:

$$\Delta H = \Delta H^0 \times \operatorname{erfc} \left( \frac{x + \Delta L_t}{2\sqrt{at}} \right). \quad (5)$$

Enter the designation:

$$\lambda = \frac{x}{2\sqrt{at}}, \quad \theta = 2\sqrt{at}/\Delta L_t, \quad (6)$$

where  $\operatorname{erfc} \lambda$  is the special tabulated error function;  $a = T/\mu$  is the conductivity coefficient, m<sup>2</sup>/day;  $T$  is the water conductivity of the horizon, m<sup>2</sup>/day;  $\mu$  is the gravity capacity coefficient, shares of unites.

The dependence  $\theta = f(\Delta L_t / \Delta L)$  is presented in Fig. 2.

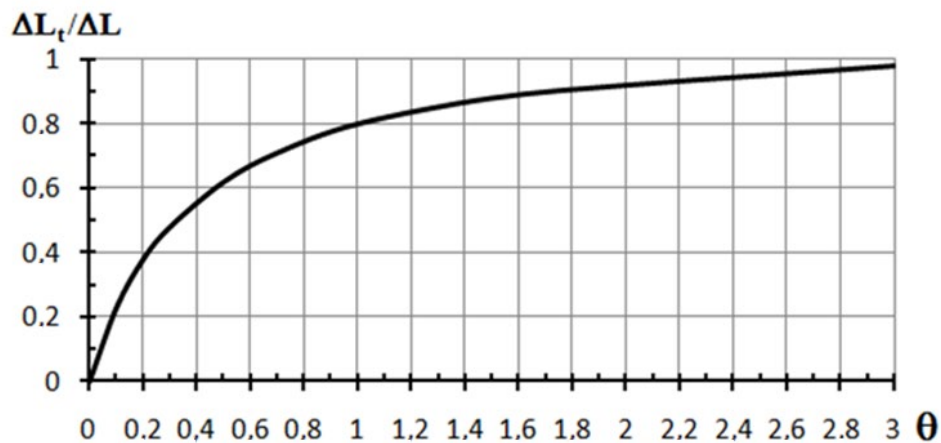


Figure 2. Dependence of  $f(\Delta L_t / \Delta L)$  on  $\theta$ .

With a high degree of accuracy, with a pairwise correlation coefficient of  $r = 0.9997$ , the value  $\Delta L_t$  can be expressed by a regression equation:

$$\Delta L_t = \Delta L \times \left( \frac{1}{0.904 + \frac{0.353}{\theta}} \right). \quad (7)$$

Given the value of  $\Delta L_t$ , the equation (7) can be presented as follows:

$$\Delta H = \Delta H^0 \times \operatorname{erfc} \left( \frac{x + \Delta L \left( \frac{1}{0.904 + \frac{0.353}{\theta}} \right)}{2\sqrt{at}} \right). \quad (8)$$

The magnitude of the change in specific two-way inflow (flow rate per linear meter) is determined by the relationship:

$$\Delta q = \frac{4T\Delta H^0}{\sqrt{\pi \times at}} \times \exp \left( - \frac{1}{2\sqrt{at}} \times \frac{\Delta L}{0.904 + \frac{0.353 \times \Delta L}{\sqrt{at}}} \right). \quad (9)$$

The average flow is determined by numerical integration. For trenches and horizontal drainage, the value  $\Delta L$  can be expressed through the parameter  $L_{ld}$  ( $\Delta L = 2L_{ld}$ ). For a drain located in a homogeneous reservoir,  $L_{ld}$  is determined by the formula [24, 25]:

$$L_{ld} = 0.73 \times \lg \frac{2d}{\pi d_d}, \quad (10)$$

where  $d_d$  is the calculated drain diameter,  $d_d \approx 0.56 \cdot P_d$ ;  $P_d$  is the wetted perimeter of the drain;  $m_d$  is the power of the flow under the drain.

For a two-layer reservoir, consisting of a slightly conductive top layer  $m_n$  with filtration coefficient  $k_n$  and a lower aquifer, with a drain in the top layer, we obtain:

$$ld = 0.73 \frac{T}{k_n} \cdot \lg \frac{8m_n}{\pi d_d}. \quad (11)$$

Analytical solutions according to dependencies (8, 9) are considered for the scheme of infinite linear source of disturbance in an infinite reservoir. However, in real conditions during construction dewatering, open laying of utilities, work is carried out at limited intervals. In this case, dewatering is carried out either at once on the entire interval (trench) – about 100 m, or on a limited section of 20–40 m long, which moves as the pit is dug. The flow pattern gradually becomes radial as it moves away from the source of disturbance.

The analytical values were compared with the numerical values obtained for typical hydrogeological conditions in order to adjust the limitations of the dewatering areas. The averaged discharges appear to be proportionally dependent on the decrease in the level in the dewatering site ( $S_c$ ), so the relationship between the average discharges is also linear, regardless of the design linear scheme. Using this relationship, the analytical solutions  $Q_a$  were refined:

- when dewatering occurs throughout the entire interval during the entire period of work:

$$Q_o = 1.2244 \cdot Q_a; \quad (12)$$

- when the dewatering section shifts in time:

$$Q_v = 1.0332 \cdot Q_a. \quad (13)$$

It is obvious that the result of analytical solution is practically no different from the result of the numerical solution in the case of section mobility and can be accepted without corrections, since the accuracy is about 3 %. However, the maximum water inflows are observed with a simultaneous decrease in the level over the entire interval, therefore, the obtained analytical solution, according to (12), should be increased by 22.4 %.

### 3. Results and Discussion

During construction work on laying utility lines, the geological environment will be changed by removing soil from open trenches and pits, as well as under the influence of a number of measures aimed at changing the hydrogeological conditions to prevent flooding in the area of the small river basins. The main impacts on the geological environment during construction is dewatering, which will be carried out in the areas of urban and storm sewerage and water supply systems [26–29].

The input data and calculation results for water inflows into the building drainage system are shown in Fig. 3.

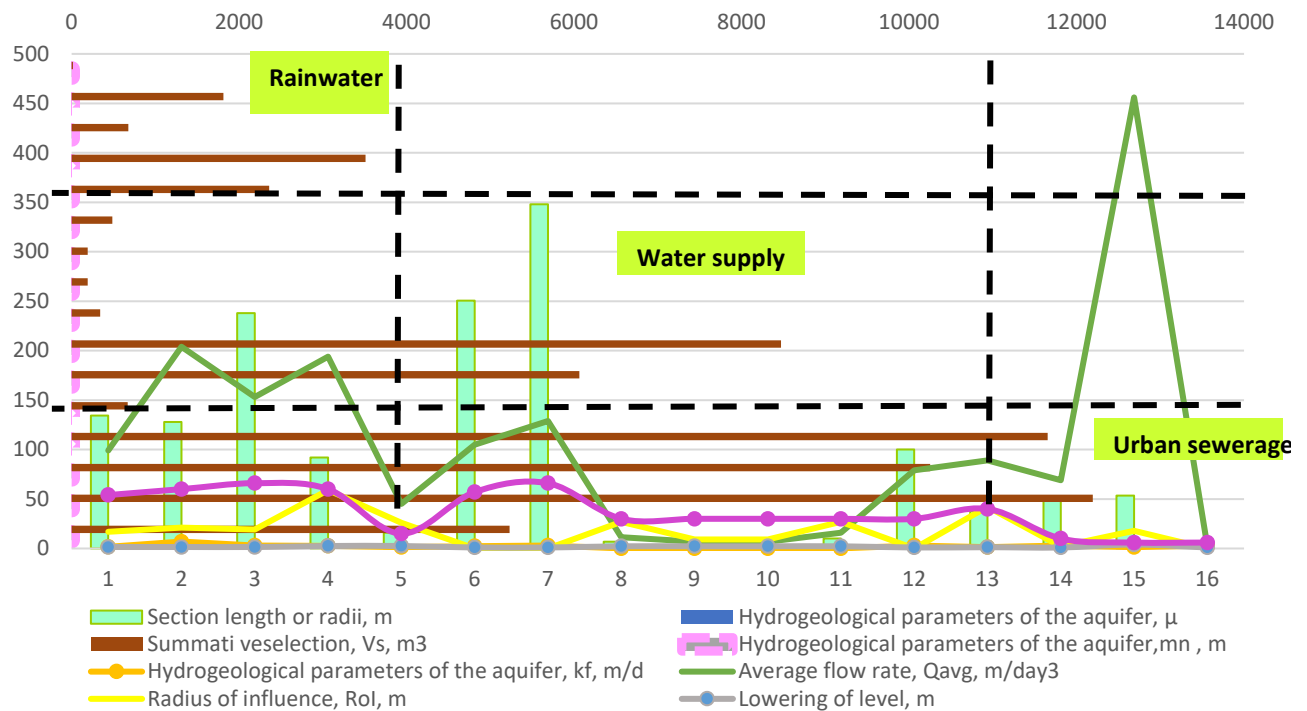


**Figure 3. Calculation results of water inflows in the building drainage system.**

The studies have shown that the level drop in the supra-moraine aquifer at different areas ranges from 1 to 4 m. The water-bearing rocks of the horizon are upper quaternary deposits, represented by sands and sandy loams; the water yield coefficient is taken to be 0.07–0.15. As the calculations have shown, the average groundwater discharge during the period of level decrease will vary for each calculated area from 2 to 456 m<sup>3</sup>/day. At the same time, the total volume of water withdrawal will be 64112 m<sup>3</sup>. When determining the size of the zone of influence of the level decrease in the aquifer, a level decrease of 1 m is taken as the boundary, which corresponds to the amplitude of natural fluctuations in the groundwater level. The maximum zone of influence from the conducted dewatering will be 59 m in the storm sewer zone.

Calculations of building subsidence as a result of lowering the water table have been made using the recommendations given in [30, 31] and the dependencies of moisture transport in the aeration zone [18, 32].

In order to assess the filtration calculations of dewatering, a model of the filtration calculations was developed and carried out in Microsoft Excel. During the model calculations, it was found that the depression funnel from construction dewatering with a groundwater subsidence of more than 1 m would include non-residential buildings in the industrial area, where the maximum subsidence under them would be 2 m (Fig. 4).

	A	B	C	D	E	F	G	H	I	J	K	L	M	N																																																																																																
1	<b>Table 1</b>																																																																																																													
2	<b>Baseline data for the calculation of precipitation at the RT 1 design point</b>																																																																																																													
3	Absolute ground mark, m				148,6		Number of water-tightness layer:				6																																																																																																			
4	Baseline groundwater he=				146,1		Deep, m				2,5																																																																																																			
5	Level reduction value				2		Horizontal wrinkle m =				2,8																																																																																																			
6																																																																																																														
7	<table border="1"> <thead> <tr> <th>No</th> <th>lytology of Rocks</th> <th>Mark Note of the bottom of the layer, m</th> <th>Engineering and geological parameters</th> <th>density of skeleton, g/cm3</th> <th>Coef, porosity, d.d.</th> <th>Maximum molecules, moisture-intensive, d.e.</th> <th>Capillar, tower, m</th> <th>Deformation module, Mpa</th> </tr> </thead> <tbody> <tr> <td>1</td> <td>PesGlsM</td> <td>145,1</td> <td>1,46</td> <td>0,65</td> <td>0,07</td> <td>0,7</td> <td>3,5</td> </tr> <tr> <td>2</td> <td>black Ql</td> <td>144,1</td> <td>1,7</td> <td>0,72</td> <td>0,16</td> <td>1,4</td> <td>8</td> </tr> <tr> <td>3</td> <td>p.m./s al</td> <td>142,8</td> <td>1,52</td> <td>0,75</td> <td>0,02</td> <td>0,5</td> <td>13</td> </tr> <tr> <td>4</td> <td>black Ql</td> <td>142,4</td> <td>1,7</td> <td>0,72</td> <td>0,16</td> <td>1,4</td> <td>8</td> </tr> <tr> <td>5</td> <td>p.s./s. al</td> <td>141,3</td> <td>1,62</td> <td>0,7</td> <td>0,02</td> <td>2</td> <td>20</td> </tr> <tr> <td>6</td> <td>cyrn.qQll</td> <td>132,4</td> <td>1,79</td> <td>0,45</td> <td>0,12</td> <td>1,4</td> <td>25</td> </tr> </tbody> </table>														No	lytology of Rocks	Mark Note of the bottom of the layer, m	Engineering and geological parameters	density of skeleton, g/cm3	Coef, porosity, d.d.	Maximum molecules, moisture-intensive, d.e.	Capillar, tower, m	Deformation module, Mpa	1	PesGlsM	145,1	1,46	0,65	0,07	0,7	3,5	2	black Ql	144,1	1,7	0,72	0,16	1,4	8	3	p.m./s al	142,8	1,52	0,75	0,02	0,5	13	4	black Ql	142,4	1,7	0,72	0,16	1,4	8	5	p.s./s. al	141,3	1,62	0,7	0,02	2	20	6	cyrn.qQll	132,4	1,79	0,45	0,12	1,4	25																																							
No	lytology of Rocks	Mark Note of the bottom of the layer, m	Engineering and geological parameters	density of skeleton, g/cm3	Coef, porosity, d.d.	Maximum molecules, moisture-intensive, d.e.	Capillar, tower, m	Deformation module, Mpa																																																																																																						
1	PesGlsM	145,1	1,46	0,65	0,07	0,7	3,5																																																																																																							
2	black Ql	144,1	1,7	0,72	0,16	1,4	8																																																																																																							
3	p.m./s al	142,8	1,52	0,75	0,02	0,5	13																																																																																																							
4	black Ql	142,4	1,7	0,72	0,16	1,4	8																																																																																																							
5	p.s./s. al	141,3	1,62	0,7	0,02	2	20																																																																																																							
6	cyrn.qQll	132,4	1,79	0,45	0,12	1,4	25																																																																																																							
8																																																																																																														
9																																																																																																														
10																																																																																																														
11																																																																																																														
12																																																																																																														
13																																																																																																														
14																																																																																																														
15																																																																																																														
16	<b>Table 2</b>																																																																																																													
17	<b>Results of the sediment calculation at RT 1</b>																																																																																																													
18	(excluding the distribution of humidity and the capacity of the compressible column of the non-conforming capacity of the aquifer)																																																																																																													
19	<table border="1"> <thead> <tr> <th rowspan="2">No of the</th> <th rowspan="2">Lithology of the design layers</th> <th rowspan="2">Power of the design layers, m</th> <th rowspan="2">Density skeleton, g/cm3</th> <th colspan="2">Nature characteristics of the ground</th> <th colspan="3">The crime of a lower level</th> <th rowspan="2">Module E, Mpa</th> <th rowspan="2">Change pressure dP</th> <th rowspan="2">Sprout in layer, dS, mm</th> </tr> <tr> <th>Humidity.</th> <th>Ge density</th> <th>Pressure, Pe</th> <th>Wet. Ws.</th> <th>Density Gs</th> <th>Pressure, Ps</th> </tr> </thead> <tbody> <tr> <td>1</td> <td>PesGlsM</td> <td>1,00</td> <td>1,46</td> <td>0,39</td> <td>0,85</td> <td>4,50</td> <td>0,18</td> <td>1,46</td> <td>5,11</td> <td>3,50</td> <td>0,30</td> <td>0,87</td> </tr> <tr> <td>2</td> <td>black Ql</td> <td>1,00</td> <td>1,70</td> <td>0,42</td> <td>1,12</td> <td>5,62</td> <td>0,34</td> <td>1,70</td> <td>6,81</td> <td>8,00</td> <td>0,90</td> <td>1,12</td> </tr> <tr> <td>3</td> <td>p.m./s al</td> <td>1,30</td> <td>1,52</td> <td>0,43</td> <td>0,95</td> <td>6,86</td> <td>0,43</td> <td>0,95</td> <td>8,04</td> <td>13,00</td> <td>1,19</td> <td>1,19</td> </tr> <tr> <td>4</td> <td>black Ql</td> <td>0,40</td> <td>1,70</td> <td>0,42</td> <td>1,12</td> <td>7,30</td> <td>0,42</td> <td>1,12</td> <td>8,49</td> <td>8,00</td> <td>1,19</td> <td>0,59</td> </tr> <tr> <td>5</td> <td>p.s./s. al</td> <td>1,10</td> <td>1,62</td> <td>0,41</td> <td>1,03</td> <td>8,44</td> <td>0,41</td> <td>1,03</td> <td>9,63</td> <td>20,00</td> <td>1,19</td> <td>0,65</td> </tr> <tr> <td>6</td> <td>cyrn.qQll</td> <td>8,90</td> <td>1,79</td> <td>0,31</td> <td>1,10</td> <td>18,23</td> <td>0,31</td> <td>1,10</td> <td>19,42</td> <td>25,00</td> <td>1,19</td> <td>0,00</td> </tr> </tbody> </table>														No of the	Lithology of the design layers	Power of the design layers, m	Density skeleton, g/cm3	Nature characteristics of the ground		The crime of a lower level			Module E, Mpa	Change pressure dP	Sprout in layer, dS, mm	Humidity.	Ge density	Pressure, Pe	Wet. Ws.	Density Gs	Pressure, Ps	1	PesGlsM	1,00	1,46	0,39	0,85	4,50	0,18	1,46	5,11	3,50	0,30	0,87	2	black Ql	1,00	1,70	0,42	1,12	5,62	0,34	1,70	6,81	8,00	0,90	1,12	3	p.m./s al	1,30	1,52	0,43	0,95	6,86	0,43	0,95	8,04	13,00	1,19	1,19	4	black Ql	0,40	1,70	0,42	1,12	7,30	0,42	1,12	8,49	8,00	1,19	0,59	5	p.s./s. al	1,10	1,62	0,41	1,03	8,44	0,41	1,03	9,63	20,00	1,19	0,65	6	cyrn.qQll	8,90	1,79	0,31	1,10	18,23	0,31	1,10	19,42	25,00	1,19	0,00
No of the	Lithology of the design layers	Power of the design layers, m	Density skeleton, g/cm3	Nature characteristics of the ground		The crime of a lower level			Module E, Mpa	Change pressure dP	Sprout in layer, dS, mm																																																																																																			
				Humidity.	Ge density	Pressure, Pe	Wet. Ws.	Density Gs				Pressure, Ps																																																																																																		
1	PesGlsM	1,00	1,46	0,39	0,85	4,50	0,18	1,46	5,11	3,50	0,30	0,87																																																																																																		
2	black Ql	1,00	1,70	0,42	1,12	5,62	0,34	1,70	6,81	8,00	0,90	1,12																																																																																																		
3	p.m./s al	1,30	1,52	0,43	0,95	6,86	0,43	0,95	8,04	13,00	1,19	1,19																																																																																																		
4	black Ql	0,40	1,70	0,42	1,12	7,30	0,42	1,12	8,49	8,00	1,19	0,59																																																																																																		
5	p.s./s. al	1,10	1,62	0,41	1,03	8,44	0,41	1,03	9,63	20,00	1,19	0,65																																																																																																		
6	cyrn.qQll	8,90	1,79	0,31	1,10	18,23	0,31	1,10	19,42	25,00	1,19	0,00																																																																																																		
20																																																																																																														
21																																																																																																														
22																																																																																																														
23																																																																																																														
24																																																																																																														
25																																																																																																														
26																																																																																																														
27																																																																																																														
28	With total pressure change dP= 1.187458																																																																																																													
29	The area of influence will be H = 7.30006 m																																																																																																													
30	The draught shall be dS = 4.421056 mm																																																																																																													

**Figure 4. Calculation results of geotechnical parameters and building settlement.**

The modeling has revealed a pattern of changes in building settlement depending on the water table. The plot of building settlement in the area of PT-1 at different depths of the water table  $H_e$  and its different geotechnical parameters and building settlement  $S_o$  is shown in Fig. 5.

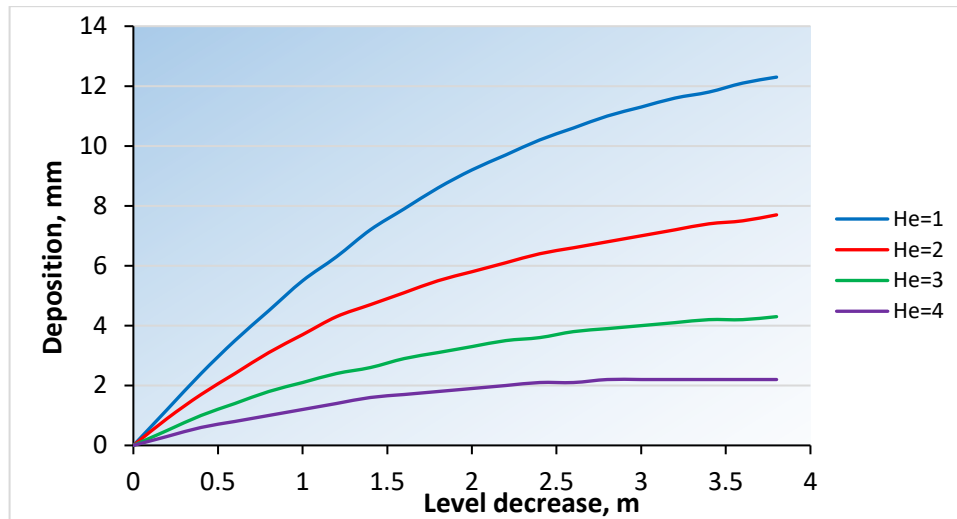


**Figure 5. Dependence of deposition on lowering and depth of groundwater level.**

The modeling showed that the estimated maximum subsidence at the design point PT-1 under the multi-storey non-residential administrative building was 4.4 m, which is less than the maximum permissible deformations.

#### 4. Conclusions

Dependencies for estimation of filtration calculations of dewatering in the area of construction of utility lines and laying of urban and storm sewers in the territory of the highway construction zone are proposed.

It was revealed that the main factor influencing the hydrogeological conditions of the area of construction of utility lines, where minor catchments of small rivers are located, is dewatering.

Analytical dependencies for the infinite linear perturbation source scheme in an infinite soil layer were proposed and improved.

It was found that the average discharges appear to be proportionally dependent on the amount of the drawdown at the dewatering site, with the relationship between the average discharges being linear regardless of the design linear scheme.

The conducted modeling showed that calculations on estimation of maximum depression at the design point under the multi-storey non-residential administrative building was 4.4 m, which was less than the maximum allowable deformations. It was revealed that the maximum water inflows were observed at lowering of water table over the entire limited area of 20–40 m length simultaneously; therefore, the obtained analytical solution should be increased by 22.4 %.

The building subsidence due to water table lowering was calculated and a model for geofiltration calculations was developed in Microsoft Excel. The model calculations showed that the maximum subsidence of the soil at the design point of the multi-storey non-residential administrative building did not exceed the maximum allowable deformation values.

## References

1. Vedernikov, V.V. Prognozirovanie vodnogo rezhima gruntov zony aeratsii zastroennykh territorii: avtoreferat dis. dokt. tekhn. nauk [Forecasting the water regime of soils in the aeration zone of built-up areas. Dr. tech. sci. diss.]. Doctor thesis. Moscow: Moscow State University of Printing Arts, 1997. 73 p.
2. Bolgov, M.V., Golubash, T.Y., Volgin, S.A. Water regime of urbanized soils and grounds in the aeration zone of Rostov Velikii town: Analysis of experimental data. *Water Resources*. 2010. 37(5). Pp. 611–622. DOI: 10.1134/S0097807810050027
3. Aver'yanov, S.F. Fil'tratsiia iz kanalov i ee vliianie na rezhim gruntovykh vod [Filtration from canals and its impact on groundwater regime]. Moscow: Kolos, 1982. 237 p.
4. Pashkovskii, I.S., Ionova, O.N., Pozdniakov, S.P., Potapova, E.Iu., Shestakov, V.M. Developing of a Physic-Mathematical Model of Ground Water Runoff for Different Environments of River Basins. *Russian Foundation for Basic Research Journal*. 1997. 5.
5. Chalov, S.R., Platonov, V.S., Moreido, V.M., Samokhin, M.A., Yarynich, Yu.I., Korshunova, N.N., Bolgov, M.V., Kasimov, N.S. Small Urban River Runoff Response to 2020 and 2021 Extreme Rainfalls on the Territory of Moscow. *Russian Meteorology and Hydrology*. 2023. 48(2). Pp. 138–146. DOI: 10.3103/S1068373923020061
6. Hersbach, H., Bell, B., Berrisford, P., Hirahara, S. et.al. The ERA5 global reanalysis. *Quarterly Journal of the Royal Meteorological Society*. 2020. 146(730). Pp. 1999–2049. DOI: 10.1002/qj.3803
7. Sokolov, D.I., Erina, O.N., Tereshina, M.A., Puklakov, V.V. Impact of Mozhaysk Dam on the Moscow River Sediment Transport. *Geography, Environment, Sustainability*. 2020. 13(4). Pp. 24–31. DOI: 10.24057/2071-9388-2019-150
8. Zhao, G., Kondolf, G.M., Mu, X., Han, M., He, Z., Rubin, Z., Wang, F., Gao, P., Sun, W. Sediment yield reduction associated with land use changes and check dams in a catchment of the Loess Plateau, China. *Catena*. 2017. 148(2). Pp.126–137. DOI: 10.1016/j.catena.2016.05.010
9. Brusova, N.E., Kuznetsova, I.N., Nahaev, M.I. Precipitation regime features in the Moscow region in 2008–2017. *Hydrometeorological Research and Forecasting*. 2019. 1(371). Pp. 127–142.
10. Bakshatin, A.M., Glazunova, I.V., Markin, V.N., Matveeva, T.I., Sokolova, S.A. Vodokhoziaistvennye meropriiatiia po snizheniiu zagriazniaiushchei nagruzki drenazhnogo stoka [Water management measures to reduce the polluting load of drainage runoff]. Patent Russia no. 2022621519, 2022.
11. Wu, J.T.H., Tung, S.C.-Y. Determination of Model Parameters for the Hardening Soil Model. *Transportation Infrastructure Geotechnology*. 2020. 7(1). Pp. 55–68. DOI: 10.1007/s40515-019-00085-8
12. Liang, P., Ding, Y. The long-term variation of extreme heavy precipitation and its link to urbanization effects in Shanghai during 1916–2014. *Advances in Atmospheric Sciences*. 2017. 34. Pp. 321–334. DOI: 10.1007/s00376-016-6120-0
13. Tereshina, M., Erina, O., Sokolov, D., Efimova, L., Kasimov, N. Nutrient dynamics along the Moskva River under heavy pollution and limited self-purification capacity. *E3S Web of Conferences*. 2020. 163. Article no. 05014. DOI: 10.1051/e3sconf/202016305014
14. Markin, V.N., Glazunova, I.V., Matveeva, T.I., Sokolova, S.A. Issues on soil moisture management substantiation for the steppe conditions in the European part of Russia. *IOP Conference Series: Earth and Environmental Science*. 2022. 1010. Article no. 012024. DOI: 10.1088/1755-1315/1010/1/012024
15. Dzhamalov, R.G., Medovar, Y.A., Yushmanov, I.O. Principles of MSW Landfill Sites' Placement Depending on Geological and Hydrogeological Conditions of Territories (Based on Moscow Region). *Water Resources*. 2019. 46. Pp. S51–S58. DOI: 10.1134/S0097807819080062
16. Dzhamalov, R.G., Medovar, Iu.A., Iushmanov, I.O. Vliianie poligona tverdykh bytovykh otkhodov na kachestvo podzemnykh i poverkhnostnykh vod (na primere Vladimirskoi oblasti) [The impact of a solid municipal waste landfill on the quality of groundwater and surface water (using the Vladimir region as an example)]. *Proceedings of the Scientific Conference "Sergeevskie chteniia"*. Moscow: RUDN University, 2018. Pp. 175–178.
17. Berezhaia, T.V., Golubev, A.D., Parshina, L.N. Anomal'nye gidrometeorologicheskie iavleniia na territorii Rossiiskoi Federatsii v mae 2016 g. [Abnormal hydrometeorological phenomena in the Russian Federation in May 2016]. *Meteorologiya i Gidrologiya*. 2016. 8. Pp. 114–128.
18. Shestakov, V.M. *Gidrogeodinamika* [Hydrogeodynamics]. Moscow: KDU, 2009. 334 pp.
19. Karpenko, N.P., Glazunova, I.V. Management of land and water resources to reduce river pollution based on expert efficiency estimates of environmental protection activities. *Prirodoobustrojstvo (Environmental Engineering)*. 2019. 4. Pp. 102–108. DOI: 10.34677/1997-6011/2019-4-102-108
20. Karpenko, N.P., Lomakin, I.M. Consideration of rocks heterogeneity of the aeration zone in filtration calculations of drainage on reclamation systems. *Prirodoobustrojstvo (Environmental Engineering)*. 2017. 1. Pp. 66–72.

21. Jiang, B., Wang, X. Research on the Training Approach and Practical Ability of Master of Civil Engineering and Water Conservancy in China. *Journal of Education and Educational Research*. 2022. 1(2). Pp. 112–115. DOI: 10.54097/jeer.v1i2.3675
22. Grinevskii, S.O. *Gidrogeodinamicheskoe modelirovanie vzaimodeistviia podzemnykh i poverkhnostnykh vod* [Hydrogeodynamic modeling of the interaction of ground and surface waters], monograph. Moscow: Infra-M, 2012. 152 pp.
23. Mahlknrecht, J., Mora, A. Editorial overview: Management of groundwater resources and pollution prevention. *Current Opinion in Environmental Science & Health*. 2022. 28. Article no. 100365. DOI: 10.1016/j.coesh.2022.100365
24. Karpenko, N.P., Shiryayeva, M.A. Assessment of the impact of oil production on the quality of water bodies of the Perm Territory using GIS technologies. *Prirodobustrojstvo (Environmental Engineering)*. 2023. 1. Pp. 95–101. DOI: 10.26897/1997-6011-2023-1-95-101
25. Gao, X.-W., Gao, L.-F., Zhang, Y., Cui, M., Lv, J. Free element collocation method: A new method combining advantages of finite element and mesh free methods. *Computers & Structures*. 2019. 215. Pp. 10–26. DOI: 10.1016/j.compstruc.2019.02.002
26. Popescu, R., Deodatis, G., Nobahar, A. Effects of random heterogeneity of soil properties on bearing capacity. *Probabilistic Engineering Mechanics*. 2005. 20(4). Pp. 324–341. DOI: 10.1016/j.probengmech.2005.06.003
27. Sun, K., Zhao, Q., Zou, J. A review of building occupancy measurement systems. *Energy and Buildings*. 2020. 216. Article no. 109965. DOI: 10.1016/j.enbuild.2020.109965
28. Ushakova, I., Korchevskaya, Yu., Trotsenko, I., Kondrateva, T. Methodology for Determining the Filtration Parameters of Drainage Bedding during Engineering Surveying. *Advances in Social Science, Education and Humanities Research*. 2020. 393. Proceedings of the International Scientific Conference the Fifth Technological Order: Prospects for the Development and Modernization of the Russian Agro-Industrial Sector (TFTS 2019). Pp. 42–45. DOI: 10.2991/assehr.k.200113.135
29. Guerrero Sedeno, A.A., Kolesnikov, A.G. Analiz metodiki rascheta drenaznykh sistem [Analysis of the calculation methodology for drainage systems]. *Proceedings of the IV International Youth Scientific Conference Youth and the 21<sup>st</sup> Century – 2012*. 2012. Pp. 57–59.
30. Sologaeu, V.I. On the modeling geofiltration problems in the design of highways. *The Russian Automobile and Highway Industry Journal*. 2011. 2 (24). Pp. 64–69.
31. Prokopov, A.Yu., Lasun, V.S. Assessment of change in engineering and geological and hydrogeological conditions as a result of heights development of residential district Leventsovsky in Rostov-on-Don. *Izvestiya Tula State University. Earth Sciences*. 2021. 1. Pp. 217–224.
32. Konukhov, D.S., Mazhirin, M.Yu. Use of geotechnological monitoring to ensure technological safety of subway facilities construction in Moscow. *Metro i Tonneli [Metro and Tunnels]*. 2020. 2. Pp. 43–47.

**Information about the authors:**

**Irina Glazunova, PhD in Technical Sciences**

ORCID: <https://orcid.org/0000-0003-4931-2008>

E-mail: [ivglazunova@mail.ru](mailto:ivglazunova@mail.ru)

**Svetlana Sokolova, PhD in Technical Sciences**

ORCID: <https://orcid.org/0000-0003-3997-6994>

E-mail: [sokolovasvetlana@mail.ru](mailto:sokolovasvetlana@mail.ru)

**Margarita Shiryayeva,**

ORCID: <https://orcid.org/0000-0001-8019-1203>

E-mail: [Shiryayeva.MA@fncg.ru](mailto:Shiryayeva.MA@fncg.ru)

Received: 11.07.2023. Approved after reviewing: 06.09.2024. Accepted: 11.09.2024.





Research article

UDC 624.04

DOI: 10.34910/MCE.130.8



## Artificial intelligence models for determining the strength of centrally compressed pipe-concrete columns with square cross-section

A.S. Chepurnenko<sup>✉</sup> , B.M. Yazyev , V.S. Turina , V.F. Akopyan 

Don State Technical University, Rostov-on-Don, Russian Federation

✉ [anton\\_chepurnenk@mail.ru](mailto:anton_chepurnenk@mail.ru)

**Keywords:** tubular steel structures, concrete, finite element method, compressive strength, artificial neural networks, forecasting

**Abstract.** The article is devoted to the development of machine learning models for predicting the ultimate load during central compression of concrete-filled steel tubular (CFST) columns with square cross-section. Artificial intelligence is currently widely used in data processing and analysis, including data on the load-bearing capacity of building structures. The use of machine learning models can become an alternative to the empirical formulas from current building design codes. The models built by artificial neural networks are based on four different architectures: cascade forward backpropagation network, Elman neural network, feedforward neural network and layer recurrent neural network. The models were trained on synthetic data obtained as a result of finite element analysis of CFST columns in a simplified formulation with varying input parameters. The input parameters of the models were the outer cross-sectional size, wall thickness, concrete compressive strength and steel yield strength. The difference from previous works is the large size of the dataset, which amounts to 22308 samples. This dataset size allows to cover the entire currently possible range of changes in input parameters. The trained models showed high performance in terms of mean squared error. The correlation coefficients between predicted and target values are close to one. The developed models were also tested on experimental data for 123 samples presented in 15 different works. The best agreement with experimental data was obtained using the layer recurrent neural network model.

**Citation:** Chepurnenko, A.S., Yazyev, B.M., Turina, V.S., Akopyan, V.F. Artificial intelligence models for determining the strength of centrally compressed pipe-concrete columns with square cross-section. Magazine of Civil Engineering. 2024. 17(6). Article no. 13008. DOI: 10.34910/MCE.130.8

### 1. Introduction

In modern construction, there is a tendency to increase the height of structures and floor spans. This requires the use of columns with high load-bearing capacity at small cross-sections. One solution to this problem is the use of concrete-filled steel tubular (CFST) structures [1–3]. The reason for the high efficiency of CFST structures lies in a number of positive qualities that they possess. This is the plastic nature of destruction even when using high-strength concrete [4–6], no need for formwork, an increase in the load-bearing capacity of concrete due to its lateral compression with a steel shell [7–9], etc.

Russian set of rules 266.1325800.2016 “Composite steel and concrete structures. Design rules” contains calculation methods only for columns of circular cross-section. At the same time, square cross-section CFST columns are widely used [10–12], for which there are no design recommendations in the current Russian design codes.

Most of the existing calculation methods are based on an empirical approach [13–15], the calculation dependencies used in this case will be applicable only for a specific design solution (for example, the absence of reinforcement of the concrete core) and the type of concrete. One of the reliable ways to predict the load-bearing capacity of CFST structures is finite element modeling [16–18]. However, this approach requires analysis in a three-dimensional physically nonlinear formulation, which leads to large time costs for preparing the calculation model and the calculation itself [19].

Currently, machine learning algorithms are widely used for determining the load-bearing capacity of building structures along with analytical and numerical algorithms [20].

The authors of [21] proposed an interpretable machine learning method based on the adaptive surrogate model with adaptive neuro-fuzzy inference system (ANFIS). To train the model, the results of 99 central compression tests on square CFST columns were collected from various sources. The quality of training was assessed using 11-fold cross-validation.

In [22], an artificial neural network (ANN) model was built to determine the load-bearing capacity of CFST columns with square and circular cross-section under central and eccentric compression. The data from 3091 full-scale experiments were used to train the model. Of these, 895 experiments were conducted for centrally compressed columns of square cross-section.

In [23], the training dataset included 1022 square-section samples, of which 685 samples were short columns and 337 were slender columns. The prediction results were compared with calculations according to Eurocode 4.

The authors of [24] considered the joint use of gene expression programming and ANNs for predicting the load-bearing capacity of CFST columns with circular and square cross-section. The experimental base for training included data from 993 samples. To validate the results, comparisons were made with design codes from six different countries.

The authors of the listed works claim that surrogate models based on machine learning have an advantage over the formulas from design codes. However, ANNs and other machine learning models are, in fact, multidimensional interpolation of data, and provide reliable results only in the range of parameters in which they were trained.

Since conducting full-scale experiments is a rather expensive and time-consuming process, some researchers use synthetic data obtained from finite element modeling to form a training dataset. An example of such an approach is the work [25]. Since the modeling is performed in a three-dimensional setting, which is also a rather labor-intensive process, the final volume of the training dataset remains small. As a rule, the volume of the training dataset does not exceed 1000 samples, which does not allow covering the entire possible range of changes in material characteristics and geometric parameters.

The purpose of this work is to develop the machine learning models for predicting the load-bearing capacity of centrally compressed square-section CFST columns, which could correctly predict the ultimate load over the entire possible range of changes in the characteristics of steel and concrete, as well as the geometric characteristics of profiled square-section pipes. The size of the training dataset in this article is 22308 samples, which is tens of times larger than the size of the datasets in previous works.

## 2. Materials and Methods

This article considers short columns, for which deflections do not lead to any significant increase in the eccentricity of the axial force. The following values were chosen as input parameters of ANNs: cross-sectional size  $a$  (mm); pipe wall thickness  $t$  (mm); pipe material yield strength  $R_y$  (MPa); ultimate compressive strength of concrete (prismatic strength)  $R_b$  (MPa). At the output, the ANN must predict one parameter, which is the value of the ultimate load  $N_{ult}$ .

Parameters, such as the modulus of elasticity of concrete, its tensile strength, Poisson's ratio, as well as the modulus of elasticity of steel, to a certain extent also influence the load-bearing capacity of CFST columns. However, they were not included among the input parameters. For the modulus of elasticity of concrete and its tensile strength, this is explained by the fact that they are in correlation with the prismatic compressive strength [26, 27]. The initial Poisson's ratio of ordinary concrete (under elastic work of material) varies from 0.16 to 0.20 [28]. When training the models, the value presented in the Russian design codes for the reinforced concrete structures was taken ( $\nu = 0.2$ ). As for the modulus of elasticity of steel, it also has a small spread from 196 to 222 GPa [29], and when training the models, it was taken equal to 200 GPa.

The supervised learning method was used to train the models. Training was carried out on synthetic data obtained by finite element modeling using a simplified method given in [30]. The essence of this

technique is to reduce the three-dimensional problem of determining the stress-strain state to a two-dimensional one based on the hypothesis of plane sections. Rectangular finite elements were used to model the concrete core, and one-dimensional finite elements were used to model the steel shell. The rounding of corners in steel profile pipes was not taken into account in the calculations. A quarter of the section was considered due to the symmetry of the problem. The side size of the concrete finite element was taken to be 1/20 of the size of the concrete core. The physical nonlinearity of concrete was specified by the equations of the deformation theory of concrete plasticity by G.A. Geniev as in [30]. Steel was considered an ideal elastoplastic material. The Huber–Mises–Henky criterion was used as a yield criterion for steel. The following formulas were used as correlation relationships between the prismatic strength of concrete  $R_b$ , tensile strength  $R_{bt}$  and the initial modulus of elasticity of concrete  $E_0$  [31]:

$$R_{bt} = 0.29 \cdot \left( \frac{R_b}{0.788} \right)^{0.6};$$

$$E_0 = 1000 \cdot \frac{0.05R_b + 57}{1 + \frac{29}{3.8 + R_b}}. \quad (1)$$

The dataset containing 22308 numerical experiments was generated<sup>1</sup>. The range of changes in parameters  $a$  and  $t$  (Table 1) corresponded to the current Interstate standard GOST 30245-2012 “Steel bent closed welded square and rectangular section for building. Specifications”. For each value of  $a$  from the range, the calculation was performed with 11 values of wall thickness from  $t_{\min}$  to  $t_{\max}$  with a uniform step. The concrete compressive strength varied from 10 to 120 MPa in increments of 10 MPa, the yield strength of steel varied from 220 to 840 MPa in increments of 62 MPa. A fragment of the training dataset is shown in Table 2.

**Table 1. Values of parameter  $a$ , as well as ranges of variation of parameter  $t$  when constructing a training dataset.**

$a$ , mm	$t_{\min}$ , mm	$t_{\max}$ , mm
100	3	8
120	3	8
140	4	8
150	4	8
160	4	8
180	5	16
200	5	12
250	6	12
300	6	22
350	6	22
400	7	22
450	7	22
500	8	22

**Table 2. Fragment of the training dataset.**

No.	$a$ , mm	$t$ , mm	$R_y$ , MPa	$R_b$ , MPa	$N_{ult}$ , kN
1	100	3.00	220	10	349.71
2	100	3.45	220	10	385.27
3	100	3.91	220	10	420.72
4	100	4.36	220	10	455.76
5	100	4.82	220	10	490.38
6	100	5.27	220	10	524.59
7	100	5.73	220	10	558.38
8	100	6.18	220	10	591.76
9	100	6.64	220	10	625.31

<sup>1</sup> The dataset is available at the following link: <https://disk.yandex.ru/i/y2y0eTlaYox3Rw>.

No.	$a$ , mm	$t$ , mm	$R_y$ , MPa	$R_b$ , MPa	$N_{ult}$ , kN
10	100	7.09	220	10	657.89
11	100	7.55	220	10	690.07
12	100	8.00	220	10	722.50
13	100	3.00	282	10	422.21
14	100	3.45	282	10	468.22
15	100	3.91	282	10	514.09
16	100	4.36	282	10	559.41
17	100	4.82	282	10	604.20
18	100	5.27	282	10	648.45
19	100	5.73	282	10	692.81
20	100	6.18	282	10	736.03
21	100	6.64	282	10	778.72
22	100	7.09	282	10	821.63
23	100	3.00	220	10	349.71
...	...	...	...	...	...
22286	500	9.27	778	120	42107.78
22287	500	10.55	778	120	43721.33
22288	500	11.82	778	120	45326.32
22289	500	13.09	778	120	46878.91
22290	500	14.36	778	120	48465.31
22291	500	15.64	778	120	49996.36
22292	500	16.91	778	120	51564.20
22293	500	18.18	778	120	53073.77
22294	500	19.45	778	120	54623.09
22295	500	20.73	778	120	56111.24
22296	500	22.00	778	120	57642.06
22297	500	8.00	840	120	40922.32
22298	500	9.27	840	120	42593.22
22299	500	10.55	840	120	44248.28
22300	500	11.82	840	120	45887.56
22301	500	13.09	840	120	47511.10
22302	500	14.36	840	120	49118.97
22303	500	15.64	840	120	50759.78
22304	500	16.91	840	120	52338.05
22305	500	18.18	840	120	53900.79
22306	500	19.45	840	120	55501.41
22307	500	20.73	840	120	57089.77
22308	500	22.00	840	120	58609.37

Several options were considered for the architecture of the ANN: cascade forward backpropagation network, Elman neural network, feedforward neural network and layer recurrent neural network. For each option, the number of hidden layers was taken to be one, the number of neurons in the hidden layer was taken to be 10, and the hyperbolic tangent was used as the activation function. ANNs with one hidden layer are among the simplest ones, but as will be shown below, one hidden layer is enough for high quality prediction with a sufficient volume of training dataset. ANN models were implemented in MATLAB software (Neural Network Toolbox). The architecture of the ANNs used is shown schematically in Fig. 1.

Levenberg–Marquardt algorithm was used to train the models. During training, the dataset was randomly divided into three parts: Training, Validation and Test in proportions of 70%, 15% and 15%, respectively. The value of the mean squared error (MSE) was chosen as a metric for the quality of training:

$$MSE = \frac{1}{n} \sum_{i=1}^n (T_i - Y_i)^2, \quad (2)$$

where  $n$  is the volume of the training dataset;  $Y_i$  are the ultimate load values predicted by the neural network;  $T_i$  are the target values of the ultimate load.

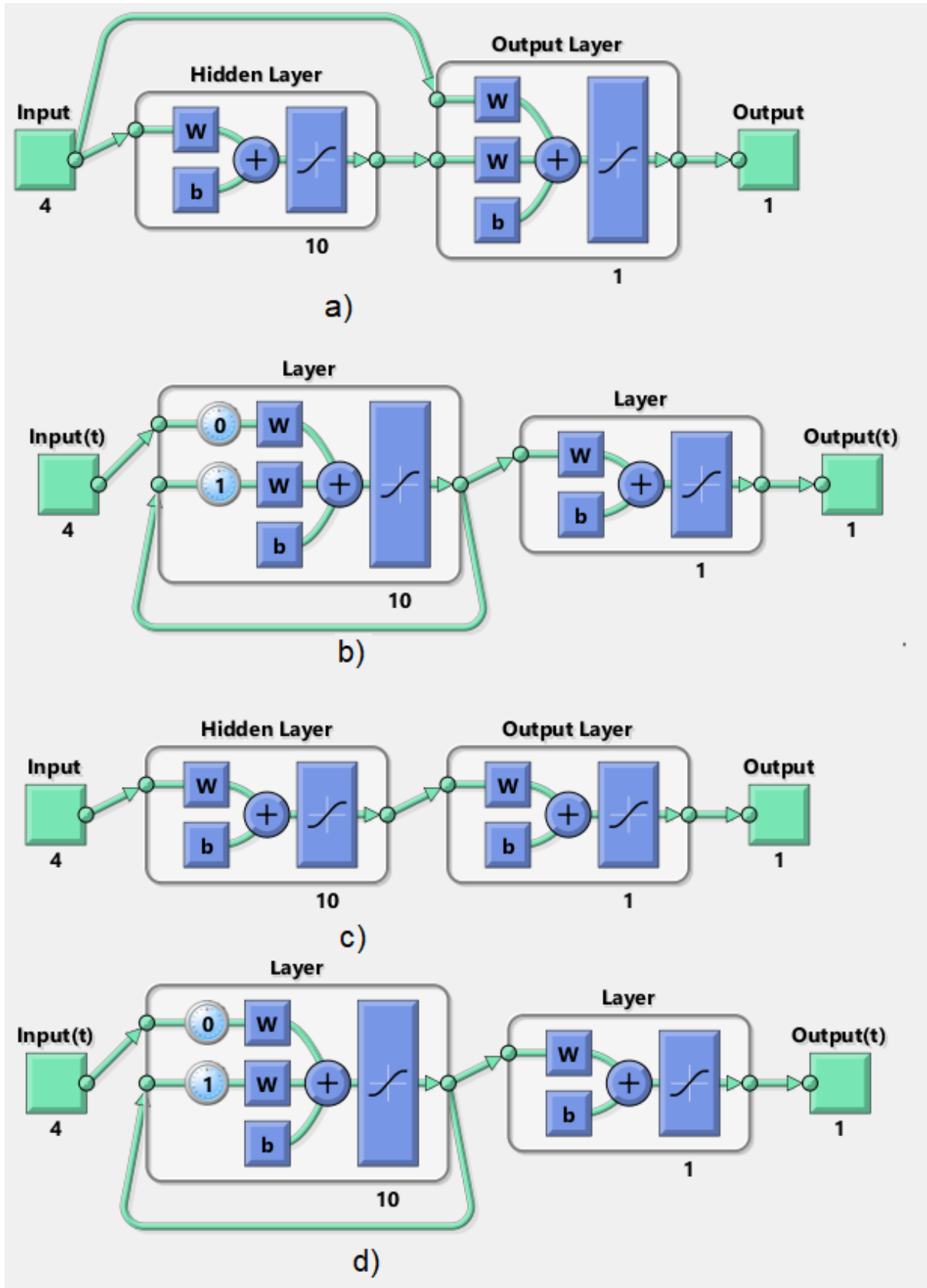


Figure 1. Architecture used for ANN: a) cascade forward backpropagation network; b) Elman neural network; c) feedforward neural network; d) layer recurrent neural network.

### 3. Results and Discussion

Table 3 shows the MSE values obtained as a result of models training, calculated from the "Validation" part of the dataset. The best results were obtained using the Elman architecture neural network. Training performance graph for this model is shown in Fig. 2. Fig. 3 represents regression plot for the Elman neural network model. The  $x$  axis corresponds to the target values of the ultimate loads  $T$ , and  $y$  axis corresponds to the predicted values  $Y$ . Most of the points on the graphs fit on the straight line  $Y = T$ . The correlation coefficients  $R$  between target and predicted values are close to 1, and for the entire sample  $R$  is equal to 0.99997. For ANN models built on cascade forward backpropagation network, feedforward neural network and layer recurrent neural network architectures correlation coefficients are also close to 1.

**Table 3. MSE values obtained as a result of training ANN models.**

Model	MSE
Cascade forward backpropagation network	12635.45
Elman neural network	6624.35
Feedforward neural network	9954.31
Layer recurrent neural network	7728.31

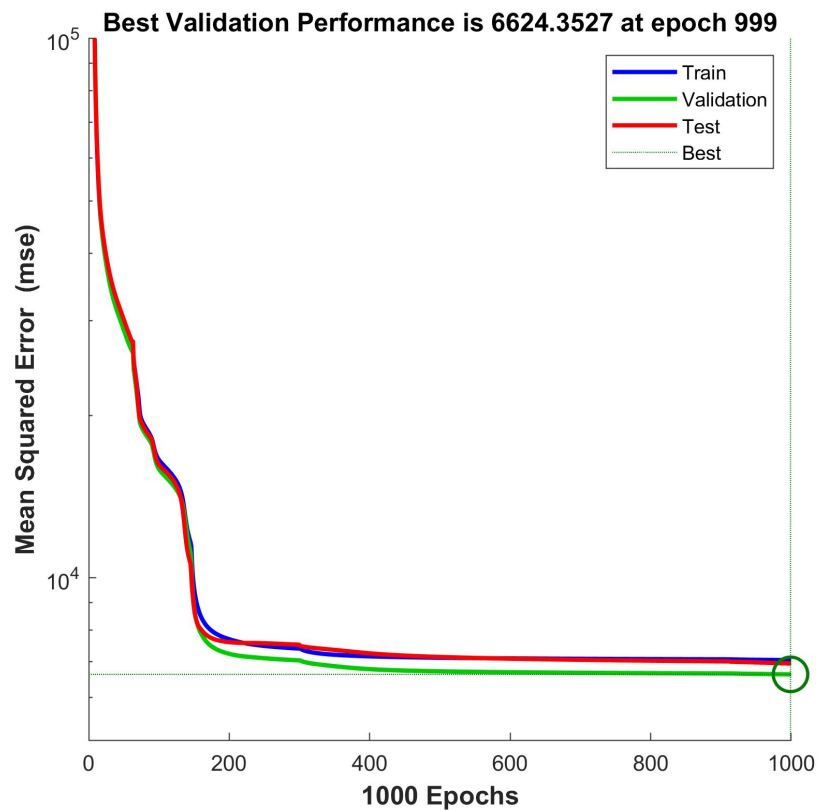


**Figure 2. Training performance graph for Elman neural network.**

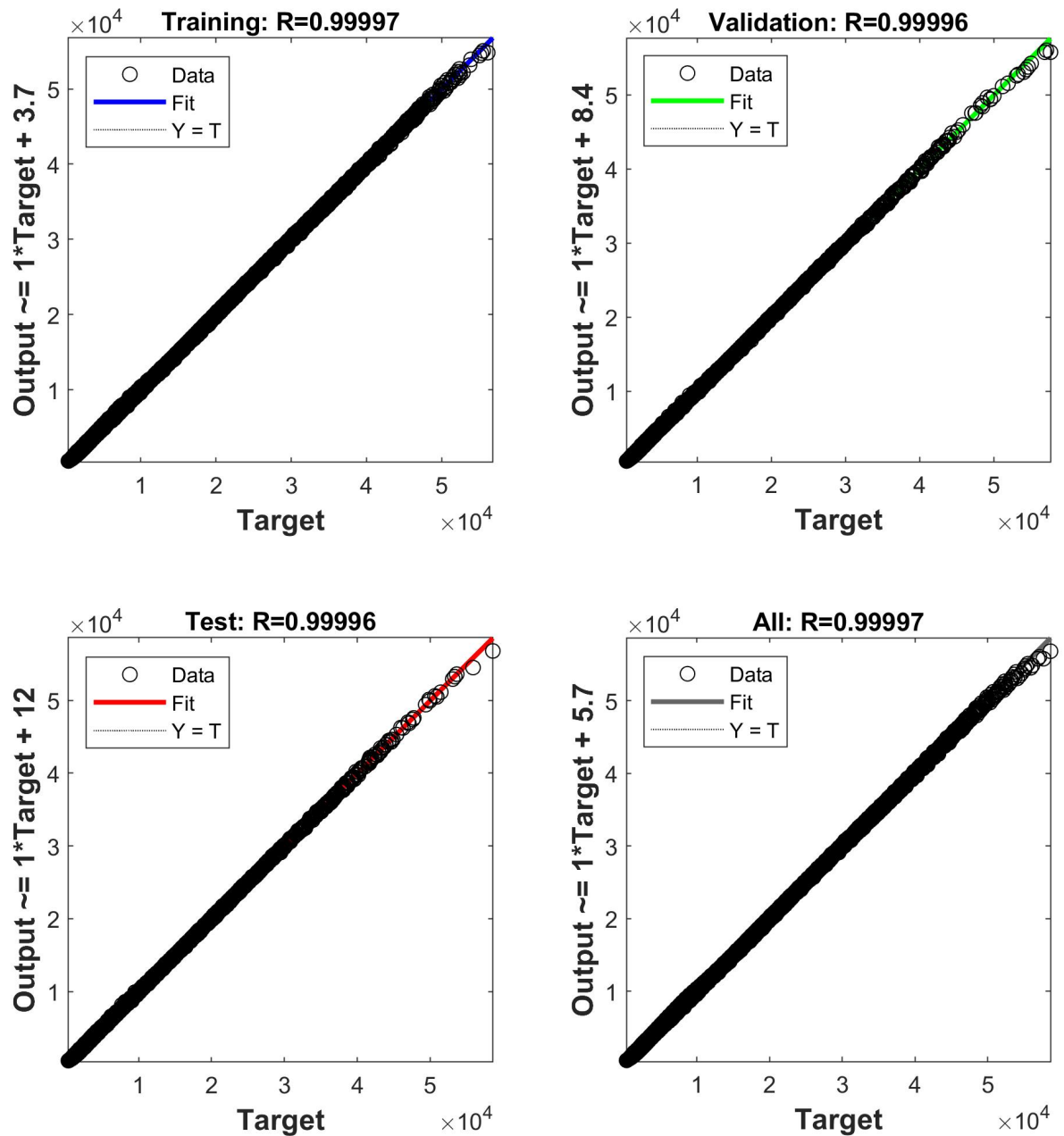


Figure 3. Regression plot for Elman neural network.

After training on synthetic data, the developed ANN models were tested on experimental data presented in [32–46]. Dimension  $a$  varied from 70 to 500 mm, wall thickness  $t$  varied from 0.7 to 16 mm, concrete compressive strength  $R_b$  varied from 21 to 121.6 MPa, and yield strength of steel varied from 228 to 835 MPa. The test results are given in Table 4. ANN 1 are the results obtained using cascade forward backpropagation network, ANN 2 corresponds to Elman neural network, ANN 3 corresponds to feedforward neural network and ANN 4 corresponds to layer recurrent neural network. Table 4 shows that despite the different architecture, the results predicted by the four models are quite close to each other. Table 5 shows the average values of the ratio of predicted ultimate loads  $N_{predict}$  to experimental ones  $N_{exp}$ , the maximum and minimum values of the ratio  $N_{predict}/N_{exp}$ , standard deviations of the value  $N_{predict}/N_{exp}$ , as well as the coefficients of variation for each of the ANN 1–ANN 4 models.

**Table 4. Results of testing the developed models on experimental data.**

No.	Sample	$a$ , mm	$t$ , mm	$R_y$ , MPa	$R_b$ , MPa	$N_{ult}$ , kN				
						experiment	ANN1	ANN2	ANN3	ANN4
Ouyang, Y., Kwan, A.K.H. (2018) [32]										
1	CR4-A-2	148	4.38	262	25.4	1153	1213	1166	1187	1178
2	CR4-A-4-1	148	4.38	262	40.5	1414	1501	1407	1453	1450
3	CR4-A-4-2	148	4.38	262	40.5	1402	1501	1407	1453	1450
4	CR4-A-8	148	4.38	262	77	2108	2135	2059	2071	2064
5	CR4-C-2	215	4.38	262	25.4	1777	2092	2052	2071	2005
6	CR4-C-4-1	215	4.38	262	41.1	2424	2746	2607	2701	2643
7	CR4-C-4-2	215	4.38	262	41.1	2393	2746	2607	2701	2643
8	CR4-C-8	215	4.38	262	80.3	3837	4304	4170	4238	4235
9	CR4-D-2	323	4.38	262	25.4	3367	3867	3947	3789	3713
10	CR4-D-4-1	323	4.38	262	41.1	4950	5358	5238	5305	5260
11	CR4-D-4-2	323	4.38	262	41.1	4830	5358	5238	5305	5260
12	CR4-D-8	324	4.38	262	80.3	7481	9212	8994	9225	9329
13	CR6-A-2	144	6.36	618	25.4	2572	2573	2563	2560	2591
14	CR6-A-4-1	144	6.36	618	40.5	2808	2850	2862	2864	2876
15	CR6-A-4-2	144	6.36	618	40.5	2765	2850	2862	2864	2876
16	CR6-A-8	144	6.36	618	77	3399	3485	3520	3502	3476
17	CR6-C-2	211	6.36	618	25.4	3920	4335	4280	4351	4346
18	CR6-C-4-1	211	6.36	618	40.5	4428	4927	4901	4980	4973
19	CR6-C-4-2	211	6.36	618	40.5	4484	4927	4901	4980	4973
20	CR6-C-8	211	6.36	618	77	5758	6335	6353	6340	6354
21	CR6-D-2	319	6.36	618	25.4	6320	7463	7402	7498	7526
22	CR6-D-4-1	319	6.36	618	41.1	7780	8879	8848	8992	9058
23	CR6-D-4-2	318	6.36	618	41.1	7473	8839	8808	8952	9017
24	CR6-D-8	319	6.36	618	85.1	10357	12996	13018	12965	13004
25	CR8-A-2	120	6.47	835	25.4	2819	2603	2592	2598	2624
26	CR8-A-4-1	120	6.47	835	40.5	2957	2815	2818	2802	2800
27	CR8-A-4-2	120	6.47	835	40.5	2961	2815	2818	2802	2800
28	CR8-A-8	119	6.47	835	77	3318	3252	3249	3189	3159
29	CR8-C-2	175	6.47	835	25.4	4210	4198	4196	4270	4272
30	CR8-C-4-1	175	6.47	835	40.5	4493	4617	4648	4680	4662
31	CR8-C-4-2	175	6.47	835	40.5	4542	4617	4648	4680	4662
32	CR8-C-8	175	6.47	835	77	5366	5581	5639	5565	5563
33	CR8-D-2	265	6.47	835	25.4	6546	7120	7089	7256	7236
34	CR8-D-4-1	264	6.47	835	41.1	7117	8052	8078	8202	8190
35	CR8-D-4-2	265	6.47	835	41.1	7172	8093	8119	8244	8232
36	CR8-D-8	265	6.47	835	80.3	8990	10537	10610	10590	10597
37	CR4-A-4-3	210	5.48	294	39.1	3183	2943	2845	2896	2860
38	CR4-A-9	211	5.48	294	91.1	4773	4909	4873	4856	4879
39	CR4-C-4-3	210	4.5	277	39.1	2713	2646	2537	2611	2562
40	CR4-C-9	211	4.5	277	91.1	4371	4641	4559	4589	4609
41	CR6-A-4-3	211	8.83	536	39.1	5898	5404	5397	5378	5360
42	CR6-A-9	211	8.83	536	91.1	7008	7280	7274	7276	7263
43	CR6-C-4-3	204	5.95	540	39.1	4026	4069	4082	4156	4136
44	CR6-C-9	204	5.95	540	91.1	5303	5932	5977	5979	5980
45	CR8-A-4-3	180	9.45	825	39.1	6803	6241	6288	6189	6165
46	CR8-A-9	180	9.45	825	91.1	7402	7506	7562	7485	7504
47	CR8-C-4-3	180	6.6	824	39.1	5028	4797	4836	4880	4849
48	CR8-C-9	180	6.6	824	91.1	5873	6235	6302	6217	6240



No.	Sample	$a$ , mm	$t$ , mm	$R_y$ , MPa	$R_b$ , MPa	$N_{ult}$ , kN				
						experiment	ANN1	ANN2	ANN3	ANN4
Schneider, S.P. (1998) [33]										
49	S1	127.3	3.15	356	30.454	917	1080	1070	1056	1074
50	S2	126.9	4.34	357	26.044	1095	1171	1154	1136	1158
51	S3	126.95	4.55	322	23.805	1113	1101	1072	1063	1081
52	S4	125.9	5.67	312	23.805	1202	1199	1158	1160	1184
53	S5	127	7.47	347	23.805	2069	1521	1506	1494	1538
Lin, C.Y. (1988) [34]										
54	D7	150	0.7	250	23	569	743	790	748	742
55	D8	150	0.7	250	23	624	743	790	748	742
56	D10	150	1.4	250	23	726	815	844	812	804
57	D12	150	2.1	250	23	809	891	902	883	871
58	E7	150	0.7	250	34.4	762	911	912	913	903
59	E10	150	1.4	250	36	993	1023	997	1015	1003
Zhu, A. et al. (2017) [35]										
60	Pa-6-1	197	6.3	438	26.58	2730	3063	3083	3075	3062
61	Pa-6-2	198.5	6.2	438	25.81	3010	3039	3061	3052	3036
62	Pa-6-3	200.5	6.25	438	24.47	2830	3050	3072	3058	3041
63	Pa-10-1	201	10.2	382	26.58	3980	3858	3912	3849	3874
64	Pa-10-2	201	10.1	382	25.81	3920	3806	3858	3797	3821
65	Pa-10-3	199.5	10	382	24.47	3900	3694	3744	3686	3712
Yamamoto, T. et al. (2022) [36]										
66	S10D-2A	100.2	2.18	300	25.7	609	667	631	617	633
67	S20D-2A	200.3	4.35	322	29.6	2230	2232	2219	2232	2196
68	S30D-2A	300.5	6.1	395	26.5	5102	5160	5177	5151	5107
69	S10D-4A	100	2.18	300	53.7	851	884	795	804	830
70	S20D-2A	200.1	4.35	322	57.9	3201	3204	3159	3219	3208
71	S30D-4A	300.6	6.1	395	52.2	6494	7228	7185	7297	7333
72	S10D-6A	101.1	2.18	300	61	911	951	855	865	891
73	S20D-6A	200.2	4.35	322	63.7	3417	3403	3363	3417	3412
Han, L.-H. (2002) [37]										
74	rc1-1	100	2.86	228	48.3	760	836	717	745	762
75	rc1-2	100	2.86	228	48.3	800	836	717	745	762
76	rc2-1	120	2.86	228	48.3	992	1029	909	951	959
77	rc2-2	120	2.86	228	48.3	1050	1029	909	951	959
Liu, D. et al. (2003) [38]										
78	C1-1	99.25	4.18	550	70.8	1490	1544	1488	1486	1491
79	C1-2	101.05	4.18	550	70.8	1535	1578	1526	1525	1529
80	C2-1	101.05	4.18	550	82.1	1740	1682	1618	1618	1613
81	C2-2	100.55	4.18	550	82.1	1775	1671	1606	1607	1602
82	C3	182	4.18	550	70.8	3590	3747	3849	3927	3917
83	C4	181.1	4.18	550	82.1	4210	4043	4143	4195	4190
Han, L.-H., Yao, G.H. (2003) [39]										
84	M-1-1	130	2.65	340.1	22	760	909	924	889	898
85	M-1-2	130	2.65	340.1	22	770	909	924	889	898
Han, L.-H., Yao, G.H. (2004) [40]										
86	ssh-1	200	3	303.5	40	2306	2200	2177	2240	2203
87	ssh-2	200	3	303.5	40	2284	2200	2177	2240	2203
Yu, Q. et al. (2008) [41]										
88	S30-1	100	1.9	404	121.6	1209	1500	1352	1372	1377
89	S30-2	100	1.9	404	121.6	1220	1500	1352	1372	1377

No.	Sample	$a$ , mm	$t$ , mm	$R_y$ , MPa	$R_b$ , MPa	$N_{ult}$ , kN				
						experiment	ANN1	ANN2	ANN3	ANN4
90	S30-3	100	1.9	404	121.6	1190	1500	1352	1372	1377
91	S30-4	100	1.9	404	121.6	1220	1500	1352	1372	1377
Chen, C.-C. et al. (2002) [42]										
92	AA-48	500	10	389	42.5	16500	17619	17626	17696	17633
93	AA-40	500	12	378	42.5	17900	18683	18674	18697	18672
94	AA-32	410	12	378	42.5	12800	13623	13716	13715	13765
95	AA-24	410	16	358	42.5	15300	15114	15209	15252	15279
Ding, F.-X. et al. (2014) [43]										
96	SST1-A	249.6	3.7	324.3	40.4	3131	3525	3486	3575	3529
97	SST1-B	251	3.75	324.3	40.4	2832	3575	3533	3622	3577
98	SST1-C	251.1	3.73	324.3	40.4	2677	3570	3529	3619	3573
Aslani, F. et al. (2015) [44]										
99	SC1A	70	5	701	21	1122	1085	978	964	999
100	SC2A	100	5	701	21	1417	1496	1448	1444	1477
Khan, M. et al. (2017) [45]										
101	CB15-SH (A)	74.04	4.91	762	100	1636	1708	1506	1521	1486
102	CB15-SH (B)	72.87	4.88	762	100	1755	1678	1473	1488	1453
103	CB20-SH (A)	99.56	4.91	762	100	2520	2352	2237	2234	2205
104	CB20-SH (B)	99.2	4.93	762	100	2632	2346	2229	2227	2197
105	CB25-SH (A)	124.43	4.93	762	100	3023	3159	3128	3110	3093
106	CB25-SH (B)	124.94	4.94	762	100	2962	3180	3151	3132	3116
107	CB30-SH (A)	149.99	4.92	762	100	4115	4156	4192	4162	4164
108	CB30-SH (B)	149.87	4.92	762	100	3968	4151	4187	4157	4159
Xiong, M.-X. et al. (2017) [46]										
109	S1	150	8	779	193	6536	6842	7047	6953	7581
110	S2	150	8	779	199	6715	6926	7216	7074	7793
111	S3	150	8	779	187	6616	6755	6889	6835	7380
112	S4	150	8	779	208	7276	7044	7488	7257	8135
113	S5	150	8	779	188	6974	6770	6915	6855	7413
114	S6	150	12	756	193	8585	7790	8346	8038	8807
115	S7	150	12	756	199	8452	7852	8529	8137	9009
116	S8	150	12	756	187	8687	7723	8173	7940	8618
117	S9	150	12	756	208	8730	7935	8822	8289	9335
118	S10	150	12	756	188	8912	7734	8201	7957	8648
119	S11	150	12.5	446	193	5953	5557	6194	6027	6340
120	S12	150	12.5	446	199	5911	5591	6333	6095	6444
121	S13	150	12.5	446	187	6039	5519	6061	5959	6239
122	S14	150	12.5	446	208	6409	5632	6552	6194	6609
123	S15	150	12.5	446	188	6285	5525	6083	5971	6256

**Table 5. Characteristics of the quality of model forecasting.**

		ANN1	ANN2	ANN3	ANN4
$N_{predict}/N_{exp}$	mean	1.046579	1.037273	1.037224	1.046729
	max	1.333582	1.388401	1.351886	1.334703
	min	0.735138	0.727888	0.722088	0.743354
Standard deviation		0.102275	0.101901	0.100931	0.097743
Coefficient of variation		9.77234	9.823902	9.730883	9.337981

Table 5 shows that quality metrics of the models are quite close, and layer recurrent neural network provides the best agreement with the experimental data. The results deviation from the experimental data can be primarily explained by the fact that when training the ANN, the simplified model of the CFST columns

deformation was used. This model did not take into account the slipping of the concrete core in the steel shell, the separation of the steel shell from the concrete core, and the effects of local buckling. In addition, of course, there was a scatter in the experimental data, which can be observed in Table 3. Our further research will be aimed at developing ANNs based on more complex theoretical models [47–48].

## 4. Conclusion

1. Four ANN models have been developed to predict the load-bearing capacity of centrally compressed CFST columns of square cross-section based on the following architectures: cascade forward backpropagation network, Elman neural network, feedforward neural network, layer recurrent neural network. The ANNs were trained on synthetic data obtained through a numerical experiment using a simplified method for 22308 samples.
2. The trained neural networks are characterized by low MSE, and the correlation coefficients between the predicted and target values are close to one. The best MSE value was achieved using the Elman neural network architecture that has a feedback.
3. The developed models of ANNs were tested on experimental data for 123 samples presented in 15 different papers. The model based on the layer recurrent neural network architecture, which has feedback like Elman neural network, showed the best forecasting quality. The average ratio of the predicted ultimate loads values to the experimental ones was 1.047, the maximum was 1.335, and the minimum was 0.743.
4. Further research can be aimed at training ANNs using more complex theoretical models that take into account the features of the contact interaction between the concrete core and the steel shell, the effects of local buckling, the slenderness of the elements, the presence of eccentricities, etc.

## References

1. Tran, H., Thai, H.T., Ngo, T., Uy, B., Li, D., Mo, J. Nonlinear inelastic simulation of high-rise buildings with innovative composite coupling shear walls and CFST columns. *The Structural Design of Tall and Special Buildings*. 2021. 30(13). Article no. e1883. DOI: 10.1002/tal.1883
2. Chen, Z., Gao, F., Hu, J., Liang, H., Huang, S. Creep and shrinkage monitoring and modelling of CFST columns in a super high-rise under-construction building. *Journal of Building Engineering*. 2023. 76. Article no. 107282. DOI: 10.1016/j.jobe.2023.107282
3. Thai, H.-T., Thai, S., Ngo, T., Uy, B., Kang, W.-H., Hicks, S.J. Reliability considerations of modern design codes for CFST columns. *Journal of Constructional Steel Research*. 2021. 177. Article no. 106482. DOI: 10.1016/j.jcsr.2020.106482
4. Yuan, H.-H., She, Z.-M., Wu, Q.-X., Huang, Y.-F. Experimental and parametric investigation on elastoplastic seismic response of CFST battened built-up columns. *Soil Dynamics and Earthquake Engineering*. 2021. 145. Article no. 106726. DOI: 10.1016/j.soildyn.2021.106726
5. Grzeszykowski, B., Szmigiera, E.D. Experimental Investigation on the Vertical Ductility of Rectangular CFST Columns Loaded Axially. *Materials*. 2022. 15(6). Article no. 2231. DOI: 10.3390/ma15062231
6. Cai, W.-Z., Wang, B., Shi, Q.-X. Hysteretic model and seismic energy response of CFST columns in diagrid structure. *Journal of Building Engineering*. 2023. 68. Article no. 106185. DOI: 10.1016/j.jobe.2023.106185
7. Hassooni, A.N., Al Zaidee, S.R. Behavior and Strength of Composite Columns under the Impact of Uniaxial Compression Loading. *Engineering, Technology & Applied Science Research*. 2022. 12(4). Pp. 8843–8849. DOI: 10.48084/etasr.4753
8. Du, Y., Zhang, Y., Chen, Z., Yan, J.-B., Zheng, Z. Axial compressive performance of CFRP confined rectangular CFST columns using high-strength materials with moderate slenderness. *Construction and Building Materials*. 2021. 299. Article no. 123912. DOI: 10.1016/j.conbuildmat.2021.123912
9. Yang, Y., Wu, C., Liu, Z., Qin, Y., Wang, W. Comparative study on square and rectangular UHPFRC-Filled steel tubular (CFST) columns under axial compression. *Structures*. 2021. 34. Pp. 2054–2068. DOI: 10.1016/j.istruc.2021.08.104
10. Wu, S., Liu, W., Zhang, J., He, W., Guo, Y. Experimental and analytical investigation of square-shaped concrete-filled steel tube columns. *Journal of Constructional Steel Research*. 2023. 201. Article no. 107737. DOI: 10.1016/j.jcsr.2022.107737
11. Chen, J., Chan, T.-M., Chung, K.-F. Design of square and rectangular CFST cross-sectional capacities in compression. *Journal of Constructional Steel Research*. 2021. 176. Article no. 106419. DOI: 10.1016/j.jcsr.2020.106419
12. Zhao, P., Huang, Y., Lu, Y., Liang, H., Zhu, T. Eccentric behaviour of square CFST columns strengthened using square steel tube and high-performance concrete jackets. *Engineering Structures*. 2022. 253. Article no. 113772. DOI: 10.1016/j.engstruct.2021.113772
13. Yang, C., Gao, P., Wu, X., Chen, Y.F., Li, Q., Li, Z. Practical formula for predicting axial strength of circular-CFST columns considering size effect. *Journal of Constructional Steel Research*. 2020. 168. Article no. 105979. DOI: 10.1016/j.jcsr.2020.105979
14. Al Zand, A.W., Badaruzzaman, W.H.W., Tawfeeq, W.M. New empirical methods for predicting flexural capacity and stiffness of CFST beam. *Journal of Constructional Steel Research*. 2020. 164. Article no. 105778. DOI: 10.1016/j.jcsr.2019.105778
15. Jin, L., Fan, L., Li, D., Du, X. Size effect of square concrete-filled steel tubular columns subjected to lateral shear and axial compression: Modelling and formulation. *Thin-Walled Structures*. 2020. 157. Article no. 107158. DOI: 10.1016/j.tws.2020.107158
16. Wang, K., Chen, M., Zhang, R., Fang, W. Finite element simulation of load bearing capacity of circular CFST long columns with localized corrosion under eccentric load. *Structures*. 2022. 43. Pp. 1629–1642. DOI: 10.1016/j.istruc.2022.07.029
17. Sarir, P., Jiang, H., Asteris, P.G., Formisano, A., Armaghani, D.J. Iterative Finite Element Analysis of Concrete-Filled Steel Tube Columns Subjected to Axial Compression. *Buildings*. 2022. 12(12). Article no. 2071. DOI: 10.3390/buildings12122071

18. Liu, J., Yu, W., Fang, Y., Pan, Z., Cao, G. Finite Element Analysis on the Seismic Performance of Concrete-Filled Steel Tube Columns with a Multiple-Chamber Round-Ended Cross-Section. *Buildings*. 2024. 14(4). Article no. 1154. DOI: 10.3390/buildings14041154
19. Tao, Z., Katwal, U., Uy, B., Wang, W.-D. Simplified Nonlinear Simulation of Rectangular Concrete-Filled Steel Tubular Columns. *Journal of Structural Engineering*. 2021. 147(6). Article no. 04021061. DOI: 10.1061/(ASCE)ST.1943-541X.0003021
20. Naser, M.Z., Thai, S., Thai, H.-T. Evaluating structural response of concrete-filled steel tubular columns through machine learning. *Journal of Building Engineering*. 2021. 34. Article no. 101888. DOI: 10.1016/j.jobbe.2020.101888
21. Le, T.-T., Phan, H.C. Prediction of Ultimate Load of Rectangular CFST Columns Using Interpretable Machine Learning Method. *Advances in Civil Engineering*. 2020. 1. Article no. 8855069. DOI: 10.1155/2020/8855069
22. Zarringol, M., Thai, H.-T., Thai, S., Patel, V. Application of ANN to the design of CFST columns. *Structures*. 2020. 28. Pp. 2203–2220. DOI: 10.1016/j.istruc.2020.10.048
23. Đorđević, F., Kostić, S.M. Practical ANN prediction models for the axial capacity of square CFST columns. *Journal of Big Data*. 2023. 10(1). Article no. 67. DOI: 10.1186/s40537-023-00739-y
24. Memarzadeh, A., Sabetifar, H., Nematzadeh, M. A comprehensive and reliable investigation of axial capacity of Sy-CFST columns using machine learning-based models. *Engineering Structures*. 2023. 284. Article no. 115956. DOI: 10.1016/j.engstruct.2023.115956
25. Tran, V.-L., Thai, D.-K., Nguyen, D.-D. Practical artificial neural network tool for predicting the axial compression capacity of circular concrete-filled steel tube columns with ultra-high-strength concrete. *Thin-Walled Structures*. 2020. 151. Article no. 106720. DOI: 10.1016/j.tws.2020.106720
26. Nesvetaev, G., Koryanova, Y., Kolleganov, A. E-Modulus and Creep Coefficient of Self-Compacting Concretes and Concretes with some Mineral Additives. *Solid State Phenomena*. 2018. 284. Pp. 963–969. DOI: 10.4028/www.scientific.net/SSP.284.963
27. Nesvetaev, G., Koryanova, Y., Chepurnenko, A. Comparison of the shear strength in heavy and self-compacting concrete. *Architecture and Engineering*. 2023. 8(2). Pp. 63–71. DOI: 10.23968/2500-0055-2023-8-2-63-71
28. Lu, X., Hsu, C.-T.T. Tangent Poisson's ratio of high-strength concrete in triaxial compression. *Magazine of Concrete Research*. 2007. 59(1). Pp. 69–77. DOI: 10.1680/macrc.2007.59.1.69
29. Chen, Z., Gandhi, U., Lee, J., Wagoner, R.H. Variation and consistency of Young's modulus in steel. *Journal of Materials Processing Technology*. 2016. 227. Pp. 227–243. DOI: 10.1016/j.jmatprotec.2015.08.024
30. Chepurnenko, A., Yazyev, B., Meskhi, B., Beskopylny, A., Khashkhozhev, K., Chepurnenko, V. Simplified 2D Finite Element Model for Calculation of the Bearing Capacity of Eccentrically Compressed Concrete-Filled Steel Tubular Columns. *Applied Sciences*. 2021. 11(24). Article no. 11645. DOI: 10.3390/app112411645
31. Chepurnenko, A.S., Turina, V.S., Akopyan, V.F. Artificial intelligence model for predicting the load-bearing capacity of eccentrically compressed short concrete filled steel tubular columns. *Construction Materials and Products*. 2024. 7(2). Article no. 2. DOI: 10.58224/2618-7183-2024-7-2-2
32. Ouyang, Y., Kwan, A.K.H. Finite element analysis of square concrete-filled steel tube (CFST) columns under axial compressive load. *Engineering Structures*. 2018. 156. Pp. 443–459. DOI: 10.1016/j.engstruct.2017.11.055
33. Schneider, S.P. Axially Loaded Concrete-Filled Steel Tubes. *Journal of Structural Engineering*. 1998. 124(10). Pp. 1125–1138. DOI: 10.1061/(ASCE)0733-9445(1998)124:10(1125)
34. Lin, C.Y. Axial Capacity of Concrete Infilled Cold-formed Steel Columns. *Proceedings of the International Specialty Conference on Cold-Formed Steel Structures*. 2. University of Missouri. Rolla, 1988. Pp. 443–457.
35. Zhu, A., Zhang, X., Zhu, H., Zhu, J., Lu, Y. Experimental study of concrete filled cold-formed steel tubular stub columns. *Journal of Constructional Steel Research*. 2017. 134. Pp. 17–27. DOI: 10.1016/j.jcsr.2017.03.003
36. Yamamoto, T., Kawaguchi, J., Morino, S. Experimental Study of Scale Effects on the Compressive Behavior of Short Concrete-Filled Steel Tube Columns. *Composite Construction in Steel and Concrete IV*. 2002. Pp. 879–890. DOI: 10.1061/40616(281)76
37. Han, L.-H. Tests on stub columns of concrete-filled RHS sections. *Journal of Constructional Steel Research*. 2002. 58(3). Pp. 353–372. DOI: 10.1016/S0143-974X(01)00059-1
38. Liu, D., Gho, W.-M., Yuan, J. Ultimate capacity of high-strength rectangular concrete-filled steel hollow section stub columns. *Journal of Constructional Steel Research*. 2003. 59(12). Pp. 1499–1515. DOI: 10.1016/S0143-974X(03)00106-8
39. Han, L.-H., Yao, G.-H. Influence of concrete compaction on the strength of concrete-filled steel RHS columns. *Journal of Constructional Steel Research*. 2003. 59(6). Pp. 751–767. DOI: 10.1016/S0143-974X(02)00076-7
40. Han, L.-H., Yao, G.-H. Experimental behaviour of thin-walled hollow structural steel (HSS) columns filled with self-consolidating concrete (SCC). *Thin-Walled Structures*. 2004. 42(9). Pp. 1357–1377. DOI: 10.1016/j.tws.2004.03.016
41. Yu, Q., Tao, Z., Wu, Y.-X. Experimental behaviour of high performance concrete-filled steel tubular columns. *Thin-Walled Structures*. 2008. 46(4). Pp. 362–370. DOI: 10.1016/j.tws.2007.10.001
42. Chen, C.-C., Ko, J.-W., Huang, G.-L., Chang, Y.-M. Local buckling and concrete confinement of concrete-filled box columns under axial load. *Journal of Constructional Steel Research*. 2012. 78. Pp. 8–21. DOI: 10.1016/j.jcsr.2012.06.006
43. Ding, F.-X., Fang, C., Bai, Y., Gong, Y.-Z. Mechanical performance of stirrup-confined concrete-filled steel tubular stub columns under axial loading. *Journal of Constructional Steel Research*. 2014. 98. Pp. 146–157. DOI: 10.1016/j.jcsr.2014.03.005
44. Aslani, F., Uy, B., Tao, Z., Mashiri, F. Behaviour and design of composite columns incorporating compact high-strength steel plates. *Journal of Constructional Steel Research*. 2015. 107. Pp. 94–110. DOI: 10.1016/j.jcsr.2015.01.005
45. Khan, M., Uy, B., Tao, Z., Mashiri, F. Behaviour and design of short high-strength steel welded box and concrete-filled tube (CFT) sections. *Engineering Structures*. 2017. 147. Pp. 458–472. DOI: 10.1016/j.engstruct.2017.06.016
46. Xiong, M.-X., Xiong, D.-X., Liew, J.Y.R. Axial performance of short concrete filled steel tubes with high-and ultra-high-strength materials. *Engineering Structures*. 2017. 136. Pp. 494–510. DOI: 10.1016/j.engstruct.2017.01.037
47. Novoselov, O.G., Sabitov, L.S., Sibgatullin, K.E., Sibgatullin, E.S., Klyuev, A.V., Klyuev, S.V., Shorstova, E.S. Method for calculating the strength of massive structural elements in the general case of their stress-strain state (parametric equations of the strength surface). *Construction Materials and Products*. 2023. 6(2). Pp. 104–120. DOI: 10.58224/2618-7183-2023-6-2-104-120
48. Novoselov, O.G., Sabitov, L.S., Sibgatullin, K.E., Sibgatullin, E.S., Klyuev, A.S., Klyuev, S.V., Shorstova, E.S. Method for calculating the strength of massive structural elements in the general case of their stress-strain state (kinematic method). *Construction Materials and Products*. 2023. 6(3). Pp. 5–17. DOI: 10.58224/2618-7183-2023-6-3-5-17

**Information about the authors:**

**Anton Chepurnenko**, Doctor of Technical Sciences

ORCID: <https://orcid.org/0000-0002-9133-8546>

E-mail: [anton\\_chepurnenk@mail.ru](mailto:anton_chepurnenk@mail.ru)

**Batyr Yazhev**, Doctor of Technical Sciences

ORCID: <https://orcid.org/0000-0002-5205-1446>

E-mail: [ps62@yandex.ru](mailto:ps62@yandex.ru)

**Vasilina Turina**, PhD in Technical Sciences

ORCID: <https://orcid.org/0009-0001-6399-401X>

E-mail: [vasilina.93@mail.ru](mailto:vasilina.93@mail.ru)

**Vladimir Akopyan**, PhD in Technical Sciences

ORCID: <https://orcid.org/0000-0003-3976-9346>

E-mail: [vovaakop@mail.ru](mailto:vovaakop@mail.ru)

Received: 08.07.2024. Approved after reviewing: 31.08.2024. Accepted: 03.09.2024.



Research article

UDC 624

DOI: 10.34910/MCE.130.9



## Evaluation of prior probability distribution of undrained cohesion for soil in Nasiriyah

R.S. Shakir , Z. Abd Al-Haleem

University of Thi-Qar, Nasiriyah, Iraq

 [rrshakir@utq.edu.iq](mailto:rrshakir@utq.edu.iq)

**Keywords:** clay soil, prior distribution, prior knowledge, site characterization, undrained cohesion

**Abstract.** The objective of the study is to evaluate the prior probability distribution (PPD) of undrained cohesion ( $C_u$ ) parameter for soil in Nasiriyah, southern Iraq, based on prior knowledge and observations. Estimated PPD of  $C_u$  can be used in Bayesian approach to update the observed value in any project in this region using the posterior probability distribution, because it is considered as a measure of the initial belief about a random variable before considering any data. The research used five methods to express the PPD of  $C_u$ . Two of them are for non-informative data, i.e. uniform distribution and Jeffreys prior, and three of them – for informative data, which include maximum entropy, regression analysis and subjective probability. They were applied to data collected from different sources in Nasiriyah, based on site investigation reports. The ranges of mean, standard deviation and vertical scale of  $C_u$  fluctuation were found to be 12–62 kPa, 0.5–27.6 kPa and 6–8 m, respectively. It was concluded that Jeffreys method is used well with individual models at the mean value of cohesion of 28.66 kPa and the standard deviation of 1.19 kPa. The maximum entropy can be used for the least informative data, while respecting the given constraints. The mean value of cohesion was 28.7 kPa, and the standard deviation was 1.2 kPa. Finally, for a finite number of 152 cohesion values, the subjective probability assessment approach, which takes into account expert knowledge and judgment, is the most appropriate method with the mean value of cohesion of 37 kPa and the standard deviation of 8.8 kPa.

**Acknowledgements:** The authors gratefully acknowledge the data provided by the Office of Scientific and Advisory Services (College of Engineering, University of Al-Qadisiyah), the National Company for Engineering Examination and Designs, and the Al-Sabtain Company for Engineering Tests.

**Citation:** Shakir, R.R., Al-Haleem, Z. Abd. Evaluation of prior probability distribution of undrained cohesion for soil in Nasiriyah. Magazine of Civil Engineering. 2024. 17(6). Article no. 13009. DOI: 10.34910/MCE.130.9

### 1. Introduction

Undrained cohesion ( $C_u$ ) is a significant and necessary property used to characterize the undrained shear strength of soil. It can be used to design and analyze different geotechnical problems, such as bearing capacity of shallow and deep (pile) foundation. Laboratory tests, such as triaxial shear or unconfined compression tests are commonly used to measure the  $C_u$  value performed on undisturbed samples from field investigation. These processes are relatively time-consuming and expensive, and there are many sources of error that make the  $C_u$  value uncertain, such as quality of consistency and degree of saturation.

Prior distribution is an essential and first step in the Bayesian approach, which includes knowledge of the uncertain parameters combined with the probability distribution of recent data to get the posterior distribution [1]. It is used in the Bayesian approach to update the observed value of cohesion in a project in this area. Prior knowledge includes general information about the hypothesis that may be relevant or unclear. It may be previously gained knowledge of any type of distribution that correctly reflects the state of the model or parameter under study. When the posterior distributions belong to the same family of

probability distribution of prior distribution, they are known as conjugate distributions [2]. Previously gained information can be divided into two groups: informative prior knowledge and non-informative prior knowledge, according to its accuracy and quantity.

Non-informative prior knowledge can be used to probabilistically characterize a homogeneous soil layer, which requires three model parameters, e.g. mean  $\mu$ , standard deviation  $\sigma$ , vertical scale of fluctuation  $\lambda$  [3]. It depends on the value of the rate, i.e. the limits of the parameter, with the most dependent uniform distribution in describing the uncertainty [2]. It led to the conclusion that prior knowledge is consistent with the rates cited in [4, 5]. Jeffreys [6] analyzed the optimal selection of non-informative prior distributions. He found that the prior probabilities should be assumed to be uniform over the parameter for variables with domains of  $(-\infty, \infty)$  and uniform over the logarithm for variables with domains of  $[0, \infty]$ . The latter becomes inversely proportional to the soil parameter in arithmetic space [7].

Informative prior knowledge shows that certain prior estimates are preferable to others. It is used, when there is an abundance of collected information about soil properties, which is divided into three methods that help to obtain the probability distribution (e.g., subjective probability, maximum entropy, regression analysis). Subjective probability assessment framework (SPAF) is used to evaluate the plausibility of previously acquired uncertain statistical estimation [8, 9]. There are some circumstances, in which a different kind of distribution might be necessary to hold the available data without the risk of obstructing the conclusions of the analysis. The maximum entropy principle could be used to define the prior prior distribution [10, 11]. In this situation, entropy refers to randomness of the information and is relatively similar to the concept of entropy in physical systems [12]. The maximum entropy method was used to estimate the probability distribution and to develop the reliability of the slopes [13]. The probability distribution can also be obtained through regression analysis [14, 15] with the  $\mu$  and  $\sigma$  of the data. This analysis provides a practical way to construct prior distributions from prior knowledge. It usually provides a weight similar to the prior information. In addition, it is challenging to include systematically subjective judgments in statistical analysis, which are sometimes a crucial component of prior knowledge [16].

The objective of geotechnical site description is to identify the soil layers and to evaluate the properties of the soil and rocks for the analysis of geological and geotechnical systems [9, 17]. The correct site characterization requires comprehensive measures at several places since soils are common geomaterials with spatial heterogeneity [18]. The process of geotechnical site characterization involves several steps, including desk research, site surveys, laboratory tests [3], analysis or comprehension of site data, and inference of soil and rock properties [19]. Any method used in the site characterization that solely relies on measured data is called "data-driven site characterization", and this includes both site-specific data collected for the current project and existing data of any kind collected from previous stages of the same project or previous projects at the same site, adjacent sites, or elsewhere [20, 21]. Geotechnical engineering frequently deals with uncertainty, and engineering design must take it into account [22]. There are three main categories of uncertainties: test errors, existing model uncertainty, and inherent variability [23, 24]. The evaluation of soil properties and their statistics based on past information are not clearly known results rather than clear-cut conclusions because of uncertainties in the currently studied information and engineers' qualification. As a result, such not clearly known evaluations are referred to as uncertain evaluation [3].

This article investigated approaches to enhance and estimate prior knowledge. It included data obtained from the geotechnical reports of projects implemented in Nasiriyah in southern Iraq. The purpose of collecting this data, which was considered as prior knowledge, is to quantify it and calculate its prior distributions to achieve the most appropriate geometric judgment sense and insert it into a Bayesian framework. The non-informative knowledge (e.g. uniform distribution) was based on the average maximum and minimum value of  $\mu$ ,  $\sigma$ , and  $\lambda$  of  $C_u$ , in addition to the maximum entropy method and the regression analysis method, besides the SPAF, which in turn was based on many stages to achieve the prior distribution appropriate to the soil property.

## 2. Methods

### 2.1. Study Area

Thi-Qar is a province in the south of Iraq that borders the provinces of Basra, Wassit, Muthanna, Missan, and Qadissiya (Fig. 1) [25, 26]. The province is located about 370 km southeast of Baghdad between latitude  $31^{\circ}14'$  N and longitude  $46^{\circ}19'$  E. It has a total area of 13552 km<sup>2</sup> [27]. The province features a hot desert climate with very hot and dry summers and mild winters. The mean daily maximum in the summer exceeds 40 °C [28]. It is located in the Mesopotamian plain. There are deposits of alluvial silt from the Euphrates and Tigris rivers. The soil in this region is a floodplain formation consisting of clay, silt,

and sand, where the silt forms 60 % of the deposits. The silt soil and sand settle in the swamps, the mud runs below the Shatt al-Arab, and one million tons of sediments are dried up annually (12000 years) in these rivers that flow from the northwest to the southeast of Turkey through this basin [29, 30]. Since the area is free from surface erosion of ancient rocks, the city of Nasiriyah belongs to the floodplain zone and represents the last formation of surface of Iraqi geology [31, 32].



**Figure 1. Location of Thi-Qar Province on the map of Iraq.**

## 2.2. Data Collection

In this study, the data was gathered from a variety of places within Thi-Qar Province. The province is divided into many sections (for example, Nasiriyah, Al-Chibayish, Suq Al-Shuyukh, Al-Rifai, Al-Shatrah, Qalat Sukkar and Al-Nasr), as shown in Fig. 2. The available soil investigations for these areas were included in the data. To analyze the geotechnical properties, as well as to measure soil consistency at various depths, the standard penetration test of approximately 200 boreholes was used.

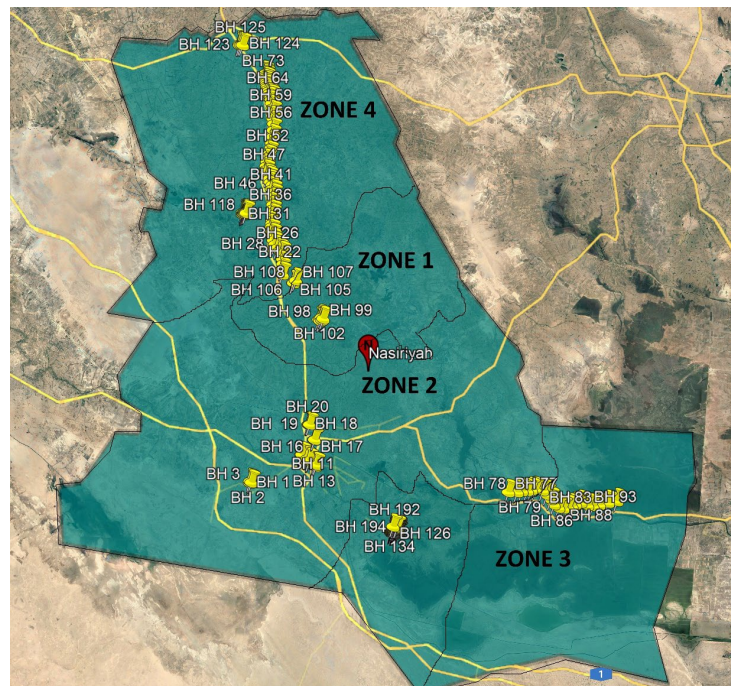


**Figure 2. Location of the study area.**



### 2.3. Description of Thi-Qar Soil

The data collected from multiple projects in Nasiriyah included zones 1–4 (Fig. 2). Zone 1 represents the description of soils of Qalat Sukkar and Al-Nasr. Zone 2 represents the soils of Al-Shatrah. Zone 3 and 4 represent the soils of Nasiriyah, Al-Chibayish, and Suq Al-Shuyukh, respectively.

The soil layers consist of silty clayey or silty clay soils of little to medium plasticity ML, that varies in color from light gray to light brown and have a fairly firm texture. It is also characterized by patches of salt and gypsum crystals that extend in Zone 1 at a depth of 14 m and 20–24 m, and in Zone 2 at a depth of 12–14 m and in Zone 3 at a depth of 11–13 m.

Zone 3 consists of a hard to very hard layer and medium plasticity. Layer of light green clay appears in the upper layer at a depth of 4 m, at 8–12 m, and also at 14–24 m. Zone 4 extends at a depth of 2–12 m and at 15–24 m. It classified by type CL.

Soil layers of little plasticity or non-plasticity are located in Zone 1, as it consists of medium to dense gray soil to soft brown of soft sandy grains (SM), at a depth of 14–20 m. The same applies to Zone 2 at a depth of 15–18 m and at a depth of 4–8 m and at a depth of 12–14 m in Zones 3 and 4, respectively. Fig. 3 shows the profile of each of these layers of Nasiriyah soils in the Thi-Qar Province.

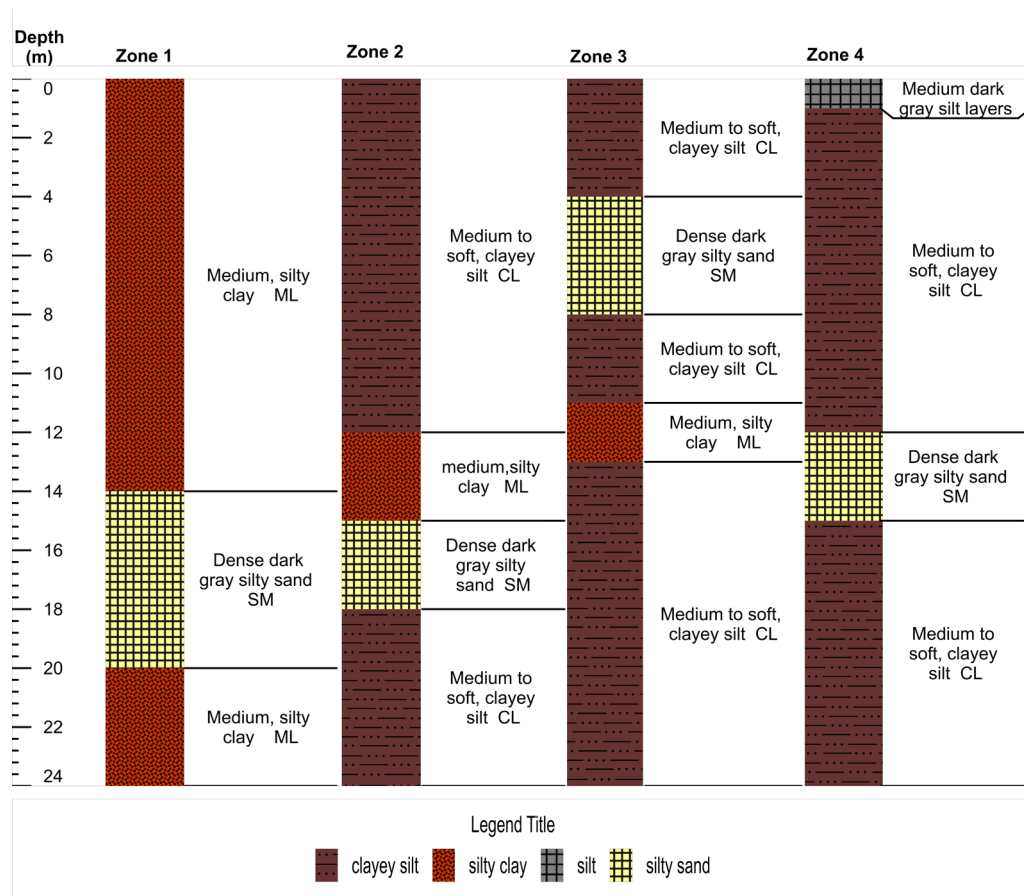


Figure 3. Soil profile of Nasiriyah based on borehole samples considered in the current study.

### 2.4. Prior knowledge

During geotechnical site characterization, both previously acquired knowledge and observation data that are site-specific are used to determine soil parameters, that can be expressed as  $\theta_i$  (e.g.,  $\mu$ ,  $\sigma$ ,  $\lambda$ ). From a Bayesian perspective, such a procedure may be viewed as an update of previously acquired knowledge using observational data from a project site [19]. The previously acquired distribution is an essential part of Bayesian inference because it resembles information about an uncertain parameter that is accompanied by the probability distribution of new data to produce the posterior distribution. The prior distribution can be obtained by applying the methods shown in Fig. 4.

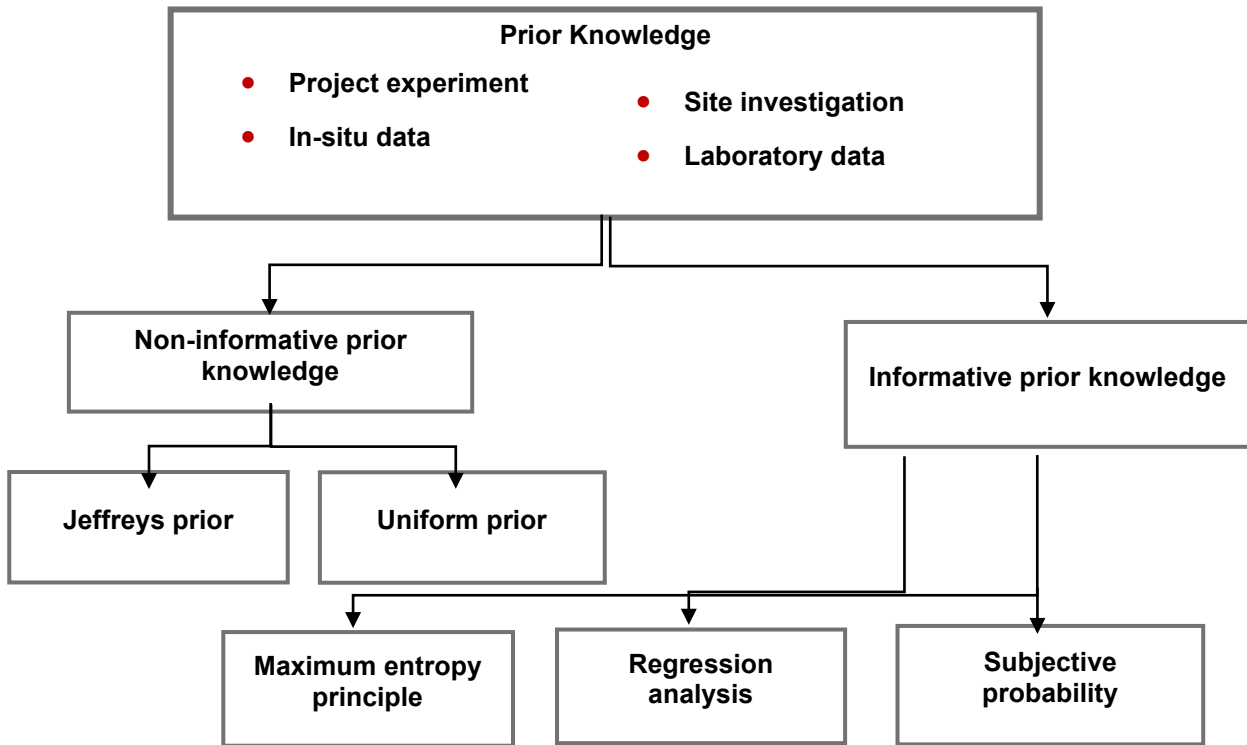


Figure 4. Methods of expressing the prior knowledge.

#### 2.4.1. Non-informative prior knowledge

Since the early studies of Bayes and Laplace [33], there has been some consensus that assigning a uniform distribution to a scalar parameter  $\theta_i$  is one of the easiest methods to depict a state of ignorance about its value. Each value of  $\theta_i$  has the same prior probability with a uniform prior (or probability density). It expresses vague data regarding the specified variable. In the lack of specific prior knowledge, vague priors are frequently used as the default prior option, however, it is crucial to emphasize that ambiguous priors are not always non-informative to the analysis, which is a common mistake in the literature with vague priors being incorrectly referred to as non-informative priors. The use of a non-informative antecedent in parameter estimation issues yields findings that are not materially different from those of conventional statistical analysis. Based on prior distribution, there is no predisposition for any value that falls within the range of potential values  $\theta_i$ . The prior distribution of  $\theta_i$  can be written as follows.

$$P(\theta_p) = \prod_{i=1}^{n_m} P(\theta_i); \quad (1)$$

$$P(\theta_i) = \begin{cases} \frac{1}{\theta_{i,\max} - \theta_{i,\min}} & \text{for } \theta_i \in [\theta_{i,\min}, \theta_{i,\max}], i = 1, 2, \dots, n_m \\ 0 & \text{otherwise} \end{cases}. \quad (2)$$

Consider a model parameter  $\theta_i$  (e.g.,  $\mu$ ,  $\sigma$ ,  $\lambda$ ).

$$P(\mu) = \begin{cases} \frac{1}{\mu_{\max} - \mu_{\min}} & \text{for } \mu \in [\mu_{\min}, \mu_{\max}], \\ 0 & \text{otherwise} \end{cases}; \quad (3)$$

$$P(\sigma) = \begin{cases} \frac{1}{\sigma_{\max} - \sigma_{\min}} & \text{for } \sigma \in [\sigma_{\min}, \sigma_{\max}], \\ 0 & \text{otherwise} \end{cases}; \quad (4)$$

$$P(\theta_p) = \begin{cases} \frac{1}{\mu_{\max} - \mu_{\min}} \times \frac{1}{\sigma_{\max} - \sigma_{\min}} \times \frac{1}{\lambda_{\max} - \lambda_{\min}} & \text{for } \mu \in [\mu_{\min}, \mu_{\max}], \sigma \in [\sigma_{\min}, \sigma_{\max}], \text{ and } \lambda \in [\lambda_{\min}, \lambda_{\max}] \\ 0 & \text{others} \end{cases} \quad (5)$$

$P(\theta_p)$  refers to the prior probability distribution,  $\mu$  is the mean,  $\sigma$  is the standard deviation,  $\lambda$  is the vertical scale of fluctuation.

This form of prior knowledge of the soil property  $C_u$  in Nasiriyah city was investigated. During the site characterization, the maximum and minimum values of the mean, standard deviation and vertical fluctuation scale were determined and presented as shown in Tables 1 and 2.

**Table 1. Ranges of the mean and standard deviation of soil properties of Thi-Qar.**

Soil property	Range of prior evaluation of mean	Range of the prior evaluation of standard deviation	Range of COV%
Cohesion $C_u$ (kPa)	12–62	0.5–27.58	1.6–84.85

**Table 2. Ranges of the vertical scale of fluctuation of soil properties of Thi-Qar.**

Soil property	Range of the prior evaluation of vertical scale of fluctuation(m)
$C_u$ (kPa)	6–8

Jeffreys proposed prior, non-informative method used to estimate parameters when an appropriate prior distribution is not obtainable.

Jeffreys noticed that a non-informative prior proportionate to the square root of the information matrix's determinant is non-informative. Then, Jeffreys prior is:

$$P(\theta) \propto I(\theta)^{-\frac{1}{2}} \quad (6)$$

Regarding the non-invariance of prior distributions based on Fisher's information matrix, Jeffreys shows up a larger finding. Fisher [34] proposed that the data contained in a set of observations  $x = x_1, \dots, x_n$ , with regard to a parameter  $\theta$ , are to be as follows:

$$I(\theta) = E_{\theta} \left[ \left( \frac{d}{d\theta} \ln(p(x/\theta)) \right)^2 \right] \quad (7)$$

$I(\theta)$  is the Fisher information.

Please note that  $p(x/\theta)$  is the probability of  $\theta$ .

#### 2.4.2. Informative prior knowledge

Informative prior distributions are those based on knowledge other than the immediate measured data at hand (e.g., prior data or engineering opinion). Prior information about the value of a parameter exists, the prior distribution might be informative rather than non-informative. Any probability distribution may be used to depict prior information. Increase in prior knowledge or data is more beneficial. The right informative distribution of prior  $\theta_i$  information must be estimated by appropriate evaluating of the plausibility of various prior  $\theta_i$  evaluation in light of previous experience.

##### 2.4.2.1. Maximum entropy principle and statistical analysis method

This method is the least biased method and by selecting a distribution with entropy, the most appropriate probability distribution of  $C_u$  can be determined, which increases the uncertainty measure. Prior knowledge regarding the model parameters may also be used to evaluate the informative prior distribution, which resembles the degree of belief (or certainty level) of prior information according to the model

parameters. When there is insufficient prior information on  $\theta_i$ , the maximum entropy method can also be used to infer the prior distribution from the established data [35, 11]. Using the maximum entropy principle, prior probability distributions for Bayesian inference are frequently generated. Jaynes [36] was an ardent supporter of this method, believing that the distribution with the maximum entropy was the least informative. Within the maximal entropy technique, the information entropy  $H_I$  is used as a measure of the uncertainty of the prior probability density function (PDF)  $P(\theta_i)$  of  $\theta_i$  and is defined as [35]:

$$H_I = -\int P(\theta_i) \ln[P(\theta_i)] d\theta, \quad (8)$$

where  $\theta_i$  is a random variable with a continuous distribution and  $P(\theta_i)$  is the PDF. A function is constructed to assess the entropy difference between  $P_1(\theta_i)$  and  $P_2(\theta_i)$  probability assignments [37].

$$H[P_1(\theta_i), P_2(\theta_i)] = \int P_1(\theta_i) \ln \left[ \frac{P_1(\theta_i)}{P_2(\theta_i)} \right] d\theta. \quad (9)$$

According to Jaynes, the minimum biased assignment of probabilities is one that reduces entropy while satisfying the restrictions given by the available information.

$$H[P(\theta_i), P_0(\theta_i)] = \int P(\theta_i) \ln \left[ \frac{P(\theta_i)}{P_0(\theta_i)} \right] d\theta. \quad (10)$$

The maximum entropy principle implies that, given specified restrictions on the prior, the prior should be the distribution with the maximum entropy that follows these requirements. The most fundamental condition is that  $P$  must reside in the probability simplex, i.e.

$$\begin{aligned} P(\theta_i) &= 1 \text{ and } P(\theta_i) \geq 0. \\ \int \theta_i P(\theta_i) d\theta &= \mu_i, \quad i = 1, 2, \dots, n_m, \end{aligned} \quad (11)$$

where  $P_0(\theta_i)$  is the prior distribution function,  $P(\theta_i)$  is the actual distribution function of the random variable  $\theta_i$ , and  $n_m$  is the greatest level of moments examined for the random variable.

The maximum entropy of the normal distribution gives the following equation:

$$E(x) = \mu, \quad E(x - \mu)^2 = \sigma^2. \quad (12)$$

The statistical analysis method can also be used to produce the prior distribution. The following equation represents the probability density function of normal distribution.

$$f(x) = \frac{1}{\sigma\sqrt{2\pi}} \exp \left[ -\frac{1}{2} \left( \frac{x - \mu}{\sigma} \right)^2 \right] \text{ for } -\infty < x < \infty. \quad (13)$$

The first step in this technique is to obtain the maximum likelihood equation applied to normal distribution equation. The following statistical quantities were obtained for average and variance, respectively.

$$\bar{\mu} = \frac{1}{n} \sum_{i=1}^n x_i = \bar{x}; \quad (14)$$

$$\bar{\sigma}^2 = \frac{1}{n} \sum_{i=1}^n (x_i - \bar{\mu})^2; \quad (15a)$$

$$s^2 = \frac{1}{n-1} \sum_{i=1}^n (x_i - \bar{\mu})^2. \quad (15b)$$

#### 2.4.2.2. Subjective probability

The SPAF method was established in response to cognitive biases. Each action taken by the engineer demonstrates the effective application of prior information and the reduction of unfavorable effects

and complications [3]. It is developed using the cognitive process, which is broken down into a number of cognitive models, including the following.

### Specification of assessment objectives

Evaluation objectives are an essential and important step during information gathering because they can cause cognitive biases and the evaluation objective must be clearly understood. In the start of the SPAF, it helps engineers to know and understand the objective of the assessment clearly by providing many solutions:

a) Record the soil property  $C_u$  of interest and establish an overall evaluation target (for example, "probabilistic characterization of the soil attribute  $C_u$ ").

b) Break the overall objective into multiple sub-goals. Each sub-goal corresponds to the statistic  $\theta_i$ ,  $i = [1, 2, \dots, n_m]$  of  $C_u$ . The relevant statistics  $\theta_i = [\theta_1, \theta_2, \dots, \theta_{n_m}]$ , which depends on the theory of probability, used to explain the underlying variability of  $C_u$  within a Bayesian framework. The important statistics are the model parameters of the random field, namely  $\mu$ ,  $\sigma$ , and  $\lambda$  of  $C_u$ . Thus,  $\theta$  is composed of three random variables.

c) Identify unfamiliar probability terminology (including  $C_u$  statistics) for engineers.

### Collecting relevant data and making a preliminary estimate

The second stage is to compile the essential information on evaluation objectives from the prior knowledge (i.e. the acquired existing data and the engineers' ability). Using known correlations (e.g., real regressions or theoretical correlations) or intuitive reasoning, a key part of knowledge may result in several questionable estimates of the soil property  $C_u$  and/or its statistics in the past. It then provides several examples of assessment goals. Two sorts of evidence exist: disconfirming evidence and supporting evidence [8]. These evidences provide a set of information that is consistent with prior information and engineering experience, which includes soil property  $C_u$  or its statistics. The serious attempts to uncover information and evidence that are related to prior information, which was obtained from a number of projects of geotechnical exploration implemented in the province. The cohesion value were obtained for Al-Shatrah, Nasiriyah, Suq Al-Shuyukh and Al-Rifai, depending on the data collected from many projects for each region with the depth as shown in Fig. 5.

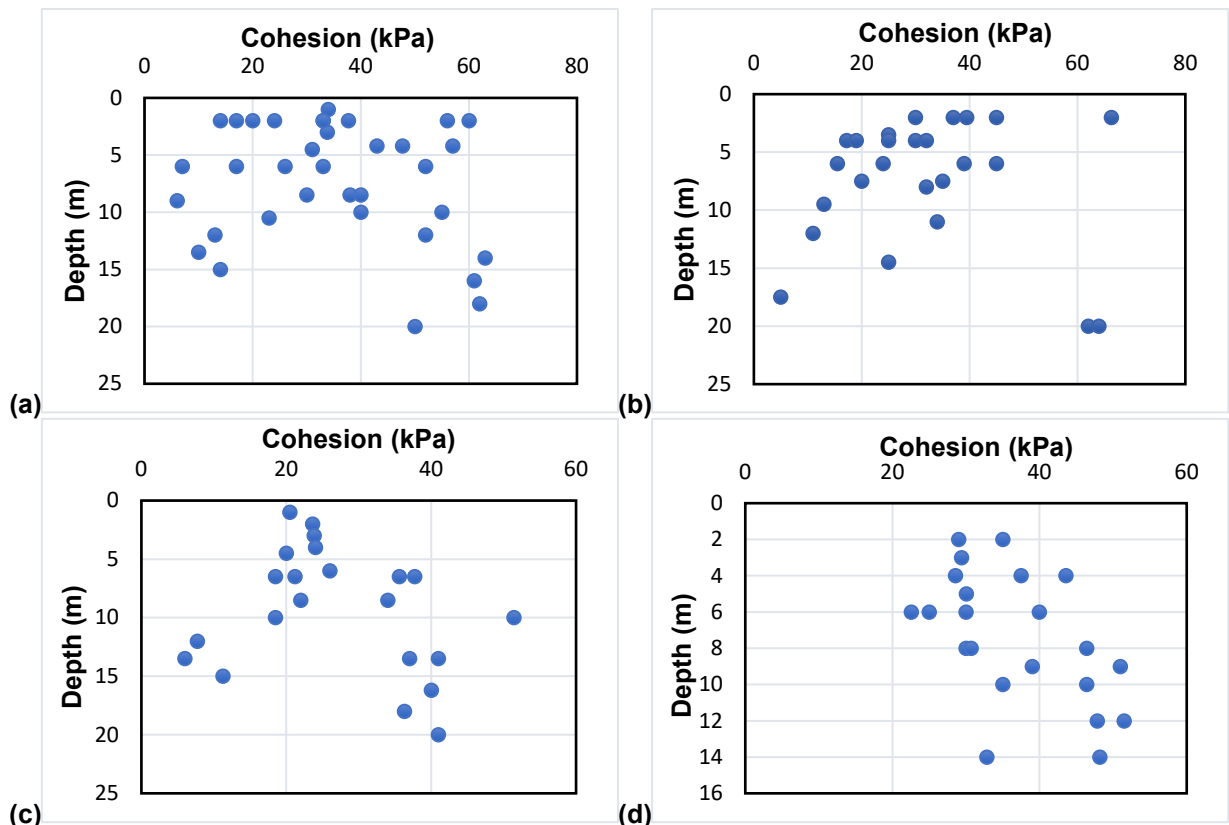


Figure 5. Mean value of cohesion with depth for (a) AL-Shatrah; (b) AL-Nasiriyah; (c) Suq AL-Shuyukh, AI-Chibayish; (d) AL-Rifai.

### Synthesis of the evidence

Engineers make use of the collected data to develop internal engineering judgments, for example property of soil  $C_u$  and its statistics. The evidence shows two crucial cognitive attributes: weight and strength [8]. Evidence synthesis is a research process that helps researchers to gather all relevant information about the research subject. This occasionally leads to engineers being overconfident in powerful but untrustworthy evidence while underemphasizing (or ignoring) fairly weak proof with relatively high weight (e.g., huge quantity and good quality), which leads to overconfidence bias, representativeness bias, and inadequate correction. There is a requirement to correctly balance the impacts of evidence strength and weight, as well as further synthesis the evidence for subjective probability evaluation. Table 3 shows the strength and weight of the cohesive soil property  $C_u$  obtained from in-situ SPTs N and the calculation of the correlation function, which were evaluated according to synthesis of the evidence. Strength in group (I) is represented as weak, (II) – moderate, (III) – weak, while in regions (IV) it is characterized as strong, (V) – moderate, (VI) – weak, (VII) – weak, (VIII) – moderate, and moderate weight.

**Table 3. Summary of the evidence's strength and weight.**

No. of evidence	Source of the information	Type of correlation	Strength	Weight
1	A formal report on the location of the clay	Empirical correlation	Strong	Strong
2	A formal report on the location of the clay	Intuitive inference	Weak	Intermediate
3	A formal report on the location of the clay	Intuitive inference	Weak	Intermediate
4	A formal report on the location of the clay	Empirical correlation	Weak	Intermediate
5	A formal report on the location of the clay	Empirical correlation and logical inference	Intermediate	Intermediate
6	A formal report on the location of the clay	Empirical correlation	Strong	Intermediate
7	A formal report on the location of the clay	Empirical correlation and logical inference	Intermediate	Intermediate
8	A formal report on the location of the clay	Empirical correlation	Strong	Intermediate
9	A formal report on the location of the clay	Intuitive inference	Weak	Intermediate
10	A formal report on the location of the clay	Empirical correlation	Strong	Intermediate
11	A formal report on the location of the clay	Intuitive inference	Weak	Intermediate
12	A formal report on the location of the clay	Intuitive inference	Weak	Intermediate
13	A formal report on the location of the clay	Empirical correlation	Strong	Intermediate
14	A formal report on the location of the clay	Intuitive inference	Weak	Intermediate
15	A formal report on the location of the clay	Intuitive inference	weak	Intermediate
16	A formal report on the location of the clay	Intuitive inference	Weak	Intermediate
17	A formal report on the location of the clay	Intuitive inference	weak	Intermediate

### Numerical assignment

The numerical assignment is a method for selecting simple and compound random probabilities that consider how prior distributions of non-random parameters are determined and derived. It involves applying many probabilities with repeated significance to randomness, and Bayesian analysis avoids it. The median value of  $\theta_i$  for a given range from 0.5 to 1, 2, ...,  $n_m$  is 0.5. The similar "equivalent" lottery technique

requires a range of  $\theta_i$ , namely  $\theta_{i,\min}$ ,  $\theta_{i,\max}$  to estimate the average value of the statistics. Using various ranges in a similar lottery approach results in different median values.

### Final confirmation

The SPAF methods mentioned above are repeated to produce the relevant PDFs of the model parameters  $\theta_i$ ,  $i = 1, 2, \dots, n_m$ , based on prior information. The prior information about  $\theta_i$  is represented in the probability distributions (e.g., CDF) and PDF, which provides means of assessing the impact of uncertainty on characterizing conditions, in which uncertainty is high or low. This theory requires a large amount of data, and the latter requires a sufficient time and effort, which provides means of assessing the impact of uncertainty on characterizing conditions, in which uncertainty is high or low.

## 3. Results and Discussion

### 3.1. Uniform distribution

This method relied on the results shown in Tables 1, 2 for the characteristic of undrained cohesion and based on (5). The details of uniform distribution of the  $C_u$  soil parameters for the three statistical quantities are as follows:

$$P(\mu) = \begin{cases} \frac{1}{62-12} = \frac{1}{50} & \text{for } \mu \in [12, 62], \\ 0 & \text{otherwise} \end{cases}$$

$$P(\sigma) = \begin{cases} \frac{1}{27.6-0.5} = \frac{10}{271} & \text{for } \sigma \in [0.5, 27.6], \\ 0 & \text{otherwise} \end{cases}$$

$$P(\lambda) = \begin{cases} \frac{1}{8-6} = \frac{1}{2} & \text{for } \lambda \in [6, 8], \\ 0 & \text{otherwise} \end{cases}$$

$$P(\theta_p) = \begin{cases} \frac{1}{50} \times \frac{10}{271} \times \frac{1}{2} = \frac{1}{2710} & \text{for } \mu \in [12, 62], \sigma \in [0.5, 27.6], \text{ and } \lambda \in [6, 8] \\ 0 & \text{others} \end{cases}$$

It implies that all combinations of  $\mu$ ,  $\sigma$ ,  $\lambda$ , and within their respective potential ranges have the same probability  $1/2710$ . Only the ranges of soil parameters are given, they can be used in the Bayesian framework to describe  $C_u$  at the clay location according to the probability distribution. Fig. 6 shows the uniform probability distributions for  $C_u$  based on the data set depended on in the current study.

Fig. 6a shows the CDF of  $\mu$  of  $C_u$  as a solid line. It was calculated using the simpler procedure. The relation between CDF and the mean value of  $C_u$  shows a linear relationship. The CDF increases linearly from 0.01 to 0.99 at mean values of 12 to 62. The PDF can be presented using a histogram with a single bin (i.e. a uniform distribution with a range of 12–62), and the PDF value of  $\mu$  is around 0.019. The uniform PDF of  $\mu$  (Fig. 6b) may serve as the prior distribution of  $\mu$  in the Bayesian framework.

Fig. 6c displays the CDF of  $\sigma$  as a solid line calculated using the simpler procedure. The CDF increases linearly from 0.01 to 0.99 as  $\sigma$  rises from 0.5 to 27.6. The PDF of  $\sigma$  determined using the simpler approach was represented a histogram with a single bin (i.e. a uniform distribution with a range of 0.5–27.6), and the PDF value of  $\sigma$  is around 0.037 (Fig. 6d). The uniform PDF of  $\sigma$  (Fig. 6d) may serve as the prior distribution of  $\sigma$  in the Bayesian framework.

The solid line shown in Fig. 6e represents the CDF of  $\lambda$ . The value of  $\lambda$  increases from 6 to 8; the CDF increases linearly from 0.01 to 0.99. Fig. 6e shows the PDF of  $\lambda$  using a histogram with a single bin (i.e. a uniform distribution with a range of 6–8), and the PDF value of  $\lambda$  is around 0.5. The uniform PDF of  $\lambda$  (Fig. 6f) may serve as the prior distribution of  $\lambda$  in the Bayesian framework.

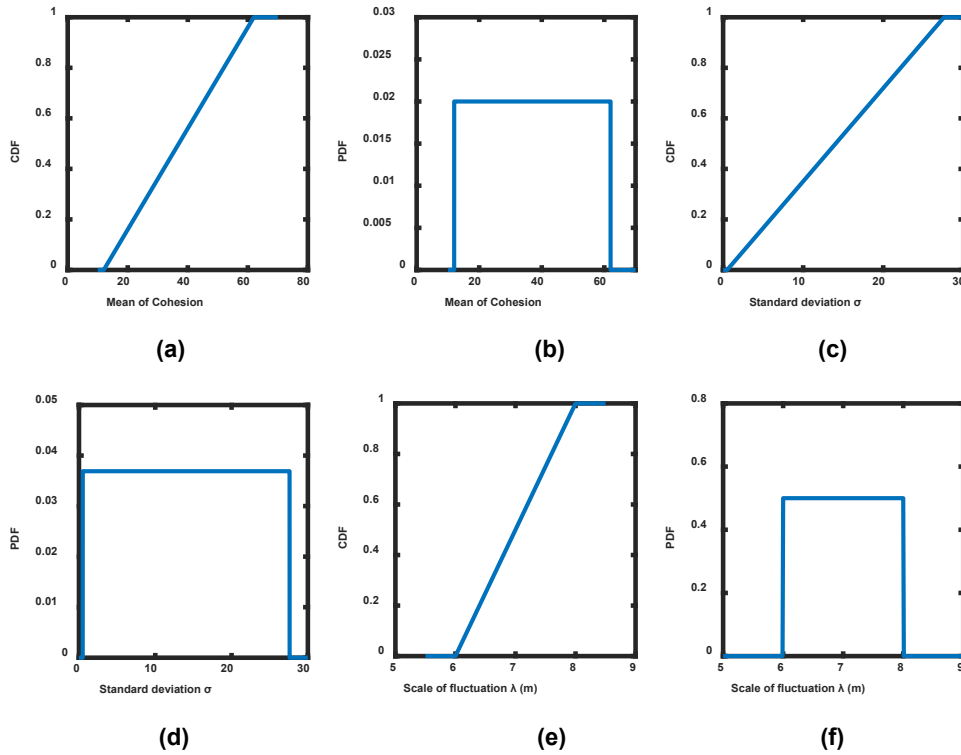


**Figure 6. Non-informative prior distribution of  $\mu$ ,  $\sigma$ ,  $\lambda$ .**

### 3.2. Jeffreys method

Jeffreys prior has a limited effect on the posterior distribution. Application of this method shows that the mean was 28.7 kPa, with a standard deviation of 1.19 kPa, based on the data included in the MATLAB code developed in this paper. Fig. 7 shows the probability and cumulative distributions. It is noteworthy that the maximum probability distribution reaches 0.33.

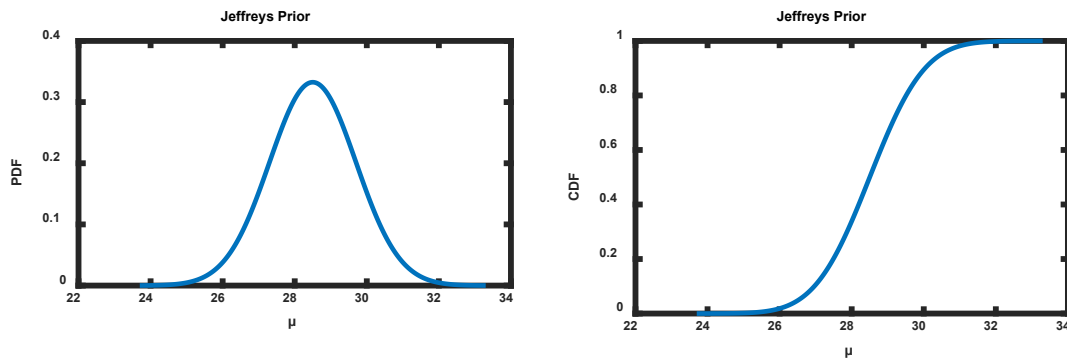


**Figure 7. Non-informative prior distribution (Jeffreys prior) of  $C_u$ .**

### 3.3. Regression analysis

In this method, the probability distribution of prior knowledge can be found based on the data of undrained cohesion. Producing the probability distribution implies computing the average and standard deviation of the data and the maximum likelihood function. The data can be fitted with a suitable probability distribution using regression analysis. In this research, two types of probability distribution were introduced for the data: normal and lognormal distribution. The disadvantage of this method was that the data collected from different sources had similar weight and no strength or weakness for the evidence was taken into account. Fig. 8 shows the normal and lognormal probability distribution fitted to the cohesion data. The results of this statistical analysis do not reflect the reality of data because some data may be very significant and some of them are not significant based on the source of data that has not been taken into account in the analysis. Engineering judgment in this analysis will be difficult to make since the data is not recognized according to its quality.



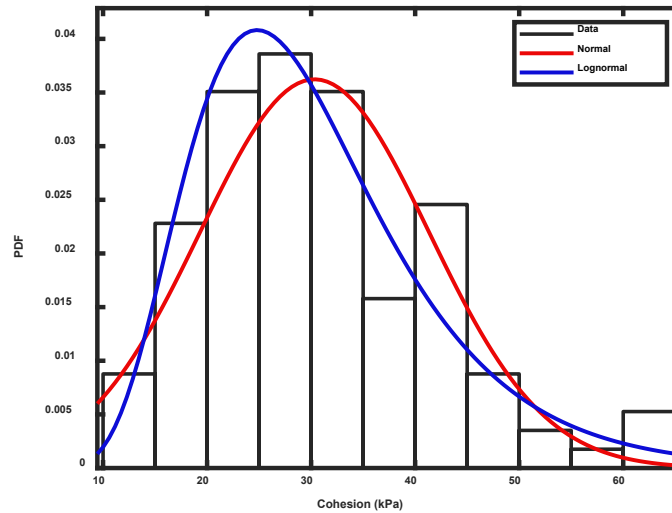


**Figure 8. Informative prior distribution.**

### 3.4. Maximum entropy

The prior probability distribution was obtained based on the maximum entropy method. With this method, the uncertainty of the prior probability distribution can be measured using information entropy  $H_I$ . The prior distribution can then be found by maximizing the information entropy subject to constraints or prior knowledge. This method can be used when the data is small but can offer a probability constraints.

The maximum entropy approach was also applied on the mean value of  $C_u$ . Fig. 9 shows the PDF and CDF distribution of the maximum entropy. In addition to the maximum entropy approach and regression analysis, the prior probability distribution was determined using the mean and standard deviation of the undrained cohesion data, respectively 28.7 and 1.2 kPa, as shown in Fig. 9.

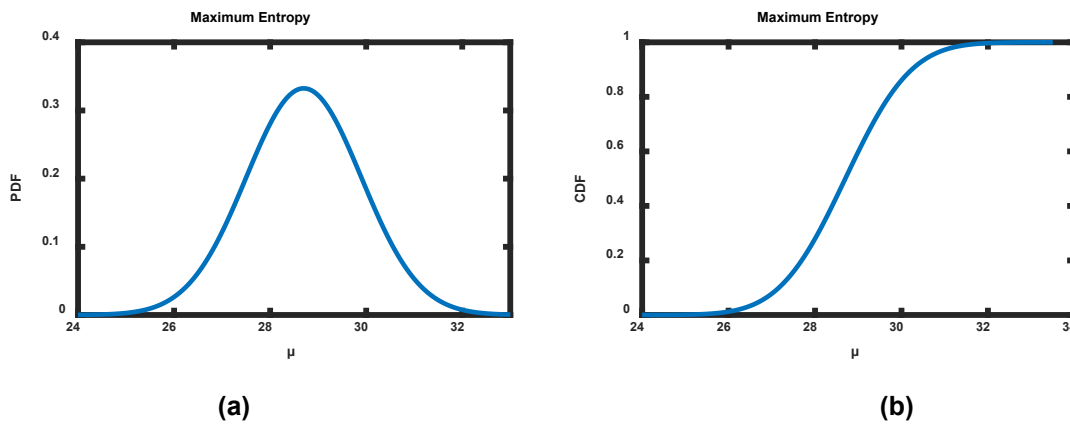


**Figure 9. Informative prior distribution.**

### 3.5. Subjective probability

Table 4 summarizes the evidence related to the parameters  $C_u$ , which include mean value ( $\mu$ ), standard deviation ( $\sigma$ ), and correlation length ( $\lambda$ ). The evidences were obtained from eight sets of items, each of which was categorized by strength and weight.

For  $C_u$ , the evidence is based on three item groups: (I), (II), and (III). Item Group (I) includes four guides with strong strength and moderate weight (evidence 1, 6, 8, 13). Item Group (II) includes a single guide with moderate strength and weight (evidence 7). Item Group (III) includes evidence 2, 9, and 14, which are characterized by weak strength and moderate weight. The equations (16) and (17) are used.

$$X = \frac{X_{\max} + X_{\min}}{2}; \tag{16}$$

$$w_x = \frac{X_{\max} - X_{\min}}{6} \quad (17)$$

$X$  is the mean of  $x$ ;  $w_x$  is the standard deviation of  $x$ ;  $x$  is the cohesion.

The  $C_u$  rates were calculated for Item Group (I), resulting in the following ranges:

$\mu = 32$ ,  $\sigma = 4$ , range: 20–44;

$\mu = 37$ ,  $\sigma = 1.6$ , range: 32.4–42.2;

$\mu = 21.3$ ,  $\sigma = 0.25$ , range: 20.5–22;

$\mu = 30$ ,  $\sigma = 1.6$ , range: 25.5–35.

Similar calculations were performed for the rest of the Table contents.

**Table 4. Summary of the evidence undrained cohesion for soil in Nasiriyah.**

Variable	No. of evidence	Item	Previous uncertain evaluation	Strength	Weight
Cohesion (kPa)	(1)	(I)	20.5–44	Strong	Intermediate
	(6)		32.36–42.16	Strong	Intermediate
	(8)		20.5–22	Strong	Intermediate
	(13)		25.5–35	Strong	Intermediate
	(7)	(II)	14.55–62	Intermediate	Intermediate
	(2)	(III)	13.75–28.15	Weak	Intermediate
	(9)		19–24	Weak	Intermediate
	(14)		12–62	Weak	Intermediate
$\mu$	(10)	(IV)	31.55	Strong	Intermediate
	(5)	(V)	49	Intermediate	Intermediate
	(11)	(VI)	22.05	Weak	Intermediate
	(12)		20	Weak	Intermediate
	(15)		37.2	Weak	Intermediate
	(16)		26.67	Weak	Intermediate
	(17)	18.29	Weak	Intermediate	
$\sigma$	(19)	(VII)	5.02–20.3	Weak	Intermediate
$\lambda$	(18)	(VIII)	6–8	Intermediate	Intermediate

Depending on the self-assessment solution stages and the data shown in Table 4,  $\mu$  and  $\sigma$  were obtained as shown in Table 5.

The average cohesion and standard deviation were 37 and 8.8 kPa, respectively (Table 5). Figure 10a shows the probability distribution based on the SPAF. The value of the probability distribution reaches 0.043. It follows from the obtained results that there is a significant difference in the mean and standard deviation value in this method compared with other methods. Other probability distribution of  $C_u$  is presented in Fig. 10: a, b for  $\mu$ ; c, d for  $\sigma$ ; e, f for  $\lambda$ .

**Table 5. The prior percentiles of the mean,  $\mu$ ,  $\sigma$ ,  $\lambda$ .**

Cumulative of probability	0.01	0.25	0.5	0.75	0.99
Mean $\mu$	12	24.5	37	49.5	62
Standard deviation $\sigma$	0.25	5.3	10.3	NA	20.3
Length of the correlation $\lambda$	6	NA	NA	NA	8

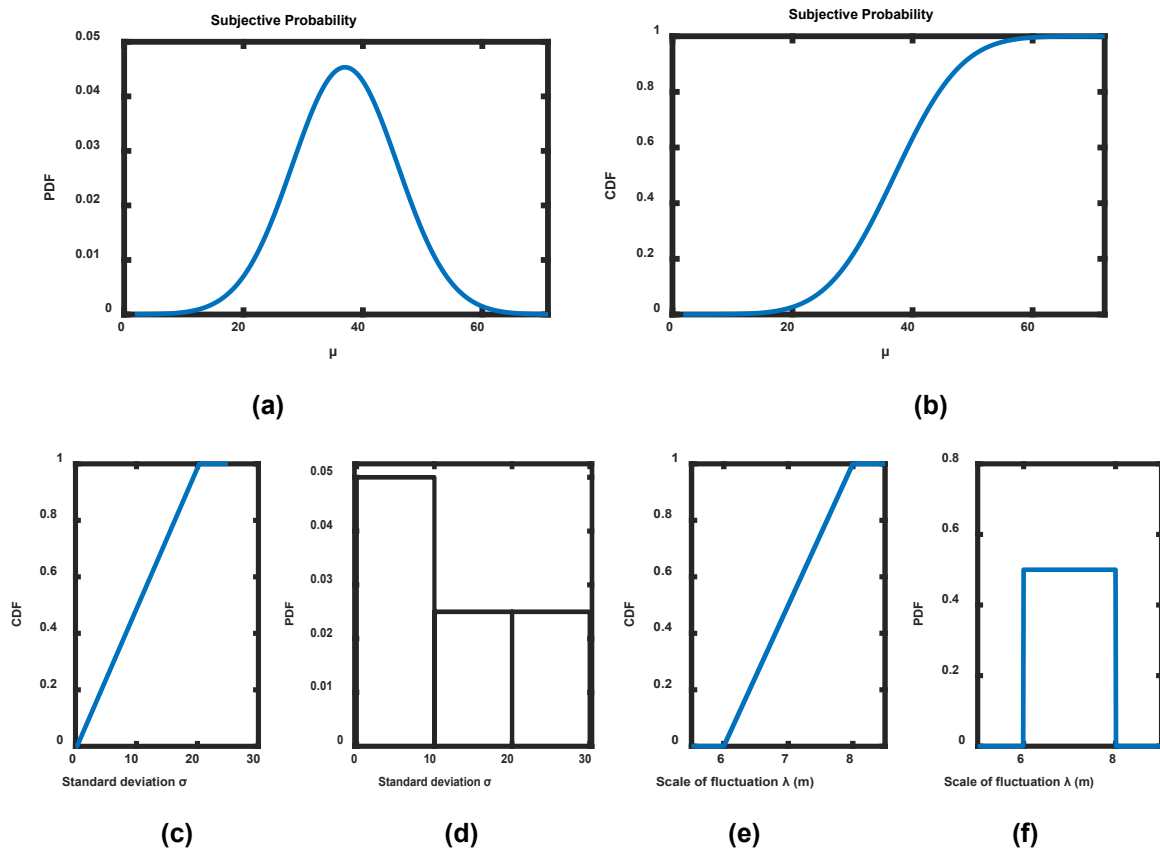


Figure 10. Informative prior distribution of  $\mu$ ,  $\sigma$ ,  $\lambda$ .

#### 4. Conclusion

This research examines the indicating of the prior probability distribution of undrained cohesion parameter based on a collected database of prior knowledge about this parameter in Nasiriyah, southern Iraq. About 152  $C_u$  values from different boreholes presented in various geotechnical investigation reports were used in this research. A wide range of conditions for selecting the suitable probability distribution was considered. The following points can be outlined based on the results of this study.

1. The range of cohesion values based on database of 152 value was between 28 kPa and 46 kPa. The uniform distribution is simple and easy to use when there is little prior knowledge or when all outcomes are considered equally likely. It can be used as a non-informative prior in Bayesian analysis when no other information is available. Since it implies all cohesion values within the given range are equally likely, it may not be the case in reality.
2. The Jeffreys prior provided a prior probability distribution based on the given mean and standard deviation. The effectiveness of Jeffreys prior might be limited to 152 data points, and the prior could dominate the posterior distribution, leading to biased results. The Jeffreys prior is particularly useful when dealing with transformation-based parameters.
3. The maximum entropy can be used for the least informative while satisfying given constraints. In this case, the mean of cohesion was given as 28.7 kPa, and the standard deviation was 1.2 kPa. By applying the principle of maximum entropy, we can find a probability distribution that is consistent with these constraints. The maximum entropy distribution fits the available information (mean and standard deviation) while being as unbiased as possible. The resulting distribution is expected to be relatively smooth and not make strong assumptions about the underlying data.
4. Regression analysis can be effective when dealing with larger data sets because it allows relationships between variables to be modeled and predictions to be made based on those relationships. With 152 data points, it may be necessary to increase the data, especially when there are significant analysis challenges, to provide useful and reliable results.
5. When working with a limited number of data points, the subjective probability assessment approach, which considers expert knowledge and judgment, might be the most suitable method. However, it is essential to be transparent about the assumptions and uncertainties introduced by the subjective assessment and to carefully interpret and validate the results against any available data.

Additionally, if further data becomes available, it could be useful to reassess the analysis using methods that are better suited for larger datasets, such as regression analysis. The subjective probability assessment heavily relies on the knowledge and judgment of the expert providing the assessment. It can be subjective and may lead to varying results depending on different expert opinions.

## References

1. Gelman, A. Prior distribution. *Encyclopedia of Environmetrics*. 2002. 3. Pp. 1634–1637.
2. Contreras, L.F., Serati, M., Williams, D.J. Bayesian approach for the assessment of sufficiency of geotechnical data. *Slope Stability 2020: Proceedings of the 2020 International Symposium on Slope Stability in Open Pit Mining and Civil Engineering*. 2020. Pp. 609–624. DOI: 10.36487/ACG\_repo/2025\_37
3. Cao, Z.-J., Wang, Y., Li, D.-Q. Probabilistic approaches for geotechnical site characterization and slope stability analysis. Heidelberg: Springer Berlin, 2017. 190 p. DOI: 10.1007/978-3-662-52914-0
4. Phoon, K.-K., Kulhawey, F.-H. Evaluation of geotechnical property variability. *Canadian Geotechnical Journal*. 1999. 36 (4). Pp. 625–639. DOI: 10.1139/t99-039
5. Cao, Z.-J., Wang, Y., Li, D.-Q. Site-specific characterization of soil properties using multiple measurements from different test procedures at different locations – A Bayesian sequential updating approach. *Engineering Geology*. 2016. 211. Pp. 150–161. DOI: 10.1016/j.enggeo.2016.06.021
6. Jeffreys, H. An invariant form for the prior probability in estimation problems. *Proceedings of the Royal Society A. Mathematical, Physical and Engineering Sciences*. 1946. 186 (1007). Pp. 453–461. DOI: 10.1098/rspa.1946.0056
7. Baecher, G.B., Christian, J.T. *Reliability and statistics in geotechnical engineering*, 1<sup>st</sup> ed. NJ: John Wiley & Sons, 2003. 616 p.
8. Vick, S.G. *Degrees of belief: Subjective probability and engineering judgment*. USA: Amer Society of Civil Engineers (ASCE), 2002. 472 p.
9. Cao, Z.-J., Wang, Y., Li, D.-Q. Quantification of prior knowledge in geotechnical site characterization. *Engineering Geology*. 2016. 203. Pp. 107–116. DOI: 10.1016/j.enggeo.2015.08.018
10. Sivia, D., *Skilling, J. Data analysis: a Bayesian tutorial*, 2<sup>nd</sup> ed. UK: Oxford University Press, 2006. 246 p.
11. Ching, J., Phoon, K.-K., Li, K.-H., Weng, M.-C. Multivariate probability distribution for some intact rock properties. *Canadian Geotechnical Journal*. 2019. 56 (8). Pp. 1080–1097. DOI: 10.1139/cgj-2018-0175
12. Zhao, T., Wang, Y., Xu, L. Efficient CPT locations for characterizing spatial variability of soil properties within a multilayer vertical cross-section using information entropy and Bayesian compressive sensing. *Computers and Geotechnics*. 2021. 137. Article no. 104260. DOI: 10.1016/j.compgeo.2021.104260
13. Li, C., Wang, W., Wang, S. Maximum-entropy method for evaluating the slope stability of earth dams. *Entropy*. 2012. 14 (10). Pp. 1864–1876. DOI: 10.3390/e14101864
14. Siu, N.O., Kelly, D.L. Bayesian parameter estimation in probabilistic risk assessment. *Reliability Engineering & System Safety*. 1998. 62 (1–2). Pp. 89–116. DOI: 10.1016/S0951-8320(97)00159-2
15. Carlin, B.P., Louis, T.A. *Bayes and empirical Bayes methods for data analysis*, 2<sup>nd</sup> ed. UK: Chapman and Hall/CRC, 2000. 440 p.
16. Feng, Y. *Development of Bayesian approaches for uncertainty quantification in in situ stress estimation*. Ph.D. thesis. University of Toronto, Canada, 2021.
17. Cao, Z.-J., Wang, Y., Li, D.-Q. Bayesian perspective on geotechnical variability and site characterization. *Engineering Geology*. 2016. 203. Pp. 117–125. DOI: 10.1016/j.enggeo.2015.08.017
18. Xu, J., Zhang, L., Wang, Y., Wang, C., Zheng, J., Yu, Y. Probabilistic estimation of cross-variogram based on Bayesian inference. *Engineering Geology*. 2020. 277. Article no. 105813. DOI: 10.1016/j.enggeo.2020.105813
19. Wang, Y., Zhao, T., Cao, Z. Bayesian perspective on ground property variability for geotechnical practice. *Proceedings of the 7<sup>th</sup> International Symposium on Geotechnical Safety and Risk (ISGSR)*. 2019. Pp. 63–74. DOI: 10.3850/978-981-11-2725-0-key5-cd
20. Otake, Y., Honjo, Y. Challenges in geotechnical design revealed by reliability assessment: Review and future perspectives. *Soils and Foundations*. 2022. 62 (3). Article no. 101129. DOI: 10.1016/j.sandf.2022.101129
21. Phoon, K.-K., Cao, Z.-J., Ji, J., Leung, Y.F., Najjar, S., et al. Geotechnical uncertainty, modeling, and decision making. *Soils and Foundations*. 2022. 62 (5). Article no. 101189. DOI: 10.1016/j.sandf.2022.101189
22. Zhang, P., Yin, Z.-Y., Jin, Y.-F. Bayesian neural network-based uncertainty modelling: application to soil compressibility and undrained shear strength prediction. *Canadian Geotechnical Journal*. 2022. 59 (4). Pp. 546–557. DOI: 10.1139/cgj-2020-0751
23. Zhao, Z., Congress, S.S.C., Cai, G., Duan, W. Bayesian probabilistic characterization of consolidation behavior of clays using CPTU data. *Acta Geotechnica*. 2022. 17 (3). Pp. 931–948. DOI: 10.1007/s11440-021-01277-8
24. Gong, W., Zhao, C., Juang, C.H., Zhang, Y., Tang, H., Lu, Y. Coupled characterization of stratigraphic and geo-properties uncertainties – A conditional random field approach. *Engineering Geology*. 2021. 294. Article no. 106348. DOI: 10.1016/j.enggeo.2021.106348
25. Muhsin, D., Shakir, R.R. Evaluation of soil classification methods based on CPT data for soil in Nasiriyah, Iraq. *AIP Conference Proceedings*. 2023. 2830. Article no. 030018. DOI: 10.1063/5.0157813
26. Adel, R., Shakir, R.R. Evaluation of static pile load test results of ultimate bearing capacity by interpreting methods. *IOP Conference Series: Earth and Environmental Science*. 2022. 961. Article no. 012013. DOI: 10.1088/1755-1315/961/1/012013
27. Ewaid, S.H., Abed, S.A., Al-Ansari, N. Crop water requirements and irrigation schedules for some major crops in Southern Iraq. *Water*. 2019. 11 (4). Article no. 756. DOI: 10.3390/w11040756
28. Ali, H.M. *Characteristic Values Of Geotechnical Data And Bearing Capacity Mapping For Soils In Nasiriyah*. [Online]. System requirements: AdobeAcrobatReader. URL: <https://dspace.utq.edu.iq/items/cdac6587-e97c-49ea-9500-c78420e02037> (Accessed: 02.12.2024).
29. Shakir, R.R. Probabilistic-based analysis of a shallow square footing using Monte Carlo simulation. *Engineering Science and Technology, an International Journal*. 2019. 22 (1). Pp. 313–333. DOI: 10.1016/j.jestch.2018.08.011

30. Ali, H.M., Shakir, R.R. Geotechnical map of Thi Qar governorate using geographical information systems (GIS). *Materials Today: Proceedings*. 2022. 60 (3). Pp. 1286–1296. DOI: 10.1016/j.matpr.2021.09.138
31. Thajeel, J.K., Adel, R., Ali, H.M., Shakir, R.R. Effect of the covariance matrix type on the CPT based soil stratification utilizing the Gaussian mixture model. *Journal of the Mechanical Behavior of Materials*. 2022. 31 (1). Pp. 492–500. DOI: 10.1515/jmbm-2022-0049
32. Shakir, R.R. Selecting the probability distribution of cone tip resistance using moment ratio diagram for soil in Nasiriyah. *Geotechnical and Geological Engineering*. 2019. 37 (3). Pp. 1703–1728. DOI: 10.1007/s10706-018-0716-3
33. Fienberg, S.E. Does it make sense to be an “objective Bayesian”? (Comment on articles by Berger and by Goldstein). *Bayesian Analysis*. 2006. 1 (3). Pp. 429–432. DOI: 10.1214/06-BA116C
34. Fisher, R.A. Theory of statistical estimation. *Mathematical Proceedings of the Cambridge Philosophical Society*. 1925. 22 (5). Pp. 700–725. DOI: 10.1017/S0305004100009580
35. Shannon, C.E., Weaver, W. *The mathematical theory of communication*. USA: The University of Illinois Press, 1964. 131 p.
36. Niven, R.K., Andresen, B. Jaynes' maximum entropy principle, Riemannian metrics and generalised least action bound. *Complex Physical, Biophysical and Econophysical Systems*. 2010. Pp. 283–317. DOI: 10.48550/arXiv.0907.2732
37. Kanwar, N.S., Deng, J. A comparison of probabilistic distributions of undrained shear strength of soils in Nipigon River, Canada. *IOP Conference Series: Earth and Environmental Science*. 2019. 351. Article no. 012024. DOI: 10.1088/1755-1315/351/1/012024

**Information about the authors:**

**Ressol R. Shakir,**

E-mail: [rrshakir@utq.edu.iq](mailto:rrshakir@utq.edu.iq)

**Zainab Abd AL-Haleem,**

E-mail: [zainababd96@utq.edu.iq](mailto:zainababd96@utq.edu.iq)

Received: 15.02.2023. Approved after reviewing: 19.02.2024. Accepted: 05.08.2024.



Research article

UDC 626

DOI: 10.34910/MCE.130.10



## Cut-off wall in foundation of reservoir dam and tailing dam: comparative evaluation

M.P. Sainov , N.S. Talalaev 

Moscow State University of Civil Engineering (National Research University), Moscow, Russia Federation  
✉ [mp\\_sainov@mail.ru](mailto:mp_sainov@mail.ru)

**Keywords:** Dam, cut-off wall, tailing, stress-strain state, numerical modeling, strength

**Abstract.** Cut-off wall is used to prevent seepage in foundations of embankment dams of reservoirs and tailing dams. Under the action of external loads, they may be subject to stresses comparable with strength of the wall material. There is a risk of loss of the wall both tensile strength and compressive strength. To decrease stresses, the cut-off wall is made of clay-cement concrete more deformed as compared to material concrete. To compare conditions of operation and strength of the cut-off wall in foundation of the reservoir dam and the cut-off wall in foundation of the tailing dam, there was fulfilled the study of their stress-strain state. Abstract rockfill dam 100 m high with geomembrane face was considered. A 2 m thick cut-off wall is located under the dam upstream slope: it crosses the layer of deformed foundation 15 m thick and is embedded in rock. Mohr–Coulomb model was used for description of behavior. Computations showed that the cut-off wall of the tailing dam performs in less favorable conditions than the cut-off wall of the reservoir dam. It is subject to greater by value vertical and horizontal loads. Due to pressure of slimes, it is subject to several times as much by value vertical compressive stresses. The value of stresses is highly dependent on deformation of the foundation soil. To provide strength, the deformation modulus of the cut-off wall should not exceed the foundation soil deformation modulus by more than 4 times. In spite of the fact that the tailing dam cut-off wall is subject to greater horizontal loads, it has less displacements than the reservoir dam cut-off wall. It was revealed that this is explained by more favorable stress state of soil in foundation of the tailing dam.

**Citation:** Sainov, M.P., Talalaev, N.S. Cut-off wall in foundation of reservoir dam and tailing dam: comparative evaluation. Magazine of Civil Engineering. 2024. 17(6). Article no. 13010. DOI: 10.34910/MCE.130.10

### 1. Introduction

**Subject of research.** In foundations of dams and dikes composed of soils, the cut-off walls (COW) arranged by one of the methods of slurry trench are frequently used as seepage-control facilities. They may be fulfilled for a considerable depth reaching several dozen meters. The examples of such structures are COWs in embankment dams Xiaolangdi (China, 2000), Karkhe (Iran, 2001), Peribonka (Canada, 2008), Sylvenstein (Germany, 2012) [1–4]. The main seepage-control wall arranged in foundation of Peribonka dam is 116 m deep. The wall up to 80 m deep in the foundation of Karkhe dam is long and the square area of its upstream face is approximately 190000 sq.m.

COW is also used in structural designs of dams of tailings ponds in metal mining industry, namely in Chile and Peru [5]. As an example, we may indicate COW, which was arranged in tailing dam Aznallcolar (1978, Spain) [6, 7].

#### Literature review

To provide safe operation of COW, proper strength of its material should be provided. Publications [9–20] are dedicated to study of stress-strain state (SSS) of COW in foundation of an embankment dam.

The results of scarce field measurements of displacements and stresses in COW are generalized in [8]. Mainly the study of SSS of COW in foundation of an embankment dam is fulfilled with the aid of numerical modeling.

Publications [9–11, 17, 19] are dedicated to SSS of COW made in foundations under the cores of earth-rockfill dams, [16] – to study of SSS of COW arranged in the dam with asphalt concrete diaphragm. In articles [12–14, 20], there studied SSS of COW made in the foundation of Miaojiaba concrete faced rockfill dam in China.

By the results of studies, there was formulated the theory of forming SSS of COW in the dam foundation. Its main concepts are as follows. COW is subject not only to bend deformations but also to deformations of longitudinal (vertical) compression. Bending moments, longitudinal and transversal forces appear in the wall. Longitudinal compressive force is the results of not only pressure on the upper end (head) of the wall but also of soil friction forces on the wall lateral surface. Pressure on the upper end is determined by dead weight of the dam soil located above the wall and by water pressure.

Under the action of vertical forces, COW may be subject to high compressive stresses comparable with strength of the wall material. This may present a serious danger for COW strength. In order to avoid loss of strength, the wall should be made of material which by its rigidity is close to surrounding soil. By recommendations of ICOLD (International Commission on Large Dams), the ratio between the wall modulus of linear deformation and the soil modulus of linear deformation should not exceed 5.

The results of numerical modeling show that conditions of COW operation also depend on its depth, structural design of an embankment dam and other factors. L. Wen et al. [14] note that conditions of operation, SSS of COW are determined by position of the wall within the embankment dam profile. It is obvious that the wall located at the toe of the embankment dam upstream slope will be subject to less vertical loads than the wall located under the dam central part.

With this regard, it is logical to propose that operation conditions of COW made in foundations of tailing dams should differ from operation conditions of COW arranged in reservoir embankment dam foundation. However, investigations dedicated to studies of SSS of COW in foundations of tailing dams were not found.

**Formulation of relevance of research.** The urgent issue is evaluation of workability of COW arranged in the layer of soil (deformed) foundation under the tailing dam in comparison with COW in the deformed foundation of the reservoir dam. To fulfill this comparative evaluation, it is necessary to analyze SSS of COW on the example of a certain structure

**Aims and tasks of study.** Studies of SSS should answer the following questions:

Question no. 1. What is the difference between SSS of COW in foundation of the tailing dam and that of COW made in the reservoir dam foundation? Are operation conditions of COW in foundation of a tailing dam more favorable or unfavorable as compared to those of COW in the reservoir dam foundation?

Question no. 2. Is there the risk of strength loss of COW made in foundation of the tailing dam? In what case the COW strength may not be provided?

## 2. Materials and Methods

### **Description of the studied structure**

Investigation was conducted on the example of an abstract tailing dam, which is 100 m high. It was assumed that the dam is made of rockfill and grows in several stages towards the downstream side (Fig. 1). Maximum depth of the tailing dam filling is 98 m.

There considered the dam, which is built on 15 m thick layer of cohesionless alluvial soil under which rock is bedded. To provide water tightness of the alluvial layer, a 2 m thick seepage-control wall made of clay-cement concrete is arranged in it.

The dam structural design is assumed to be as follows. The dam seepage-control element is the face made of geomembrane placed along the upstream face. To provide stability of the face, the upstream slope was chosen to be 2.5. The dam downstream slope is 1.6.

The face and the COW are connected with the aid of a concrete apron 2 m long and 0.4 m thick.

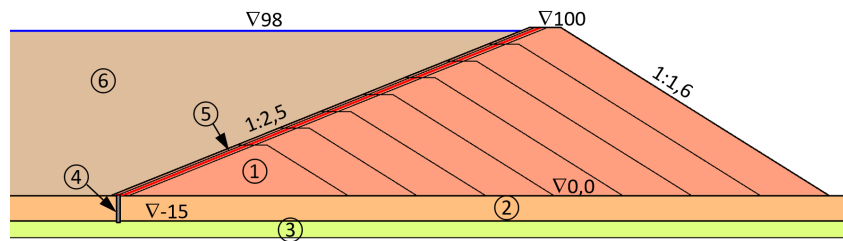


**Figure 1. Diagram of the tailing dam structural design: 1 – rockfill; 2 – foundation alluvial layer; 3 – rock foundation; 4 – cut-off wall made of clay-cement concrete; 5 – face made of polymer geomembrane; 6 – slimes.**

#### **Description of finite-element model**

The structure SSS analysis was conducted by finite-element method with the aid of computer program NDS\_N, developed by M.P. Sainov. Analysis was fulfilled in 2D formulation.

The structure computational domain included the dam itself, the layers of soil and rock foundations as well as part of a tailing dam.

The developed finite-element model of the computational domain includes 1273 elements (Fig. 2). The use was made of the elements with square degree of approximation of displacements inside the element. 115 elements out of the total number of elements were Goodman's elements, which are intended for modeling non-linear character of interaction between soils and rigid structures.

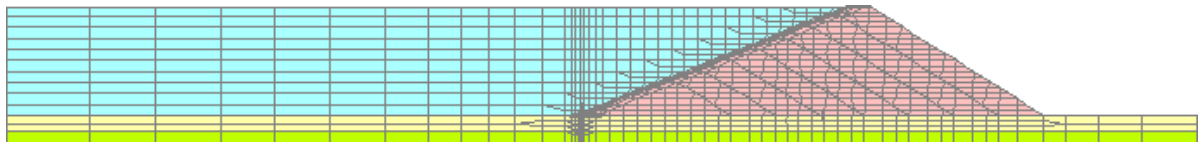


**Figure 2. Diagram of dividing the structure into finite elements.**

Computations were conducted for loads from the structure dead weight and hydrostatic pressure. Slimes located below the water level were assumed to be in suspended state. Lengthwise distributed load from hydrostatic pressure was applied to upstream faces of seepage-control facilities.

SSS analysis was conducted taking into account the sequence of the dam construction and the tailing dam filling. The dam is constructed in 8 stages. The first stage is 30 m high. Its construction is preceded by arrangement of COW in the layer of the deformed foundation. Each subsequent stage is 10 m higher than the preceding one.

For comparative evaluation, the analysis was also conducted for the reservoir embankment dam with similar structural design. Its only difference is the fact that there are no loads from slimes.

#### **Selection of physical-mechanical properties of medium**

Two alternatives of soil deformation of the dam and foundation were considered.

In alternative 1, rockfill modulus of linear deformation was taken equal 75 MPa, and foundation alluvial soil modulus of linear deformation was 40 MPa. They correspond to not high quality of soil compaction. In alternative 2, the moduli of linear deformation of rockfill and foundation soil were two times as much as in alternative 1.

Mohr–Coulomb model was used for description of soil behavior. Tensile strength of soils was assumed to be close to 0.

Rock material was assumed to be elastic and absolutely strong. It was proposed that COW is made of clay-cement concrete. By Russian building code, for clay-cement concrete, the modulus of linear deformation is assumed to be 300–500 MPa, and uniaxial compressive strength is 1–2 MPa.

The most complicated issue is assigning physical-mechanical properties of slimes: strength  $\rho$ , modulus of linear deformation  $E$ , angle of internal friction  $\varphi$  and cohesion  $c$ . With this purpose, the literary sources [21–25] were analyzed.

Publications [21, 22] are dedicated to analysis of tailing dams. In [22], for slimes, the following design characteristics were assumed:  $\rho = 1.7 \text{ kg/cm}^3$ ,  $\varphi = 40^\circ$ ,  $c = 10 \text{ kPa}$ . In [21], they were assumed as follows:  $\rho = 2 \text{ kg/cm}^3$ ,  $E = 12.1 \text{ MPa}$ ,  $\varphi = 21^\circ$ ,  $c = 16 \text{ kPa}$ .



In [24], by the results of tests in stabilometer, the followings strength indices of slimes were obtained:  $c = 20 \text{ kPa}$ ,  $\varphi \approx 40^\circ$ .

Publications [23, 25] are dedicated to the issue of determining parameters of slimes for Hardening Soil model. In publication [25], the properties of slimes in different zones of Aitik tailing dam (Sweden) were investigated. The following characteristics of slimes were obtained: density in dry state  $1.43\text{--}1.62 \text{ kg/cm}^3$ , averaged modulus of linear deformation  $E_{50}$  amounts to  $5.5\text{--}8.3 \text{ MPa}$ , angle of internal friction  $\varphi = 38\text{--}40^\circ$ , cohesion  $c = 0\text{--}7 \text{ kPa}$ .

In [23], there described the results of investigations of slimes properties in the largest tailing dam of Bulgaria. Soil samples were taken in the interval of depths  $12\text{--}81 \text{ m}$ . There was determined the range of slimes density variation in natural state ( $1.8\text{--}2.2 \text{ kg/cm}^3$ ) and the range of modulus of linear deformation ( $6\text{--}21 \text{ GPa}$ ). Processing of the results showed that deformation of slimes decreases with growth of lateral compression.

The indicated effect is explained by the fact that due to pressure of lying above layers, consolidation processes, the density of slimes increases with depth and their deformation decreases. Therefore, in calculation, the tailing dam storage was conditionally divided in two zones by depth. In the lower zone, the slimes were assumed to be denser and less deformed. The depth of the upper zone was taken equal  $20 \text{ m}$ . As the dam height increased and the tailing dam was filled, the boundary between the zones was also raised.

Parameters of physical-mechanical properties of the structure materials are presented in Table 1.

**Table 1. Physical-mechanical properties of materials.**

Material	Density, $\text{kg/cm}^3$		E, MPa	$\nu$	$\varphi$	c, kPa
	unsaturated	saturated				
Rockfill (alternative 1)	2.00	2.28	75	0.30	$45^\circ$	–
Rockfill (alternative 2)	2.00	2.28	150	0.30	$45^\circ$	–
Foundation alluvium (alternative 1)	1.85	2.16	40	0.30	$38^\circ$	–
Foundation alluvium (alternative 2)	1.85	2.16	80	0.30	$38^\circ$	–
Slimes (upper zone)	1.64	2.02	10	0.38	$35^\circ$	1
Clay-cement concrete	1.74	2.10	25	0.38	$35^\circ$	1
Clay-cement concrete	1.90		300	0.35	strong	
Concrete	2.40		30000	0.20	strong	
Rock	2.55	2.63	5000	0.25	strong	

Note: E – modulus of linear deformation;  $\nu$  – Poisson's ratio;  $\varphi$  – angle of internal friction; c – specific cohesion.

Shear stiffness of contacts between rock structures and soils was taken equal  $500 \text{ MPa/m}$ . Preliminary calculations showed that variation of shear stiffness in the interval  $500\text{--}2500 \text{ MPa/m}$  does not greatly affect the results of calculations.

### 3. Results and Discussion

SSS analysis of the dam and COW was fulfilled for the last construction stage of the tailing dam.

#### **Stress-strain state of the dam**

In order to evaluate difference in SSS of a tailing dam and a reservoir dam, Figs. 3, 4 show distribution of displacements, and Figs. 5, 6 – distribution of stresses. They are plotted with consideration of the dam construction sequence.

Values of stresses in the dam body and foundation are mainly determined by acting loads (function of the structure) and are less depended on the variant of deformation properties of soils. The tailing dam is subject to greater by value stresses.

In the reservoir dam, vertical stresses  $\sigma_y$  reach maximum value ( $1.8 \text{ MPa}$ ) at the toe, in the internal zone (Fig. 5,b). In COW zone, they amount to approximately  $0.7 \text{ MPa}$ . In the tailing dam, due to the weight

of slimes, the vertical stresses reach 2.1 MPa (Fig. 5,a). In COW zone, they comprise approximately 1.2 MPa.

Horizontal compressive stresses  $\sigma_x$  reach their maximum in the rock foundation layer, as a rule, in the zone from the downstream side from COW. At construction of a tailing dam, they exceed 1.1 MPa (Fig. 6,a), and at creation of an reservoir, they are 1.0 MPa (Fig. 6,b).

Considerable difference is noted in soil stress state from the downstream side of the wall. In case of a reservoir, the zone of soil loosening appears in front of the wall; there the soil loses compressive strength and/or shear strength. In this zone, horizontal stresses  $\sigma_x$  are close to 0 (Fig. 6,b). In case of a tailing dam, from the upstream side of the wall, the soil is subject to compressive stresses  $\sigma_x$  with value at least 0.15 MPa (Fig. 6,a). This compression arises from pressure of slimes lying above.

The tailing dam is characterized by greater by value displacements and settlements than those of the reservoir dam. This is explained by existence of additional loads from the weight and pressure of slimes. However, the difference in displacements is not large. Horizontal displacements of a tailing dam exceed the displacements of a reservoir dam by approximately 15 % (Table 2). The tailing dam displacements reach their maximum at the upstream face (Fig. 3). The tailing dam settlements also reach their maximum near the upstream face and for the reservoir dam they are in its internal part (Fig. 4). But maximum values of settlements differ not greatly.

**Table 2. Maximum values of the tailing dam displacements and settlements.**

Parameter	Tailing		Reservoir	
	Alternative 1	Alternative 2	Alternative 1	Alternative 2
$U_x$ [cm]	41	21	36	18
$U_y$ [cm]	88	44	85	43

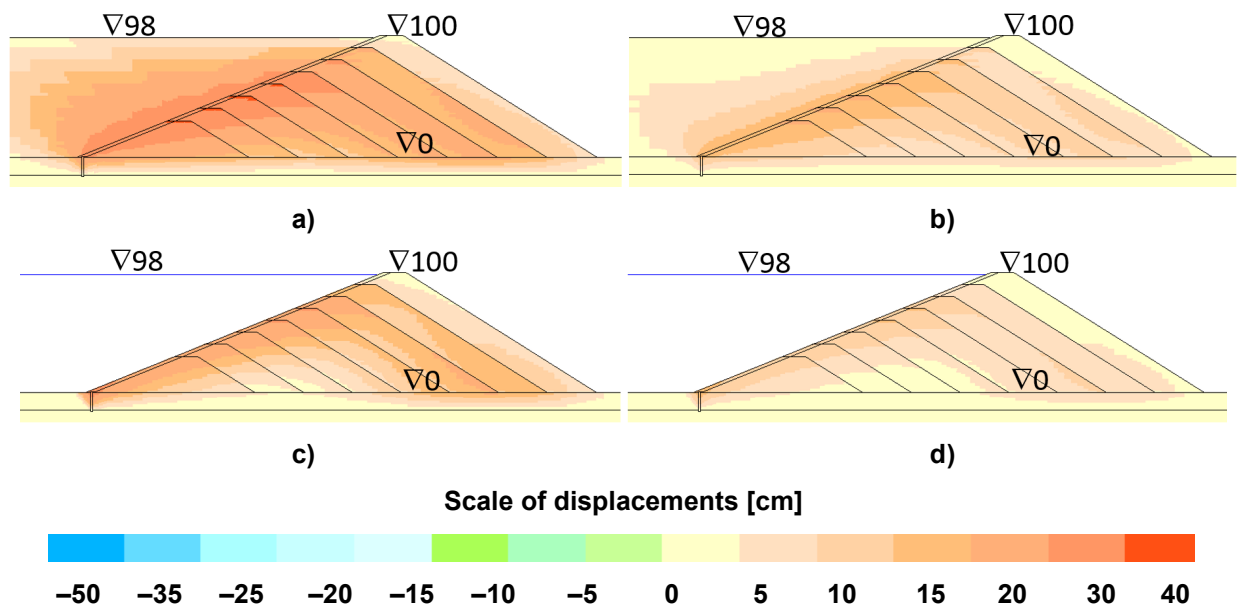


**Figure 3. Tailing dam horizontal displacements<sup>^</sup>**  
a), b) – tailing dam; c), d) – reservoir dam; a), c) – alternative 2; b), d) – alternative 1.

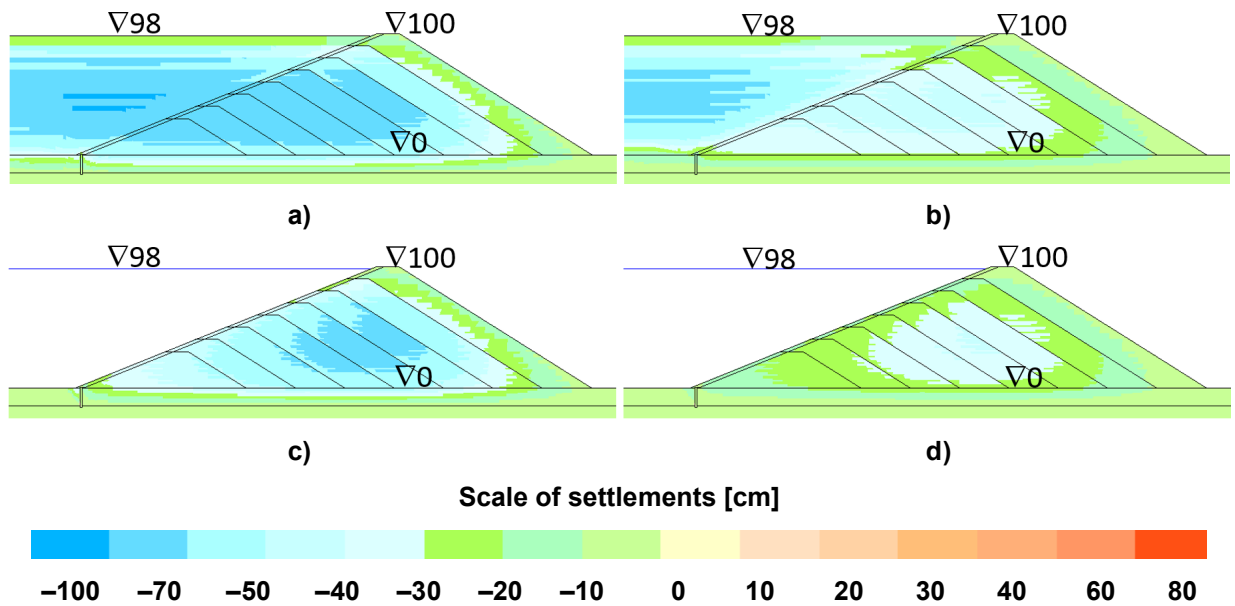


**Figure 4. Tailing dam vertical settlements:**  
 a), b) – tailing dam; c), d) – reservoir dam; a), c) – alternative 2; b), d) – alternative 1.

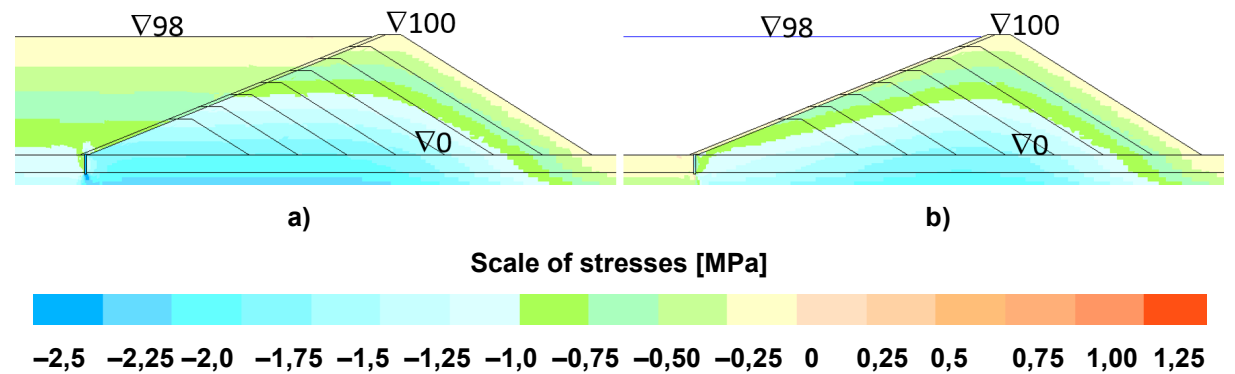


**Figure 5. Vertical stresses in a tailing dam foundation and body (alternative 1):**  
 a) – tailing dam; b) – reservoir dam.

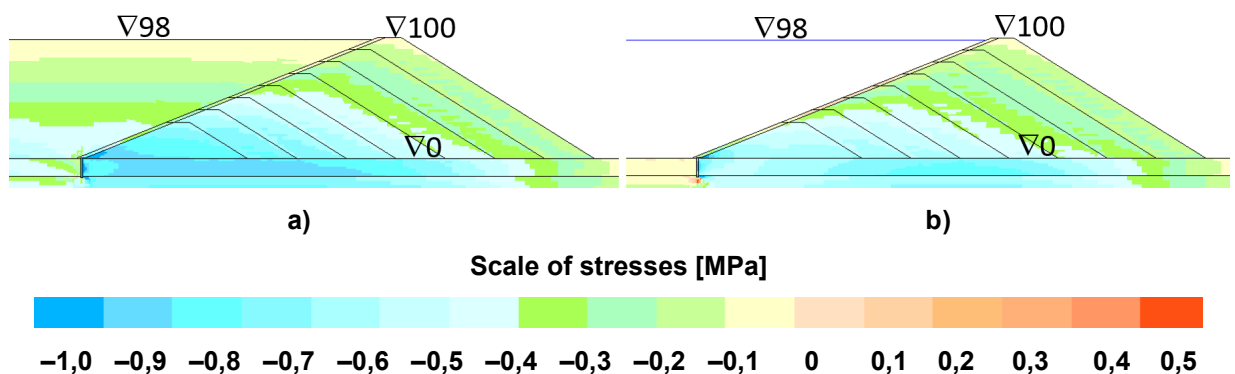


**Figure 6. Horizontal stresses in a tailing dam foundation and body (alternative 1):**  
 a) – tailing dam; b) – reservoir dam.

***Stress-strain state of a cut-off wall***

In SSS of COW in a tailing dam and a reservoir dam, the difference is expressed more vividly.

The first difference refers to the values of COW horizontal displacements.

In all the considered cases, COW is displaced towards the downstream side and displacements reach their maximum in COW upper part. By the results of calculations, it was revealed that a tailing dam COW horizontal displacements are always less than those of a reservoir dam COW (Fig. 7). It seems that it should be vice versa because in a tailing dam the wall is subject to more by value horizontal loads from the upstream side than that in a reservoir. However, it was revealed that such effect is explained by specific feature of soil stress state from the upstream side of the wall.

With the aid of additional calculations, it was shown that a tailing dam COW displacements would be more than a reservoir COW displacements in case if soils were assumed to be strong and able to perceive any by value tensile and shear stresses. However, in real conditions, the soils tensile strength is close to 0 and this results in increase of a reservoir COW displacements. At displacements of a reservoir dam, the soils bedded from the upstream side of the wall turn to be unable to resist shear displacements.

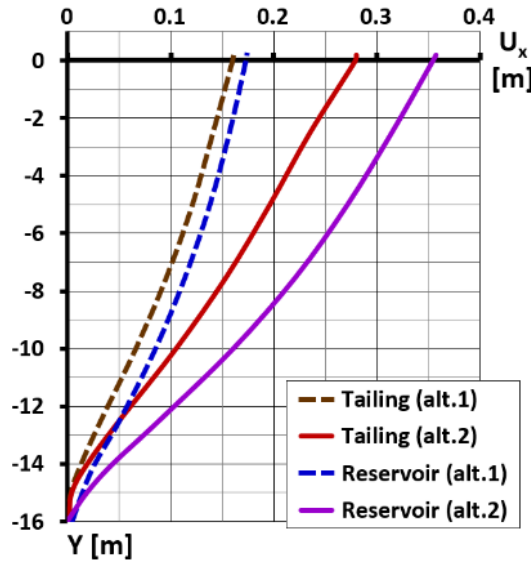


Figure 7. COW horizontal displacements.

The second difference is in the character of COW stress state. In both cases, SSS is formed by two processes.

The first process is the wall bend deformations. At horizontal displacements, COW bends towards the upstream side. In the wall upper part and in the zone of its embedment into rock foundation, the bend occurs towards the upstream side. The highest wall bend deformations are revealed in the zone of embedment. Bend deformations are expressed in non-uniform distribution of vertical stresses  $\sigma_y$  between the wall faces (Fig. 8). In the tailing dam wall, they are revealed to some more extent.

The second process is wall longitudinal compression, which is mainly formed by the forces acting on its upper end. From the point of view of longitudinal forces value, the tailing dam wall principally differs from the reservoir wall. Vertical load on the reservoir wall is mainly formed due to hydrostatic pressure. In a tailing dam COW, it is added by pressure from the weight of slimes. Calculations showed that the tailing dam wall is subject to compressive force approximately 3 times as much as compared to the reservoir wall. This creates danger of loss of compressive strength of clay-cement concrete of which the wall is built.

Calculations showed that in all the considered cases in COW, there are zones where vertical stresses  $\sigma_y$  exceed uniaxial compressive strength of clay-cement concrete (2 MPa). In the reservoir COW, as a rule, this is the downstream face of the wall in the zone of its embedment into rock foundation (Fig. 8). At that, the values of stresses slightly vary depending on deformation of the foundation alluvial soil.

In the tailing dam wall, vertical stresses exceed uniaxial compressive strength of clay-cement concrete actually height-wise. They amount to 4–6 MPa, and in the zone of embedment into rock, they exceed 5 MPa in alternative 2 (Fig. 8,b) and 10 MPa in alternative 1 (Fig. 8,a).

However, as clay-cement concrete is a plastic material, at evaluation of its compressive strength, it is necessary to take into account the effect of strength increase if lateral compression takes place. This effect is known from experimental results of a number of authors [26, 27].

Mohr–Coulomb theory was used to determine compressive strength of clay-cement concrete in conditions of complicated stress state. The value of hydrostatic pressure on the wall was approximately used as compressive stress. At that, it was assumed that the angle of internal friction of clay-cement concrete was equal to  $\varphi = 30^\circ$ .

Analysis showed that with consideration of the indicated effect, the strength of clay-cement concrete in the reservoir wall would be provided in all the considered alternatives. COW strength of the tailing dam will be provided only in case if deformation modulus of foundation soil will not be less than 80 MPa (alternative 2, Fig. 8, b). In alternative 1, when deformation modulus of foundation soil amounts to 40 MPa, the wall strength will not be provided in any sections height-wise (Fig. 8, a); its integrity will be damaged.

Thus, the tailing dam COW operates in more unfavorable conditions than the reservoir COW and not always it may serve as a safe seepage-control facility of the tailing dam.

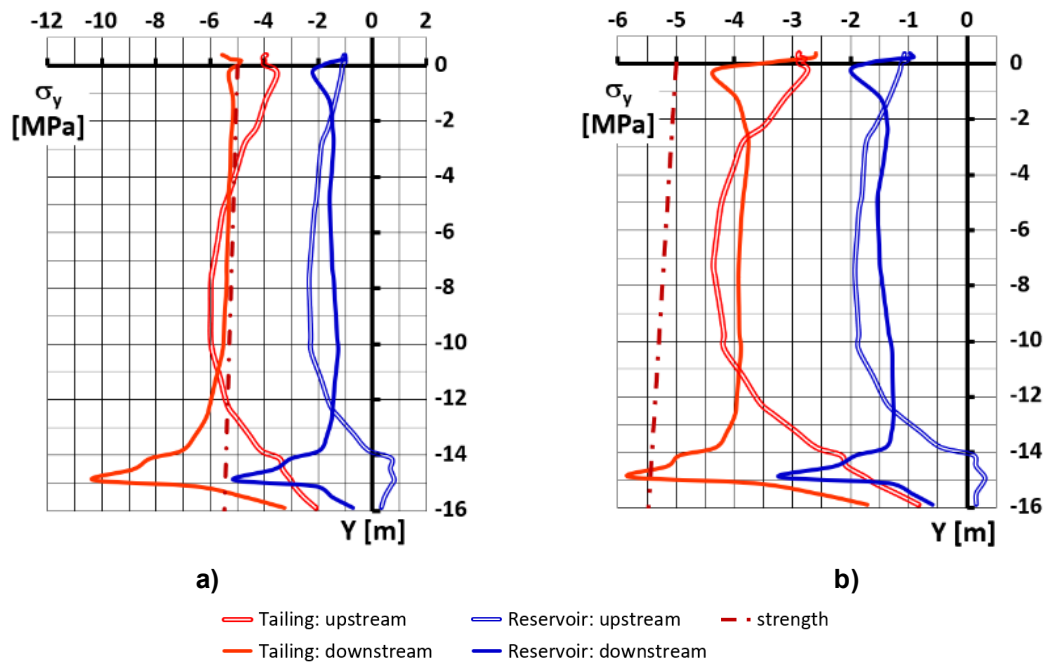


**Fig.8. Vertical stresses in a COW: a) – alternative 1; b) – alternative 2.**

#### 4. Conclusion

The fulfilled study shows that COW in the foundation of the tailing dam operates in more unfavorable conditions than the COW in the reservoir dam foundation. This is related to existence of additional vertical and horizontal loads.

Pressure from the weight of slimes creates additional vertical force in the wall and increases the risk of compressive strength loss of its material. Selection of mix and properties of clay-cement concrete for COW should be accomplished with consideration of deformation properties of foundation soil. For the considered case of a high tailing dam, the wall strength will not be provided if clay-cement concrete modulus of deformation will be 4 times as much as deformation modulus of foundation soil.

As a result of investigations, an interesting effect was revealed: under other equal conditions, the wall displacements in foundation of a tailing dam may be a little bit less than displacements of the wall in foundation of the reservoir dam. This is related to specific feature of elastic-plastic behavior of soils embedded in the tailing dam foundation.

#### References

- Balian, S. Cut-Off Wall Construction at Peribonka dam. *International Water Power & Dam Construction*. 2007. 59(2). Pp. 42–44.
- Noll, H., Langhagen, K., Popp, M., Lang, T. Rehabilitation of the Sylvenstein earth-fill dam – Design and Construction of the Cut-Off Wall [Ertüchtigung des Sylvenstein-Staudamms – Planung und Ausführung der Dichtwand]. *WasserWirtschaft*. 2013. 103(5). Pp. 76–79.
- Mirghasemi, A.A., Pakzad, M., Shadravan, B. The world's largest cutoff wall at Karkheh dam. *The International Journal on Hydropower & Dams*. 2005. 2. Pp. 2–6.
- Faridmehr, I., YazdaniPour, M.R., Jokar, M.J., Ozbakkaloglu, T. Construction and Monitoring of Cement/Bentonite Cutoff Walls: Case Study of Karkheh Dam, Iran. *Studia Geotechnica et Mechanica*. 2019. 41(4). Pp. 184–199. DOI: 10.2478/sgem-2019-0019
- Cacciuttolo, C., Pastor, A., Valderrama, P., Atencio, E. Process Water Management and Seepage Control in Tailings Storage Facilities: Engineered Environmental Solutions Applied in Chile and Peru. *Water*. 2023. 15(1). Article no. 196. DOI: 10.3390/w15010196
- Alonso, E. The Failure of the Aznalcóllar Tailings Dam in SW Spain. *Mine Water and the Environment*. 2021. 40. Pp. 209–224. DOI: 10.1007/s10230-021-00751-9
- Alonso, E., Gens, A. Aznalcóllar dam failure. Part 1: Field observations and material properties. *Geotechnique*. 2006. 56(3). Pp. 165–183. DOI: 10.1680/geot.2006.56.3.165
- Wen, L., Chai, J., Xu, Z., Qin, Y., Li, Y. A statistical analysis on concrete cut-off wall behaviour. *Proceedings of the Institution of Civil Engineers: Geotechnical Engineering*. 2018. 171(2). Pp. 160–173. DOI: 10.1680/jgeen.17.00142
- Pan, Y., He, Y.-L., Zhou, X.-X., Cao, X.-X. Analysis of effect of canyon terrain on stress and displacement of cutoff wall in dam foundation with deep overburden. *Yantu Lixue / Rock and Soil Mechanics*. 2013. 34(7). Pp. 2023–2030.

10. Liu, S.-h., Wang, L.-j., Wang, Z.-j., Bauer, E. Numerical stress-deformation analysis of cut-off wall in clay-core rockfill dam on thick overburden. *Water Science and Engineering*. 2016. 9(3). Pp. 219–226. DOI: 10.1016/j.wse.2016.11.002
11. Pisheh, Y.P., Hosseini, S.M.M.M. Numerical analyses of embankment dams containing plastic concrete cut-off walls using finite difference method (A case study: The Karkheh Embankment Dam). *Global Journal of Engineering and Technology Advances*. 2021. 9(3). Pp. 143–153. DOI: 10.30574/gjeta.2021.9.3.0176
12. Wen, L., Chai, J., Wang, X., Xu, Z., Qin, Y., Li, Y. Behaviour of concrete-face rockfill dam on sand and gravel foundation. *Proceedings of the Institution of Civil Engineers: Geotechnical Engineering*. 2015. 168(5). 439–456. DOI: 10.1680/geng.14.00103
13. Wen, L., Chai, J., Xu, Z., Qin, Y., Li, Y. Monitoring and numerical analysis of behaviour of Miaojiaba concrete-face rockfill dam built on river gravel foundation in China. *Computers and Geotechnics*. 2017. 85. Pp. 230–248. DOI: 10.1016/j.compgeo.2016.12.018
14. Wen, L., Chai, J., Xu, Z., Qin, Y., Li, Y. (2019) Comparative and Numerical Analyses of Response of Concrete Cutoff Walls of Earthen Dams on Alluvium Foundations. *Journal of Geotechnical and Geoenvironmental Engineering*. 2019. 145(10). Article no. 04019069. DOI: 10.1061/(ASCE)GT.1943-5606.0002132
15. Yu, H., Yu, S., Li, C., Li, W. FEM Analysis of Stress Characteristics of Cut-off Wall in Rushan River Groundwater Reservoir. *IOP Conference Series: Earth and Environmental Science*. 2019. 384. Article no. 012171. DOI: 10.1088/1755-1315/384/1/012171
16. Yu, X., Kong, X., Zou, D., Zhou, Y., Hu, Z. Linear elastic and plastic-damage analyses of a concrete cut-off wall constructed in deep overburden. *Computers and Geotechnics*. 2015. 69. Pp. 462–473. DOI: 10.1016/j.compgeo.2015.05.015
17. Sainov, M.P. 3D performance of a seepage control wall in dam and foundation. *Magazine of Civil Engineering*. 2015. 57(5). Pp. 20–33. DOI: 10.5862/MCE.57.2
18. Sainov, M.P., Anisimov, O.V. Stress-strain state of seepage-control wall constructed for repairs of earth rock-fill dam. *Magazine of Civil Engineering*. 2016. (68)8. 3–17. DOI: 10.5862/MCE.68.1
19. Sainov, M.P., Lubyantsev, L.V. Stress-strain state of seepage-control walls in foundations of embankment dams. *Magazine of Civil Engineering*. 2017. 73(5). 96–112. DOI: 10.18720/MCE.73.9
20. Sainov, M., Soroka, V., Gunasekaran, M. Combination of rockfill dam reinforced concrete face and seepage control wall in the foundation: stress-strain state. *Construction of Unique Buildings and Structures*. 2022. 99(1). Article no. 9902. DOI: 10.4123/CUBS.99.2
21. Li, Q., Ma, G., Li, P., Su, Z. Dynamic characteristics of tailings dam with geotextile tubes under seismic load. *Reviews on Advanced Materials Science*. 2021. 60(1). Pp. 599–614. DOI: 10.1515/rams-2021-0046
22. Solans, D., Kontoe, S., Zdravković, L. Impact of foundation layer characteristics on the seismic response of a tailings dam. 10th European Conference on Numerical Methods in Geotechnical Engineering (NUMGE 2023). Imperial College. London, 2023. DOI: 10.53243/NUMGE2023-307
23. Kerenchev, N. On the E50 modulus of Tailings dam materials. 19<sup>th</sup> International Multidisciplinary Scientific GeoConference (SGEM 2019). STEF92 Technology Ltd. Sofia, 2019. DOI: 10.5593/sgem2019/1.2/S02.051
24. Luo, P. Investigation on Shear Wave Velocity and Triaxial Mechanical Performance of Tailings Core from Tailings Dam. *Advances in Civil Engineering*. 2021. Article no. 5848324. DOI: 10.1155/2021/5848324
25. Bhanbhro, R., Knutsson, R., Auchar Zardari, M., Edeskär, T., Knutsson, S. Mechanical properties of soft tailings from different depths of a Swedish tailings dam: Results from triaxial tests. *Scientia Iranica*. 2020. 27(3). Pp. 1066–1074. DOI: 10.24200/sci.2018.20418
26. Rasskazov, L.N., Radzinskii, A.V., Sainov, M.P. Strength and Deformability of Clay-Cement Concrete in a Complex Stress State. *Power Technology and Engineering*. 2015. 48(5). Pp. 361–365. DOI: 10.1007/s10749-015-0534-1
27. Razavi, S.-K., Hajjalilue-Bonab, M., Pak, A. Design of a Plastic Concrete Cutoff Wall as a Remediation Plan for an Earth-Fill Dam Subjected to an Internal Erosion. *International Journal of Geomechanics*. 2021. 21(5). Article no. 04021061. DOI: 10.1061/(ASCE)GM.1943-5622.0001991

#### **Contacts:**

**Mikhail Sainov, Doctor of Technical Sciences**

ORCID: <https://orcid.org/0000-0003-1139-3164>

E-mail: [mp\\_sainov@mail.ru](mailto:mp_sainov@mail.ru)

**Nikita Talalaev,**

ORCID: <https://orcid.org/0009-0001-9424-9661>

E-mail: [talalaevnicita@yandex.ru](mailto:talalaevnicita@yandex.ru)

*Received 25.12.2023. Approved after reviewing 18.09.2024. Accepted 26.09.2024.*

